Lava accretion processes around fast-spreading ridges:

Volcanology and petrology in the northern Oman ophiolite

高速拡大海嶺における溶岩層形成プロセスの解明
～オマーンオフィオライトの例～

Yuki Kusano

Doctoral Program in Fundamental Sciences
Graduate School of Science and Technology

Niigata University

Abstract

Detailed lithological study with geochemical variations of lavas reveals the across-axis accretionary process at Wadi Fizh in the northern Oman ophiolite. The > 900-m thick V1 sequence is divided into the lower V1 (LV1), middle V1 (MV1) and upper V1 (UV1) sequences by 0.4-m and 0.8-m thick umber layer at 410 mab (meters above the base of the extrusive rocks) and 670 mab, respectively. The lowest part of the LV1 (LV1a) consists of lobate sheet and pillow lava flows extruded on the relatively flat ridge crest. Elongate pillows at 230 mab are flows draping downslope from the ridge crest which characterize the lithofacies on the ridge flank. Just above a jasper layer at 270 mab, 130-m thick voluminous flows of evolved lava were transported from the crest and emplaced on the ridge flank (LV1b). Off-axial accretionary processes recorded in the MV1 and UV1 sequences resulted in alternating flows of less evolved and depleted lava with evolved lavas, suggesting that the MV1 off-axial lava sequence comprises flows emanated from both on- and off-axial source vents. The less-evolved and depleted UV1 flows suggest independent sources distinct from the axial lavas. The Lasail Unit is regarded as a subunit of the V1 sequence because it corresponds to the UV1 based on the geological, petrological, and geochemical characteristics. The broad compositional range of the V1 sequence as well as the wide spectrum of geochemistry of the underlying sheeted dike complexendorse a view that the Wadi Fizh area corresponds to a segment end of the Oman paleospreading system accompanied by off-axis volcanisms as in segment boundaries of the present East Pacific Rise.

Comparing eight sections spanning 70 km, the along-axis volcanic system is reconstructed. The thickness of on-axis lava section decrease from the center to the margin of the ridge segment. Appearance of pillow lavas around the segment margin indicates that more ragged seafloor topography than the center where pahoehoe flows dominate. Their lava compositions are also varied systematically. Homogenized mildly-evolved lavas characterize the segment center. The larger melt lens and the higher ability of melt concentration below the segment center would produce the thick and homogenized lava sequence. On the other hand, both evolved and less-evolved lavas showing lower degrees of partial melting occur in the segment margin. Smaller melt lenses would promote highly evolved and less-evolved lavas. Vigorous off-axis volcanisms are recognized around the second- and third-order segment margins. They might be rooted at less-evolved melt avoiding the focus on the axis area.

The V2 sequence generated at later arc-like setting is also studied. The 1115-m thick V2

consists of the lower tholeiitic (LV2) and the upper boninitic magmatism (UV2). The stratigraphy indicates that boninite had erupted after the tholeiitic volcanism and characterized the end of V2 in this area. This discovery gives a new constraint for the petrogenesis of the V2 magmatism.

概要

海嶺火成活動は、4 階層のセグメントによって活動の範囲や規模などが規制され、セグメントの中心から末端にかけて系統的に変化すると考えられている（Macdonald et al., 1991）。海底の音波探査等でこうした変化が解析されているが，その実体，特に深さ方向を観察することは困難で、溶岩層の表層に限られている。溶岩層自体もすべてが海嶺軸上で形成されたのではなく、海嶺軸から 1-4 km 離れたオフアクシスで 2 倍近い厚さになることが知られている（Hooft et al., 1996）。これは海嶺軸上で噴出した溶岩が流下したり，軸とは別の割れ目から噴出したりすることによって、オフアクシスで溶岩が定置するためと考えられている（e.g. Perfit and Chadwick, 1998）。これらの問題を解決するため本研究では、アラビア半島東端に露出するオマーンオフィオライトにおいて詳細な調査を行った。本オフィオライトには上部マントルから溶岩層までの海洋リソスフェアが連続的に露出しており、海洋地殻形成プロセスを解析できるフィールドとして世界各地から注目されている。オマーンオフィオライト溶岩層最下部を構成する V1 溶岩には、海嶺およびその周囲で起こった火成活動が火山岩層序として記録されている。本研究ではこれらの溶岩を詳細に検討し、海嶺軸と直行方向および海嶺軸方向の火成活動の変化を明らかにした。現世の海洋調査の結果に基づいて議論することによって、従来続いてきたオマーンオフィオライト固有の層序問題を解決する手がかりともなった。また、オフィオライトの生成場を検討するために上位の V2 溶岩層についても調査を行った結果、ボニナイト溶岩が見いだされた。 Wadi Fizh では、厚さ 900 m 以上の V1 溶岩層が連続して露出し、厚さ 40 cm および 80 cm のアンバー層により下位から LV1、MV1 と UV1 に区分される。LV1 最下部（LV1a）はロベートシートフローと枕状溶岩で構成され、比較的平滑な海嶺軸上に噴出したことが推定される。230 mab（meters above the base of the extrusive rocks）に出現する伸長した枕状溶岩は、海嶺の斜面を流下して形成されたとみられる。270 mab よりも上位（LV1b）には厚さ 130 m もの分化した溶岩が出現し、大規模な溶岩流が海嶺軸部から流下して海嶺の側面で定置したと推定される。MV1 と UV1 には、オフリッジでの溶岩定置・噴出プロセスが保存されている。MV1 はあまり分化していない溶岩と分化した溶岩が交互に積み重なり、海嶺軸上溶岩とオフアクシス溶岩の両方で構成されたと考えられる。UV1 はあまり分化していない溶岩で構成され海嶺軸上溶岩とは別のソースを持っていると推測される。Fizh ではシート状岩脈群と同様、溶岩組成が広い範囲を示し、本地域が古海嶺システムのセグメント境界部に相当することと調和的である。EPR ではセグメント境界部にオフアクシス海山が偏在することが報告されており、本地域の MV1 や UV1 はこうしたオフアクシスでの溶岩定置プロセスを反映していると考えられる。本研究では南北 70 km にわたる 8 つの地域で溶岩層の層序学的検討を行い、古海嶺軸方向の火成活動システムを復元した。V1 溶岩層全体の厚さには大きく影響しないが、海嶺軸上火成活動で形成される溶岩の厚さはセグメント中心部から境界部へと薄くなる傾向がある。中心部では全体にパホイホイ溶岩が卓越して観察されるが、境界部では枕状溶岩が形成されており、より険しい海底地形が推測される。溶岩組

成も系統的に変化し、セグメント中心部では均質化した、あまり分化していない溶岩が支配的である。中心部では比較的大きな安定したメルトレンズがあり、下部地殻から次々と上昇してくるメルトがそこで均質化されるため溶岩も厚く、均質になると考えられる。一方、セグメント境界部では分化したものからあまり分化していない溶岩、また部分溶融度の低い溶岩まで、幅広い組成を示す。より小さいメルトレンズで著しく分化した溶岩や、メルトレンズを経ずに下部地殻から直接上昇した溶岩などがこれらの起源として推測される。2 次および 3 次のセグメント境界に相当する 3 地域ではオフアクシス火成活動の痕跡が認められ、これらは海嶺軸下のメルトレンズへの上昇を免れたメルトが噴出した可能性がある。　V2 溶岩は V1 火成活動後、オマーンオフィオライトがアラビア半島に衝上する以前に島弧セッティングで形成されたもので V1 溶岩とは異なる生成プロセスを有する。Wadi Suhayli と Hilti の合流点に産する厚さ 1115 m の V2 溶岩は、ソレアイト質溶岩からなる主体部とボニナイト溶岩からなる上部に区分される。つまり本地域では、ボニナイトは V2 火成活動の最末期、ソレアイト質火成活動の後に噴出したことが明らかとなった。　上述のように層序的に確立した V1 と V2 溶岩の組成を比較すると、単斜輝石の TiO_2 および Na_2O、全岩石の希土類元素比（Nd/Yb）n において大局的に両者が区分できることが判明した。しかし局所的にみると重複する範囲も多い。V1 溶岩は海嶺軸上からオフアクシス火成活動への変化や海嶺軸方向のセグメント構造に支配されたマグマシステムによって広い組成範囲を有する。V2 溶岩は一部でマグマやフルイド混合の痕跡を示しており、組成範囲が広くなる場合もある。したがってオフィオライト形成場の議論に化学組成は欠かせないものの、比較する際には十分な吟味が必要である。

Contents

Chapter 1

Lava accretion system around mid-ocean-ridges: Volcanic stratigraphy in the Wadi Fizh area, Northern Oman ophiolite

1.1. Introduction

Recent ocean-floor explorations based on high-resolution bathymetry surveys, submersible and deep-tow camera observations and sampling as well as dredging and ocean-floor drilling have revealed construction processes of the present oceanic crust. A number of observations of on- and off-axis regions of fast spreading ridges have confirmed the occurrence of pahoehoe and lobate sheet flows on shallow slopes (< 5°) on the ridge summit and off-axial plains, whereas steeper axial slopes are dominantly covered with pillow lavas [e.g. Auzende et al., 1996; Gregg and Smith, 2003; Umino et al., 2002]. Generally, extrusive rocks emplaced on the spreading axis show a temporal variation through the crustal accretion process on the ridge axis. However, Hooft et al. [1996] reported that oceanic crustal layer 2A thickens double or more off axis compared to the thickness on axis. Such off-axis lavas are considered to have been emplaced by transportation through lava channels and tubes downslope from the sources on the ridge crest or by extrusion from off-axial vents [Geshi et al., 2007; Perfit et al., 1994; Reynolds and Langmuir, 2000; White et al., 2000, 2002 and 2006]. Detailed geological mapping of axial terrain of fast-spreading ridges have revealed narrow and shallow troughs accompanied by small pillow mounds, some flows filling the axial troughs and draping downslope [Fornari et al., 1998]. In addition to these, recent accurate acoustic imagery shows many submarine volcanoes erupted off axis around the East Pacific Rise (EPR) [Scheirer and Macdonald, 1995; White et al., 2006]. Although a large number of off-ridge volcanoes exist in the vicinity (-3 km) of fast-spreading ridge axes, their distribution is clearly biased and clustered at around second- and third-order segment boundaries [Haymon et al., 1991; Macdonald et al., 1991; White et al., 2000, 2002, 2006]. On the EPR, lava tubes and channels have been found to extend several kilometers in length from the ridge crest to the flanks [Soule et al., 2005].Off-ridge lavas from the EPR 9°-12°N show a larger compositional variation ranging from highly depleted to enriched basalts compared to axial N-MORBs [Perfit et al., 1994; Niu and Batiza, 1997; Reynolds and Langmuir, 2000; Sims et al., 2003]. This diversity may inherit from the heterogeneity of the mantle source because they are free from mixing in the axial magma chambers [Niu and Batiza, 1997].

It is apparent that extrusive layers thicken almost continuously as the oceanic crust moves away from the ridge crest to fault-bounded basins. Eruptive style and lava flow morphology may change along with the varying basement topography and distance from the source to the site of emplacement. From lab-based fluid-dynamics experiments, lava flow morphology varies in response to the change in density, viscosity and flow rate of lava, and slope of the basement [Griffiths and Fink, 1992; Gregg and Fink, 1995; Gregg and Fink, 2000]. From seafloor observations, steep flanks (over four degree in gradient) of submarine volcanoes off Hawaii Islands and rise slopes of the EPR are covered predominantly with elongate pillows, but subhorizontal summits and rise crests are overwhelmingly underlain by lobate sheets and pahoehoe flows [Auzende et al., 1996; Gregg and Smith, 2003; Umino et al., 2002]. The formation microscanning imagery interpretations of in-situ crust at Ocean Drilling Program (ODP) Hole 1256D, located at a super-fast spread, 15Ma EPR seafloor, almost half of the extrusive layers were emplaced off axis and the uppermost 100-m thick ponded lava layer was emplaced by off-axis volcanism [Crispini et al., 2006].

In order to understand the constructional processes of upper oceanic crust, it is critical to pursue detailed analyses of stratigraphic variations of the lava accretion styles. However, it has been challenging to directly observe the sequence of in situ upper oceanic crust because of its rare exposure [e.g. Francheteau et al., 1992] as well as the difficulty in scientific ocean drilling [Teagle et al., 2006, etc.]. On the other hand, ophiolites provide superb exposures based on which we can reconstruct detailed three dimensional architecture of oceanic crust.

The Oman ophiolite is the largest and best exposed ophiolite in the world that preserves the original structure of oceanic lithosphere formed at a fast-spread Neotethys ridge system [e.g. Nicolas, 1989]. Detailed structures of ridge segments have been identified in the northern Oman ophiolite based on the geological and petrological lines of evidence on the gabbros and sheeted dike complex [Adachi and Miyashita, 2003; Miyashita et al., 2003; Umino et al., 2003]. Wadi Fizh area is considered to be a second- or third-order discontinuity of a paleoridge segment, because plutonic complexes (blocks) consisting of layered gabbro, upper gabbro and wehrlitic intrusions are penetrated by dolerite dikes [Adachi and Miyashita, 2003]. From the segment center at Wadi ath Thuqbah toward the end at Wadi Fizh, the dike thickness increases and the number of dikes decreases [Umino et al., 2003]. Comparatively uniform and moderately evolved dikes occur in the segment center while those from the segment end show a larger variation from highly evolved to primitive compositions [Miyashita et al., 2003; Umino et al., 2003].

The volcanic formations in the Oman ophiolite are divided into three units: V1 (Geotimes unit), V2 (Alley unit) and V3 (Salahi unit) [Alabaster et al., 1982; Lippard et al., 1986; Ernewin et al., 1988; Umino et al., 1990]. Despite of different ideas for the genesis of magmatism, the stratigraphic division of V1=Geotimes, V2=Alley and V3=Salahi unit is broadly accepted. However, there is a debate on the lava stratigraphy in particular for the

Lasail Unit. Alabaster et al. [1982] and Lippard et al. [1986] define the Lasail Unit between Geotimes and Alley Unit. Umino et al. [1990] and A'Shaikh et al. [2005] regard the Lasail Unit as a part of the Geotimes Unit, while Ernewein et al. [1988] and Godard et al. [2003] regard as a subdivision of the V2 unit. Detailed stratigraphic analyses are indispensable to solve this problem, but only a part of V1 extrusive rocks exposed in the Wadi Shaffan area has been studied yet [Einaudi et al., 2000; 2003].

This paper presents the first thorough description of the whole V1 sequence in the Wadi Fizh area and detailed stratigraphic variation of lava configuration and geochemistry, and discusses the accretionary processes of the upper crust at a paleoridge segment boundary (Figure 1.1).

1.2. Geology

1.2.1. Geology and description of lithofacies

V1 unit was generated in a mid-ocean ridge setting [Nicolas, 1989; Umino et al., 1990; Godard et al., 2003], or in a supra-subduction zone setting [Alabaster et al., 1982; Pearce, 1980; Lippard et al., 1986], whereas V2 unit was formed by subduction-related [Alabaster et al., 1982; Pearce, 1980; Lippard et al., 1986] or intraoceanic detachment magmatism [Ernewein et al., 1988; Boudier et al., 1988]. The collision event by which the Oman ophiolite was emplaced on the Arabian continent occurred after V2 magmatism. V3 magmatism would have been originated during the 85-Ma collision event [Alabaster et al., 1982; Lippard et al., 1986; Ernewin et al., 1988; Umino et al., 1990].

The extrusive rocks in Wadi Fizh area is more than 900 m in thick, striking N-S to NWN-SES and diping 25°-40° east (Figure 1). The extrusive rocks gradually change into the underlying sheeted dike complex, through 20-m thick transition zone with an increasing number of 0.8- to 1.5-m thick dikes downward. The sheeted dike complex striking N-S to NW-SE and dipping 20°-45° west, and it is nearly perpendicular to the extrusives.

Although V2 lavas appear at the eastern end of the mapped area (Figure 1.1), the direct relationship between the V1 and V2 flows is not observed because of lack of exposure. A 0.3-m thick umber layer intercalated with the V2 pillow lavas trends N50W and dips 20° east, which is concordant to the general structure of the underlying V1 extrusive rocks.

Based on a series of observations on the modern-day submarine lava formation described below, we have identified four lithofacies in the V1 sequence; pillow, pahoehoe, lobate sheet and massive lava flows.

Pillow flows comprise 31% of the V1 section. Pillow flows consist mainly of "bulbous" pillows (Figure 1.2b) and only locally of "elongate" pillows (Figure 1.2c). Characteristic features indicative of pillow budding are sometimes observed such as transverse spreading cracks, but none of corrugations on pillow surfaces are preserved due to weathering. However, flow directions of pillow lobes could be determined by the alignment of elongate, cylindrical pillow lobes, which sometimes bifurcate downslope [Auzende et al., 1996; Gregg and Smith, 2003; Umino et al., 2002].

Pahoehoe flows are abundant in the UV1. Individual pahoehoe flows have a minimum thickness of 30 m and attains to 20% of the entire V1 sequence. Subaqueous pahoehoe lobes have been mistaken as pillow lobes but the former has much smaller ratios of thickness to width than the latter [Walker, 1992; Umino and Nakano, 2007]. Pahoehoe lobes are approximately 1-3 x 2-5 m in extension and 0.2-1 m thickness. They are characterized by their bun-like or amoeboid shapes and smooth surfaces without corrugations and are intimately associated with lobate sheet flows like their subaerial equivalents accompanying pahoehoe sheet (lava rise) (Figure 1.2d) [Hon et al., 1994; Umino et al., 2002]. Some pahoehoe lobes are interconnected upstream to a larger and thicker lobate sheet, to which coalesced adjacent pahoehoe lobes merge [Gregg and Chadwick, 1996]. Hollow lobes are present in pahoehoe flows, which form by drainage of molten lava within partially solidified lobes [Batiza and White, 2000; Umino et al., 2000].

Lobate sheet flows occupy 41% of the V1 sequence and are the dominant lithofacies in this section (Figure 1.2e). A lobate sheet has a gently curved upper surface with well-developed columnar joints perpendicular to the surface. A lobate sheet flow is a compound flow consisting of numerous lobes about 2 m in thickness and lateral extension of 20 m or more, which are piled up to form a domal structure as a whole (Figure 1.2f). Some lobate sheet flows include breccias 0.1-0.2 m thick and are underlain by lenses of pillows less than 0.5 m thick. Varioles less than 1 cm in diameter are locally present in the chilled margin of a lobate sheet.

Massive lava constitutes 7% of the V1 sequence, which is the least abundant among the four lithofacies. Unlike lobate sheet flows, massive lava has a flat surface with well-developed columnar joints perpendicular to the surface. A massive flow is 1.5-35 m thick and extends at least 100 m long.

The 900-m thick sequential V1 unit is separated by 0.4- and 0.8-m thick metalliferous sedimentary layers (umber) (Figure 1.2a), on which the V1 units is divided into three subunits: the lower V1 (LV1), the middle V1 (MV1) and the upper V1 (UV1) (Figure 1.3). The uppermost UV1 with at least 200 m thickness shows shallower dips of 25°-32° east than the LV1 and MV1 unit dipping 30°-40° east. Stratigraphic levels are indicated by the height in meters above the base (mab) of the V1 sequence resting on the sheeted dike complex (Table 1.1).

1.2.2. The lower V1 sequence (LV1)

The LV1 is 410 m thick and consists mainly of pillow and lobate sheet flows with a subordinate amount of massive lava. Massive lava occurs in the lowermost V1 sequence directly overlying the sheeted dike complex. Pillow flows comprise 54% in the LV1. Most pillow lobes are bulbous pillows about 1.0-m across, while elongate pillows are locally present. Distinction of individual lithofacies is relatively easy at outcrops as shown in Figure 2f and is usually identified by the occurrence of different lava flow type and/or structure. At 330 mab, a sharp color change in thick pillow flows marks a boundary of superposed two flow units with a thickness of 45 and 25 m, respectively, which show different flow directions as indicated by the difference in elongated pillow alignment (Figure 1.2g). At 230 mab, a 20-m thick elongate pillow flow is underlain by a 40-m thick lobate sheet flow associated with bulbous pillows (Figure 1.2c). At 270 mab, a jasper layer is interbedded between the lower LV1 (LV1a) and the upper LV1 (LV1b) (Figure 1.3). The jasper forms a thin wavy layer with a variable thickness about 0.05 to 0.2 m and a lateral extension about 50 m, filling interpillow spaces and radial cracks of the underlying pillow lava. The jasper layer is overlain by lobate sheet flows, which are in turn overlain by a 70-m thick pillow flow unit. The top of the LV1 is conformably overlain by a 0.4-m thick metalliferous sedimentary layer extending approximately 3 km to the south (Figure 1.2a) where no erosion is observed along the boundary. At 410 mab, a 0.2-m thick dike trending NW-SE and dipping 60° westward intruded into the LV1b and the MV1 through the metalliferous sedimentary layer in between (Figure 1.2c).

1.2.3. The middle V1 sequence (MV1)

The MV1 has a thickness of 260 m and consists of bulbous pillows, pahoehoe and lobate sheet flows. The basal part of MV1 is shown in Figures 1.2a and 1.2b, where thin hyaloclastite conformably overlies an umber bed. Pillow and pahoehoe flows constitute 30% and 25% of the MV1, respectively. The thickness of individual flows is 10-50 m, which is similar to that of the LV1. The lower part of the MV1 is dominated by lobate sheet and pahoehoe flows, while the upper part is dominantly composed of pillow flows. A >5 m thick dike at 480 mab intrudes into pahoehoe flows with a chilled margin. The MV1 is terminated by the appearance of a 0.8-m thick metalliferous sedimentary layer extending about 4 km to the south.

1.2.4. The upper V1 sequence (UV1)

The UV1 is more than 200 m thick in total, and consists of 46% of pahoehoe flows and 30% of variolitic lobate sheet flows. While the upper sequence is poorly exposed, the UV1 sequence begins with thick pahoehoe flows resting on a metalliferous sedimentary layer. Between 730 and 880 mab, several 1.0-m thick basaltic dikes intrudes into pahoehoe and lobate sheet flows. These dikes strike WNW and dip 22°-78° south. A 0.75-m thick boninite dike trending 72° west and dipping 74° south is present in the UV1 sequence at 770 mab (Figure 1.1 and 1.3). At 854 mab, near the upper end of continuous exposures of the extrusive section, a 6- to 7-m wide zone of elongate pillows intruded by an intense swarm of thin dikes (0.1-0.25 m thick) is present within the host pahoehoe lava which strikes 50° east and dips 28° east (Figure 1.2h). The dikes appear exclusively within the 2-m wide central portion of the zone that extends laterally a few tens meters along N70°W and dips 70° south, almost perpendicular to the surrounding pahoehoe lava structure. The dikes intruded into and are sided by elongate pillows concordant to the attitude of dikes as shown in Figure 2h. These dikes and pillows are interpreted as a fissure vent opened within a pillowed ridge. The fissure runs through the pillowed ridge >3 m in height and 6-7 m in width, which consists of subvertical elongate pillows 0.6 m in diameter bifurcating downward along the pillowed ridge.

1.3. Petrography

Based on abundance and assemblage of phenocrysts, the V1 volcanic rocks are divided into aphyric, plagioclase (Pl)-phyric, plagioclase-olivine-clinopyroxene (Pl-Ol-Cpx)-phyric and Pl-Cpx-phyric types. Hyaloophitic and intersertal textures are well observed in the groundmass and a variolitic texture commonly develops near the surface of pillows (Figure 1.4a). Lava samples underwent intensive low-temperature alteration. Most plagioclases are altered to albite, saussurite or calcite. Chlorite and clay minerals replace olivine phenocrysts.

Only clinopyroxene, Fe-Ti oxide and chrome-spinel remain as primary minerals. Clinopyroxene occurs as discrete crystals or glomerocrysts. Summary of petrography is shown in Table 1.1.

The LV1 consists mainly of aphyric and sparsely Pl-Cpx-phyric basalt. A few Pl-phyric and Pl-Ol-Cpx lavas are also present. Aphyric lava sparsely contains plagioclase and clinopyroxene microphenocrysts (Figure 1.4b) and comprises a doleritic groundmass. Clinopyroxene phenocrysts and microphenocrysts show either sector zoning or normal zoning. Vesicles are filled with quartz, calcite and clay minerals. Pl-Cpx basalt dominates in the MV1 interbedded with a few aphyric flows (Figure 1.4c). Clinopyroxene shows either a sector zoning or normal zoning as those in the LV1. In the MV1 lava, clinopyroxene occurs both as a phenocryst and a microphenocryst. Amygdules filled with calcite, zeolite and clay minerals are common. The UV1 lava consists of Pl-Ol-Cpx and few Pl and Pl-Cpx basalt. Pl-Ol-Cpx lavas contain discrete or glomerocrystic Ol (Figure 1.4d). Clinopyroxenes have no distinct zoning. Vesicles are filled with calcite and clay minerals. A 0.2-m thick dike at 410 mab is Ol-phyric and a 1.0 m-thick dike at 730 mab is Pl-Ol-Cpx-Opx (orthopyroxene) -phyric, respectively. Chrome spinel (Cr/(Cr+Al)=0.76-0.81) occurs as microphenocrysts and inclusions in altered olivine of the 0.2-m thick dike at 410 mab. A 0.75-m thick boninite dike at 770 mab is Ol-Opx-Cpx-phyric with olivine and orthopyroxene phenocrysts completely replaced by clay minerals (Figure 1.4e).

1.4. Bulk chemistry

Whole-rock major elements, Ni, Y, Zr, Cr and V contents of 55 samples were analyzed by X-ray fluorescence (XRF) (RIX3000, Rigaku Denki) at Niigata University. The analytical method is described in Takahashi and Shuto [1997]. Other trace and rare earth elements of 41 samples were analyzed by inductively-coupled plasma mass spectrometry (ICP-MS) (Agilent 7500a ICP-MS) after Roser et al. [2000] at Niigata University. When acid-resistant minerals such as zircon and titanite are present, the analyses of ICP-MS by acid digestion may give lower Zr, Hf, Th and U contents, but rare earth element (REE) concentrations by acid digestion show similar values to those by alkali fusion [Neo et al., 2009]. Therefore, we use Zr value of the XRF method and other trace element content of the ICP-MS method for this study. The results of XRF and ICP-MS analyses are given in Appendix Table 1 and 2.

As mentioned above, the analyzed samples have suffered pervasive low-temperature alteration which may have affected the primary geochemical characteristics. We will first assess the effects of low-temperature alteration before discussing the primary geochemical signatures. Loss on ignition (L.O.I.) of analyzed samples ranges from 2.0 to 6.5 wt% and shows a positive correlation with CaO contents, suggesting an enrichment of CaO during alteration (Figure 1.5). This is consistent with abundant calcite in veins and vesicles and replacing olivine crystals [Alt and Honnorez, 1984]. On the other hand, Na2O contents show a weak negative correlation with L.O.I. However, the high Na2O in low L.O.I. samples does not always represent the primary nature of the sample, because plagioclase is totally altered to albite. Therefore, the high Na2O contents seem to have increased during the secondary processes. MgO contents do not correlate with L.O.I. but they might have been modified due to the formation of chlorite replacing olivine and filling vesicles [Humphris and Thompson, 1978a; Honnorez, 1981]. Therefore, we use immobile incompatible elements such as TiO_2 and P_2O_5 for the following petrological consideration. Vesicles are commonly filled with quartz so that SiO_2 may have increased in such samples.

Large-ion lithophile (LIL) elements such as Rb, Ba and Li, and Sr are generally highly mobile during ocean floor weathering [Thompson, 1973; Humphris and Thompson, 1978b; Staudigel and Hart, 1983; Seyfried et al., 1984, 1998; Alt and Honnorez, 1984]. In fact these elements are highly scattered, suggesting an intensive modification of the initial concentration during the secondary processes. On the other hand, V, Y, Zr and Cr are generally immobile against such alteration processes [Thompson, 1973; Hart et al., 1974; Humphris and Thompson, 1978b; Pearce and Norry, 1979]. Tight positive correlations such as TiO_2-Zr and Y-Zr support this view. In the section to follow, we discuss the petrological and geochemical characteristics of the extrusive rocks on the basis of these immobile elements.

Zr contents of V1 samples range from 24 to 153 ppm, indicating that these samples span from the most primitive to most evolved MORBs [BVSP, 1981]. Samples from LV1 and MV1 range in Zr from 42 to 153 ppm, and from 24 to 132 ppm, respectively, whereas UV1 samples concentrate between 27 and 50 ppm. Thus, the LV1 is generally evolved and the UV1 is relatively primitive among the V1 sequence. The V1 samples form two clusters on the Zr-TiO_2 and Zr-P_2O_5 variation diagrams (Figure 1.6), which subdivide the LV1 samples into high- and low-TiO_2 group. The high-TiO_2 group is characterized by higher incompatible element contents than the low-TiO_2 group. Although both groups are observed in the LV1 and MV1, the high-TiO_2 group dominates in the LV1 while the low-TiO_2 group dominates in the MV1. All the UV1 samples belong to the low-TiO_2 group.

These high- and low-TiO_2 groups show different trends in the Zr-Zr/Y variation diagram (Figure 6). The high-TiO_2 group has a limited Zr/Y ratio of 2.6-3.2, which slightly increases with increasing Zr contents. This suggests that the high-TiO_2 group of LV1 and MV1 was formed by the process of simple fractional crystallization from the same parent magma [Fujimaki et al., 1984]. On the other hand, the low-TiO_2 group exhibits a broad range in Zr/Y from 1.6 to 2.6 that increase with increasing Zr contents. Four samples of the LV1, almost half of the MV1 and all the UV1 samples belonging to the low-TiO_2 group may be derived from more diverse sources from the high-TiO_2 group samples.

REE concentrations of the V1 sequence exhibit similar characters as high field strength (HFS) elements. The high-TiO_2 group of the LV1 has Yb contents from 3.5 to 5.5 ppm, (La/Yb)n ratios from 0.8 to 1.0, and shows flat REE patterns with a slight light-REE (LREE) depletion (Figure 1.7a). On the contrary, the LV1 low-TiO_2 group ranges in Yb contents from 1.5 to 1.8 ppm and in (La/Yb)n ratios from 0.7 to 0.8 with slightly LREE-depleted REE patterns. Yb contents of the MV1 also show two distinct groups, where the high-TiO_2 group ranges from 3.0 to 4.5 ppm and the low-TiO_2 group ranges from 1.5 to 1.9 ppm (Figure 1.7b). The MV1 high-TiO_2 group shows flat REE patterns ((La/Yb)n=0.9-1.1) similar to those of the LV1. On the other hand, the MV1 low-TiO_2 group shows LREE-depleted patterns ((La/Yb)n=0.3-0.7) (Figure 1.7b). The UV1 samples overlap the MV1 low-TiO_2 group and have 1.4-2.1 ppm Yb and 0.5-0.8 (La/Yb)n ratios (Figure 1.7c).

The V2 sequence has similar bulk compositions to the V1 low-TiO_2 group. The V2 samples show low Zr contents ranging from 39 to 54 ppm. V contents of the V2 samples tend to be higher than those of the V1 sequence at a given Zr content (Figure 1.6). Also, Zr/Y ratios of the V2 sequence tend to be lower than the V1 low-TiO_2 group at a given Zr content (Figure 1.6). Although major and minor element concentrations of the V2 volcanics are similar to the V1 low-TiO_2 group, REE patterns give a more distinct feature. The V2 samples have (Nd/Yb)n ratios from 0.69 to 0.74, lower than 0.75-1.25 of the V1 low-TiO_2 group (Figures 1.7c and 1.7d), that shows a crossover of the REE patterns of the V1 and the V2 samples. Dikes intruding into the V1 sequence at 410 and 730 mab have similar compositions to each other with lower (Nd/Yb)n ratios (0.56-0.58). A boninite dike in the UV1 at 770 mab is highly depleted in incompatible elements but has a slightly LREE-enriched pattern, which resembles to a typical U-shaped pattern of boninites from the Oman and other ophiolites [Ishikawa et al., 2002; Godard et al., 2003].

1.5. Mineral chemistry

Clinopyroxene phenocrysts and microphenocrysts in 37 samples were analyzed by EPMA (JEOL JXA-8600SX) at Niigata University using an accelerating voltage of 15 kV and a beam current of 1.3×10^{-8} A. Counting time was 30 seconds on the peak and 20 seconds on the background. Correction procedures followed the ZAF-Oxide method. Representative clinopyroxene analyses are given in Appendix Table 3. Because preferential partitioning of Al_2O_3, TiO_2, Na_2O and REEs in [100] sector compared to other sectors is enhanced for clinopyroxene crystals in submarine lava due to rapid cooling, cares must be taken when comparing the variation of these elements in clinopyroxene [Coish and Taylor, 1979; Dowty, 1976; Gamble and Taylor, 1980; Lofgren et al., 2006]. We use core compositions of [001] sector only in order to exclude the compositional differences arose from this kinetic effect on the trace element partitioning (Figure 1.8).

Mg# (= Mg/[Mg + Fe*] where Fe* is total Fe as Fe^{2+}) of V1 clinopyroxene ranges from 0.65 to 0.93, which is comparable to or more varied than the previous reports for volcanic rocks from the Oman ophiolite [Alabaster et al., 1982; Ernewein et al., 1988; Umino et al., 1990; Einaudi et al., 2003; A'Shaikh et al., 2005]. This is consistent with the wide Zr range of bulk rock compositions in this area as described above. Mg# of clinopyroxene ranges widely from 0.65 to 0.90 for the LV1and from 0.74 to 0.93 for the MV1, while the UV1 clinopyroxenes range from 0.81 to 0.88, implying that the UV1 is comparatively less-evolved and has a limited compositional range among the V1 lavas as the bulk rock compositions. As shown in figure 8, analyses of the V1 sequence have a tight negative correlation between Mg# and TiO_2, and Na_2O, and a positive correlation between Mg# and Wo (= 100Ca/[Ca + Fe* + Mg]) (Figures 1.8a, d and e). Cr_2O_3 content attaining 1 wt% decreases rapidly with decreasing Mg# (Figure 1.8c). Thus, the LV1, MV1 and UV1 clinopyroxenes show similar chemical variations.

Mg# of clinopyroxene of the V2 sequence spans also a wide range from 0.67 to 0.85 like that of the V1 sequence. TiO_2 of clinopyroxene of the V2 sequence, ranging from 0.21 to 0.56 wt%, shows a negative correlation with Mg# like the V1 sequence, but is lower than the latter (Figure 1.8a). Such compositional trends are also recognized in Na_2O contents (Figure 8e). Moreover, it is noted that clinopyroxene of the boninite dike in the V2 sequence is extremely depleted in TiO_2 and Na_2O (Figure 1.8a and e). Thus, the clinopyroxenes of the V2 sequence and the boninitic dike are apparently distinct from those of the V1 sequence.

1.6. Chemical stratigraphy

Bulk-rock and clinopyroxene compositions shown above are examined in respect to the lithological stratigraphy. The lithological column and geochemical variations along the Wadi Fizh are illustrated in Figure 1.9.

The LV1 lava shows overall smooth variations with evolved compositions (TiO_2: 1.5-2.3 wt%; Zr: 87-153 ppm) except for a few spikes around 180, 250 and 330 mab. The incompatible elements such as Zr and Yb of the high-TiO_2 group gradually increase upward. Four samples belonging to the low-TiO_2 group are characterized by less-evolved but slightly enriched compatible elements. Three of them are lobate sheet flows just below the jasper layer at 270 mab. These less-evolved samples have similar (La/Yb)n and Zr/Y ratios to the other evolved rocks above and below. Clinopyroxene compositions are scattered but show broadly consistent variations with the bulk compositions.

It is noticed that there is a gap in bulk and clinopyroxene compositions between above and below the jasper layer at 270 mab (Figure 1.9). The LV1b is characterized by more evolved compositions (TiO_2: 1.9-2.2 wt%; Zr: 118-153 ppm) and narrower compositional variations than the LV1a (TiO_2: 1.5-2.1 wt %; Zr: 86-141 ppm). Grayish pillow lava at 330 mab is the only exception that has a less-evolved composition (Figure 1.2f). However, the entire LV1 shows similar (La/Yb)n ratios and a slight increase in Zr/Y ratios upward.

The 0.4-m thick metalliferous sedimentary layer marks the sharp compositional gap between the LV1 below and the MV1 above. The lower part of the MV1 sequence consists of less evolved lavas with very low incompatible elements compared to the LV1b samples. The entire MV1 exhibits zigzag variations with a wide range in TiO_2 (0.6-2.1 wt%) and Cr (5-300 ppm). It is noticed that (La/Yb)n and Zr/Y ratios of the MV1 also exhibit zigzag profiles unlike those of the LV1. This fact indicates that the MV1 is composed of basalts derived from a heterogeneous source or variable degrees of partial melting.

The basal part of the UV1 sequence shows low incompatible element contents with a limited compositional range (TiO_2: 0.6-1.0 wt%; Zr: 35-54 ppm) than the lower sequence. The lowest UV1 sample is also characterized by the highest compatible element content (Ni: 59 ppm; Cr: 199 ppm). Because the top of MV1 lavas have high Zr content such as 118 ppm, there is a sharp compositional gap between the MV1 and the UV1 at 670 mab. The zigzag profile of Zr/Y ratios of the UV1 implies that the UV1 lavas are derived from a slightly heterogeneous source.

1.7. Discussion

1.7.1. Effusive section in the Wadi Fizh area—change from on- to off-ridge setting

Lobate sheet flows and bulbous pillows dominate in the lowermost V1 sequence, while elongate pillows occur at 230 mab. Gentle slopes around fast-spreading ridges exist on 1) the axial summits and troughs and 2) the ridge flanks more than several kilometers off-axis. Based on the high-resolution topographic exploration of the axial regions on fast-spreading ridges, there are narrow (1-200 m) and shallow (3-50 m) fault grabens and collapse pits on lobate sheets [Ballard et al., 1979; Engels et al., 2003; Fornari et al., 1998; Fundis et al., 2010; Gregg and Chadwick, 1996]. Therefore, the occurrence of elongate pillows is only local in small scale on slopes inside the axial troughs and as pillow mounds formed around vents at low extrusion rates during the waning stage of eruptions [Fornari et al., 1998]. On the axial-ridge scale, elongate pillows preferentially form on slopes with a gradient larger than approximately 54° and dominate on slopes >15° on submarine volcanoes off Hawaii Islands and on the rise slopes of the southern EPR at 14°S [Auzende et al., 1996; Gregg and Smith, 2003; Umino et al., 2002; Tominaga and Umino, 2010]. The result of seafloor observation indicates that the lava flow morphology correlates well with the gradient of slopes respective to a subtle difference in lava composition. On the other hand, ODP Hole 1256D penetrated through the superfast-spread upper oceanic crust has only a limited interval of pillow lava at 700-800 m below seafloor, 200 m above the top of the sheeted dike complex within the 864-m thick extrusive rocks, which is correlated to pillow-dominant facies emplaced on the ridge slope [Tominaga and Umino, 2010]. Applying the same idea, we correlate the lowermost 230 m of the LV1 to axial facies erupted on the subhorizontal paleoridge crest and the thick pillow lava interval from 230 to 410 mab to slope facies which were emplaced on the steep ridge slope outside the ridge crest (Figure 1.10).

The jasper layer at 270 mab, which divides the LV1 to LV1a and LV1b manifests the hiatus of lava flow accumulation on this part of the seafloor. A jasper layer is considered to precipitate from hydrothermal fluid as colloidal silica and iron-oxyhydroxide particles, which are easy to be dispersed and subject to erosion without capping by later volcanic products [Halbach et al., 2002; Grenne and Slack, 2003]. Its limited continuity and thin occurrence suggest that the jasper layer settled on local depressions during a short repose period before overlain by the subsequent flows. During the repose period, lava composition changed from less-evolved to more evolved lavas. This change coincides with the changes in dominant flow types from lobate sheet flows below the jasper layer to pillow lavas above. Their thick lava layers, and evolved and limited bulk compositions of the LV1b may have been derived from voluminous eruptions. Despite the wide range variations in incompatible elements such as TiO_2, Zr and Yb, the high-TiO_2 group basalts, show a narrow range in Zr/Y ratios through the entire LV1 sequence. It is noted that the LV1 Zr/Y ratios slightly increase with increasing Zr, which implies overall upward evolution of the LV1 flows. Thus, the majority of high-TiO_2 group of both LV1a and LV1b is derived from the same source, and experienced various degrees of fractional crystallization. Some low-TiO_2 LV1 lavas may not be explained by a simple fractional crystallization of the high-TiO_2 LV1 magma.

The 0.4-m thick metalliferous umber dividing the LV1 and MV1 contains more heavy metals than pelagic sediments and is considered to have been generated by hydrothermal activities [Robertson and Fleet, 1986; Karpoff et al., 1988]. Unlike the jasper layer at 270 mab, the umber layer is traced more than 3 km, suggesting a significant depositional period. Assuming a sedimentation rate of 0.01 mm/a [e.g. Berger, 1974], the 0.4-m thick umber represents a 40,000-year time interval. If a half-spreading rate was 5-10 cm/a, the MV1 should have deposited more than 2-4 km off-axis from the top of the LV1. Although this is only a rough approximation, the distance of 2-4 km seems to be in accordance with the change in characteristic lava morphology from the LV1 with elongate pillows to the MV1 with common lobate sheets. We suggest that the MV1 lavas were emplaced off axis on a subhorizontal abyssal plain by traveling a long distance from the ridge crest or by in-situ eruptions at off-axis vents.

The 70-m thick MV1 flows above the metalliferous umber are characterized by less-evolved and depleted compositions with lower (La/Yb)n and Zr/Y ratios than the lower LV1, suggesting that this part of the MV1 may be derived from a more depleted source or formed by a higher degree of partial melting. Recurrence of less-evolved flows through the MV1 suggests a discrete source other than the axial vents that fed the more evolved LV1 flows. Evolved flows in the upper two third of the MV1 have similar compositions to the LV1 high-TiO_2 group with the overall same Zr/Y ratios, indicative of a common source of these two. The evolved, more fertile lavas intervened with the MV1 may be flows that traveled a long distance through lava channels or tubes from the ridge axis [e.g. Soule et al., 2005]. The zigzag pattern of the geochemical variations of the MV1 may represent alternating sources of the on- and off-axis magmatism. This geochemical pattern is similar to the northern EPR at

9° N where pillow ridges and mounds formed above off-axial source vents are sometimes covered with large-scale flows from the ridge axis [Perfit et al. 1994].

The UV1 sequence is characterized by less-evolved and depleted homogeneous compositions belonging to the low-TiO_2 group. The less-evolved character suggests that the volcanism occurred significantly off axis beyond the limit of distance that evolved voluminous flows from the ridge axis can travel. The presence of a fissure vent at 854 mab is the evidence of such off-ridge volcanism. We suggest that the UV1 lavas were generated from a homogeneous depleted source mantle. An isolated volcano is also reported from the Wadi Shaffan area [Einaudi et al., 2000; 2003]. These findings suggest the common presence of off-ridge volcanism on the Neotethys oceanfloor.

It is noted that the UV1 may be correlated to the Lasail Unit, because they have similar geological and petrological features. The Lasail Unit was defined by Alabaster and Pearce [1980] as a fractionation sequence from basalt through andesite to felsite which directly overlie the 'axis' lavas. The basaltic member is typified by small, distinctly gray-green, non-vesicular, aphyric and frequently bun-shaped pillow lavas. The Lasail Unit shows more primitive compositions (TiO_2: 0.3-0.9 wt%; Zr: 20-50 ppm) than the Geotimes Unit (TiO_2: 0.6-1.5 wt%; Zr: 50-200 ppm) [Alabaster et al., 1982; Lippard et al., 1986]. The UV1 and less-evolved lavas of the MV1 which are roughly plotted in the field of the most primitive V1 and sheeted dikes, and the Lasail Unit by the previous studies (Figure 1.6). Alabaster et al. [1982] also claimed that the origin of the Lasail Unit is seamount based on their sporadical distributions. Both the UV1 and the less-evolved flows in the MV1 were formed by off-ridge volcanism which is broadly regarded as a part of the mid-ocean ridge magmatism. We thus conclude that the Lasail Unit is a subunit of the V1, represented by the less-evolved MV1 and UV1 in the Wadi Fizh area, and is essentially generated as a part of the mid-ocean ridge volcanism.

The V2 lavas are also characterized by depleted compositions like the LV1 low-TiO_2 group. The V2 sequence is considered to be generated in an immature arc setting [Ishikawa et al., 2002], that makes the most outstanding difference of the V1 and V2 sequence. The presence of pyroclastic deposit interbedded with V2 lavas in Ghayth area 20 km south of the study area suggests more hydrous conditions for the V2 magma, in accordance with the arc setting [Umino et al., 1990]. The best indicator that discriminates the V1 from and V2 sequence is clinopyroxene chemistry [Alabaster et al., 1982; Umino et al., 1990; Adachi and Miyashita, 2003]. The V2 clinopyroxenes show lower incompatible elements than the V1 clinopyroxenes with Mg# <0.85 (Figure 8). Distinction of the V1 low-TiO_2 group and the V2 is less obvious for the bulk-rock chemistry, however, the V2 sequence is characterized by slightly lower Zr/Y and (Nd/Yb)n ratios than the V1 low-TiO_2 group (Figure 1.6). The low Zr/Y ratios indicate a more depleted source or a higher degree of partial melting for the V2 than the V1 low-TiO2 group. Furthermore, lower (Nd/Yb)n ratios of the V2 samples result in a crossing REE patterns for the V1 and V2 volcanics indicative of discrete sources for the V1 and V2 (Figures 1.7a and b).

1.7.2. The volcanism at a segment boundary

The bulk-rock compositions of the V1 sequence in Wadi Fizh show a larger compositional variation than the V1 unit from other areas by the previous studies [Alabaster et al., 1982; Lippard et al., 1986; Ernewein et al., 1988]. The sheeted dike complex of the Wadi Fizh area coincidentally exhibits the broadest compositional range in the northern Oman ophiolite [Miyashita et al., 2003]. In contrast, the sheeted dikes have less-evolved, limited compositions toward the segment center of the paleo-spreading axis at Wadi ath Thuqbah 25 km south of the study area [Umino et al., 2003]. Seismic experiments along the EPR and Galapagos Spreading Center have shown that melt lenses are small or absent below the segment ends due to lower supply rates of magma to the upper crust [Hooft et al., 1997; Blacic et al., 2004]. This suggests that primitive melts supplied from the lower crust have more chances to extrude without mixing with the evolved magmas in a shallow magma chamber which is consistent with the observed geochemical differences of the segment center and end in the northern Oman ophiolite [Miyashita et al., 2003]. Around the segment end, it might be more enhanced cooling by hydrothermal circulation [Morgan and Chen, 1993]. At the same time, evolved melts may extrude at the segment ends because cooler conditions promote fractional crystallization of shallow melt lenses than at the segment centers. Besides, dikes and flows derived from the adjacent ridge segment veiled a larger compositional variation to the segment boundary lavas. Eventually, the large compositional variation of the V1 extrusive sequence is consistent with the model of Adachi and Miyashita [2003] that the Wadi Fizh area corresponds to the leading edge of a propagating paleo-ridge segment. Infrequent axial eruptions were followed by relatively long repose periods for hydrothermal deposits to precipitate.

Off-axis volcanoes are more abondant in second- or third-order segment ends along the EPR [Schierer and Macdonald, 1995; White et al., 2006]. Generally, lavas erupted from off axial vents show a more diverse composition than those extruded from axial vents since the off-axial lavas may retain the signatures of the source mantle heterogeneity due to a lack of persistent crustal magma chambers, which are otherwise obscured by mixing of differentiated and replenished primitive melts and assimilation of crustal materials [Perfit et al., 1994; Sims et al., 2002; 2003; Hall and Sinton, 1996; Geshi et al., 2007]. The zigzag compositional profiles of the MV1 are in good agreement with the characteristics of such off-ridge volcanism as exemplified by the off-axis lavas at EPR 9°N [Perfit et al., 1994]. The UV1 is most likely generated by off-axis volcanism as indicated by the presence of the pillowed ridge with a fissure vent among the off-axial pahoehoe flows. The less-evolved compositions of the UV1 lavas also support this interpretation that lower supply rates of magma at the segment end promoted solidification of the crustal magma chamber, thereby allowing extrusions of less-evolved magmas from the deep crust and the mantle.

1.8. Conclusions

Temporal and spatial variations of extrusive layers from the ridge crest to off-ridge area were investigated in geological and geochemical terms along Wadi Fizh in the northern Oman ophiolite. A successive exposure of the V1 extrusive sequence is divided by a 0.4-m and 0.8-m thick metalliferous sedimentary layers into three subsequences: the lower V1 (LV1), the middle V1 (MV1) and the upper V1 (UV1).

The lowest part of the LV1 consisting of lobate sheet flows and bulbous pillow lavas formed on the flat ridge crest. The presence of elongate pillows at 230 mab represents a lithofacies emplaced on relatively steep slopes flanking the ridge. The LV1 is subdivided into two subsequences by a jasper layer at 270 mab. The stratigraphic variations of the lower subsequence (LV1a) show an evolved chemical compositional profile with a few less-evolved levels. Similar Zr/Y ratios through the most LV1 sequence indicate that the LV1 originated from the same source material. Lavas in the upper subsequence (LV1b) were emplaced at the foot of the ridge slope where the gentle skirts extend away from the ridge. The 130-m thick evolved compositions of the LV1b represent voluminous lava flows fed from the axial source.

Assuming a half-spreading and sedimentation rate to be 5-10 cm/a and 0.01 mm/a, respectively, the 260-m thick MV1 sequence was emplaced 2-4 km off the ridge axis. Predominance of lobate sheet and pahoehoe flows suggest that the MV1 flowed onto a subhorizontal off-axial seafloor. Wide compositional variations with a zigzag pattern represent juxtaposing magma sources beneath the paleo-spreading system, which differ in the degrees of partial melting and/or fractional crystallization. The zigzag profile of the MV1 sequence is explained by alternating flows erupted in-situ at off-axis vents and transported from axial vents. The fissure vent at 854 mab provides a direct evidence of in-situ off-axis volcanism for the UV1. Restricted depleted compositions of the UV1 lavas indicate that they were derived from discrete sources other than the axial magma.

The UV1 and less-evolved lavas of the MV1 can be correlated to the Lasail Unit based on the geological and petrological similarity. The Lasail Unit is considered to be a subunit of V1, which formed by off-ridge mid-ocean ridge volcanism. The V2 lavas can be discriminated by their lower bulk Zr/Y (Nd/Yb)n ratios and clinopyroxene compositions more depleted in TiO_2 and Na_2O than the V1 lavas.

Broad bulk-rock compositions of the V1 sequence are consistent with volcanism at a paleo-ridge segment end. At a segment end, both primitive and evolved magmas may extrude because of smaller size or absence of a melt lens due to colder upper crust than at the segment center. The V1 flows and the sheeted dikes in the Wadi Fizh area have similarly variable compositions expected for the cold upper crust at a segment end. The UV1 is the product of off-axis volcanism, like those around second- to third-order discontinuities along the present EPR.

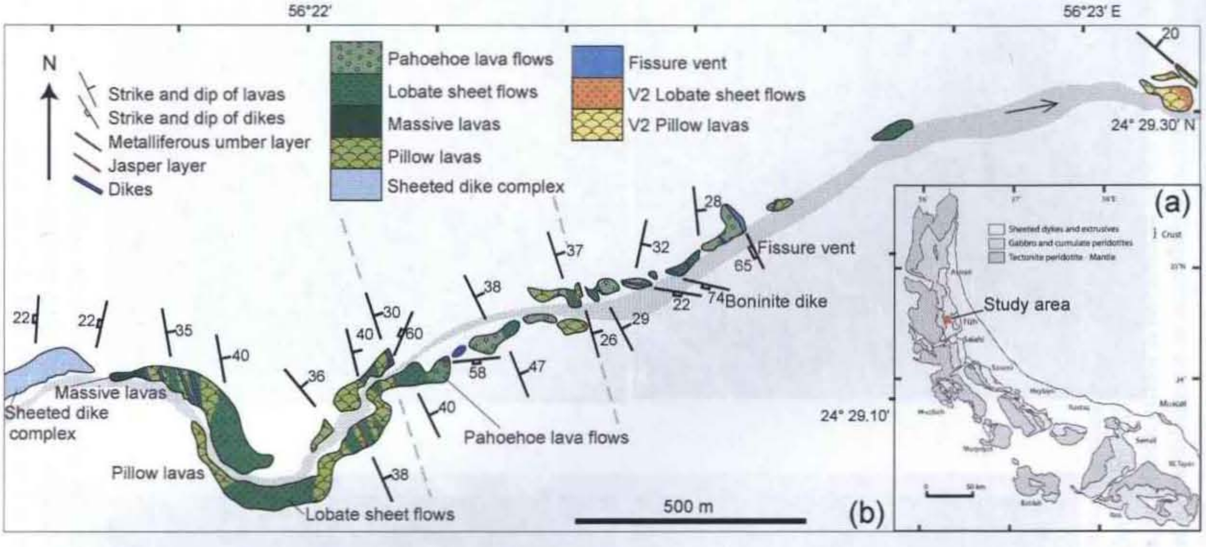

Figure 1.1 (a) Simplified geological map of Oman ophiolite after Lippard et al., [1986]. (b) Geological route map along the Wadi Fizh.

Figure 1.2 Representative lava morphology and lithofacies. (a) 0.4-m thick glossy metalliferous sedimentary layer at 410 mab dividing the LV1 and MV1 is traceable for as long as 3 km southward. (b) Bulbous pillow flows in the LV1 sequence (405 mab) just below the metalliferous sediment of (a). A 0.2-m thick dike intrudes into the flows and overlying MV1. (c) Elongate pillows at 230 mab in the LV1 showing subparallel alignment, indicative of flowage on a slope. (d) Pahoehoe flows in the UV1 at 735 mab. Pahoehoe lobes are 1 x 1.5-3 m wide and 0.1-0.3 m thick, with much smaller thickness/width ratios than pillow lobes.

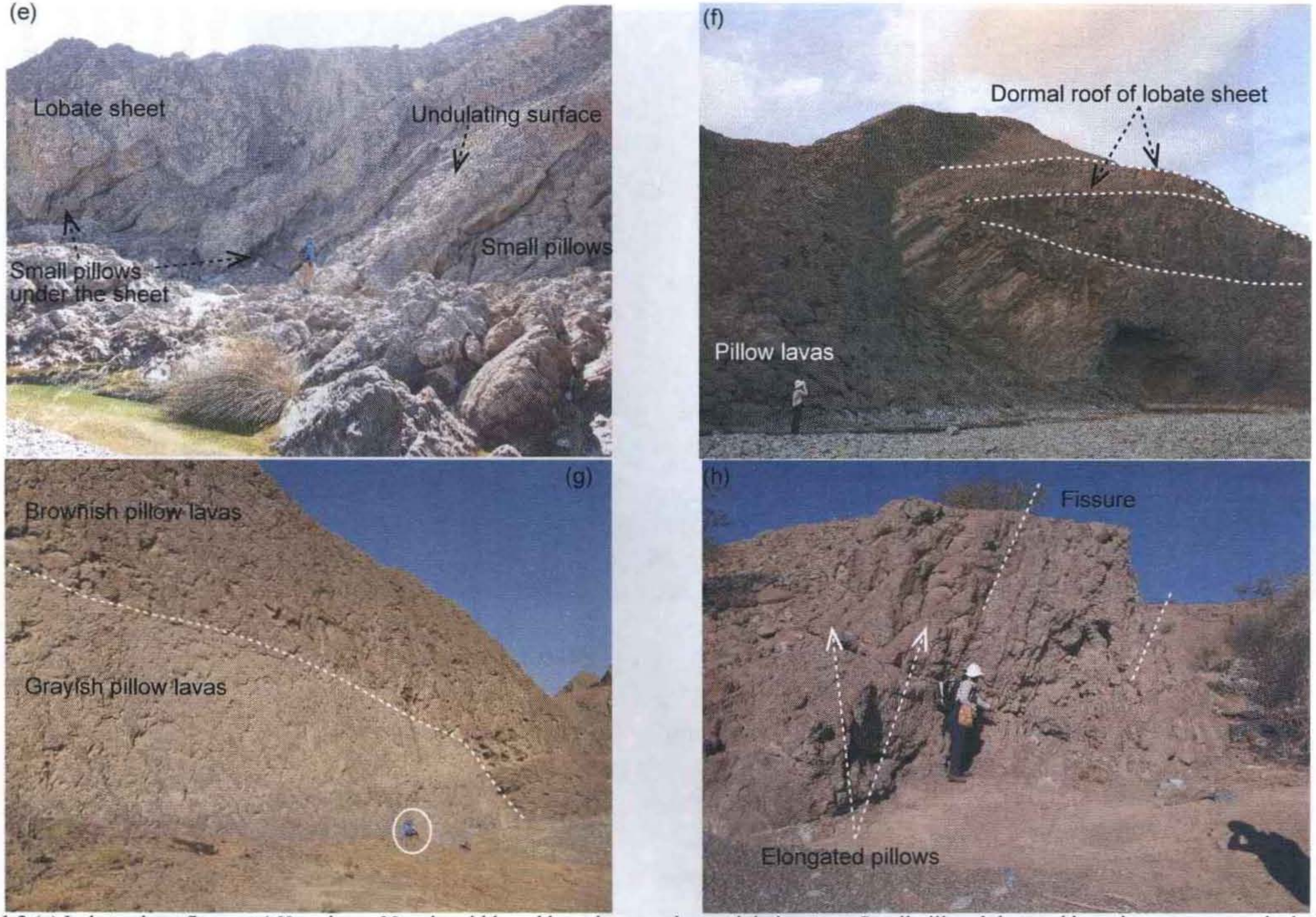

Figure 1.2 (e) Lobate sheet flows at 160 mab are 20 m in width and have hummocky, undulating tops. Small pillow lobes and breccias accompany the bottom of each flow lobe (dense and dark part). (f) Thick lobate sheet flow underlain by pillow lava at 350 mab. Columnar joints develop in the basal part of the sheet flow. Flow boundaries coincide with lithological boundaries in some cases. (g) Thick pillow lava flows in the LV1b. Sharp change in color indicates the flow unit boundary within the pillow lavas at 330 mab. Different colors are due to the difference in secondary mineralogy inherited from the different bulk compositions. The brownish pillows have evolved composition whereas the grayish pillows show less-evolved features (see the text). (h) Fissure vent at 854 mab. Note the overturned and elongated pillow lobes around the fissure.

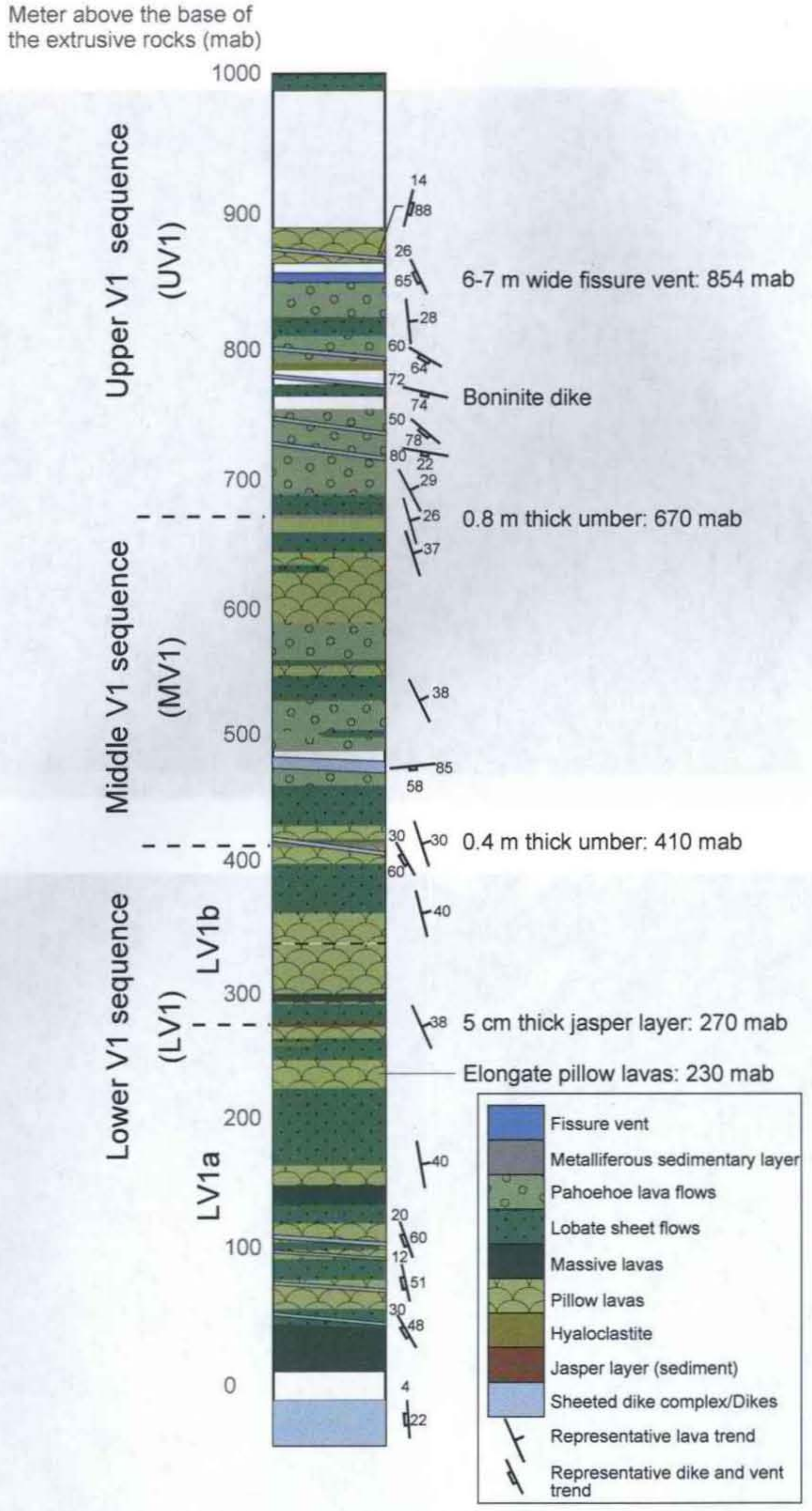

Figure 1.3 Stratigraphic column of the V1 sequence along Wadi Fizh. Broken lines indicate boundaries of each sequence.

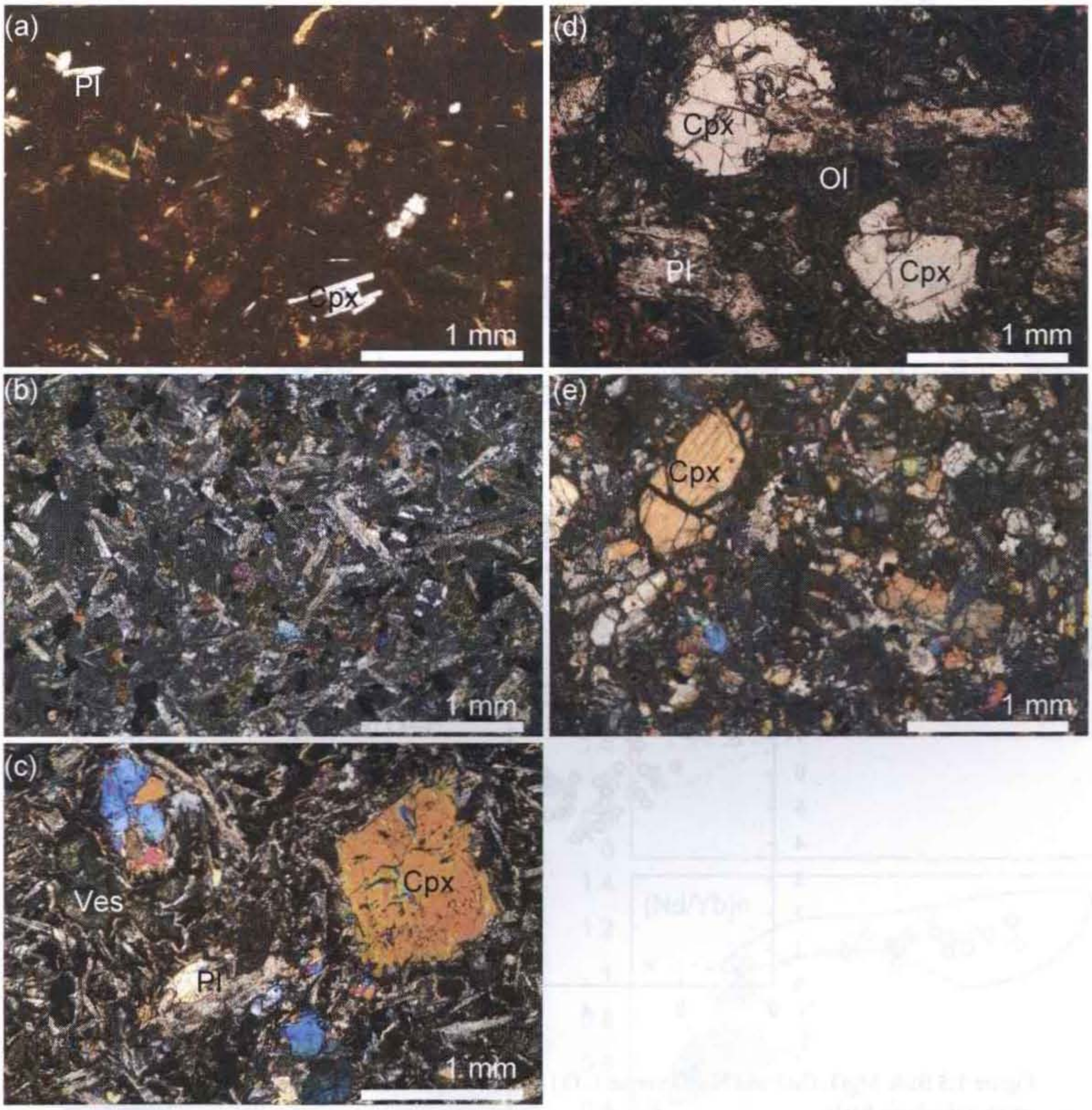

Figure 1.4 Microphotographs of flows and dikes. (a) Altered plagioclase and clinopyroxene microphenocrysts in the variolitic groundmass (LV1). (b) Aphyric lava with doleritic texture (LV1). (c) Plagioclase and clinopyroxene phenocrysts in a hyalo-ophitic matrix (MV1). (d) Olivine, plagioclase and clinopyroxene phenocrysts in a hyalo-ophitic matrix (UV1). (e) Clinopyroxene phenocrysts and clinopyroxene and orthopyroxene microphenocrysts in a boninite dike at 745 mab. Ol: olivine; Pl: plagioclase; Cpx: clinopyroxene; Ves: vesicle.

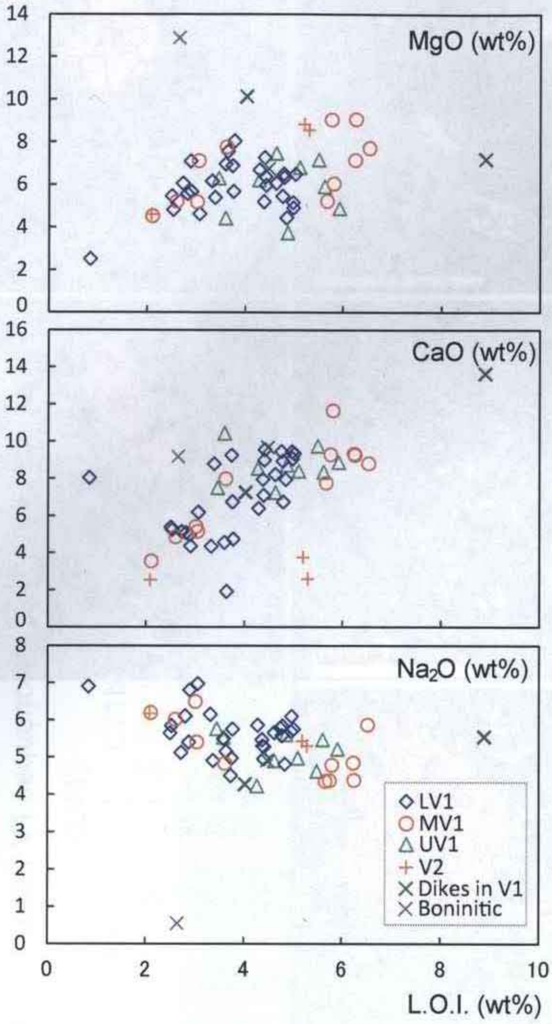

Figure 1.5 Bulk MgO, CaO and Na2O versus L.O.I (wt%). Major element compositions are recalculated on an anhydrous basis.

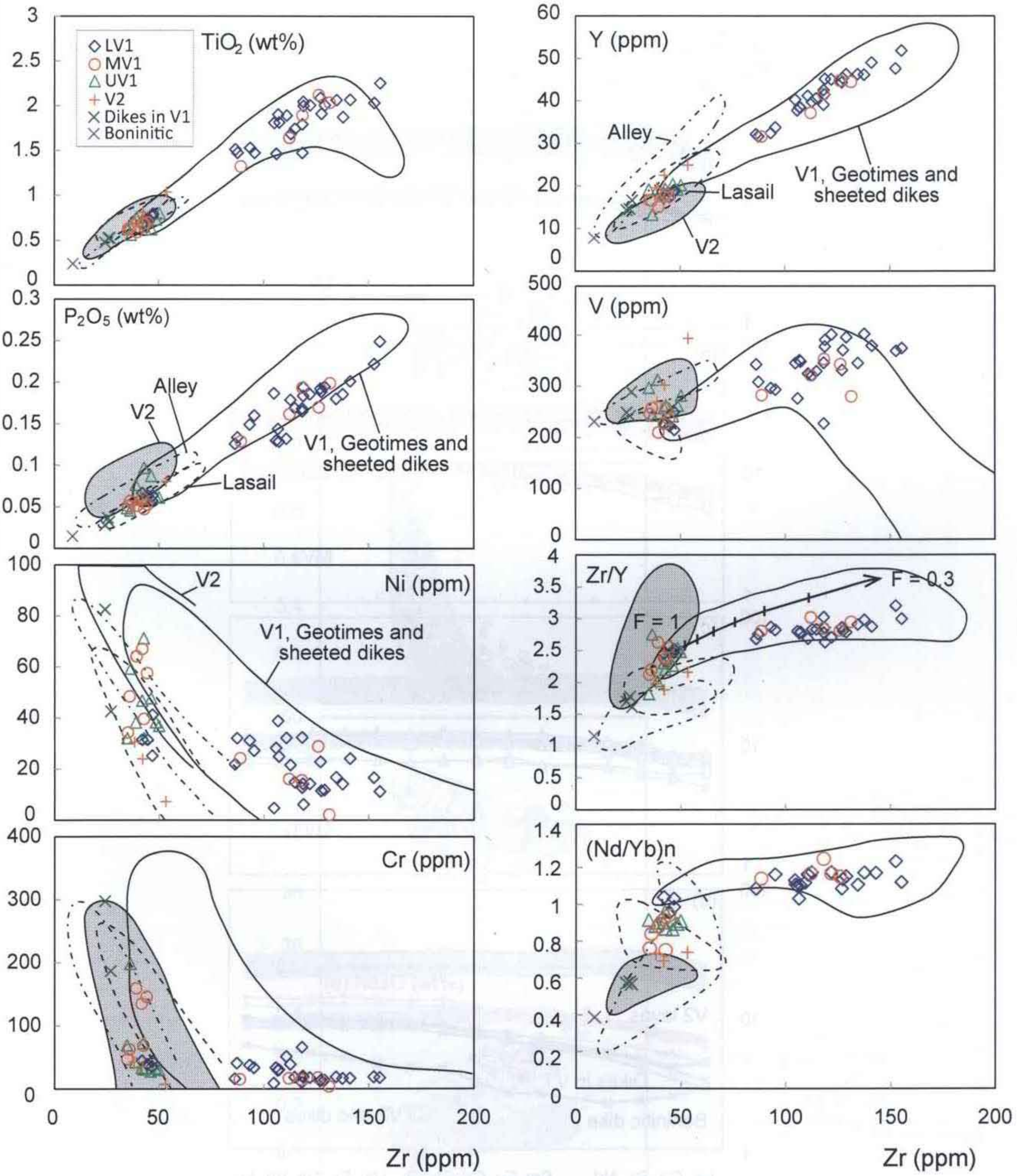

Figure 1.6 TiO2, P2O5, Ni, Cr, Y, V, Zr/Y and (Nd/Yb)n ratios plotted against Zr. TiO2 and P2O5 concentrations are recalculated on an anhydrous basis. High Ni and Cr samples are omitted. Open and shaded fields are lava compositions of previous studies; V1, Geotimes and sheeted dikes, and V2 field: A' Shaikh et al. [2005], Beurrier et al. [1989], Einaudi et al. [2003], Ernewein et al. [1988], Godard et al. [2003, 2006] and Miyashita et al. [2003]; Lasail and Alley field: Alabaster et al. [1982] and Lippard et al. [1986]. The fractionation trend in the Zr/Y plot is calculated from a parental magma corresponding to the less-evolved LV1 sample. Arrow shows fractionation F = ~0.3. Crystallization of olivine, clinopyroxene and plagioclase are assumed to be 10, 30 and 60, respectively, and partition coefficients are after Fujimaki et al. [1984].

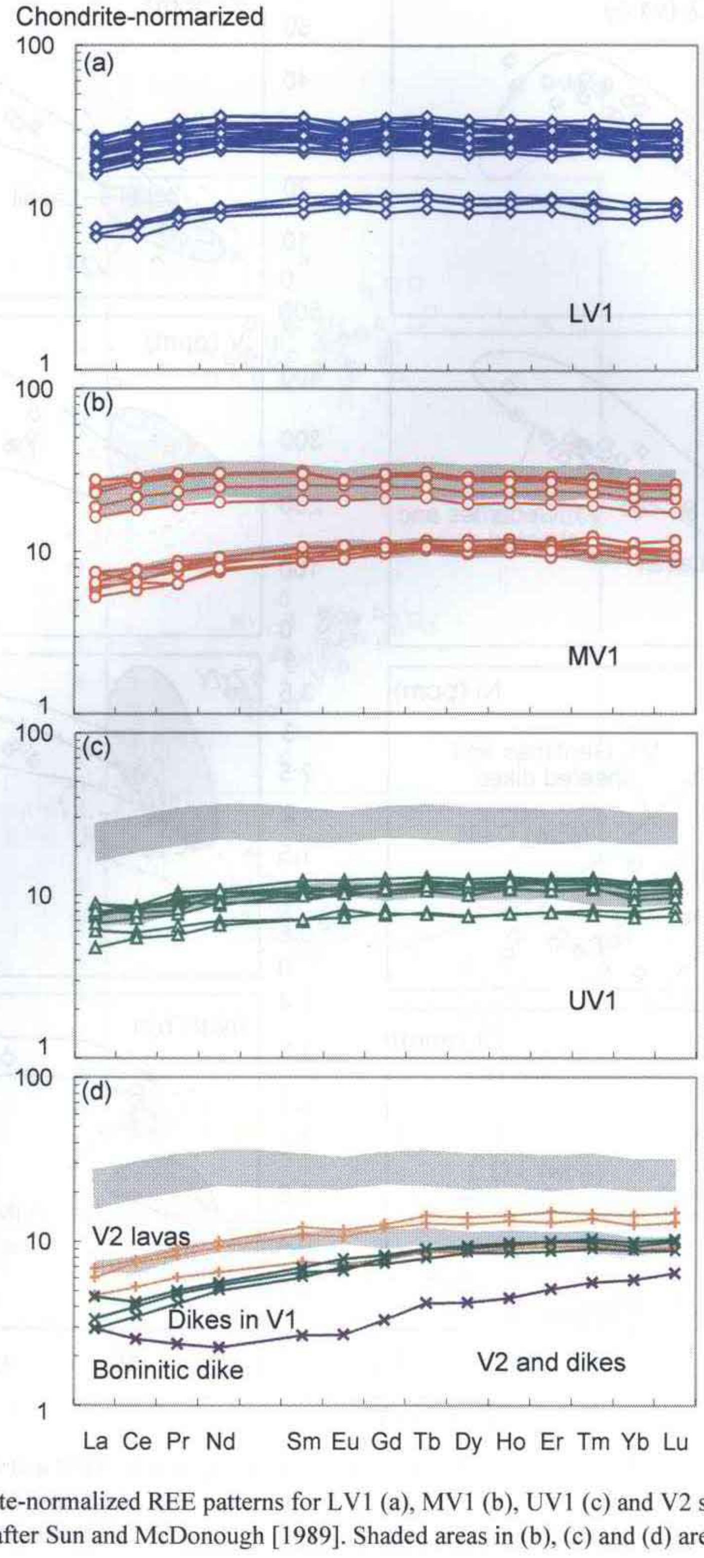

Figure 1.7 Chondrite-normalized REE patterns for LV1 (a), MV1 (b), UV1 (c) and V2 sequence (d). The chondrite value is after Sun and McDonough [1989]. Shaded areas in (b), (c) and (d) are ranges of LV1.

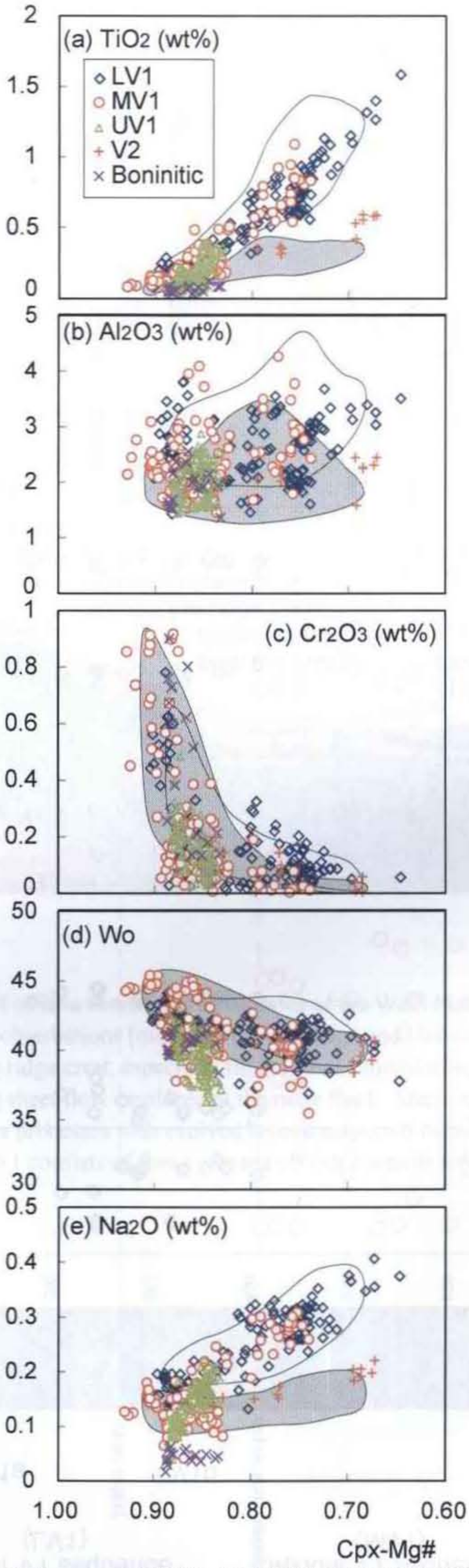

Figure 1.8 Clinopyroxexe Mg# versus (a) TiO2, (b) Al2O3, (c) Cr2O3, (d) Wo mol% and (e) Na2O. Open and shaded fields are lava compositions of V1 and V2 units from Alabaster et al. [1982], Einaudi et al. [2003] and A' Shaikh et al. [2005].

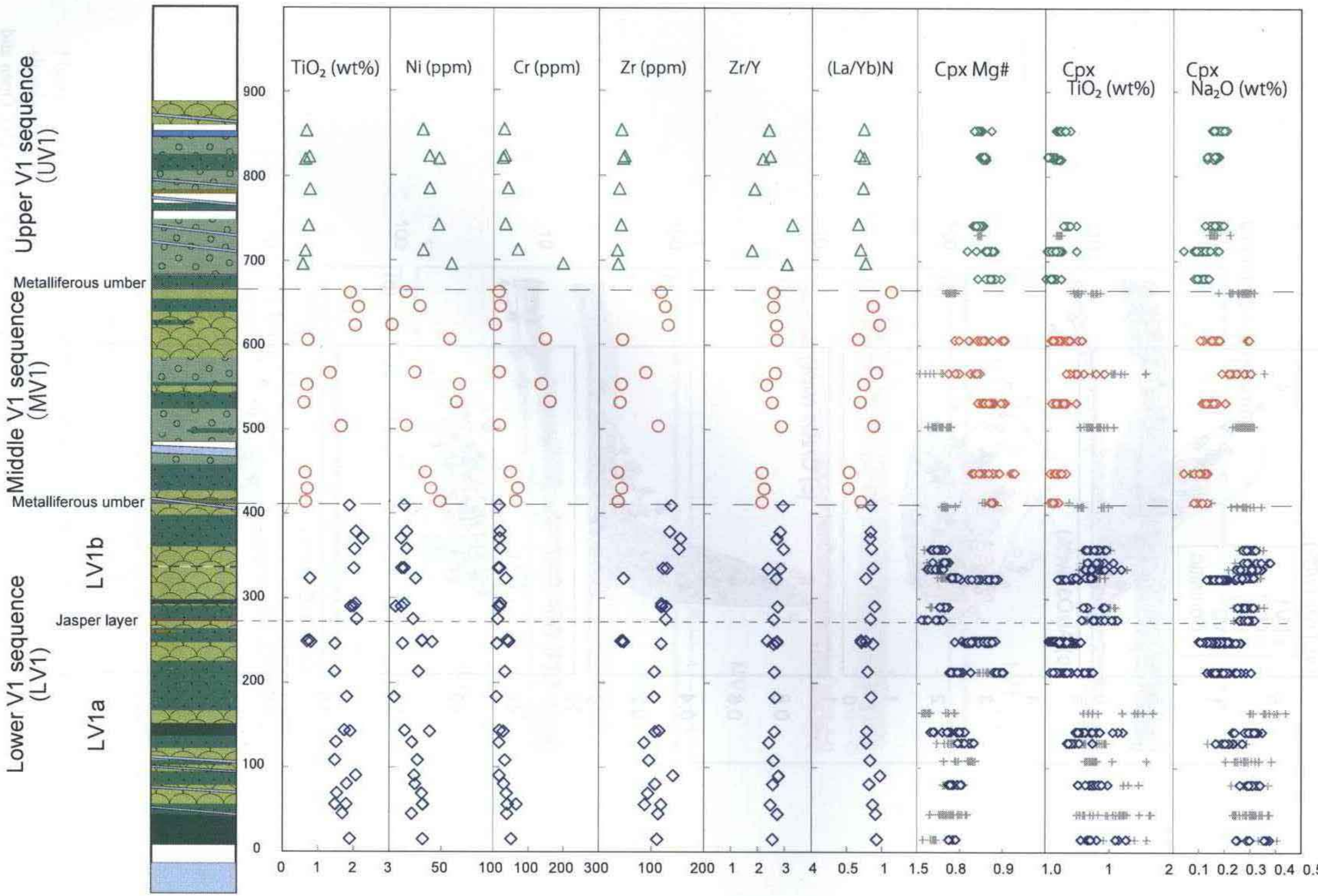

Figure 1.9 Stratigraphic variations of selected bulk-rock TiO2, Ni, Cr, Zr, Zr/Y, (La/Yb)n and clinopyroxene Mg#, TiO2 and Na2O. Grey crosses are sector zoned clinopyroxenes. See text for explanation.

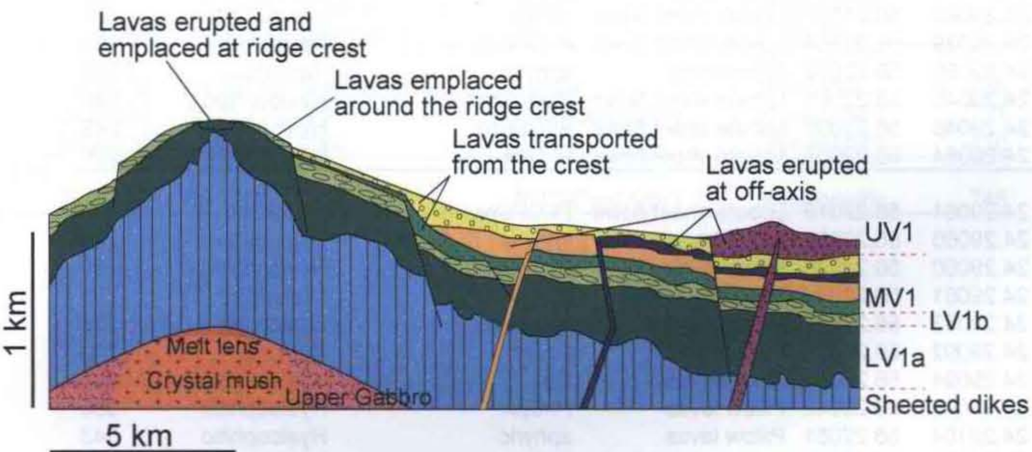

Figure 1.10 Schematic model of lava accretionary processes of the Wadi Fizh extrusive sequences based on the geological and geochemical obserbations [modified by Tominaga and Umino, 2010]. LV1a consists of flows erupted and emplaced on the ridge crest, especially fill the axial summit trough. The LV1b consisting of 20-m thick pillow lavas and lobate sheet flow emplaced at the ridge flank. After short period of quiescence, MV1 was emplaced via off-axis magma processes with evolved lavas transported from the ridge summit and less-evolved lavas erupted in-situ. The UV1 consists of flows erupted off ridge area to form off-ridge volcanoes.

Table 1.1 Locations, mode of occurrences and phenocryst assemblages of the Wadi Fizh lava flows and dikes. Pl: plagioclase; Ol: olivine; Cpx: clinopyroxene; Opx: orthopyroxene.

sample No.	Latitude	Longitude	Mode of occurrence	Mineral assemblages	Texture	mab
Lower V1 sequence						
LV1a						
07Fizh5	24.29118	56.21450	Massive lavas	aphyric	Doleritic	15
07Fizh6	24.29118	56.21478	Pillow lavas	Pl-Ol-Cpx	Variolitic	45
07Fizh7	24.29116	56.21484	Pillow lavas	aphyric	Intersertal	56
07Fizh8	24.29116	56.21484	Pillow lavas	Pl-Ol-Cpx	Intersertal	56
07Fizh9	24.29117	56.21492	Pillow lavas	Pl-Cpx	Hyaloophitic	69
07Fizh10	24.29117	56.21493	Dike	Pl-Cpx	Hyaloophitic	75
07Fizh11	24.29115	56.21495	Pillow lavas	Pl-Cpx	Variolitic	73
07Fizh12	24.29114	56.21498	Lobate sheet flows	aphyric	Hyaloophitic	80
07Fizh13	24.29109	56.21500	Lobate sheet flows	Pl	Hyaloophitic	90
07Fizh14	24.29108	56.21509	Pillow lavas	Pl	Variolitic	99
07Fizh15	24.29100	56.21514	Pillow lavas	Pl-Cpx	Variolitic	108
07Fizh16	24.29092	56.21526	Pillow lavas	Pl-Ol-Cpx	Variolitic	123
07Fizh17	24.29087	56.21532	Lobate sheet flows	aphyric	Intersertal	129
07Fizh18	24.29075	56.21533	Lobate sheet flows	Pl-Cpx	Variolitic	131
07Fizh19	24.29068	56.21535	Lobate sheet flows	aphyric	Intersertal	143
07Fizh20	24.29057	56.21534	Lobate sheet flows	Pl-Cpx	Intersertal	142
07Fizh21	24.29049	56.21542	Pillow lavas	aphyric	Intersertal	165
09vFizh1	24.29040	56.21567	Lobate sheet flows	aphyric	Intersertal	183
07Fizh22	24.29039	56.21584	Lobate sheet flows	Pl-Ol-Cpx	Intersertal	213
07Fizh23	24.29059	56.22000	Pillow lavas	aphyric	Variolitic	246
09vFizh2	24.29045	56.22006	Lobate sheet flows	Pl-Ol-Cpx	Hyaloophitic	248
09vFizh3	24.29046	56.22009	Lobate sheet flows	Pl-Ol-Cpx	Hyaloophitic	249
07Fizh24	24.29054	56.22006	Lobate sheet flows	Pl-Cpx	Intersertal	250
LV1b						
07Fizh26	24.29061	56.22018	Lobate sheet flows	Pl-Ol-Cpx	Intersertal	275
07Fizh27	24.29060	56.22028	Pillow lavas	aphyric	Hyaloophitic	290
07Fizh28	24.29060	56.22028	Pillow lavas	Pl-Cpx	Hyaloophitic	290
07Fizh29	24.29061	56.22033	Massive lavas	aphyric	Intersertal	293
07Fizh30	24.29083	56.22041	Pillow lavas	aphyric	Hyaloophitic	325
09vFizh4	24.29092	56.22030	Pillow lavas	Pl-Cpx	Variolitic	323
09vFizh5	24.29094	56.22038	Pillow lavas	Cpx	Hyaloophitic	335
07Fizh31	24.29095	56.22042	Pillow lavas	Pl-Cpx	Hyaloophitic	335
07Fizh32	24.29104	56.22051	Pillow lavas	aphyric	Hyaloophitic	343
07Fizh33	24.29109	56.22055	Lobate sheet flows	Pl-Cpx	Intersertal	358
07Fizh34	24.29116	56.22055	Lobate sheet flows	aphyric	Intersertal	370
07Fizh35	24.29123	56.22068	Lobate sheet flows	aphyric	Hyaloophitic	378
07Fizh36	24.29130	56.22074	Pillow lavas	aphyric	Variolitic	409
Middle V1 sequence						
07Fizh37	24.29132	56.22076	Lobate sheet flows	aphyric	Hyaloophitic	414
07Fizh38	24.29123	56.22081	Pillow lavas	aphyric	Hyaloophitic	416
07Fizh39	24.29123	56.22109	Lobate sheet flows	aphyric	Intersertal	430
07Fizh40	24.29122	56.22096	Lobate sheet flows	Pl-Cpx	Hyaloophitic	449
07Fizh41	24.29124	56.22100	Pillow lavas	aphyric	Hyaloophitic	467
07Fizh43	24.29140	56.22131	Pahoehoe flows	aphyric	Hyaloophitic	504
07Fizh44	24.29145	56.22143	Pahoehoe flows	Pl-Cpx	Hyaloophitic	516
07Fizh45	24.29149	56.22156	Lobate sheet flows	Pl-Cpx	Hyaloophitic	532
07Fizh46	24.29151	56.22162	Pillow lavas	Pl-Cpx	Variolitic	553
07Fizh47	24.29153	56.22171	Pahoehoe flows	Pl-Cpx	Hyaloophitic	567
07Fizh48	24.29155	56.22190	Pillow lavas	Pl-Cpx	Hyaloophitic	606
07Fizh49	24.29155	56.22203	Pillow lavas	aphyric	Hyaloophitic	623
07Fizh50	24.29170	56.22207	Lobate sheet flows	Pl-Cpx	Intersertal	645
07Fizh51	24.29174	56.22219	Pillow lavas	Pl-Cpx	Hyaloophitic	662

(Continued)

sampleNo.	Latitude	Longitude	Mode of occurrence	Mineral assemblages	Texture	mab
Upper V1 sequence						
07Fizh52	24.29174	56.22227	Lobate sheet flows	Pl-Ol(-Opx)	Intersertal	679
07Fizh53	24.29176	56.22233	Pahoehoe flows	Ol	Hyaloophitic	689
07Fizh54	24.29227	56.22191	Pillow lavas	Pl	Hyaloophitic	693
07Fizh55	24.29233	56.22196	Pillow lavas	Pl-Cpx	Variolitic	712
07Fizh56	24.29238	56.22206	Lobate sheet flows	Pl-Cpx	Hyaloophitic	742
08Fizh2	24.29185	56.22269	Pahoehoe flows	Pl	Hyaloophitic	731
09vFizh6	24.29182	56.22245	Pahoehoe flows	Pl-Ol-Cpx	Hyaloophitic	736
08Fizh3	24.29185	56.22277	Pahoehoe flows	Pl-Ol-Cpx	Variolitic	742
09vFizh7	24.29184	56.22283	Pahoehoe flows	Pl-Ol-Cpx	Hyaloophitic	753
08Fizh5	24.29202	56.22306	Hyaloclastites	Pl	Hyaloophitic	802
08Fizh6	24.29204	56.22313	Lobate sheet flows	Pl-Cpx	Hyaloophitic	820
08Fizh7	24.29206	56.22314	Lobate sheet flows	Pl-Ol-Cpx(-Opx)	Hyaloophitic	823
08Fizh8	24.29216	56.22332	Pillow lavas	Pl-Ol-Cpx	Hyaloophitic	854
09vFizh9	24.29246	56.22389	calcite vein host	aphyric	Intersertal	
V2 lavas						
08Fizh11	24.29318	56.23074	Massive lavas	Ol-Cpx	Hyaloophitic	
08Fizh13	24.29321	56.23072	Massive lavas	Pl-Ol-Cpx	Hyaloophitic	
08Fizh14	24.29317	56.23068	Massive lavas	aphyric	Hyaloophitic	
08Fizh15	24.29316	56.23066	Massive lavas	aphyric	Hyaloophitic	
08Fizh16	24.29314	56.23055	Pillow lavas	Pl	Variolitic	
Dikes						
07Fizh42	24.29132	56.22116	Massive lavas	Pl-Cpx	Intersertal	486
08Fizh1	24.29183	56.22259	Sill	Pl-Ol-Cpx(-Opx)	Hyaloophitic	731
08Fizh17	24.29130	56.22074	Dike	Ol	Hyaloophitic	410
Boninitic dike						
08Fizh4	24.29200	56.22302	Sill	Pl-Ol-Cpx(-Opx)	Hyaloophitic	745

Chapter 2

Along-axis variations of magmatism:

Implication from the V1 volcanic rocks in the northern Oman ophiolite

2.1. Introduction

Overlapping spreading centers and small offsets called 'devals' mark the boundaries of the magma supply systems [Langmuir et al., 1986] and they might be appeared as compositional variations between each segment. For example, mid-ocean-ridge basalts (MORBs) recovered from magmatically robust segments of the EPR (11°20'N and 9° 30'N) have relatively small geochemical variations whereas lavas from the magmatically 'starved' section at 10°30'N have a great range in composition, including evolved and less-evolved samples [Batiza et al., 1996]. They suggest that the differences are due to steady-state or non-steady-state behavior of magma chambers, respectively. On the other hand, digitized profiles around the ridge axis show deeper topography, narrower axial summit and deeper melt lens beneath the ridge axis in the segment margin than inflated segment center [Scheirer and Macdonald, 1993]. It indicates that magmatisms would be changed along a ridge axis. Also deeper crust around the segment margin may provide lower MgO contents responsible for the lower temperature of magma than the segment center. Seismic refraction profiles around segment center exhibit lower velocities of crustal section while higher velocities of upper crust due to abundant sheeted dike complex [Canales et al., 2003]. Therefore, it is suggested that robust and starved volcanisms are the end members and the volcanisms change gradually from the segment center to the end.

As described above (Chapter 1), the segment end (Wadi Fizh) might characterize the boundary of magma system. At the northern Oman ophiolite, sheeted dike complex shows geological and compositional variation along the segment [Umino et al., 2003; Miyashita et al., 2003]. According to their classification, the 70-km long segment is bounded at northern Wadi Fizh and southern Ahin as the second-order segment margin, and Wadi Bani Umar is recognized as the fourth-order segment margin (deval). The segment center is located around Wadi ath Thuqbah to Hayl. Thicker and finer dikes occur at the segment ends with wide compositional ranges than that of the segment center [Umino et al., 2003; Miyashita et al., 2003].

2.2. Geology

Our studied area extends about 70 km long from southern part of the Fizh block to the Hilti (or Salahi) block (Figure 2.1). Six wadis expose almost whole the V1 section and two wadis preserve lower to middle part of the V1 (lacking the V1 and V2 boundary) (Figure 2.2; Table 2.1). Extrusive sections strike NE-SW to NW-SE which depends on the seafloor topography or faulting after emplacement. Since Wadi ath Thuqbah, Bani Ghayth and Wadi Suhayli area are folded by anticline, total thickness of the V1 might be overestimated. But they show regional geological and geochemical variations enough to discuss. The northernmost Wadi Zabin is omitted in Figure 2.2 because it belongs to another segment and we need more survey.

2.2.1 Wadi Zabin

Because the segment boundary is presumed to be located between Wadi Zabin and Fizh, Wadi Zabin seems to be generated from another segment [Miyashita et al., 2003; Adachi and Miyashita, 2003]. The V1 sequence continuously exposes from sheeted dike complex however the EW-trending dike swarm intrudes into the crustal section [Ishikawa et al., 2002; Adachi and Miyashita, 2003]. The 1125-m thick V1 sequence trends N-S to NE-SW and dips 30° to 45° east. The lower part is characterized by the occurrence of pahoehoe lava flows, and the upper part preserves jointed lobate sheet flows.

2.2.2 Wadi Fizh

Detailed stratigraphy of the >900-m thick V1 sequence is discussed in the chapter 1. Approximately the 1200-m thick V1 sequence trends NW-SE and dips 25° to 40° east (Figure 2.3a). Lobate sheet flows occupy 44%, pillow lavas occupy 38%, pahoehoe flows occupy 10% and massive flows occupy 8% of the V1. Pillow lavas occur the lower part (LV1) and pahoehoe flows occur at upper part (MV1 and UV1). The 410-m thick LV1 and more than 500-m thick MV1+LV1 represent on-ridge and off-ridge volcanisms, respectively.

2.2.3 Wadi ath Thuqubah

Paleo segment center is reported around Wadi ath Thuqubah [Miyashita et al., 2003; Umino et al., 2003]. The transition zone between sheeted dike complex and V1 lavas, and the upper part of V1 sequence are preserved in this area, and the two constructions may contact with fault. The lowest part containing the transition zone trends NW-SE and dips 20°-30° NE, and crops out 130 m thick. The upper part trends NW-SE and dips 25°-45° NE, and exposes 315 m thick. Pahoehoe flows occupy 54% of the V1, massive flows have limited exposure and no pillow lava occurrences. Lobate sheet flows occur around the top of V1 in this area. 18-m thick metalliferous and pelagic sediments (Suhaylah Formation) have been overlying on the V1 with no visible erosions.

2.2.4 Bani Ghayth (near Wadi Jizi)

This area located at 2 km northward from Wadi Jizi and considered to be generated from the similar geologic setting to Wadi ath Thuqbah, the paleo segment center. But in more strictly, Ghayth area corresponds to a little southern part which lower crust and mantle section has been lost by obduction related deformation. The V1 trends N-S to NE-SW and dips 20°-30° east, the trends gradually change upward. The 890-m thick V1 is composed of 50% of pahoehoe, 30% of lobate sheet and 20% of massive flows (Figure 2.3b). The lower part is dominated in pahoehoe flows (Figure 2.3e), while the middle through upper part mainly consists of 5-20 m thick lava layers.

2.2.5 Wadi Yanbu

Wadi Yanbu has been located at northern part of Hilti block, 8 km southward from Wadi Jizi. The V1 exposes whole section from sheeted dike complex to the V2 lavas. Wadi Yanbu area occurs N-S trending and 20°-30° dipping to east. A 572-m thick section containing 60-m thick blank, is composed of 86% of pahoehoe, 13% of lobate sheet and 1% of massive flows. Thin jasper lenses and layers (<3 cm) commonly appear over 475 mab and rarely preserve ropy wrinkle of pahoehoe flows.

2.2.6 Wadi Salahi

5 km southward from Wadi Yanbu, Wadi Salahi area has 660-m thick V1 lavas. The V1 sequence between transition zone and the V2 is composed of 58% of pahoehoe, 32% of lobate sheet and 2% of massive flows. Pillow lavas occur at 332 mab and hyaloclastites are sometimes interlayered under the lobate sheet flows. The lower part of the V1 is dominated in pahoehoe flows. Three metalliferous umber layers occur above 640 mab, nearly the upper most V1.

2.2.7 Wadi Suhayli area (Suhayli N and Suhayli)

Two sections are observed in this area, 5 km (north branch of Suhayli; Suhayli N) and 7 km (along Wadi Suhayli) southward from Wadi Yanbu. Due to the existence of gentle anticline, this area trends NE-SW to E-W and dips SE to south at westward, and gradually change NE-SW trends at eastward. The Suhayli N section thickens 970 m^+ because it doesn't expose the transition zone, and the V1 and V2 boundary. Pahoehoe flows occupy 62%, lobate sheet and massive flow occupy13 and 14%, respectively. 11% of pillow lavas occur at 424 (77 m thick) and 625 mab (30 m thick). Between the 300 and 400 mab, NS-trending dikes intrude into the V1 lavas like a 'dike swarm'. Although Wadi Suhayli lacks the basement contact and has 110-m thick blank, 935-m thick V1 sequence is covered with the V2 sequence (see chapter 3 about the V2 extrusives in this area). 40% of pahoehoe and 56% of lobate sheet flows occur in Wadi Suhayli (Figure 2.3f). Pillow lavas occupying 2% of this area occur at 220 mab. The 'dike swarm' does not appear at this section, but a fissure vent is observed at 335 mab (Figure 2.3c).

2.2.8 Wadi Hilti

Location of this area is 8 km southward from Wadi Suhayli, and the southern tip of Hilti block. The V1 sequence overlying on the sheeted dike complex exposes 688-m thick sequence. The V1 and V2 boundary has been lacked in this area. NS-trending 'dike swarm' intrudes into the V1 at 220 mab as like as Suhayli N area (Figure 2.3d). Pahoehoe and lobate sheet flows occupy 44% and 38% of the V1, and 12% of pillows often occur in the lower part (Figure 2.3g and h).

2.3. Petrography

Based on abundance and assemblage of phenocrysts, the V1 volcanic rocks are divided into aphyric, Pl (plagioclase), Pl-Ol (olivine) -Cpx (clinopyroxene) and Pl-Cpx -phyric types. Hyaloophitic and intersertal textures are well observed in the groundmass and a variolitic texture commonly develops near the surface of pillows (Figure 2.4). Almost lava samples are 1-10 vol.% vesicular, dominated in lower than 5 vol.%. Lava samples underwent intensive low-temperature alterations. Most plagioclases are altered to albite, saussurite or calcite. Chlorite and clay minerals replace olivine phenocrysts. Even clinopyroxene has been locally replaced to epidote or calcite or clay minerals. Clinopyroxene occurs as discrete crystals or glomerocrysts. Summary of petrography is shown in Table 2.1.

Except for Wadi Fizh area, the V1 lava is characterized by aphyric basalts and sometimes contains a few phenocryst contents (rarely phyric: <2 vol.%). While the V1 basalts in Wadi Fizh area are often observed Pl-Cpx-phyric type attaining more than 20% phenocryst contents. Averaged minor axis length of phenocrysts both plagioclase and clinopyroxene (and olivine) is 0.55 mm in Wadi Fizh and 0.44 mm in Bani Ghayth.

2.4. Geochemical variations

2.4.1 Whole rock chemistry

Whole-rock major elements, Ni, Y, Zr, Cr and V contents of 207 samples were analyzed by XRF (RIX3000, Rigaku Denki) at Niigata University. The analytical method is described in Takahashi and Shuto [1997]. Other trace and rare earth elements of 173 samples were analyzed by ICP-MS (Agilent 7500a ICP-MS) after Roser et al. [2000] at Niigata University.

The results of major and trace element analyses are given in Appendix Table 1 and 2.

The V1 lavas show huge and continuous Zr variation ranging from 24 to 208 ppm. Zr-variation diagrams with TiO_2, Ni, Cr, Y, V and Zr/Y ratios of the V1 samples are shown in Figure 2.5. Incompatible elements increase and compatible element contents rapidly decrease with increasing Zr contents. TiO_2 and V contents of some samples decrease with increasing Zr contents at more than 150 ppm. The decreasing trend is generally caused by fractional crystallization of Fe-Ti oxide minerals. Y content positively correlates with Zr content. The V1 lavas show less compatible element content (Ni: less than 50 ppm; Cr: less than 30 ppm). High-Zr content samples (more than 90 ppm) have 1.0-1.4 in (Nd/Yb)n ratios and slightly increase with increasing Zr content (Figure 2.6). While low-Zr (less than 90 ppm) samples have 0.5-1.0 in (Nd/Yb)n ratios and rapidly increase with increasing Zr content. Nb/Ta ratios of the V1 lavas range from 12 to 17.

Volcanic rocks have generally wide compositional range of each area, but degrees of fractional crystallization are different. The segment margin areas of Wadi Zabin, Wadi Fizh and Wadi Hilti exhibit wide Zr contents ranging from 51 to 203, 27 to 155 and 47 to 189 ppm. The segment center area of Wadi ath Thuqbah shows tight compositional range from 44 to 127 ppm in Zr content. Bani Ghayth, near the segment center area shows similar compositional range to Wadi Fizh. The reason why Bani Ghayth lavas show large compositional range will be discussed later. Intermediate area of Wadi Yanbu and Wadi Salahi also exhibits wide range of Zr contents. Other incompatible elements show similar compositional range to Zr contents except for Wadi Zabin showing slightly narrow range in TiO_2 contents. Wadi Fizh, Wadi ath Thuqubah and Bani Ghayth belonging to northern part of study area contain low incompatible and high compatible element samples than the southern part (Wadi Yanbu, Wadi Salahi and Wadi Hilti). It is noted that Wadi Hilti samples have high Y content and low Zr/Y ratio at a given Zr content (Figure 2.5).

2.4.2 Clinopyroxene chemistry

Clinopyroxene phenocrysts and microphenocrysts in 55 samples were analyzed by EPMA (JEOL JXA-8600SX) in Niigata University. The accelerating voltage was 15 kV, beam current was 1.3x10-8 A, and peak intensity was counted for 30 seconds. Correction procedures followed ZAF-Oxide method. Representative clinopyroxene analyses are given in Appendix Table 3.

Mg# (Mg#=Mg/(Mg+Fe*) where Fe* is total Fe as FeO) of V1 clinopyroxenes ranges from 0.62 to 0.93, which is comparable to or more varied than the previous reports for volcanic rocks from the Oman ophiolite [Alabaster et al., 1982; Ernewein et al., 1988; Umino et al., 1990; Einaudi et al., 2003; A'Shaikh et al., 2005]. This is consistent with the wide Zr range of bulk rock compositions in this area as described above. Clinopyroxene Mg#-variation diagrams show negative correlation with TiO_2 and Na_2O, and positive correlation with Cr_2O_3 and Wo (=Ca/(Ca+Mg+Fe)) contents (Figure 2.7). Some clinopyroxene analysis showing low Mg# and incompatible element contents are responsible for crystallization of Fe-Ti oxide minerals as like as whole rock Zr-variation diagrams.

Clinopyroxenes of Wadi Fizh have the widest Mg# range from 0.93 to 0.65. While clinopyroxene Mg# of Wadi Zabin, another side of the segment end, ranges from 0.81 to 0.62 and shows oxide minaral crystallization trend in TiO_2-Zr diagram. The lines of evidence indicate more evolved feature of Zabin than Fizh. Bani Ghayth belonging to the segment center area shows wide Mg# ranging from 0.91 to 0.67 and decreasing TiO_2 and Na_2O contents at Mg# <0.75. Clinopyroxenes of Ghayth lavas seem to exhibit lower incompatible and compatible elements than that of Fizh. Intermediate area (Wadi Yanbu) shows slightly tight range of Mg# (= 0.89-0.69) and higher incompatible and compatible element contents than the segment center and end. Wadi Hilti, shows more tight Mg# ranging from 0.88 to 0.72 and higher incompatible and compatible element contents attaining to Wadi Fizh. And more, Hilti samples contain higher Na_2O than Wadi Fizh at a given clinopyroxene Mg#. These compositional variations imply that the difference of melting degrees between areas.

2.5. Discussion

2.5.1 Integration of along-axis variation

Geology and Petrology of the extrusives have given us a lot of information about generation processes. First, I integrate all analyses and discuss regional variations from the view of along-axis variation. Representative features of each section are shown in Table 2.2.

The thickness of V1 lava sequence is approximately 1000 m in the studied sections. Both the segment margin (Wadi Fizh) and center (Bani Ghayth) having 1200-m thick V1 sequence suggest that the total amount of lavas is almost fixed at around ridges. However Wadi Yanbu and Salahi having 572 m and 660 m thick show very thin lava sequence against 1000-m thick V1. It is assumed that the thickness of layer 2 (volcanic and sheeted dike complex) is almost constant in the seismic structure under the fast spreading ridge [Scheirer et al., 1998] so that the sheeted dike complex might balance the layer 2 thickness. Actually, the sheeted dike complex in this area is estimated thicker than other area [Ministry of Petroleum and Minerals, 1992]. This may be the reason that the occurrence of relatively thin V1 lavas although it needs to more detailed field surveys.

At Wadi Fizh, it is revealed that the on- and off-axis lavas are contained in the V1 sequence (see chapter 1). Off-axis magmatisms in the EPR occur wherever along the ridge axis with biased around the second- and third-order segment ends [Scheirer and Macdonald, 1995; White et al., 2006]. If the segment structure controls the mantle processes and magma system, we could trace the systematic sign along a segment. The criteria of on- and off-axis settings is the occurrence of pillow lavas and metalliferous sedimentary layer, but pillow lavas have few appearance at relatively flat seafloor and metalliferous layer frequently occurs around ore deposits. Bani Ghayth shows both these characteristics. It is assumed that the occurrence of the lowest metalliferous umber near the turning point of lithology between pahoehoe and lobate sheet flows mark off ridge setting at Bani Ghayth, on-ridge lavas attain 603 m, which is 1.5 times thicker than Wadi Fizh (410 m thick). Wadi Yanbu also has no exposure of pillow lavas and pahoehoe flows are dominated throughout the V1 sequence. Since Metalliferous umber just occurs at the V1-V2 boundary, there is little magmatism at off ridge or marked by the lowest jasper layer at 474 mab.

Wadi Salahi, Suhayli N, Suhayli and Hilti preserve the pillow lava layers and the estimation of on-axis lavas are 352 m, 380 m, 205 m and 350 m thick, respectively. Suhayli shows thin on-axis layer than Fizh consisting of 230 m thick. It might be caused by under estimation in Suhayli due to faulted boundary between sheeted dike complex and extrusives. These four areas intercalate few jasper layer or lens and it is difficult to compare the on-ridge lavas with other area. However, the occurrence of tumulus and fissure vent in Suhayli and NS-trending 'dike swarm' intruding into the V1 in Suhayli N and Hilti is the evidence of off-axis magmatisms in these areas.

Thickness of on-axis lava layer is a simple indication of magmatic activity. As compare the thickness of on-axis lavas, Bani Ghayth located at near the second-order segment center produces thick on-ridge lava layer. Comparing the lava sequences of Ghayth with that of Fizh, the amount of on-ridge lava may decrease toward the segment end. According to the hypothesis, the 205 m-thick on-axis lavas in Suhayli might be correspond to a small scale of segment end. The higher pillow lava ratios support relatively steep topography in Suhayli and

Hilti as like as Fizh (Figure 2.2). Simultaneously, it is suggested that active off-ridge volcanisms occur at these segment end because almost sections have approximately 1000 m V1 thickness.

Petrography of each section shows slightly different character between on- and off-ridge sequences. The lower parts belonging to the on-ridge lavas exhibit aphyric and a few phenocryst contents (Table 2.1) while the upper parts formed at off-ridge settings contain more abundant phenocrysts than the lower parts in every areas. For example, the LV1 of Wadi Fizh is dominated in aphyric lavas. Because the phenocrysts are considered to be crystallized in crustal section, a few phenocryst contents indicate higher temperature and shorter stagnant time in the axial magma chamber (AMC) than off-ridge conditions. Averaged phenocryst size of Fizh lavas is 1.25 times bigger than that of Ghayth lavas. It implies that the segment ends may have cooler condition than the center. Thuqbah preserving basement and off-ridge section shows few phenocryst contents supporting the most active and large AMC around the segment center.

2.5.2. Petrogenesis of the V1 lavas with reference to along-axis variations

Regional geochemical variations in this area are shown as bulk-rock Ni, Cr, Zr, Y, TiO_2, Yb and Nb/Ta histograms (Figure 2.8). Except for Fizh and Ghayth, bulk-rock analyses of each area show unimodal variation meaning comparatively homogenized compositions. Especially Thuqbah shows narrow ranges and comparatively mildly-evolved features in all elements. In Yanbu, Salahi and Hilti, lavas show similar evolved distributions, and Salahi shows slightly mildly-evolved features in the three areas. Although Yanbu has highly evolved samples, it may be caused by biased analyses below the umber layer showing most evolved feature. The bimodal distribution of Fizh has been formed due to on- and off-ridge magmatism at the segment end. Because less-evolved peaks are occupied by off-ridge samples, on-axis lavas in the segment end might be characterized by evolved features. However several less-evolved samples appear in on-axis sequence responsible for cooler circumstance or mantle heterogeneity at the segment ends. Comparison of geochemical distributions of studied areas indicates that the lava compositions change systematically along the segment. The segment margin (Fizh) shows evolved feature while the segment center (Thuqbah) shows mildly-evolved and narrow variations, therefore, the compositions gradually change from the segment centers to the ends. Applying the hypothesis, slightly mildly-evolved feature in Salahi implies the correspondence to the third- or fourth-order segment center. The third or fourth order of segment has been separated at around Suhayli, as shown by the geological feature. The along-axis variation in bulk-rock Zr compositions would be able to apply the composition of sheeted dike complex of Miyashita et al. [2003]. Sample localities are slightly different but they show systematically change from the segment margin to the center as like as V1 sequence in this study (Figure 2.9).

Zr-distribution histogram of Ghayth samples exhibits bimodal variation similar to Fizh despite located around the segment center. Many off-ridge lavas are observed around the segment margin and also at the segment center in the EPR [Scheirer and Macdonald, 1995]. For example, the superfluous melt in the AMC after segmentation in Wadi Bani Umar al Gharbi, 8 km northwest from Ghayth [Umino et al., 2003], would be available to erupt at off ridge of the segment center area. However, this area belongs to the upper nappe in the ophiolite complex, so that the upper volcanic sequence of Ghayth might preserve later volcanism than other studied areas traceable to lower crustal section.

Zabin shows unimodal distribution in Zr histogram both the V1 lavas of this study and the sheeted dike complex [Miyashita et al., 2003] (Figure 2.9). Clinopyroxene compositions of Zabin lavas also show highly fractionated features different from other areas (Figure 2.7). These highly evolved melts may be derived from fractional crystallization within the more closed system melt lens. This area is proposed that another side of Fizh corresponding to the segment margin [Adachi and Miyashita, 2003]. Propagating-side Fizh has been characterized by bimodal Zr distribution with evolved and less-evolved lavas and less-evolved lavas are dominated in off ridge (see chapter 1). Therefore, we conclude that withdrawing-side Zabin may not be concentrated magma and be resulted in few less-evolved lavas or off-ridge volcanism.

Clinopyroxene compositions show large Mg# and major element content variations. At a given Mg#, Ghayth clinopyroxenes show lower TiO_2 and Na_2O concentrations than that of Fizh (Figure 2.7). Difference of these contents is due to various melting degrees of melt which equilibrium with these clinopyroxene. Lower concentrations in Ghayth lavas suggest that these melts have been experienced higher degree of melting before crystalize clinopyroxenes than that of Fizh locating the segment margin. Clinopyroxenes of Hilti lavas belonging to the opposite segment tip of Fizh, are plotted at higher TiO_2 and Na_2O concentrations than Fizh. Therefore, Hilti extrusive section might be derived from lower degree of melting. Their low Zr/Y ratios in whole rock composition well correspond to the evidence of clinopyroxene. Lower Mg# clinopyroxenes (less than 0.8) of Yanbu as intermediate area are plotted between

Ghayth and Fizh, while higher Mg# clinopyroxenes (more than 0.8) has similar concentration to Hilti. Actually, high Mg# clinopyroxene phenocrysts are derived from upper sequence of Yanbu (Figures 2.4q and r), should be reflect off-ridge volcanisms. In sum up with melting degrees considered from clinopyroxene compositions, the degree of melting gradually increases from the segment margin to the center.

2.6. Conclusions

Comparing eight sections spanning 70 km, the along-axis volcanic system is reconstructed. It is proposed that Wadi Fizh and Hilti correspond to the second-order segment margins and Wadi ath Thuqbah corresponds to the second-order segment center, supported by geology and petrology of the sheeted dike complex and gabbros. Further, this study proposes that Wadi Salahi correlates to the third- or fourth-order segment center and Wadi Suhayli correlates to the third-order segment margin.

The thickness of on-axis lava decreases from the center to the margin of the ridge segment. Appearance of pillow lavas around the segment margins indicates that more ragged seafloor topography than that of the center where pahoehoe flows are dominated. Their lava compositions are also varied systematically. Homogenized mildly-evolved lavas characterize the segment center. The larger melt lens and the higher ability of melt concentration below the segment center would produce the thick and homogenized lava sequence. On the other hand, both evolved and less-evolved lavas showing lower degrees of partial melting occur in the segment margins. Smaller melt lenses would promote highly evolved and less-evolved lavas.

Vigorous off-axis volcanisms are recognized around the second- and third-order segment margins. They might be rooted at less-evolved melt avoiding the focus on the axis area and converse the thickness of ocean floor lava layer.

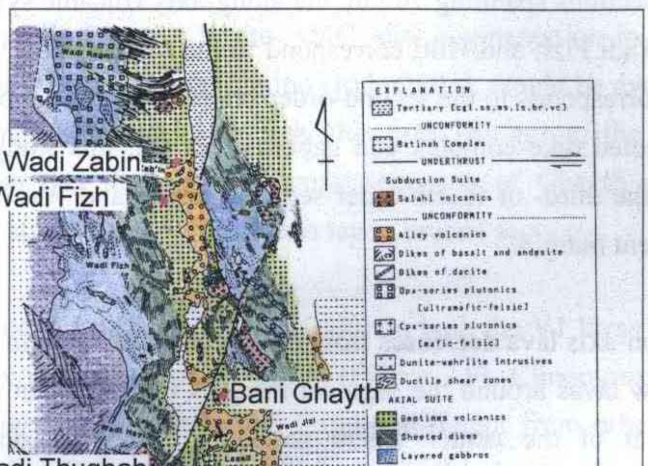

Figure 2.1 Geologic map of the northern Oman ophiolite after Umino et al. (1990). Studied sections are shown in.

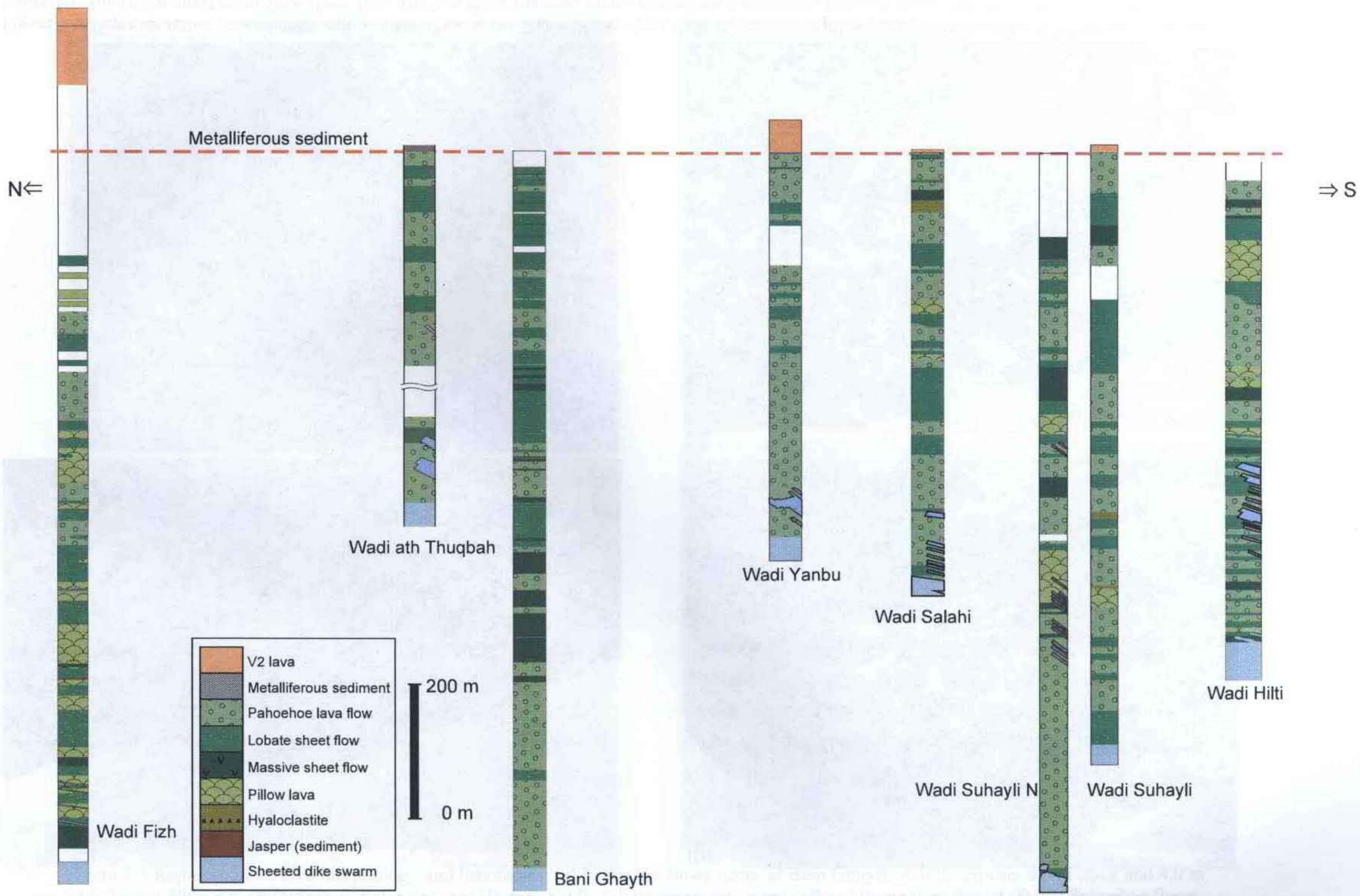

Figure 2.2 Columnar sections of V1 lavas between Wadi Fizh area and Wadi Ahin area. Red horizontal line shows V1-V2 boundary (metalliferous umber). Thickness of V1 is variable along the segment structure; thicken in segment boundary by active off-axis volcanism (Wadi Fizh, Wadi Suhayli) and segment center by active on-ridge volcanism (around Bani Ghayth). V1 lavas are composed of frequently pahoehoe flows although pillow lavas are predominant around the segment boundary.

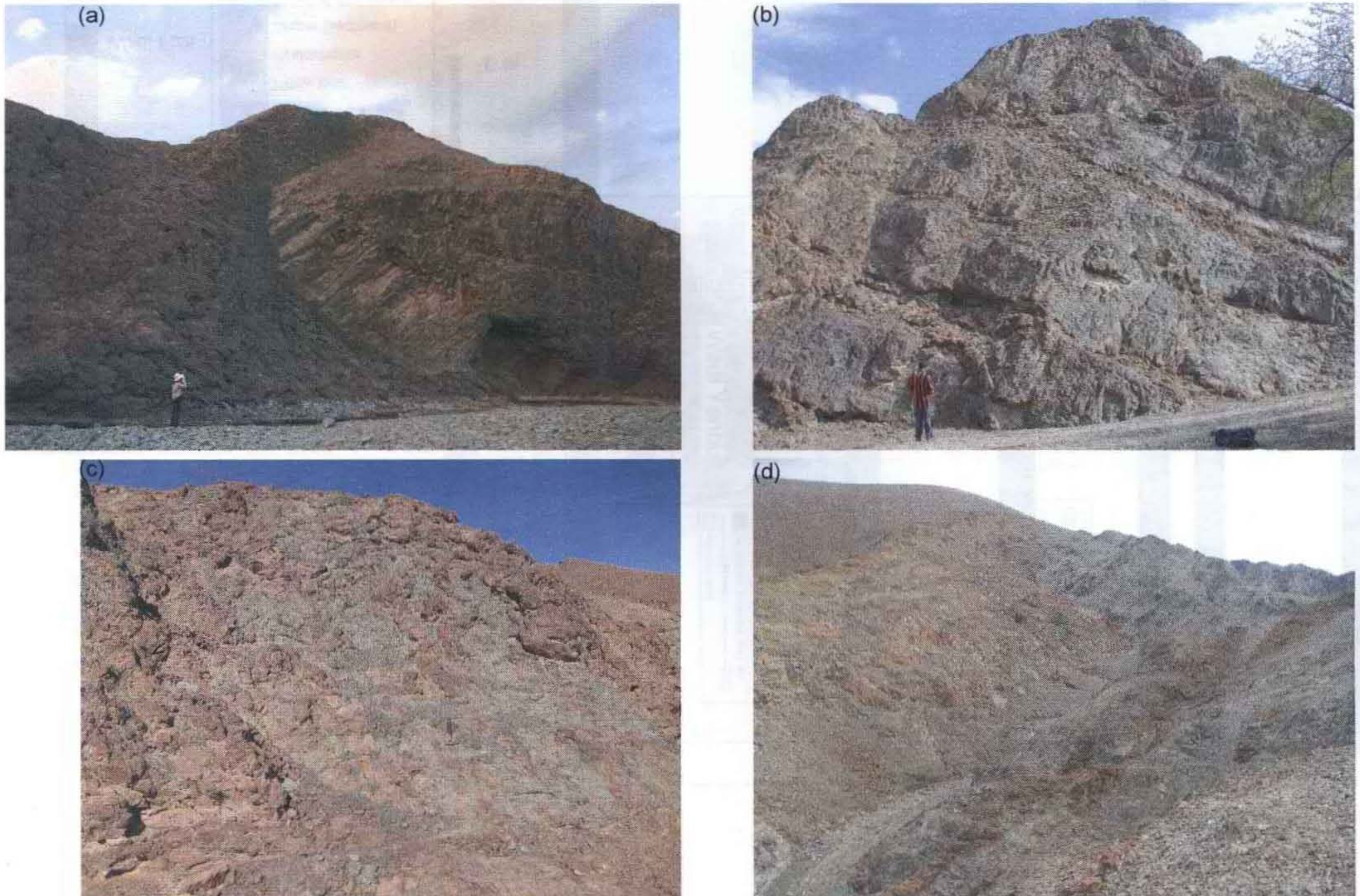

Figure 2.3 Representative lava morphology and lithofacies. (a) Thick lobate sheet flow underlain by pillow lava at 350 mab in Wadi Fizh. Columnar joints develop in the basal part of the sheet flow. (b) 2-m thick massive lavas intercalating pahoehoe flows in Bani Ghayth. (c) Fissure vent occurs in Wadi Suhayli. The 5 m vent is filled with fragmented lavas. (d) Dike swarm appears in the V1 sequence in Wadi Hilti. Host pahoehoe and lobate sheet flows are intruded by NS-trending dikes.

Figure 2.3 Representative lava morphology and lithofacies. (e) Pahoehoe flows occur at Bani Ghayth. A lobe appears 0.3 m thick and 4.0 m wide lens at 300 mab. (f) Pahoehoe flows occur at Wadi Suhayli. A lobe represents more inflated thong than that of (f). (g) Pahoehoe flows occur at Wadi Hilti. Thick blocky crust only remains the line of lobe edges. (h) Appearance of pillow lava at Wadi Hilti. Radial joints and elongate tubes characterize the mode of occurrence.

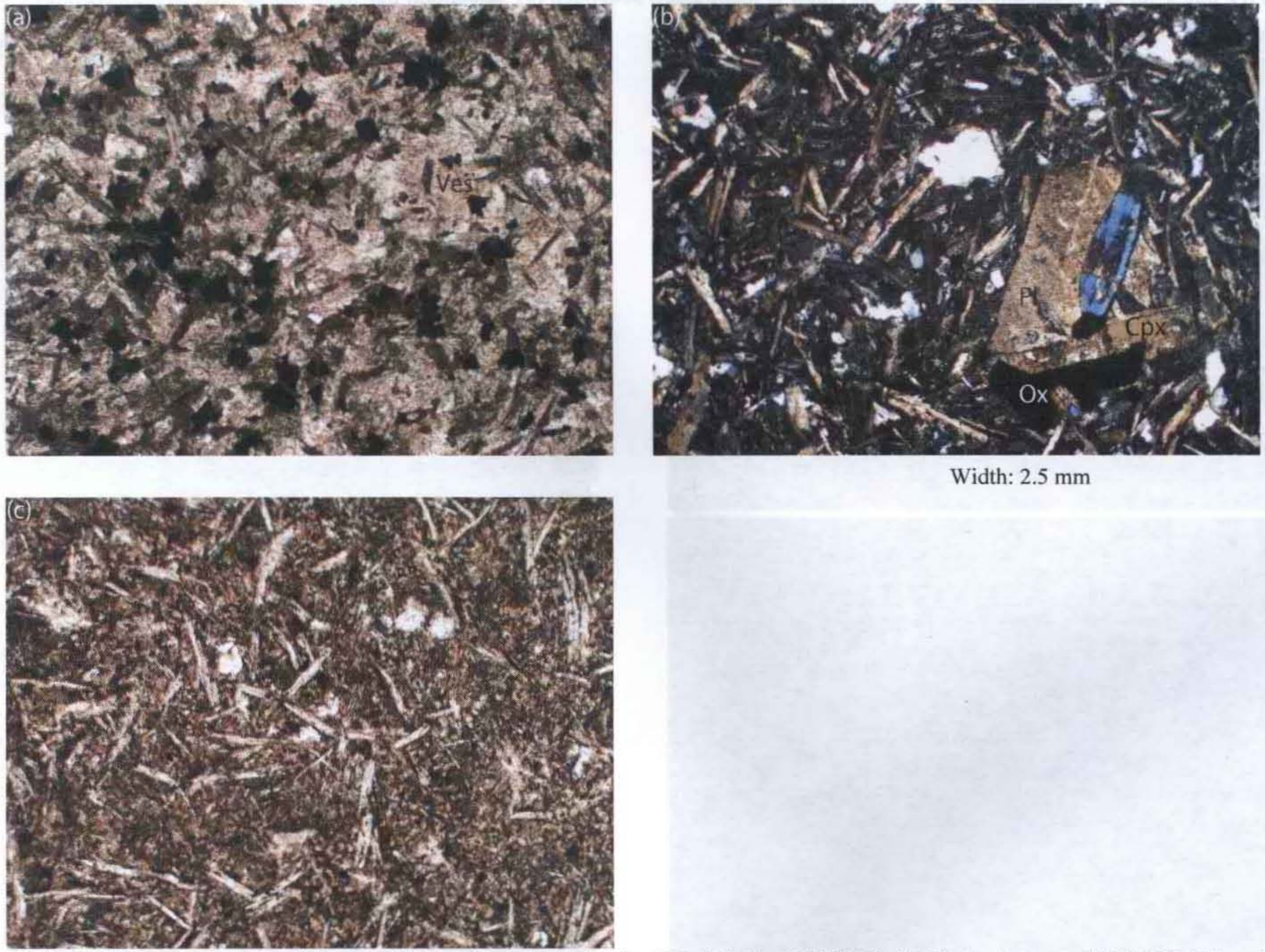

Figure 2.4 Microphotographs of flows and dikes. (a) Aphyric basalt of Wadi Zabin (08ZbN21). (b) Pl-phyric type of 08ZbN50. Microphenocryst of clinopyroxene and Fe-Ti oxide minerals occur. (c) Aphyric type of 09ZbN54. Ol: olivine; Pl: plagioclase; Cpx: clinopyroxene; Ox: oxide mineral; Ves: vesicle.

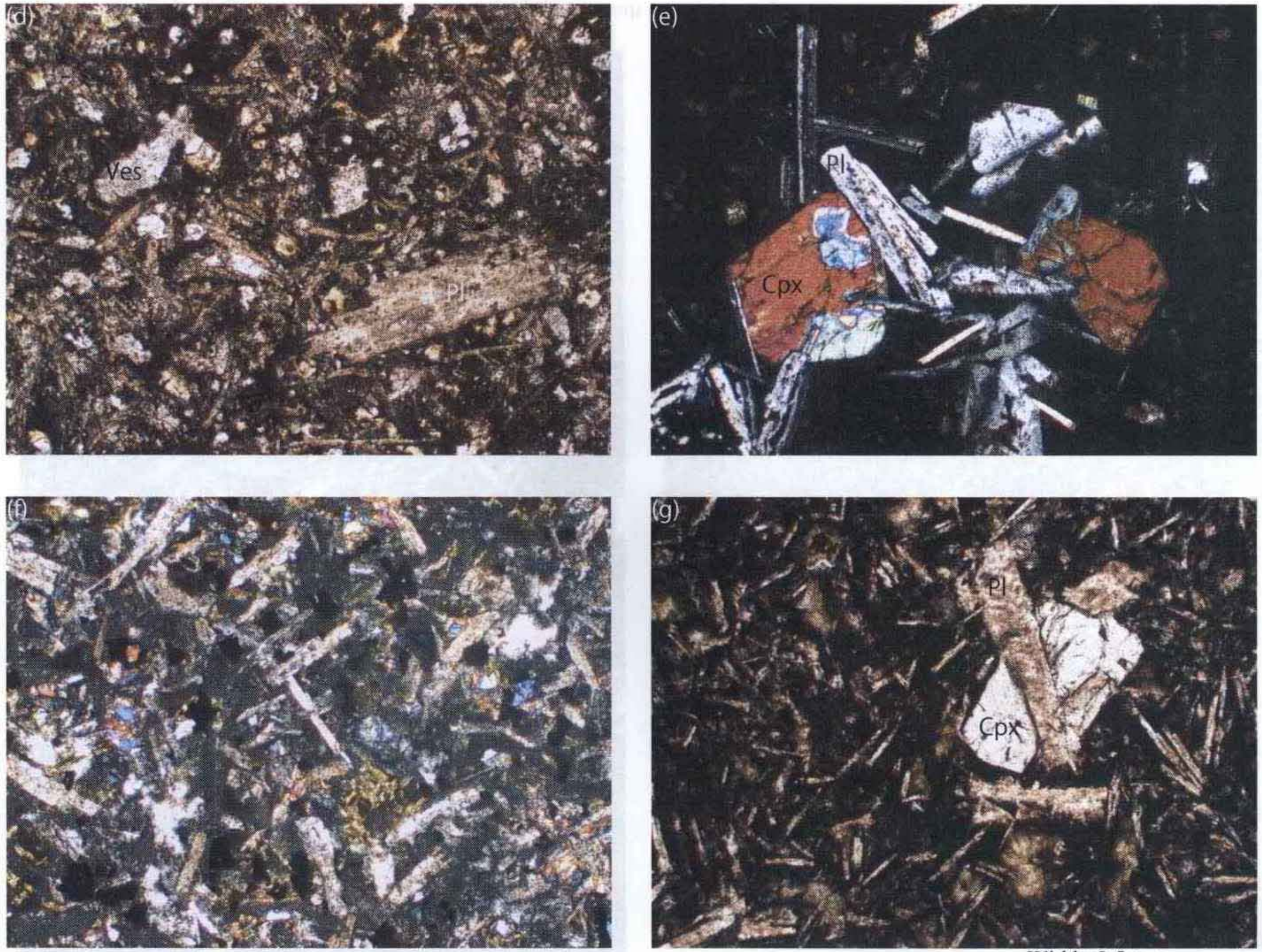

Width: 2.5 mm

Figure 2.4 Microphotographs of flows and dikes. (d) Pl-phyric type of Wadi Fizh (07Fz9). (e) Pl-Cpx-phyric type of 07Fz11 with aphanitic matrix. (f) Aphyric type of 07Fz34. (g) Pl-Cpx-type of 07Fz49. Ol: olivine; Pl: plagioclase; Cpx: clinopyroxene; Ves: vesicle.

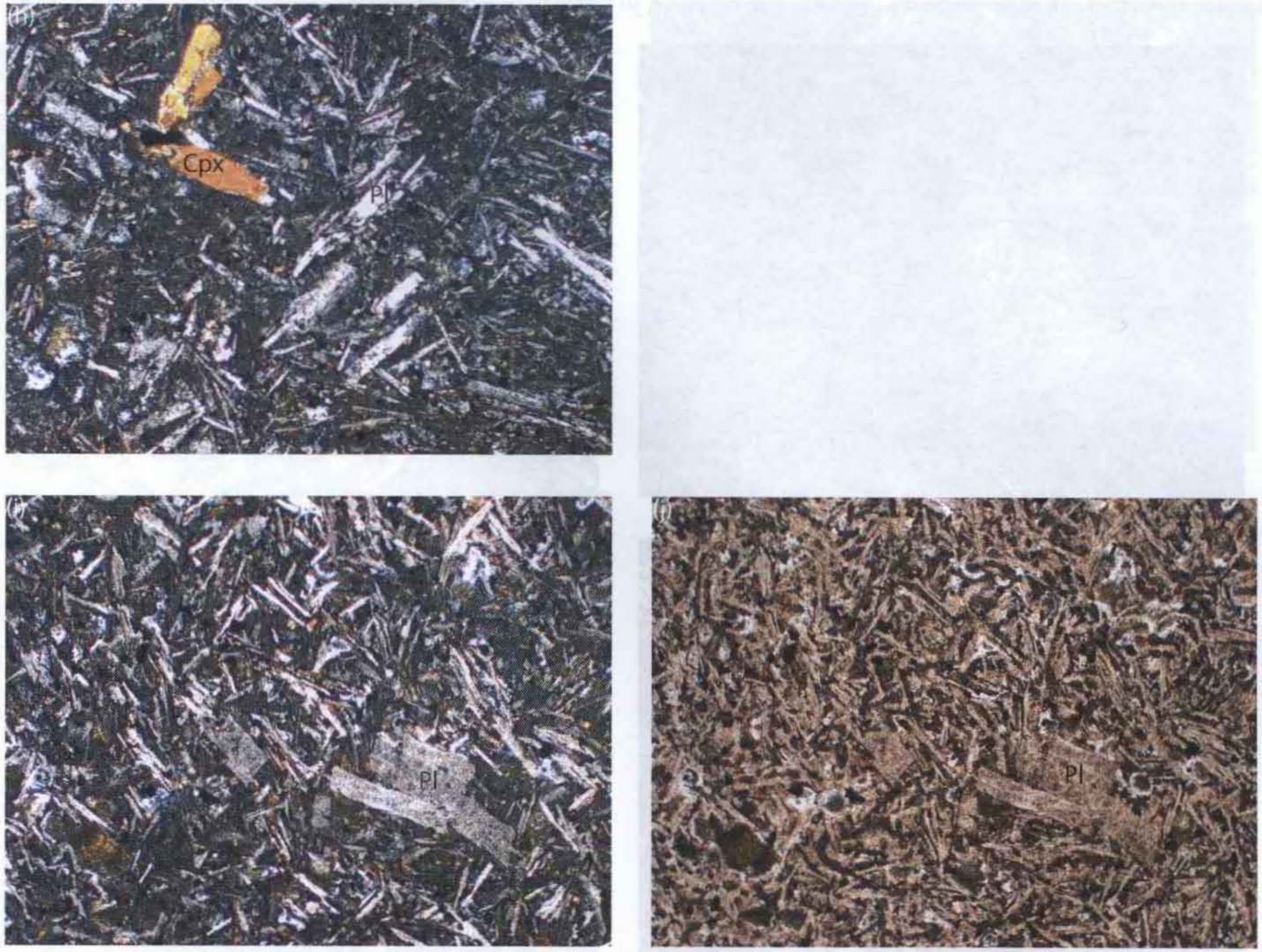

Width: 2.5 mm

Figure 2.4 Microphotographs of flows and dikes. (h) Aphyric basalt of Wadi Thuqbah (10Thu1). Plagioclase and clinopyroxene microphenocrysts sometimes occur. (i) (j) Pl-phyric type of 10Thu12 with fine grained hyalo-ophitic matrix. Pl: plagioclase; Cpx: clinopyroxene; Ves: vesicle.

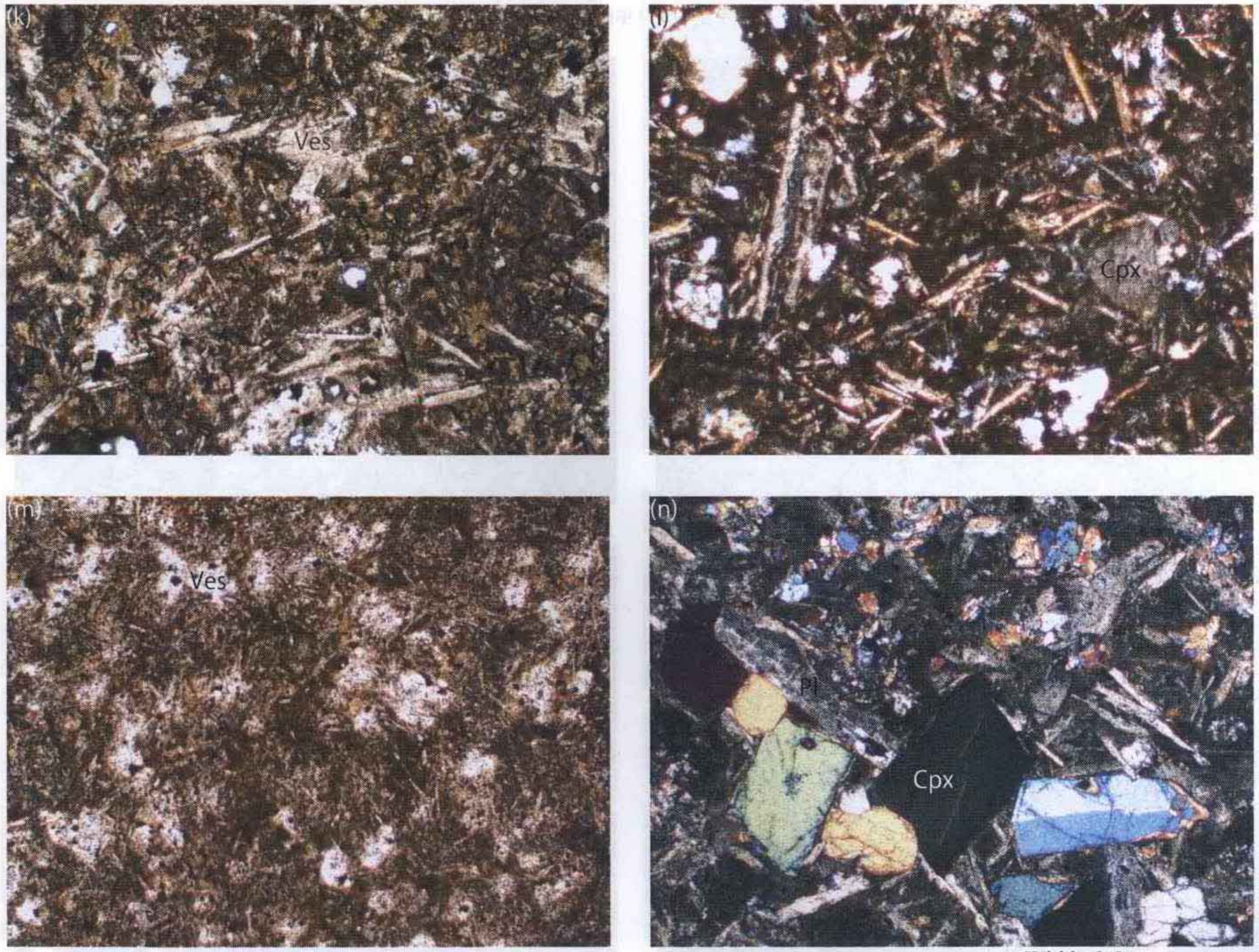

Width: 2.5 mm

Figure 2.4 Microphotographs of flows and dikes. (k) Aphyric type of Bani Ghayth (06Ghay6). (l) Aphyric type of 06Ghay49 with microphenocryst plagioclase and clinopyroxenes. Some clinopyroxenes are altered and filled with calcite. (m) Very fine grained matrix of 08Ghay4. Vesicles represent variable form filled with calcite. (n) Pl-Cpx-phyric type of 10Ghay43. Pl: plagioclase; Cpx: clinopyroxene; Ves: vesicle.

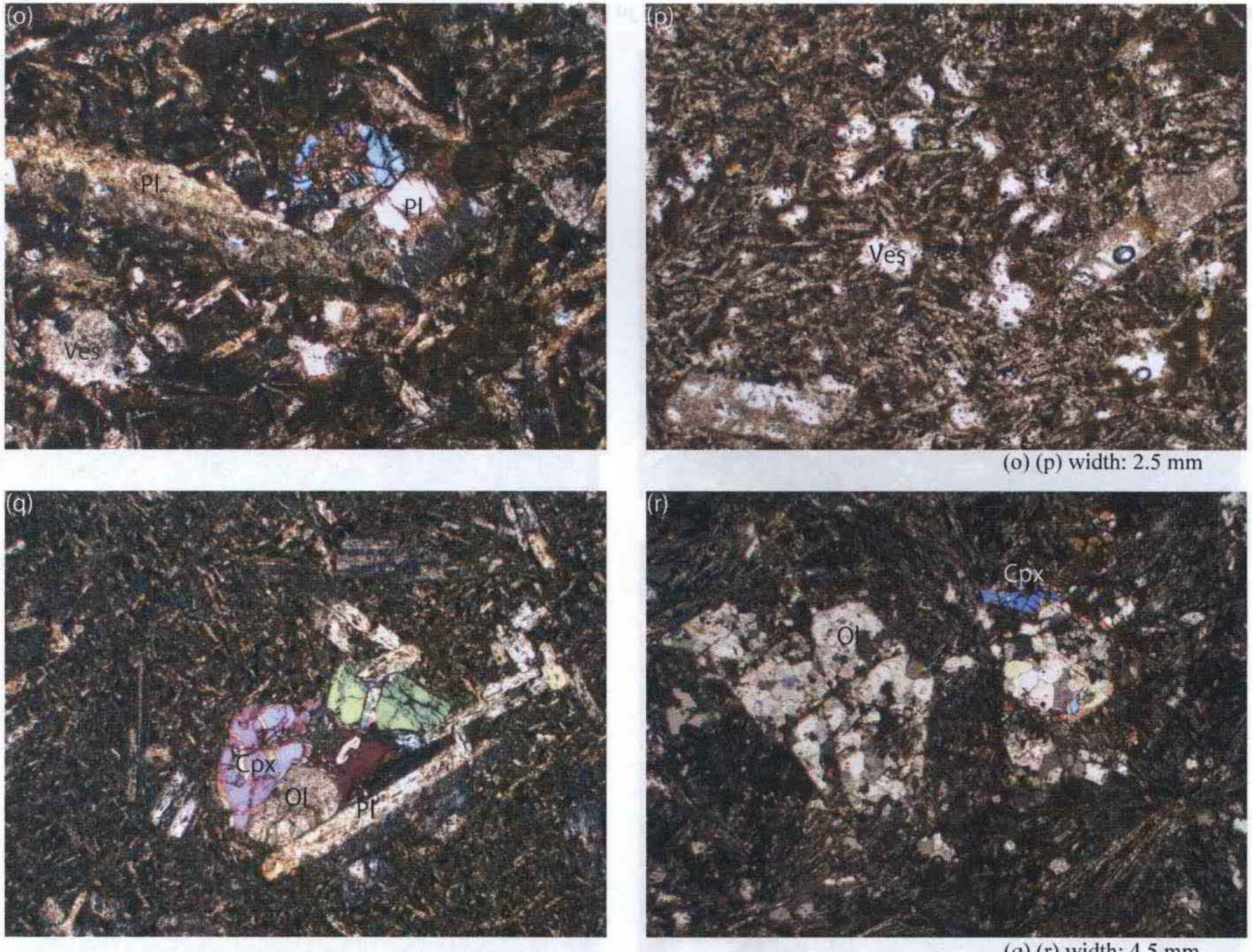

Figure 2.4 Microphotographs of flows and dikes. (o) Pl-phyric with clinopyroxene microphenocryst of Wadi Yanbu (06vsal8). (p) Aphyric type with plagioclase microphenocryst of Wadi Yanbu (06vsal29). (q) Pl-Ol-Cpx glomerocryst of Wadi Yanbu (07vsal118). (r) Ol pseudomorph (filled with calcite) phenocryst in 07vsal119. Ol: olivine; Pl: plagioclase; Cpx: clinopyroxene; Ves: vesicle.

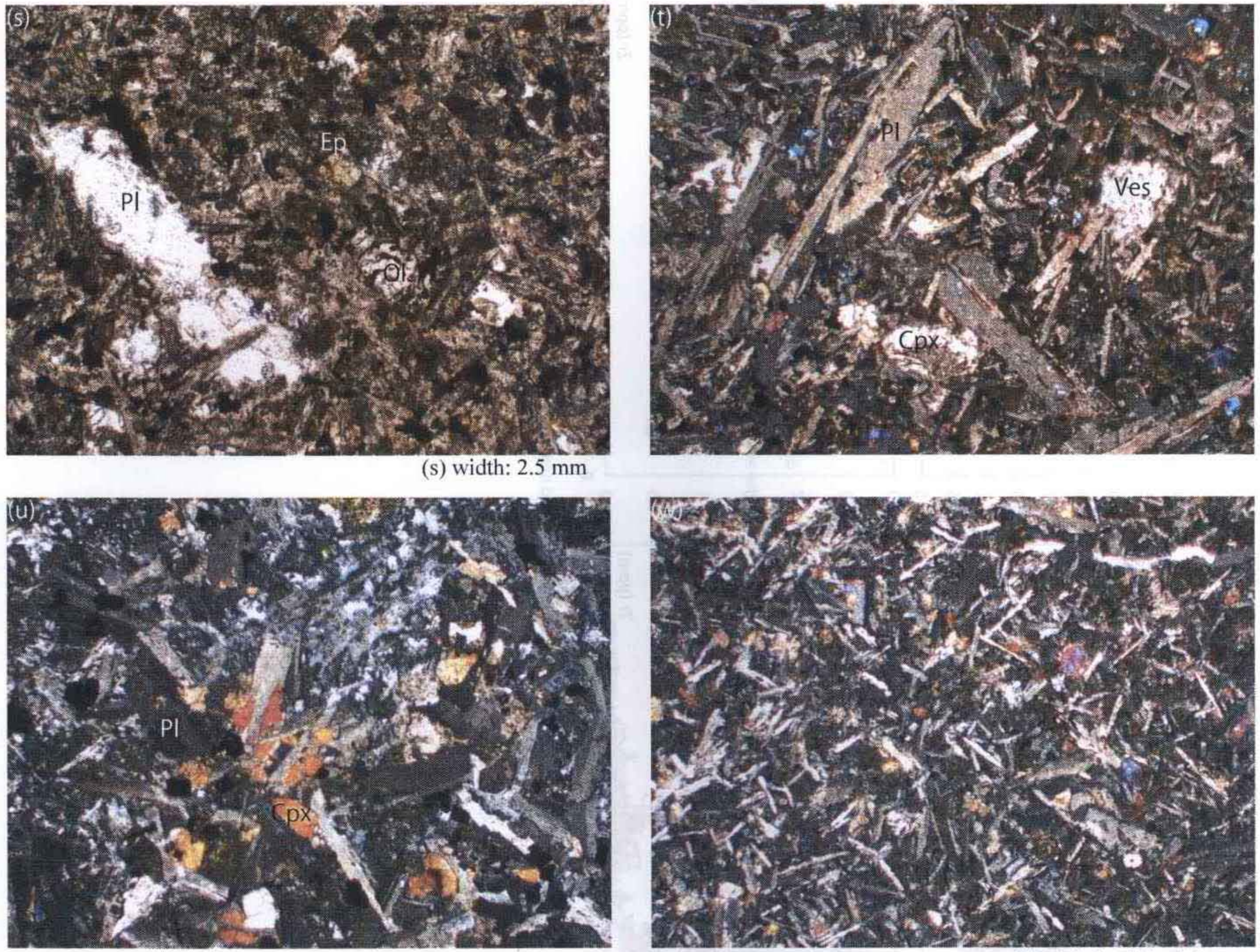

Figure 2.4 Microphotographs of flows and dikes. (s) Pl-phyric type of Wadi Salahi (07vsal29). Olivine occurs as matrix mineral. (t) Aphyric basalt of 07vsal42. Clinopyroxene is altered to calcite. (u) Coarse grained aphyric type of Wadi Hilti (09vHil10). (w) Fine grained aphyric type of pahoehoe flows (09vHil46). Ol: olivine; Pl: plagioclase; Cpx: clinopyroxene; Ep: Epidote; Ves: vesicle.

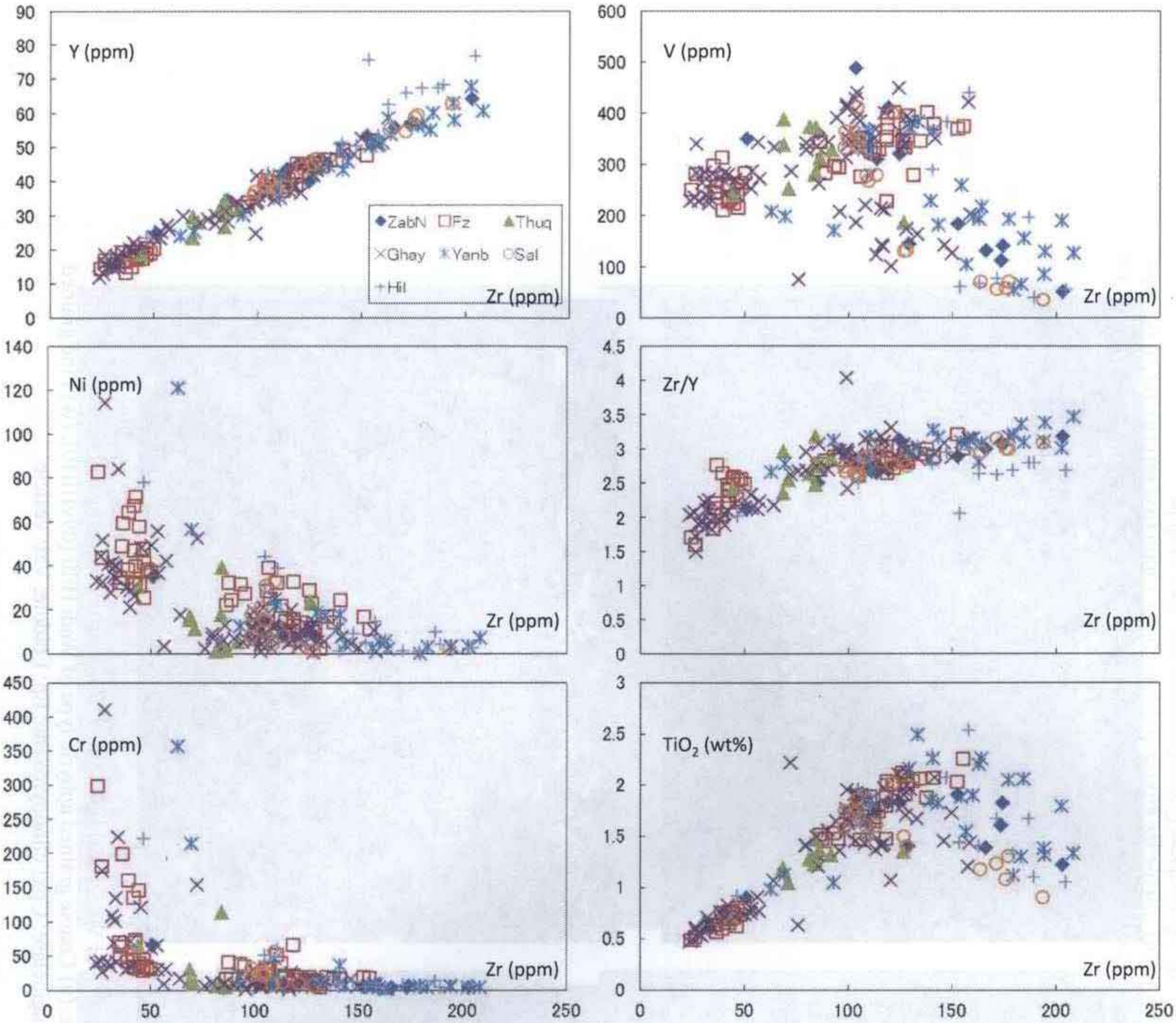

Figure 2.5 Y, Ni, Cr, V, Zr/Y ratios and TiO_2 plotted against Zr. TiO_2 is based on an anhydrous basis.

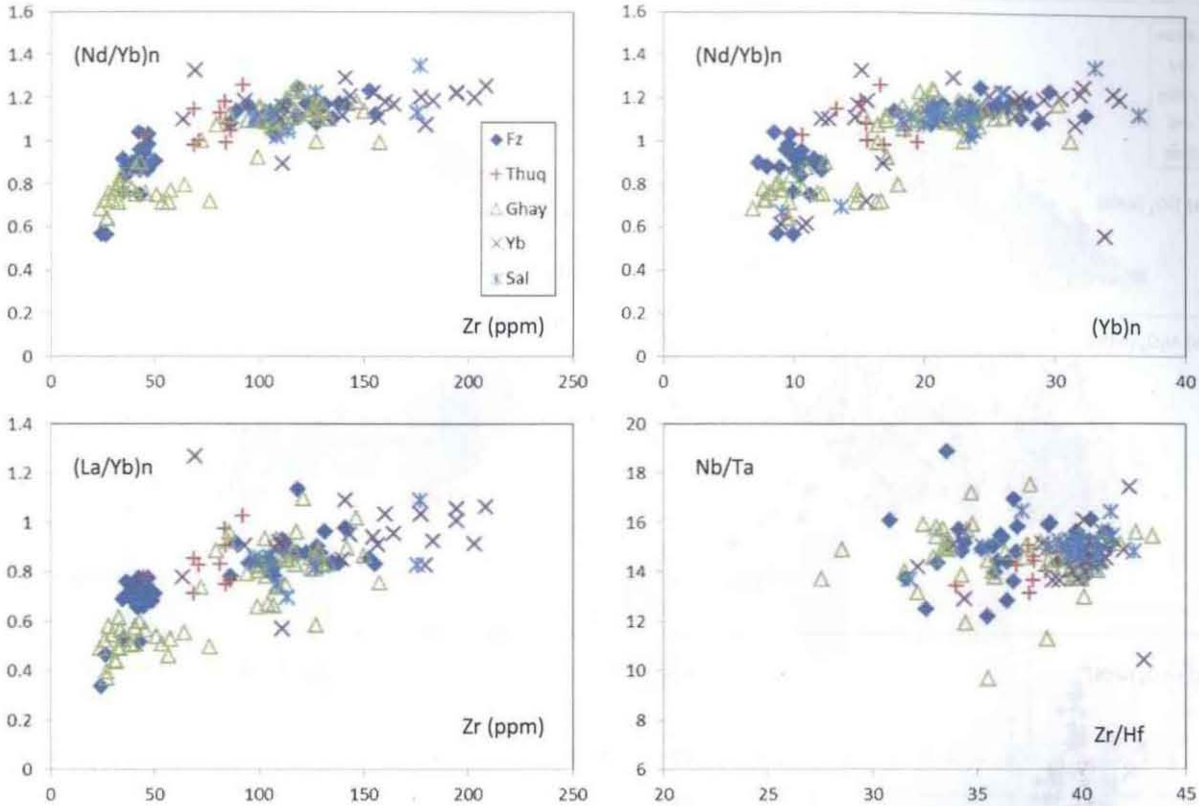

Figure 2.6 Chondrite normarized Nd/Yb and La/Yb ratios against Zr, and Chondrite normarized Nd/Yb ratios versus Yb, and Nb/Ta versus Zr/Hf ratios in this study.

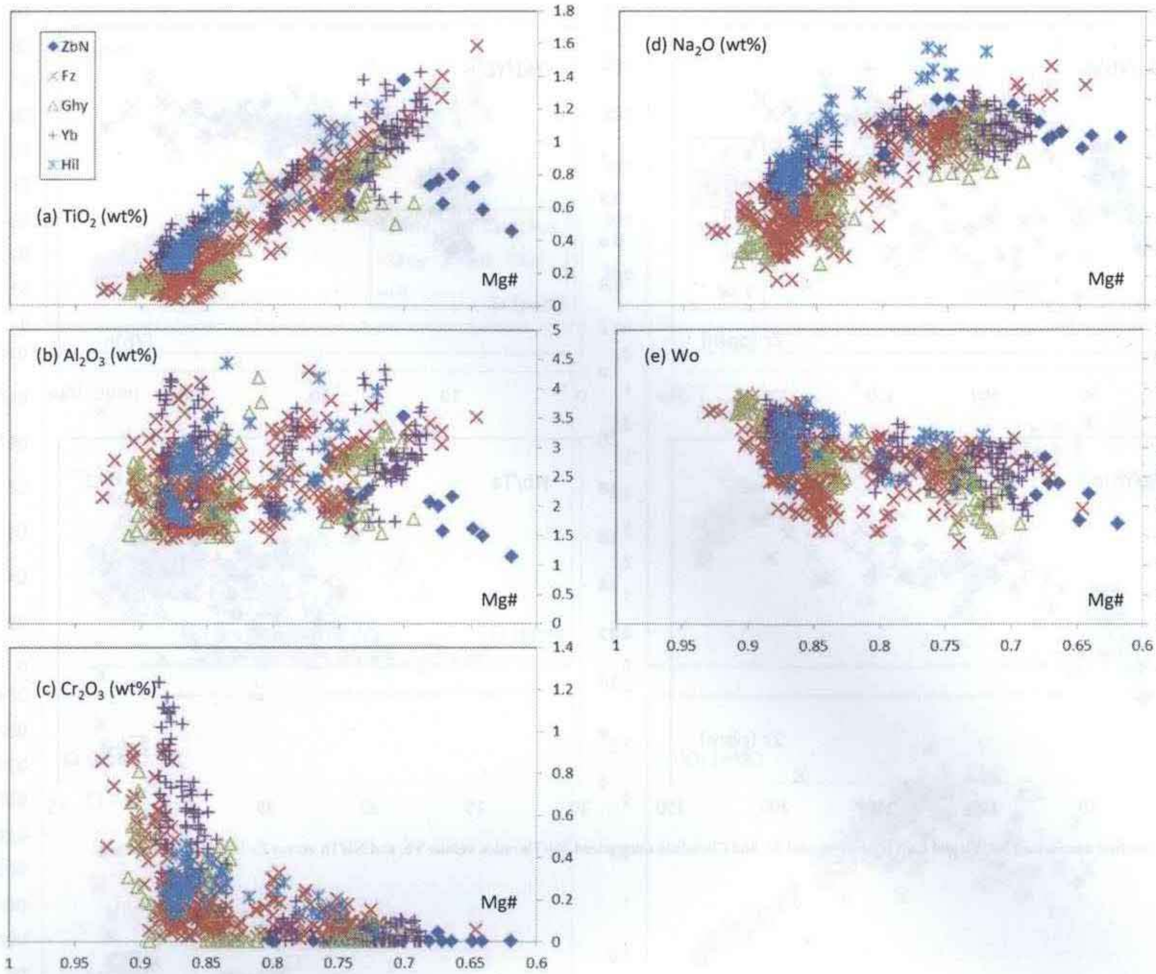

Figure 2.7 Clinopyroxexe Mg# versus (a) TiO_2, (b) Al_2O_3, (c) Cr_2O_3, (d) Na_2O and (e) Wo mol%.

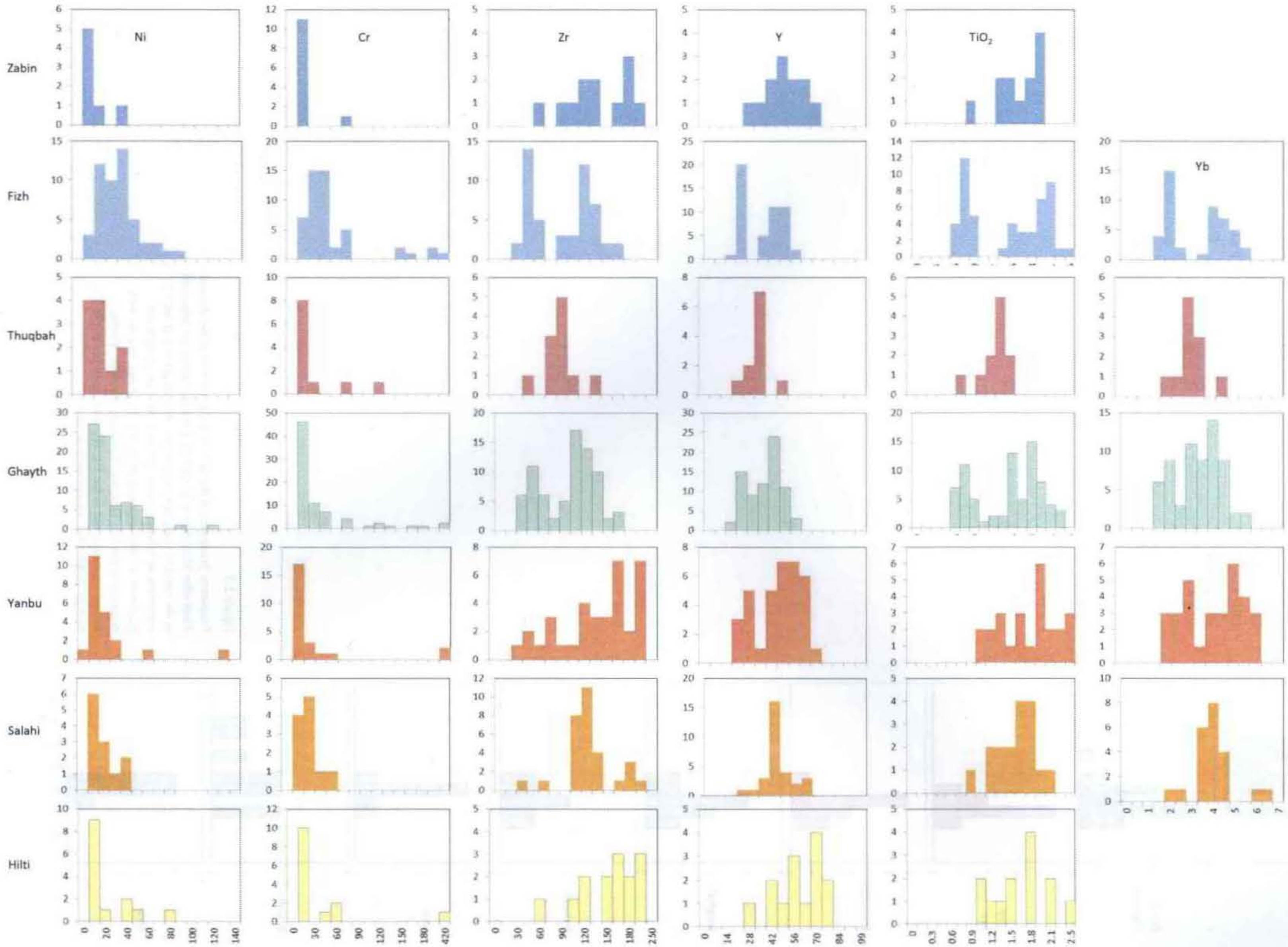

Figure 2.8 Frequency histogram of the bulk rock incompatible and compatible elements of the V1 lavas for each location. See text for explanation.

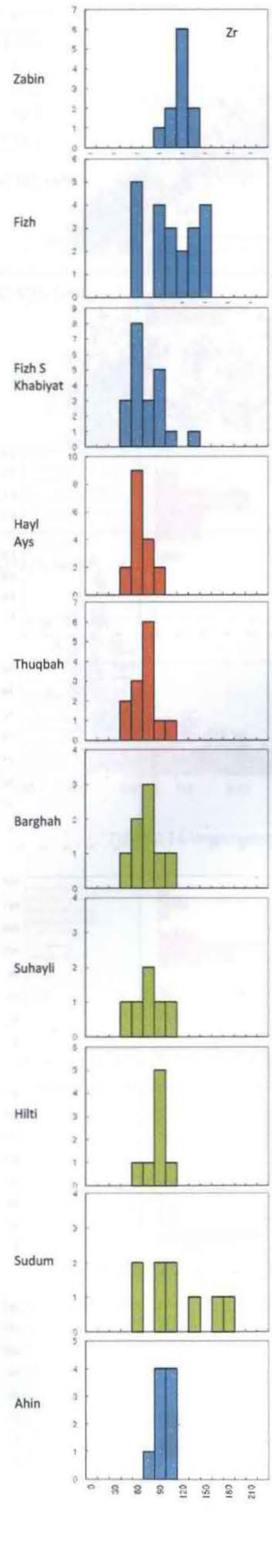

Figure 2.9

Frequency histogram of the bulk rock Zr contents of the sheeted dikes after Miyashita et al. [2003]. Locality names are improved to the name of wadi and corresponds sheeted dikes and the V1 extrusives as follows; Zabin: Zabin; Fizh: Fizh; Fizh S and Khabiyat: no well exposure in the V1; Hayl and Ays: no well exposure in the V1; Thuqbah: Thuqbah; Barghah: Yanbu; Suhayli: not analyzed in the V1; Hilti: not analyzed in the V1; Sudum: Hilti; Ahin: no exposure in the V1.

Table 2.1.1 Locations, mode of occurrences and phenocryst assemblages of the Wadi Zabin lava flows and dikes. Pl: plagioclase; Ol: olivine; Cpx: clinopyroxene.

sample No.	Mode of occurrence	Mineral assemblages	texture
08ZabinN05	Dike	aphyric	Hyaloophitic
08ZabinN10	pillow lava	aphyric	vitrophiric
08ZabinN21	massive lava	aphyric	Intersertal
08ZabinN28	massive or lobate	Pl-Ol	Hyaloophitic
08ZabinN32	massive lava	aphyric	Hyaloophitic
08ZabinN38	massive lava	aphyric	Intersertal
08ZabinN45	lobate sheet flows	aphyric	Hyaloophitic
08ZabinN50	lobate sheet flows	Pl-Cpx	Hyaloophitic
08ZabinN54	pillow lava	aphyric	Hyaloophitic
08ZabinN60	pillow lava	aphyric	Hyaloophitic
08ZabinN67	pillow lava	aphyric	Hyaloophitic
08ZabinN71	pillow lava	Cpx	Hyaloophitic

Table 2.1.2 Locations, mode of occurrences and phenocryst assemblages of the Wadi Thuqbah lava flows and dikes. Pl: plagioclase; Cpx: clinopyroxene.

Sample No.	Mode of occurrence	Mineral assemblages	Texture
10vThu1	Massive lava	sparsely Pl-Cpx	Hyaloophitic
10vThu2	Lava in Hyaloclastite	aphyric	vitrophitic
10vThu3	Pahoehoe flows	rarely Pl	Hyaloophitic
10vThu4	dike	sparsely Pl-Cpx	Hyaloophitic
10vThu5	dike	aphyric	intersertal
10vThu6	Lobate sheet flows	aphyric	Hyaloophitic
10vThu7	Pahoehoe flows	reraly Pl	Hyaloophitic
10vThu8	Pahoehoe flows	aphyric	Hyaloophitic
10vThu9	dike	aphyric	Hyaloophitic
10vThu10	Lobate sheet flows	rarely Cpx	Hyaloophitic
10vThu11	Pahoehoe flows	sparsely Pl-Cpx	Hyaloophitic
10vThu12	Pahoehoe flows	sparsely Pl	intersertal: fine
10vThu13	Lobate sheet flows	aphyric	Hyaloophitic
10vThu14	Lobate sheet flows	aphyric	Intersertal

Table 2.1.3 Locations, mode of occurrences and phenocryst assemblages of the Bani Ghayth lava flows and dikes. Pl: plagioclase; Ol: olivine; Cpx: clinopyroxene; Opx: orthopyroxene.

sample No.	Mode of occurrence	Mineral assemblages	texture	mab
06Gay1	massive	Pl-Cpx	Hyaloophitic	628
06Gay2	massive	sparsly Pl-Cpx	Hyaloophitic	610
06Gay3	massive	Pl	Hyaloophitic	607
06Gay4	pillow	aphyric	Hyaloophitic	598
06Gay5	pillow margin	rarely Pl	Hyaloophitic	598
06Gay6	pillow core	aphyric	Hyaloophitic	598
06Gay7	massive	rarely Pl	intersertal	587
06Gay8	pillow	aphyric	Hyaloophitic	587
06Gay9	pillow core	sparsly Pl-Cpx	variolitic	569
06Gay10	pillow rim	aphyric	aphanitic	567
06Gay11	pillow	aphyric	intersertal	552
06Gay12	pillow	aphyric	Hyaloophitic~variolitic	548
06Gay13	massive	Pl (-Ol) -Cpx	intersertal	547
06Gay14	massive	Pl-Ol (-Cpx)	intersertal	545
06Gay15	jasper			547
06Gay16	pillow core	Pl (-Ol)	intersertal	542
06Gay17	massive	sparsly Pl	intersertal	539
06Gay18	massive	rarely Pl-Cpx	Hyaloophitic	535
06Gay19	massive	aphyric	Hyaloophitic	531
06Gay20	vesiclated pillow	aphyric	hyaroophitic	529
06Gay21	pillow core	aphyric	hyaroophitic	524
06Gay22	pillow core	aphyric	Hyaloophitic~intersertal	508
06Gay23	pillow core	sparsly Pl-Cpx	variolitic	492
06Gay24	columner massive	aphyric	intersertal	490
06Gay25	pillow core	sparsly Pl-Cpx	Hyaloophitic	487
06Gay26	vesiclated massive	sparsly Pl	Hyaloophitic	485
06Gay27	massive	Pl	Hyaloophitic	480
06Gay28	massive	Pl (-Ol) -Cpx	Hyaloophitic	480
06Gay29	pillow hyaro mix rim	Pl	variolitic	475
06Gay30	massive	Pl	intersertal	469
06Gay32	pillow rim	aphyric	variolitic	466
06Gay33	pillow	Pl-Cpx	intersertal	466
06Gay34	massive	aphyric	Hyaloophitic	462
06Gay35	massive	aphyric	Hyaloophitic	459
06Gay36	massive	aphyric	intersertal	445
06Gay37	pillow rim	Pl-Cpx	variolitic	428
06Gay38	massive	Pl	intersertal	418
06Gay39	massive	Pl	Hyaloophitic	408
06Gay40	pillow hyaro mix rim	aphyric	variolitic	406
06Gay41	massive	aphyric	Hyaloophitic	385
06Gay42	massive	aphyric	Hyaloophitic	370
06Gay43	pillow rim	aphyric	Hyaloophitic	360
06Gay44	massive	aphyric	Hyaloophitic	356
06Gay45	dike	aphyric	Hyaloophitic	341
06Gay46	vesiclated massive	aphyric	Hyaloophitic	342
06Gay47	massive	Pl-Cpx	Hyaloophitic	338
06Gay48	massive	aphyric	intersertal	338
06Gay49	massive	aphyric	Hyaloophitic	318
06Gay50	massive	aphyric	intersertal	318
06Gay51	massive	Pl	Hyaloophitic	314
06Gay52	pillow	Pl-Cpx	varioliic	299
06Gay53	massive	sparsly Pl	Hyaloophitic	299
06Gay54	massive	Pl-Ol	hyaroophitic	280
06Gay55	pillow	Pl-Ol-Cpx	Hyaloophitic	241
06Gay56	massive	Pl-Cpx	Hyaloophitic	218
06Gay57	pillow	aphyric	Hyaloophitic	200
06Gay58	massive	aphyric	varioltic	
06Gay59	massive	Pl	Hyaloophitic	
06Gay60	massive	sparsly Pl	Hyaloophitic	

(Continued)

sampleNo.	Mode of occurrence	Mineral assemblages	texture	mab
06Gay61	massive	Pl	Hyaloophitic	
06Gay62	pillow	sparsly Pl	Hyaloophitic	
06Gay63	massive	aphyric	Hyaloophitic	
06Gay64	massive	aphyric	Hyaloophitic	
06Gay65	massive	sparsly Pl	Hyaloophitic	
06Gay66	pillow	aphyric	Hyaloophitic	
06Gay67	massive	sparsly Pl	vitrophyric	
06Gay68	massive	sparsely Pl-Cpx	Hyaloophitic	
06Gay69	massive	sparsely Pl-Cpx	Hyaloophitic	
08Ghayth1	massive lava	Ol-Cpx	variolitic	188
08Ghayth2	joint<lobate sheet	Pl	intersertal	177
08Ghayth3	lobate sheet	Pl	variolitic	138
08Ghayth4	lobate sheet	Pl-Ol	Hyaloophitic	138
08Ghayth5	massive lava	aphyric	intersertal	86
08Ghayth6	sheeted dike	aphyric	Hyaloophitic	65
08Ghayth7	joint<massive	Cpx	Hyaloophitic	50
08Ghayth8	sheeted dike	Pl-Ol-Cpx	Hyaloophitic	-25
08Ghayth9	pillow lava	aphyric	Hyaloophitic	
08Ghayth10	EW dike	aphyric	intersertal-	
08Ghayth11	massive lava	aphyric	intersertal	
08Ghayth12	massive lava	aphyric	Hyaloophitic	
08Ghayth13	massive lava	aphyric	Hyaloophitic	
08Ghayth14	EW dike	aphyric	variolitic	
10gay1	phoehoe	aphyric	Hyaloophitic	600
10gay2	lobate sheet	Pl-Ol-Cpx	Hyaloophitic	607
10gay3	lobate sheet	aphyric	Hyaloophitic	610
10gay4	pahoehoe	rarely Pl	Hyaloophitic(fine)	613
10gay5	pahoehoe	sparsly Pl	aphanitic-Hyaloophitic	625
10gay6	lobate sheet	aphyric	dolelitic	648
10gay7	lobate sheet	sparsely Pl-Cpx	Hyaloophitic	667
10gay8	lobate sheet	sparsely Pl-Cpx	Hyaloophitic	687
10gay9	lobate sheet	Pl-Cpx	intersertal	703
10gay10	lobate sheet	rarely Pl	doleritic	712
10gay11	lobate sheet	aphyric	Hyaloophitic	722
10gay12	lobate sheet			731
10gay13	pahoehoe	Pl-Cpx	Hyaloophitic(fine)	733
10gay14	lobate sheet	rarely Pl-Cpx	doleritic	742
10gay15	lobate sheet	Cpx	Hyaloophitic	750
10gay16	lobate sheet	aphyric	Hyaloophitic(fine)	759
10gay17	lobate sheet	aphyric	intersertal	762
10gay18	pahoehoe	aphyric	Hyaloophitic	773
10gay19	dike	aphyric	Hyaloophitic(fine)	
10gay20	lobate sheet	Pl-Cpx	intersertal-doleritic	789
10gay21	lobate sheet	Pl	intersertal	797
10gay22	pahoehoe	rarely Pl	Hyaloophitic	809
10gay23	pahoehoe	rarely Pl	Hyaloophitic	833
10gay24	lobate sheet	rarely Pl	Hyaloophitic	843
10gay25	lobate sheet	aphyric	intersertal	848
10gay26	lobate sheet	rarely Pl	Hyaloophitic	856
10gay27	lobate sheet	aphyric	intersertal-doleritic	863
10gay28	lobate sheet	aphyric	Hyaloophitic	867
10gay29	lobate sheet	rarely Pl	Hyaloophitic	874
10gay30	pahoehoe	Pl	Hyaloophitic	880
10gay31	pahoehoe	sparsely Pl-Cpx	Hyaloophitic	884
10gay32	pahoehoe	sparsely Pl-Cpx	Hyaloophitic	889
10gay33	pahoehoe	sparsly Pl	Hyaloophitic(fine)	887
10gay34	lobate sheet	rarely Pl-Ol-Cpx	Hyaloophitic	
10gay35	lobate sheet	Ol-Cpx	aphanitic	
10gay36	lobate sheet	rarely Pl	Hyaloophitic	
10gay37	lobate sheet			
10gay38	lobate sheet	Pl-Cpx	Hyaloophitic	
10gay39	lobate sheet	aphyric	intersertal-Hyaloophitic	
10gay40	lobate sheet			

(Continued)

sampleNo.	Mode of occurrence	Mineral assemblages	texture	mab
10gay41	lobate sheet	Pl-Cpx	Hyaloophitic	
10gay42	dike	aphyric	Hyaloophitic	
10gay43	lobate sheet	Pl-Cpx	Hyaloophitic	
10gay44	lobate sheet	Pl-Ol	Hyaloophitic	
10gay45	pahoehoe	Pl-Ol-Cpx	Hyaloophitic(fine)	
10gay46	lobate sheet	Pl-Ol	Hyaloophitic	
10gay47	lobate sheet	Pl	Hyaloophitic(fine)	
10gay48	dike	Ol-Cpx	Hyaloophitic	

Table 2.1.4 Locations, mode of occurrences and phenocryst assemblages of the Wadi Yanbu lava flows and dikes. Pl: plagioclase; Ol: olivine; Cpx: clinopyroxene.

sample No.	Mode of occurrence	Mineral assemblages	texture
06vsal1	pahoehoe flows	Pl (-Ol)	vitrophyric
06vsal2	umber		
06vsal3	V2	Pl-Cpx	Hyaloophitic
06vsal4	V2	Pl-Cpx	hyalopilitic
06vsal5	V2	aphyric	hyalopilitic
06vsal6	pahoehoe flows	Pl-Ol	hyalopilitic
06vsa7	pahoehoe flows	Pl-Ol	vitrophyric
06vsal8	pahoehoe flows	Pl-Ol	Hyaloophitic
06vsal9	pahoehoe flows	aphyric	hyaloophytic
06vsal10	pahoehoe flows	sparsly Pl-Cpx	vitrophyric
06vsal11	pahoehoe flows	sparsly Pl-Cpx	Hyaloophitic
06vsal12	pahoehoe flows	Pl-Cpx	glassic
06vsal13	pahoehoe flows	Pl-Ol-Cpx	hyalopilitic
06vsal15	V2	sparsly Pl	hyalopilitic
06vsal16	pahoehoe flows	Pl-Cpx	Hyaloophitic
06vsal17	pahoehoe flows	aphyric	vitrophyric
06vsal18	pahoehoe flows	aphyric	vitrophyric
06vsal19	pahoehoe flows	sparsly Pl-Ol	vitrophyric
06vsal20	pahoehoe flows	sparsly Pl-Cpx	Hyaloophitic
06vsal21	pahoehoe flows	aphyric	vitrophyric
06vsal22	pahoehoe flows	aphyric	Hyaloophitic
06vsal23	Lobate sheet flows	Pl-Cpx	Hyaloophitic
06vsal24	Lobate sheet flows	Pl-Cpx	Hyaloophitic
06vsal25	pahoehoe flows	sparsly Pl-Cpx	intersetal
06vsal26	Lobate sheet flows	sparsly Pl	hyalopilitic
06vsal27	pahoehoe flows	aphyric	Hyaloophitic
06vsal28	pahoehoe flows	aphyric	hyalopilitic
06vsal29	Lobate sheet flows	aphyric	hyalopilitic
06vsal30	pahoehoe flows	aphyric	hyalopilitic
06vsal31	Lobate sheet flows	aphyric	hyalopilitic
07Salahi107	pahoehoe flows	aphyric	Hyaloophitic
07Salahi108	massive	aphyric	Intersertal-Hyaloophitic
07Salahi109	massive	Pl-Ol-Cpx	Intersertal
07Salahi110	lobate sheet	aphyric	intersertal
07Salahi111	lobate sheet	Pl-Cpx	Hyaloophitic
07Salahi112	pillow	aphyric	pl
07Salahi113	lobate sheet rim?	Ol	Hyaloophitic
07Salahi114	lobate sheet	aphyric	Intersertal
07Salahi115	lobate sheet	aphyric	Intersertal
07Salahi116	lobate sheet	Pl	Intersertal
07Salahi117	lobate sheet	Ol	intersertal
07Salahi118	massive	Pl-Ol-Cpx	
07Salahi119	pahoehoe flows	Ol-Cpx	spherulitic
07Salahi120	pahoehoe flows	Pl-Ol-Cpx	intersertal
07Salahi121	lobate sheet	(Pl-) Ol-Cpx	Hyaloophitic
07Salahi122	pahoehoe flows	aphyric	varioritic
07Salahi123	pahoehoe flows	Pl-Cpx	spherulitic

Table 2.1.5 Locations, mode of occurrences and phenocryst assemblages of the Wadi Salahi lava flows and dikes. Pl: plagioclase; Ol: olivine; Cpx: clinopyroxene.

sample No.	Mode of occurrence	Mineral assemblages	texture
07Salah29	pillow lavas	aphyric	intersertal
07Salahi30	pahoehoe flows	sparsely Pl	Hyaloophitic
07Salahi31	pahoehoe flows	aphyric	intersertal
07salahi32	lobate sheet	Pl (-Ol) -Cpx	intergranular
07Salahi33	lobate sheet	aphyric	intersertal
07Salahi34	lobate sheet	Pl (-Ol)	intersertal
07Salahi35	lobate sheet	aphyric	hyaloophytic
07Salahi36	pahoehoe flows	aphyric	hyaloophytic
07Salahi37	pahoehoe flows	sparsely Pl	hyaloophytic
07Salahi38	pahoehoe flows	aphyric	intersertal
07Salahi39	lobate sheet	aphyric	intersertal
07Salahi40	pahoehoe flows	Pl	intersertal
07Salahi41	pahoehoe flows	sparsely Pl-Ol	hyaloophytic
07salahi42	lobate sheet	Pl-Cpx	intergranular
07Salahi43	Dike	aphyric	intergranular
07Salahi45	pahoehoe flows	aphyric	Hyaloophitic
07Salahi47	pahoehoe flows	Pl-Cpx	Hyaloophitic
07Salahi48	pahoehoe flows	Pl	Hyaloophitic
07Salahi50	lobate sheet	Pl	Hyaloophitic~intersertal
07Salahi51	lobate sheet	Pl-Cpx	Hyaloophitic
07salahi52	pahoehoe flows	Pl	intersertal
07Salahi54	pahoehoe flows	aphyric	intersertal
07Salahi55	Dike	aphyric	intersertal

Table 2.1.6 Locations, mode of occurrences and phenocryst assemblages of the Wadi Hilti lava flows and dikes. Pl: plagioclase; Ol: olivine; Cpx: clinopyroxene.

sample No.	Mode of occurrence	Mineral assemblages	texture
09vHil2	massive lavas	rarely Pl-Ol	Hyaloophitic
09vHil6	lobate sheet flows	rarely Pl	Hyaloophitic (coarse)
09vHil10	pahoehoe flows	aphyric	intersertal-pl, cpx
09vHil14	pahoehoe flows	Pl	Hyaloophitic (fine)
09vHil20	lobate sheet flows	doleritic	cpx-poikilitic
09vHil24	2nd dike	rarely Pl-Cpx	intersertal
09vHil25	lobate sheet flows	rarely Pl	Hyaloophitic
09vHil29	pahoehoe flows	aphyric	Hyaloophitic
09vHil36	2nd dike	Pl-Cpx	intersertal
09vHil37	pahoehoe flows	Pl	Hyaloophitic
09vHil41	lobate sheet flows	aphyric	Hyaloophitic
09vHil45	lobate sheet flows	aphyric	Hyaloophitic
09vHil46	pahoehoe flows	Pl-Cpx	Hyaloophitic (coarse)
09vHil48	massive lavas	aphyric	intersertal
09vHil51	dike	Pl-Cpx	intersertal
09vHil52	pillow lavas	aphyric	intersertal-doleritic
09vHil54	pillow lavas	Pl	intersertal
09vHil56	lobate sheet flows	sparsely Pl-Cpx	intersertal~Hyaloophitic
09vHil57	pillow lavas	Ol-Cpx	Hyaloophitic
09vHil58	lobate sheet flows	Pl	intersertal~Hyaloophitic
09vHil60	pahoehoe flows	sparsely Pl	Hyaloophitic
09vHil63	pahoehoe flows	Pl-Cpx	Hyaloophitic

Table 2.2 Summary of all intra-segment areas. Location in a second and third segment, thickness of lava sequence, modal % of lithology, mineral assemblage, special mention of lithology, bulk rock chemistry are shown. Ol: olivine; Pl: plagioclase; Cpx: clinopyroxene.

Second-order	Margin (North)	Center		Intermediate				Margin (South)
Third-order					Center	Margin		
Area	Fizh	Thuqbah	Ghayth	Yanbu	Salahi	Suhayli N	Suhayli	Hilti
Thickness of Lava sequence (m)								
Total thickness	1200	445+	900+	572	660	970+	935	688+
Axial part	410		603	474	352	380	205	350
Off-axis volcanism								
	Fissure vent					Dike swarm	Fissure vent	Dike swarm
Lithology (%)								
Pillow	38				5	11	2	12
Pahoehoe	10	70	50	86	58	62	40	44
Lobate sheet	44	24	30	13	32	13	56	38
Massive	8	6	20	1	2	14		6
Hyaloclastite					3		2	
Mineral assemblage								
	Aphyric	Aphyric	Aphyric	Aphyric	Aphyric			Aphyric
	Pl-Ol-Cpx	Pl-Cpx	Pl-Ol-Cpx	Pl-Ol-Cpx	Pl-Ol-Cpx			Pl-Ol-Cpx
	Ol	Cpx	Cpx	Ol	Pl-Ol			Ol-Cpx
	Cpx	Pl	Pl-Ol	Pl-Ol	Pl-Cpx			Pl-Ol
	Pl-Cpx		Pl-Cpx	Pl-Cpx	Pl			Pl-Cpx
	Pl		Pl	Pl				Pl
Whole rock composition								
Histogram	Bimodal	Unimodal	Bimodal	Unimodal	Unimodal			Unimodal
	Wide range	Narrow range	Wide range					Wide range
	Evolved and less-evolved	Mildly-evolved	Evolved and less-evolved		Mildly-evolved			Low Zr/Y ratio
Clinopyroxene composition								
			Low-Na_2O	Mildly High-Na_2O				High-Na_2O

Chapter 3

Discovery of boninite lava sequence in the V2:

Constriction for the tectonic setting of Oman ophiolite

3.1. Introduction

The Oman ophiolite is one of the best places to study the tectonic process and mechanism of transition from spreading ridge to island arc setting. Unfortunately, the V2 lavas have limited outcrops due to be covered with Quaternary at the southern part, and intruded by the EW-trending dikes at the northern part of the ophiolite.

Umino et al. [1990] has reported that the boninite lavas correlate with “Alley volcanics”. Although the most V2 lavas consist of tholeiitic basalts and andesite, boninites appear as intercalated lavas at Wadi Jizi area [Ishikawa et al., 2002] and intrusion into sheeted dike complex at Wadi Zabin area [Ishikawa et al., 2002; Adachi and Miyashita, 2003]. These boninites suggesting hot, hydrous shallow mantle had provided the V2 tectonic setting launching very near the spreading ridge [Ishikawa et al., 2002].

The sources of the V2 are contaminated by fluids as shown by changes in the mineral assemblages and trace element contents of the magmas [Umino et al., 1990; Ishikawa et al., 2002; Godard et al, 2006]. Whether this contamination of the V2 melts is due to a general subduction setting [e.g., Alabaster et al, 1982] or triggered by the liberation of fluids from the metamorphic sole during the early stage of obduction at the ridge [e.g., Ishikawa et al, 2005] is still on debate.

The most famous place of boninite lavas is Izu-Bonin-Mariana (IBM) arc located at fore-arc setting. The IBM arc preserves early arc volcanic history due to a change of tectionic setting from spreading ridge to subduction [Ishizuka et al., 2006]. At this region, it is indicated that the volcanisms have changed from tholeiitic to boninitic to dacite to andesitic, continuously, and their lithologies have been changed from pillow or sheet flows to volcaniclastic deposits [Umino and nakano, 2007]. On the other hand, the V2 section of the Oman ophiolite is often compared with that of the Troodos ophiolite. The upper pillow lavas of Troodos ophiolite range from 500 to 750 m thickness and consist of arc tholeiites and olivine-phyric boninites [Taylor et al., 1990].

This paper presents the first thorough description of the approximately whole V2 unit around the junction of Wadi Suhayli and Hilti, and shows detailed stratigraphic variations in terms of lithology and geochemistry. Based on these results, the formation processes of the V2 unit are discussed.

3.2. Geology

3.2.1. Geology and descriptions of lithofacies

The V2 sequence in the northern Oman ophiolite seems to be covering the V1 sequence with conformity, though the V1 and V2 boundary has 20-m thick conglomerate of the V1 pillow by unconformity at around Wadi Ahin area [Umino et al., 1990]. Typical V2 lavas are exposed in Wadi Fizh, Wadi Yanbu and Wadi Salahi area contacting with metalliferous sediment just the basal part. In this case, first V2 lavas have been preserved, but we cannot consider the whole V2 volcanism. Because the V1 sequence is directly covered with the Suhaylah Formation at Wadi ath Thuqbah where fossil ages span from V2 to V3 magmatism, the V2 sequence is absent in this area [Regba et al., 2000].

The extrusive rocks in Wadi Suhayli area generally strike NE-SW and dip 20°-30° to east, attaining approximately 2200 m in thickness. The extrusive rocks gradually change into the underlying sheeted dike complex striking N-S to NW-SE and dipping 60°-90° westward, through 20-m thick transition zone with increasing number of 0.8- to 1.5-m thick dikes downward. The 935-m thick V1 and 1115-m thick upper V2 units are separated by a 0.5-m thick metalliferous sedimentary layer (umber). The V2 unit covered with 30-m thick metalliferous umber and shale is overlain by the V3 unit. The V2 sequence is subdivided into two subunits by a 1.0-m thick metalliferous sedimentary layer (Figure 3.1). We hereafter call these subunits the lower V2 (LV2) and the upper V2 (UV2) (Figure 3.2). Actually, the V2 unit has partly been thrusted by emplacement of the V3 or primary fault, the UV2 exposures southward in this area. Stratigraphic levels are indicated by the height in meters above the basement (mab) of the V2 unit.

Based on lava morphology we identified three lithofacies in the V2 sequence; pillow, pahoehoe and lobate sheet flows.

Pillow flows comprise 1% of the V2 section and appear as several meters thick. Pillow flows consist of "bulbous" pillows. Neither corrugations nor ropy wrinkles on pillow surface are preserved due to weathering.

A pahoehoe lobe is similar to a pillow lobe but has much smaller height to width ratios than the latter [Walker, 1992] and smooth surfaces without corrugations, and are intimately associated with lobate sheet flows [Umino et al., 2002]. Some hollow lobes are present in pahoehoe flows, which formed by drainage of molten lava within partially solidified pahoehoe lobes [Batiza and White, 2000; Umino et al., 2000] (Figure 3.3c). Pahoehoe flows are abundant in this area. The lobes are observed as thick and fine grained crust with coarse grained contents (Figure 3.3d). Individual pahoehoe flows have a minimum thickness of 4 m and attains to 32% of the entire V2 sequence. Almost the V2 samples of other area appear as pahoehoe flows.

Lobate sheet flows occupy 67% of the V2 sequence and are the dominant lithofacies in this section (Figure 3.3a). A lobate sheet has a gently curved upper surface with well developed columnar joints perpendicular to the surface. A lobate sheet flow is a compound flow consisting of a number of lava lobes about 2 m thick. An upper lobe laterally piles up onto the lower lobe. Some lobate sheet flows are underlain by lenses of pillow or pahoehoe lobes less than 0.5 m thick (Figure 3.3c). Varioles less than 1 cm rarely 3 cm in diameter may be present in the chilled margin of a lobate sheet.

3.2.2. The lower V2 sequence

The lower V2 unit (LV2) is 1010 m thick although 135- and 110-m thick intervals occupying 25% of the V2 unit are hidden by gravels. The LV2 consists mainly of lobate sheet flows with a subordinate amount of pahoehoe lava and a few of pillow lava flows. The lobate sheet flows comprise 55% in the LV2. The distinction of individual lithofacies is relatively easy as shown in Figure 3.3. The boundary is usually determined by the occurrence of different lithologies and/or structures. At around 270 mab, a large tumuli with 20 m thick appears (Figure 3.3b). A cylinder conduit of 5-7 m diameter corresponds to around 720 mab (Figure 3.3h). An umber layer at 910 mab has partly been vesiculated, and branched by underlying lavas (Figure 3.3g). Thin umber lens occur above 885 mab and the top layer of LV2 consisting of lobate sheet flows is overlain by 1.0-m thick umber layer extending 1.8 km to south.

3.2.3. The upper V2 sequence

The upper V2 (UV2) has a thickness of 140 m and consists of lobate sheet flows they intercalate six sheets of discontinuous metalliferous umber. Sheet flows and umbers are piled up repeatedly between 1007 and 1045 mab. Sheet flows sometimes have 2-cm thick fine grained crust. 2-m thick pyroclastic rock occurs at the top of UV2 and it consists of 0.5-3 cm of fragments similar to the fine grained crust of sheet flows and noticeable size of clinopyroxene minerals (Figure 3.3e and 3.4d). The UV2 is terminated by the appearances of

0.5-m thick metalliferous sedimentary layer (Figure 3.3f).

3.3. Petrography

Based on abundance and assemblage of phenocrysts, the V2 volcanic rocks are divided into aphyric, Ol (olivine)-Cpx (clinopyroxene), Ol-Opx (orthopyroxene)-Cpx, Pl (plagioclace)-Ol-Cpx, Ol-Pl-Opx-Cpx and Pl-Cpx -phyric types (Figure 3.4). Aphyric rocks are displayed on the lower part of the LV2 and Pl-bearing rocks are dominated in the LV2. Hyaloophitic and intersertal textures are well observed in the groundmass and a variolitic texture frequently develops near the surface of pahoehoe flows. Mineral assemblages are not correlated with their lithologies.

Lava samples underwent intensive low-temperature alteration. Most plagioclases are altered to albite, saussurite or calcite (Figure 3.4j, l, n and o). Olivine phenocrysts sometimes with iddingsite are replaced by chlorite and clay minerals (Figure 3.4e-h, k and m-o). Chrome-spinels occur in olivine pseudomorphs (Figure 3.4h). Orthopyroxene phenocrysts are also altered to talc or clay minerals (Figure3.4i). Distinguishing olivine and orthopyroxene pseudo phenocrysts are sometimes difficult. Only clinopyroxene and chrome-spinel remain as primary minerals. Clinopyroxene occurs as discrete crystals or glomerocrysts (Figure 3.4n-p). Summary of petrography is shown in Table 3.1.

3.4. Bulk chemistry

Whole-rock major elements, Ni, Y, Zr, Cr and V contents of 80 samples were analyzed by XRF (RIX3000, Rigaku Denki) at Niigata University. The analytical method is described in Takahashi and Shuto [1997]. Other trace and rare earth elements of 27 samples were analyzed by ICP-MS (Agilent 7500a ICP-MS) after Roser et al. [2000] at Niigata University. 10 samples from other localities are also analyzed. The results of major and trace element analyses are given in Appendix Table 1 and 2.

Zr contents of the V2 samples ranges from 9 to 87 ppm, indicating that these samples are highly variable from most primitive to most evolved. Zr contents of the LV2 samples range from 13 to 87 ppm, while that of the UV2 samples range from 9 to 15 ppm. Thus, the LV2 lavas have more evolved and variable feature than the UV2. Zr contents of the V2 samples well correlate with TiO_2 contents but form two trends on Zr-Al_2O_3, -P_2O_5, -Cr, -V and -Ni variation diagrams (Figure 3.5). The UV2 samples show rapid increasing incompatible element and decreasing compatible element contents with increasing Zr content than the LV2 samples. V contents of the UV2 are slightly lower than those of the LV2 at a given Zr content. The lava unit around 900 mab represented by '09vHil213' shows more evolved and enriched feature than the host LV2.

The LV2 samples have 1.4 to 2.6 ppm Yb contents and almost samples show in (La/Yb)n ratios ranging from 0.5 to 0.7 except for a basement sample attaining 1.6 (Figure 3.6b). The LV2 samples are divided into LREE-depleted ((La/Nd)n ratios: 0.7-0.8) and slightly LREE-enriched ((La/Nd)n ratios: 0.9-1.3). On the other hand, the UV2 has low Yb contents ranging from 1.0 to 1.2 ppm and a LREE-enriched typical U-shaped pattern ((La/Nd)n ratios: 1.4-2.7) (Figure 3.6a). The UV2 has negative Nb and Zr anomaly (Nb/Ta: 10-11; Zr/Hf: 28-30) than that of the LV1 (Nb/Ta: 13-17; Zr/Hf: 33-38).

The V2 samples from other area (Wadi Fizh and Wadi Yanbu) have similar composition to the LV2 samples (Figure 3.7). Their Zr content ranges from 32 to 49 ppm concentrating in typical LV2 samples of Suhayli-Hilti. None sample is plotted in the UV2 compositional field.

3.5. Mineral chemistry

Clinopyroxene phenocrysts and microphenocrysts from 10 samples, and Cr-spinel included in olivine pseudomorphs from 5 samples were analyzed by EPMA (JEOL JXA-8600SX) at Niigata University. The accelerating voltage was 15 kV, beam current was 1.3×10^{-8} A, and peak intensity was counted for 30 seconds. Correction procedures are followed ZAF-Oxide method. Representative clinopyroxene analyses are given in Appendix Table 3 and 4.

Mg# (= Mg/(Mg+Fe*) where Fe* is total Fe as FeO) of the V2 clinopyroxene ranges from 0.66 to 0.90, which is comparable to or more varied than the previous reports for the V2 rocks from the Oman ophiolite [Alabaster et al., 1982; Ernewein et al., 1988; Umino et al., 1990]. This is consistent with the wide Zr range of bulk rock compositions in this area as described above. Mg# of clinopyroxene ranges widely from 0.66 to 0.90 for the LV2, while the UV2 clinopyroxenes range from 0.85 to 0.90, implying that the UV2 is comparatively less-evolved and has a limited compositional range among the V2 lavas as like as the bulk rock compositions.

Analyses of the V2 sequence have a negative correlation between Mg# and TiO_2, and Na_2O, and positive correlation between Mg# and Wo (=100Ca/(Ca+Fe*+Mg)) (Figures 3.8a, d and e). Cr_2O_3 contents attaining 1.2 wt% decrease rapidly with decreasing Mg# (Figure 3.8c).

Moreover, it is noted that clinopyroxene of the UV2 is extremely depleted in TiO_2 and Na_2O contents (Figure 3.8a and d). Thus, the clinopyroxene of the LV2 and UV2 are apparently distinct as similar to whole rock compositions.

The LV2 samples contains high- (>0.8) and low-Mg# (<0.7) clinopyroxenes. Clinopyroxenes in one sample generally contain similar Mg# crystals, but '09vhil 259' at 163 mab contains both high- and low-Mg# clinopyroxenes. 1.2-mm minor diameter phenocryst shows low Mg#, while 0.4-mm minor diameter microphenocryst shows high Mg#. '10vhil217' at 1000 mab belonging to the LV2 has similar composition to the UV2 in high Mg# and Cr_2O_3, and low incompatible element contents. '09vhil 213' clinopyroxenes at 900 mab show high TiO_2 content similar to the V3 clinopyroxene (Figure 3.8a).

Cr# and Mg# of chrome-spinels in the '10vhil217' range from 0.72 to 0.75 and from 0.46 to 0.50, while these in the UV2 range from 0.66 to 0.77 and from 0.43 to 0.62, respectively. TiO_2 contents of the UV2 chrome-spinels are lower at a given Cr# indicating that the UV2 is more depleted than the '10vhil217' (Figure 3.9) though they have similar clinopyroxene composition.

3.6. Chemical Stratigraphy

Bulk-rock compositions shown above are examined in respect to the lithological stratigraphy. The lithological column and geochemical variations around the Wadi Hilti are illustrated in Figure 3.10.

The LV2 lava shows overall smooth variations (TiO_2: 0.5-0.8 wt%; Zr: 35-60 ppm; Ni: 25-51 ppm) except for few spikes around 2, 172, 527, 591, 900 and 1000 mab. The trace elements show wavy variation upward and roughly five times repentance between 0 and 200 (cycle 1), 200 and 440 (cycle 2), 440 and 660 (cycle 3), 660 and 800 (cycle 4), and 800 and 1010 (cycle 5) mab are recognized. Ti/V and Th/Nd ratios are approximately constant whole the LV2 but (La/Pr)n ratio shows a weak wavy profile upward. Lower part of the LV2 shows low-(La/Pr)n ratio (less than 1.0), while the upper LV2 shows repentance of low- and high-(La/Pr)n ratios (more than 1.0). Nb/Ta ratio also shows wavy profile similar to other trace elements. This fact indicates that the LV2 is composed of lavas derived from a heterogeneous source or variable degrees of partial melting. A whole rock compositional spike at 900 mab corresponds to the occurrence of the V3-like clinopyroxene. Lobate sheet flow at 630 mab shows low- and high-clinopyroxene Mg# due to plot of two samples from separate points. A pahoehoe lava flow at 163 mab containing high- and low- Mg# clinopyroxenes has 37 ppm Zr content. It may be an evidence of magma mixing, but more detailed analysis is needed.

The 1.0-m thick metalliferous sedimentary layer marks the sharp compositional gap between the LV2 and UV2. The UV2 has extremely low incompatible element and high compatible element contents (Zr: 9-15 ppm; Cr: 399-874 ppm). The UV2 exhibits more tight compositional profiles in incompatible elements and more broad compositional profiles in compatible element such as Ni and Cr than the LV2 samples, which shows zigzag profiles with low- and high-trace element content samples. Ti/V and Nb/Ta ratios of the UV2 are lower, and (La/Pr)n and Th/Nd ratios of the UV2 are higher than that of the LV2.

3.7. Discussion

3.7.1 Volcanic history during the V2 magmatism

Although approximately 25% of outcrop of the whole V2 section have no outcrop, the predominant occurrence of pahoehoe and lobate sheet flows indicate that the V2 volcanism erupted on the flat seafloor. The pahoehoe flow unit is dominated in the lower part of LV2, and often forms tumuli. Thin pahoehoe flows are limited under the lobate sheet flows as same flows. While the upper part of LV2 and the UV2 consist of lobate sheet flows, it is suggested that eruptions with large amount of lava flows occur on the more flat field as later V2 volcanism. These lobate sheet flows sometimes intercalate 1-5 cm thick sedimentary layers indicating shallow sea level and intermittent volcanisms. Occurrence of the cylindered conduit (Figure 3.3h) may suggests that the compression environment during the V2 magmatism [Umino et al., 1990].

Metalliferous sedimentary layer at 1010 mab divides the V2 to the LV2 and UV2, but is deformed and crosscut by shale under the V3 at northward in the study area. The local appearance of the UV2 might be erupted and emplaced in somewhere like a fault basin. The UV2 consists of pahoehoe and lobate sheet flows as like as the LV2, but lapilli and tuff appears on the top. This pyroclastic fall neither show grading or imbrication (Figure 3.3g). Therefore, it indicates that at least the end of V2 magmatism was formed by subaqueous strombolian eruption fed from a conduit near the study area.

After the deposition of 30-m thick shale, the V3 magmatism occurs through huge feeder dike intruding the V2 unit [Umino et al., 2009]. Because the feeder dike appears 1.8 km southward near from the study area, the branch might intrude into the V2 sequence at around 900 mab. Vesiculated umber might be produced by the heating from such branch.

3.7.2 Timing of the boninites eruption –comparison with other boninites

The V2 section in this area records two types of volcanism represented as the LV2 and UV2. The LV2 mainly consists of Pl-Ol-Cpx-Opx with aphyric basalts. Plagioclase and olivine phenocrysts constantly occur and frequently pyroxenes occur. The lower part of LV1 is richer in phenocryst contents than the upper. Orthopyroxene phenocryst often occurs but coexistence with clinopyroxene phenocryst is limited. Also, orthopyroxene phenocrysts are not contained in high-(La/Pr)n lavas. These mineral assemblages are responsible for the wavy compositional variations. The cycle 1 (0-200 mab) consists of Pl-Ol-Cpx type and relatively phenocryst rich, the cycle 2 (200-440 mab) consists of Pl-Ol and aphyric types. The cycle 3 (440-660 mab) consists of Pl-Ol-Cpx and Pl-Ol-Opx type and the cycle 4 (660-800 mab) consists of Pl-Ol-Cpx but the amount of phenocrysts is decreased. The cycle 5 (800-1010 mab) mainly consists of few phenocrysts of Ol-Cpx type.

The LV2 lavas are plotted in an island arc tholeiite (IAT) field on the discrimination diagram of TiO_2-10MnO-10P_2O_5 after Mullen [1983]. Since the V2 samples from other area also plotted in the IAT field, IAT would be the representative character of the V2 unit. As far as the lowest part of the V2 unit, southern area shows more LREE enriched pattern. As shown in Figure 3.7, (Pr/Nd)n ratios increase from Fizh through Yanbu to Hilti UV1. Because LREE enrichment is considered to be derived from a fluid mixing, it may be influenced by hydrothermal circulation after the V1 volcanism. The most large scale unconformity exposes at Wadi Ahin [Umino et al., 1990], 5 km southward, primary ophiolite nappe boundary might feed seawater or fluids preferentially.

The UV2 lavas are plotted in boninite field on the discrimination diagram of TiO_2-10MnO-10P_2O_5 after Mullen [1983]. Whole rock content has been modified by secondary alterations, but as reference value, SiO_2, MgO and CaO content of the UV1 ranges from 48 to 64, from 7.9 to 12, and from 5.4 to 18wt%, respectively. According to the definition of boninite, the UV2 lavas divided into high-Ca boninite similar to the Troodos ophiolite and N Tonga trench [Crawford et al., 1989; Falloon et al., 1989]. The UV2 rocks are distinguished from the LV2 in moderately to highly phyric features containing olivine phenocrysts with groundmass clinopyroxenes (Figure 3.4e-h).

Although occurrence of boninite has been reported at the northern Oman ophiolite [Umino et al., 1990; Ishikawa et al., 2002; Adachi and Miyashita, 2003], this is the first sequential evidence of boninite lava flows. The UV2 overlays on the LV2 after a short rest of magmatism and has produced at least 140-m thick lava flows with a pyroclastic fall. These lines of evidence indicate that the boninitic magmatism occurred after island arc tholeiitic magmatism, as the end of the V2 magmatism. At the Tonga Arc, arc basalts cover the boninite [Cooper et al., 2010], but no arc volcanisms are represented in this area after the boninitic volcanism. Therefore, paleo geological setting seems to be different from that of the modern Tonga arc.

3.7.3 Difference between the V1 and V2 lavas

The V1 and V2 units have tend to be distinguished from the geochemical evidence [Alabaster et al., 1982; Lippard et al., 1986; Ernewein et al., 1988; Godard et al., 2003], but this study revealed that their whole rock and mineral compositions of the V1 less-evolved and the V2 rocks sometimes overlap each other. Especially the V1 lavas have large compositional variations due to on- and off-axis magmatism (see chapter 1), and along-axis variation (see chapter 2), we need to use extreme care in handling.

As mentioned in chapter 1, the useful indexes for comparing the V1 and V2 lavas are whole rock trace element and clinopyroxene compositions. Clinopyroxene TiO_2 and Na_2O contents of the V2 are lower than that of the V1 at a given clinopyroxene Mg# (Figure 3.11). Even the low-Mg# V1 samples (Zabin and Ghayth) decreasing TiO_2 or Na_2O due to crystallization of Fe-Ti oxide show higher concentration than V2 clinopyroxenes. But some analyses overlap between the V1 and V2 especially Mg#>0.8. In the most less-evolved samples both the V1 and V2 pyroxenes have lower contents in TiO_2 or Na_2O at Mg#>0.8. Moreover, because a lot of clinopyroxenes show sector zoning and/or normal zoning and such crystals tend to concentrate high TiO_2 or Na_2O, the compositional field becomes broad and finally overlaps. Some V2 samples suggesting magma mixing for their generation process might give a spread variation. Considering the along-axis compositional variations, the V1 lavas at the segment center experienced higher degree of melting show lower concentrations than other area.

It is difficult to distinguish the V1 and V2 lava in whole rock immobile element composition such as HFS elements. However, Zr-variation diagram with (Nd/Yb)n ratio gives an apparent distinction between the V1 and V2 lavas in Fizh, but Ghayth sample partly overlap with the V2 lavas (Figure 3.12). These lavas intercalated in the V1, and may be generated from mantle heterogeneity or relatively higher degree of partial melting. Nb/Ta-Zr/Hf ratio diagram shows overlapping with the V1 and V2 lavas. Particularly Thuqubah, Ghayth and off-ridge Fizh lava are plotted in the V2 field. Although Nb anomaly generally used for comparing arc component between the V1 and V2 [e.g. Godard et al., 2003], this result indicate that we need to multi-sided considerations to distinguish the V1 and V2 lavas.

3.8. Conclusions

This is the first thorough description of the approximately whole V2 unit around the junction of Wadi Suhayli and Hilti, and shows detailed stratigraphic variation in terms of lithology and geochemistry. The 1150-m thick V2 consists of the 1010-m thick LV2 and 140-m thick UV2. The LV2 shows island arc tholeiitic character based on their petrology and geochemistry, while the UV2 contains abundant olivine phenocrysts and shows boninitic feature. The stratigraphy indicates that boninite had erupted after the tholeiitic volcanism and terminated the V2 magmatism in this area. This discovery gives a new constraint for the petrogenesis of the V2 magmatism.

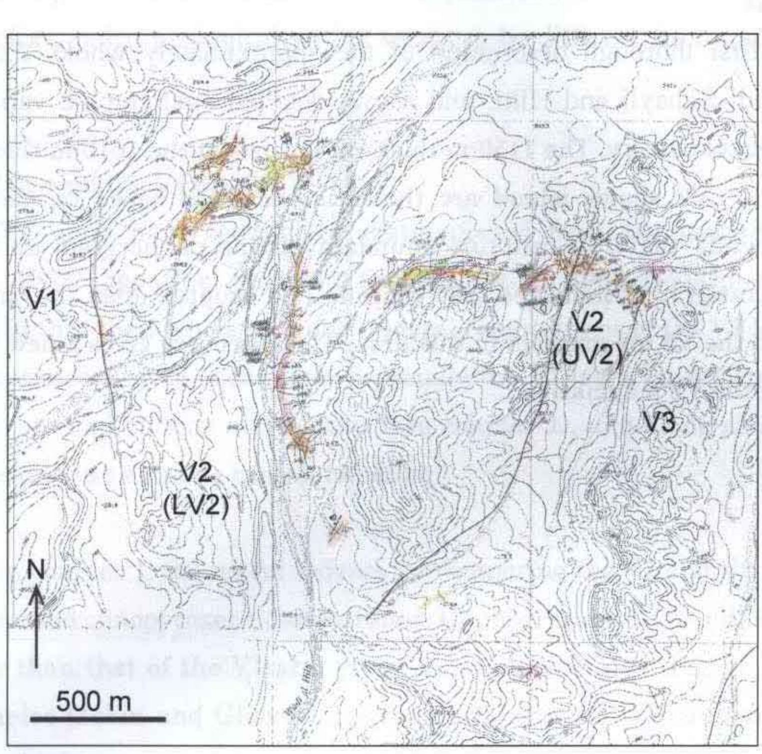

Figure 3.1 Geological map along Wadi Suhayli and Hilti.

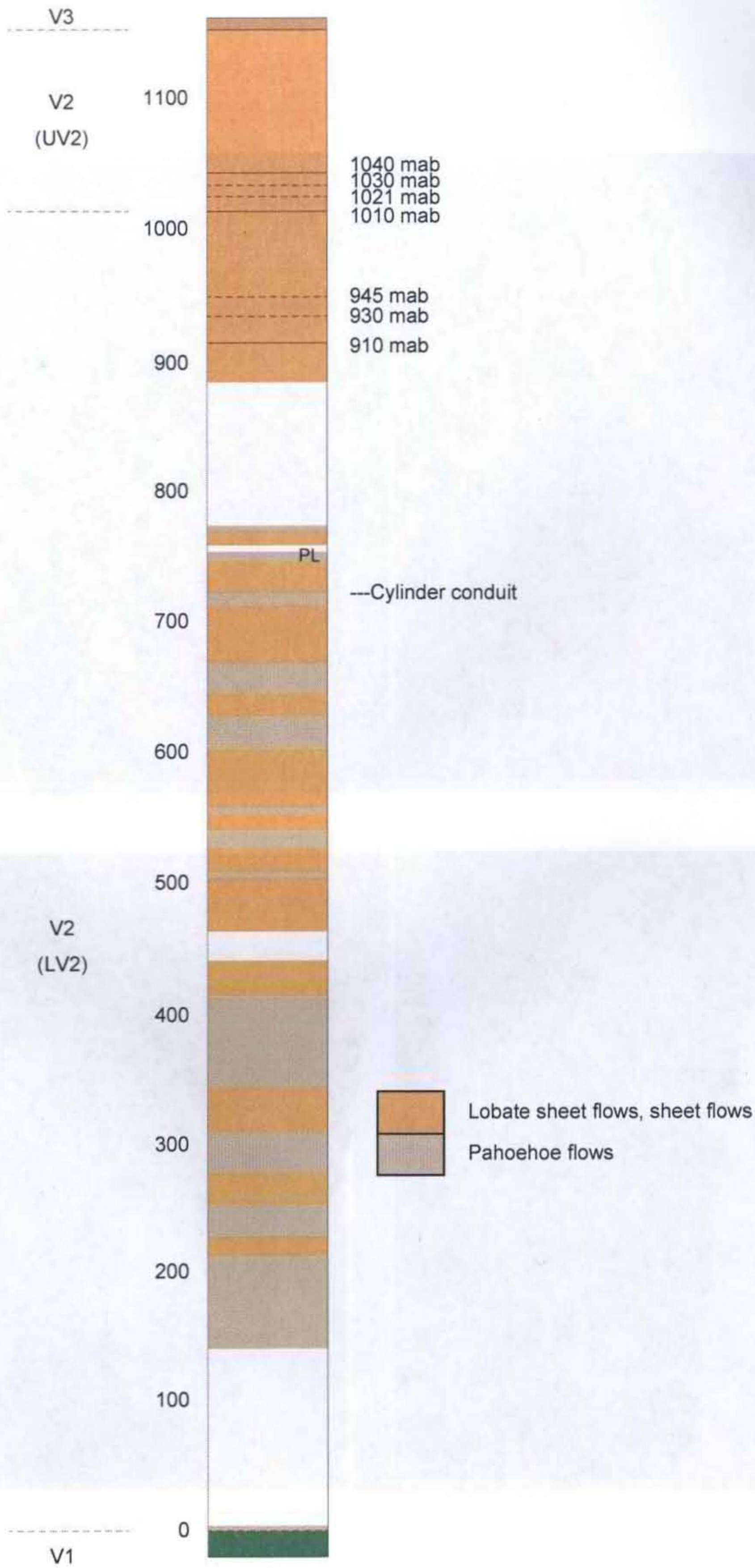

Figure 3.2 Stratigraphic column of the V2 sequence along intersection of Wadi Suhayli and Hilti. Broken lines indicate boundaries of each sequence.

Figure 3.3 Representative lava morphology and lithofacies. (a) Lobate sheet flows around 511 mab. 2-m thick jointed sheet flows gently change the dip in laterally. (b) Occurrence of tumuli around 380 mab. (c) Lobate sheet flows are sometimes underlain by pahoehoe flows. At 630 mab, a hollow appears in pahoehoe flows. (d) Occurrence of pahoehoe flows with thick crust. The coarse core is eroded.

Figure 3.3 Representative lava morphology and lithofacies. (e) Pyroclastic rock piles up at the top of V2. Red volcanic rock fragment and tuff are contained in the layer. (f) UV2 has limited occurrence due to erosion. (g) V3 intrusion at 910 mab. Metalliferous sediments are branched to thin layer. (h) Cylinder conduit in the V2 section.

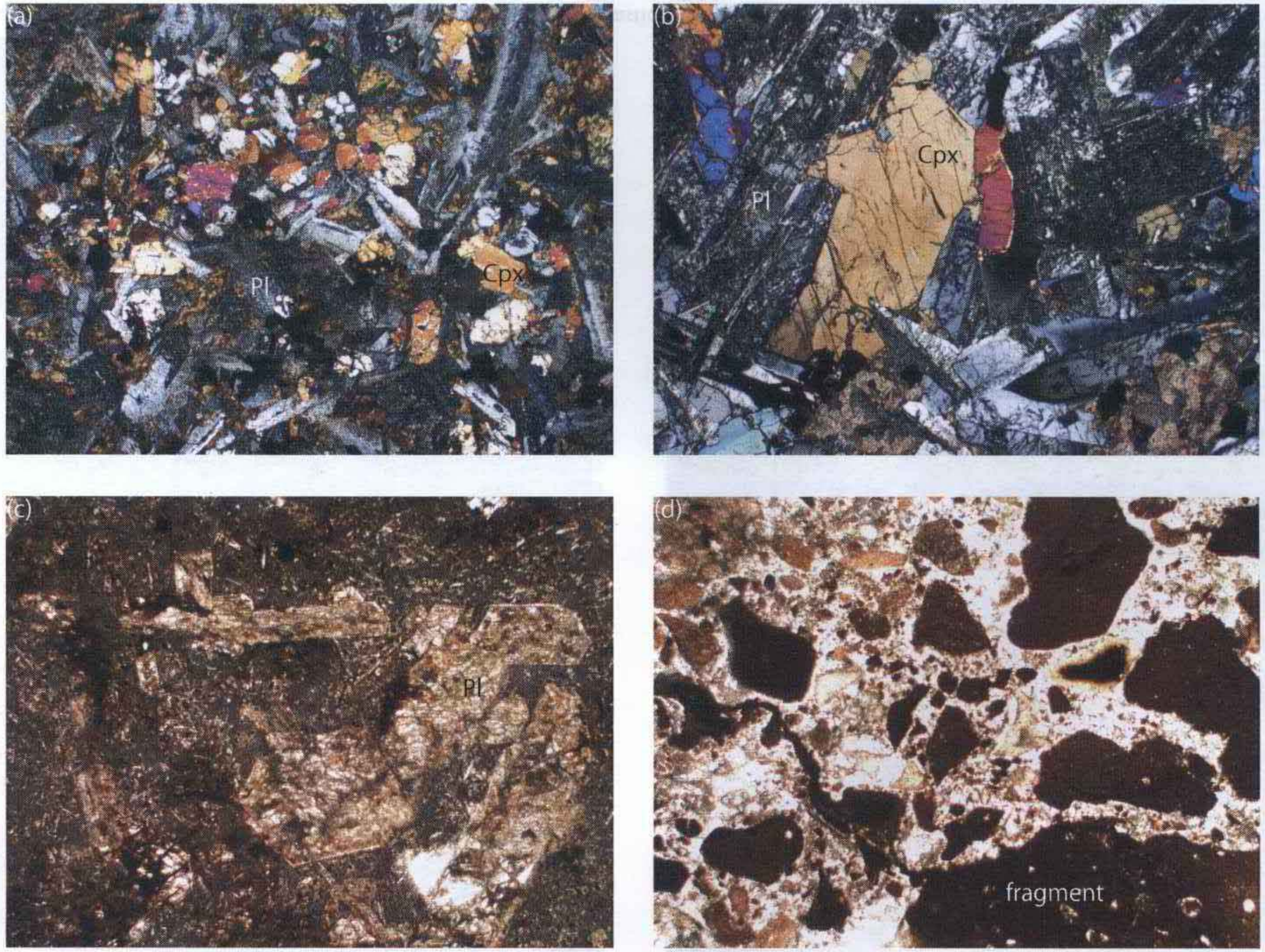

Width: 4.5 mm

Figure 3.4 Microphotographs of flows and dikes. (a) Doleritic texture of the V3 basalts. (b) Coarse grained Pl-Cpx type of 09vHil213. (c) Plagioclase phenocrysts occur at the chilled margin of intrusion at 910 mab. (d) Pyroclastic rock contains basalt fragments and colored minerals. Pl: plagioclase; Cpx: clinopyroxene; Ves: vesicle.

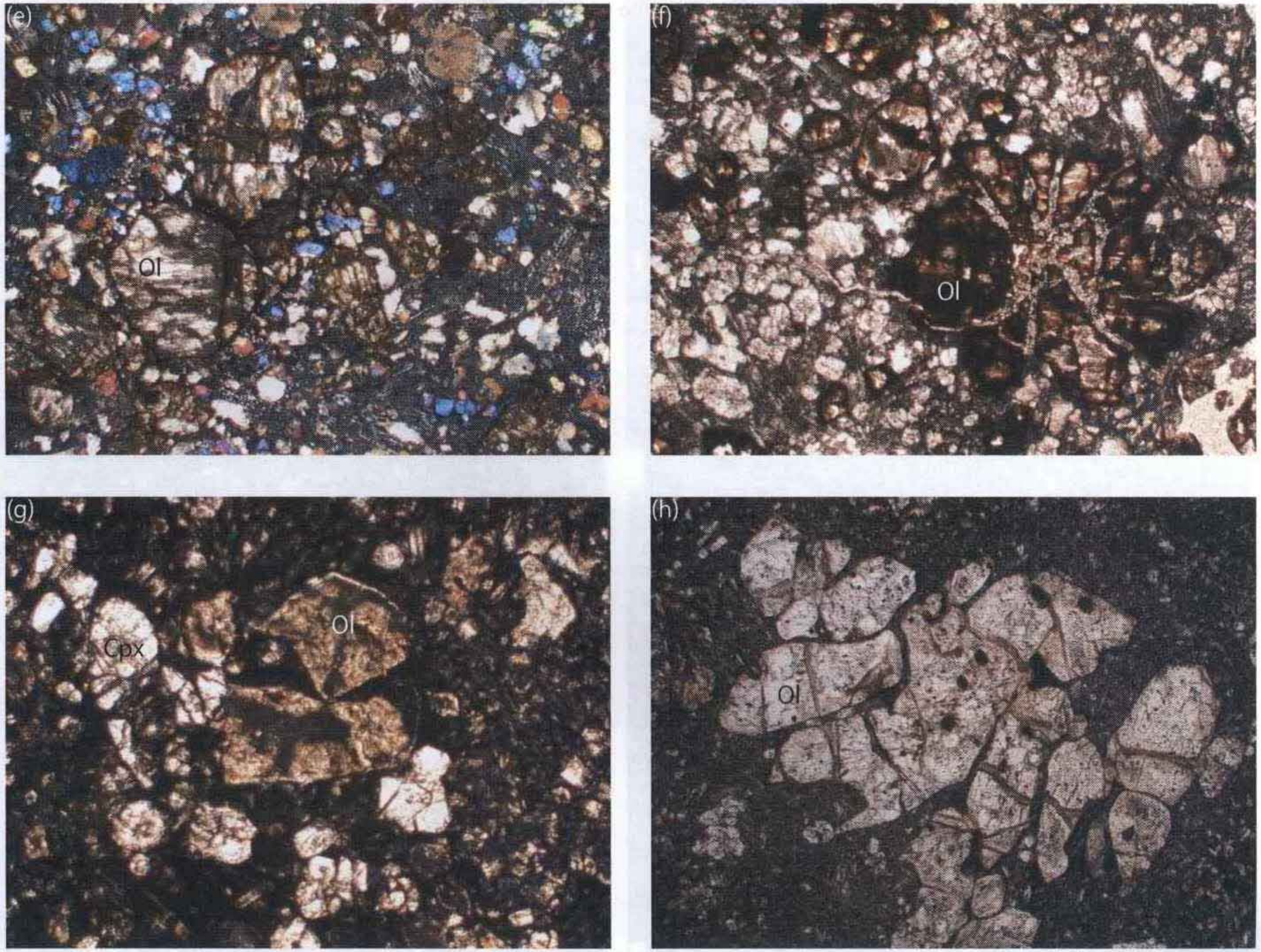

Width: 4.5 mm

Figure 3.4 Microphotographs of flows and dikes. (e) The UV2 contains olivine phenocrysts (10vHil203). Many clinopyroxenes occur in groundmass. (f) Olivine sometimes occurs like a jigsaw puzzle (10vHil204). (g) Fine grained UV2 contains olivine and clinopyroxene phenocrysts (10vHil209). (h) Olivines sometimes appear as glomerocryst. Olivine pseudomorphs frequently contain chrome-spinels (10vHil216). Ol: olivine; Pl: plagioclase; Cpx: clinopyroxene; Ves: vesicle.

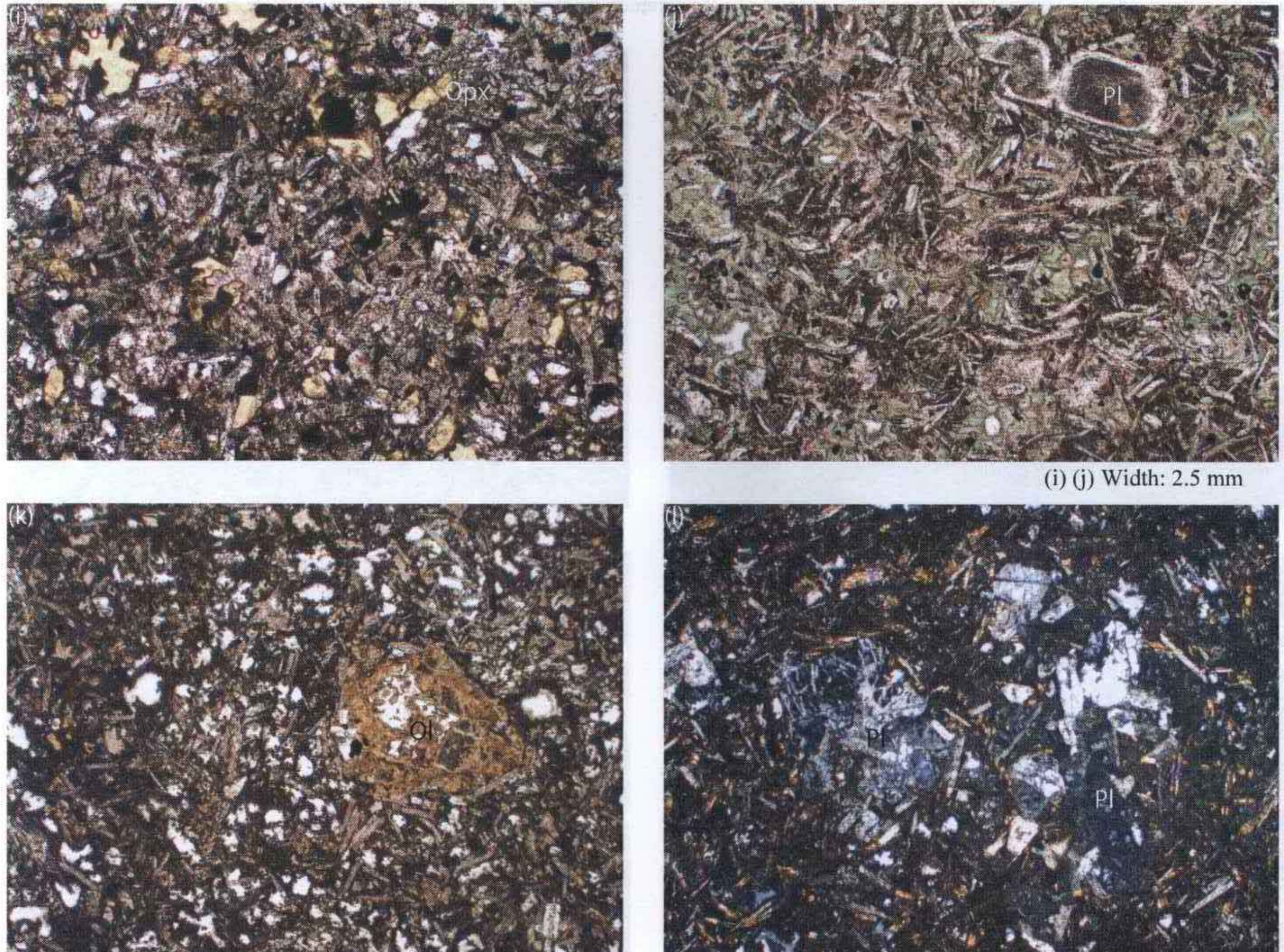

(i) (j) Width: 2.5 mm

(k) (l) Width: 4.5 mm

Figure 3.4 Microphotographs of flows and dikes. (i) Aphyric type of 09vHil238. Orthopyroxene altered to clay minerals or talc often appears at groundmass. (j) Pl-phyric type of 09vHil232. (k) Olivine has replaced clay minerals (09vHil241). (l) Plagioclase glomerocryst of 09vHil241. Ol: olivine; Pl: plagioclase; Cpx: clinopyroxene; Opx: orthopyroxene; Ves: vesicle.

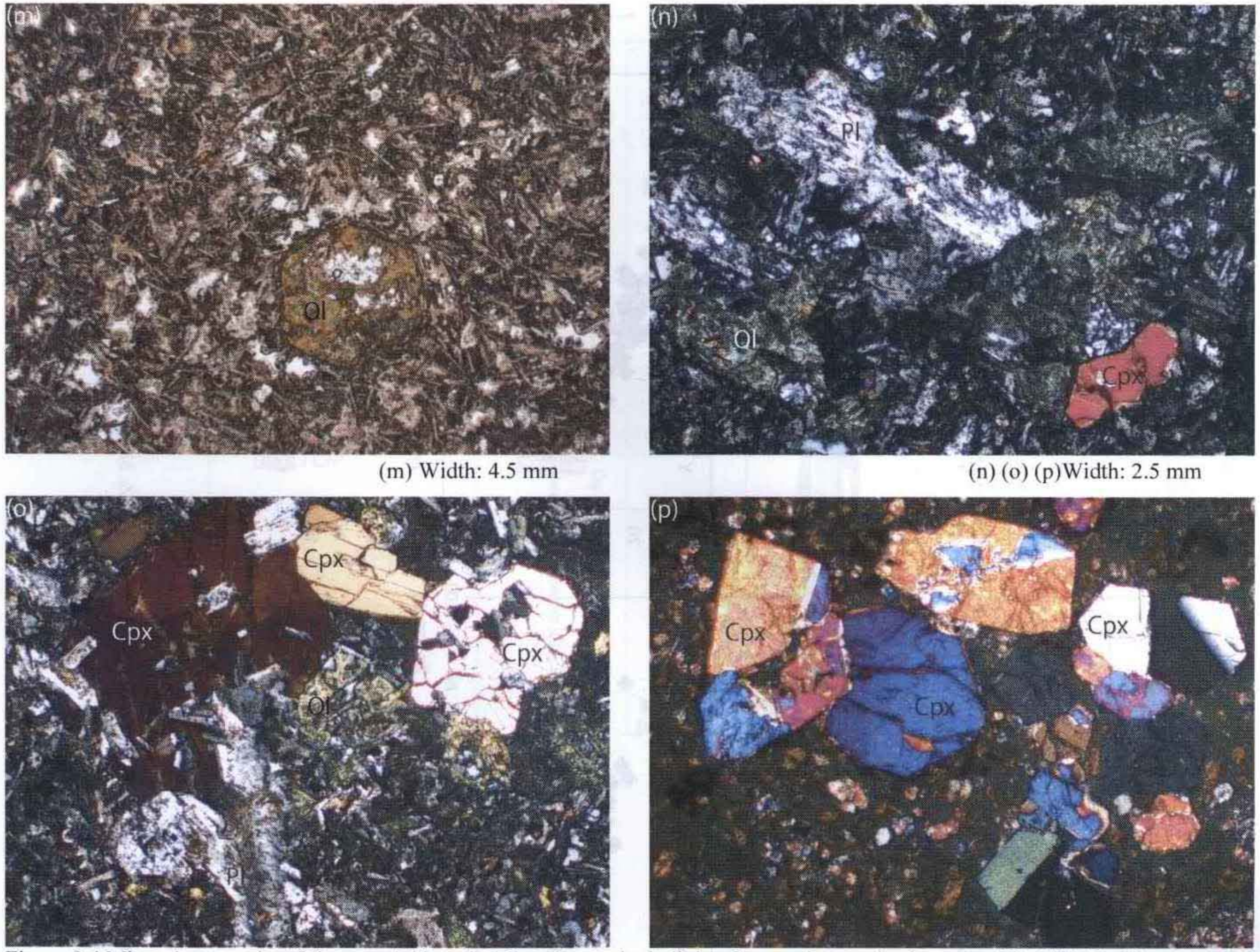

Figure 3.4 Microphotographs of flows and dikes. (m) Pseudomorphed olivine frequently remains hexagon (09vHil226). (n) Pl-Ol-Cpx-phyric type of 09vHil256. Olivine phenocrysts are replaced by chlorite. (o) Clinopyroxene phenocrysts sometimes show sector zoning (09vHil256). (p) Clinopyroxene phenocrysts in the basement flow of the V2 (10Sh21). Ol: olivine; Pl: plagioclase; Cpx: clinopyroxene; Ves: vesicle.

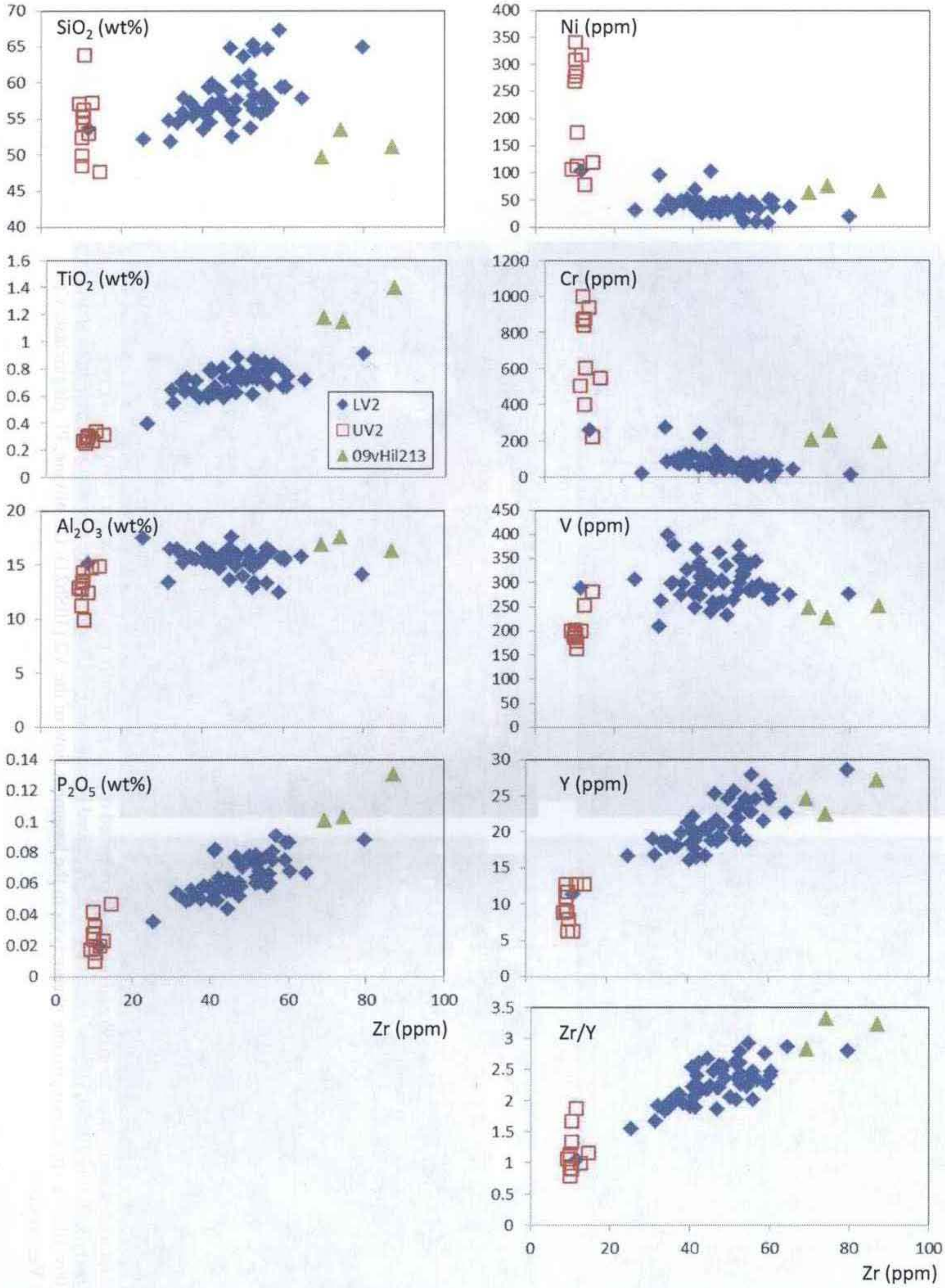

Figure 3.5 SiO_2, TiO_2, Al_2O_3, P_2O_5, Ni, Cr, V, Y and Zr/Y ratios plotted against Zr. SiO_2, TiO_2, Al_2O_3 and P_2O_5 are based on an anhydrous basis.

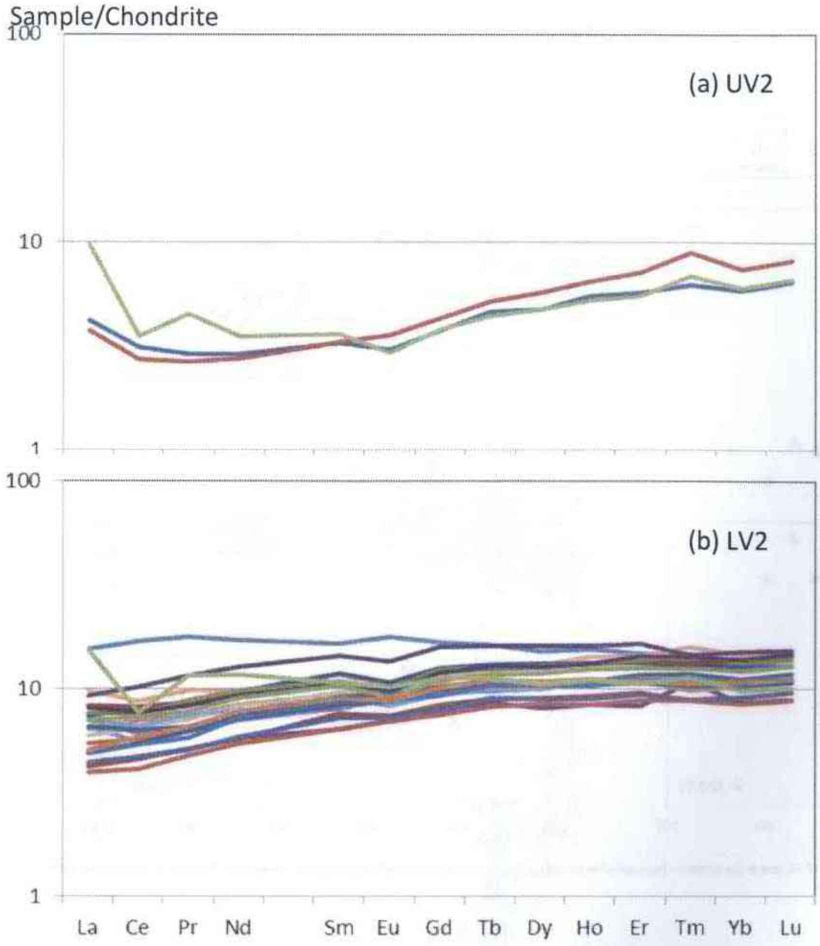

Figure 3.6 Chondrite-normalized REE patterns for UV2 (a) and LV2 sequence (b). The chondrite value is after Sun and McDonough [1989].

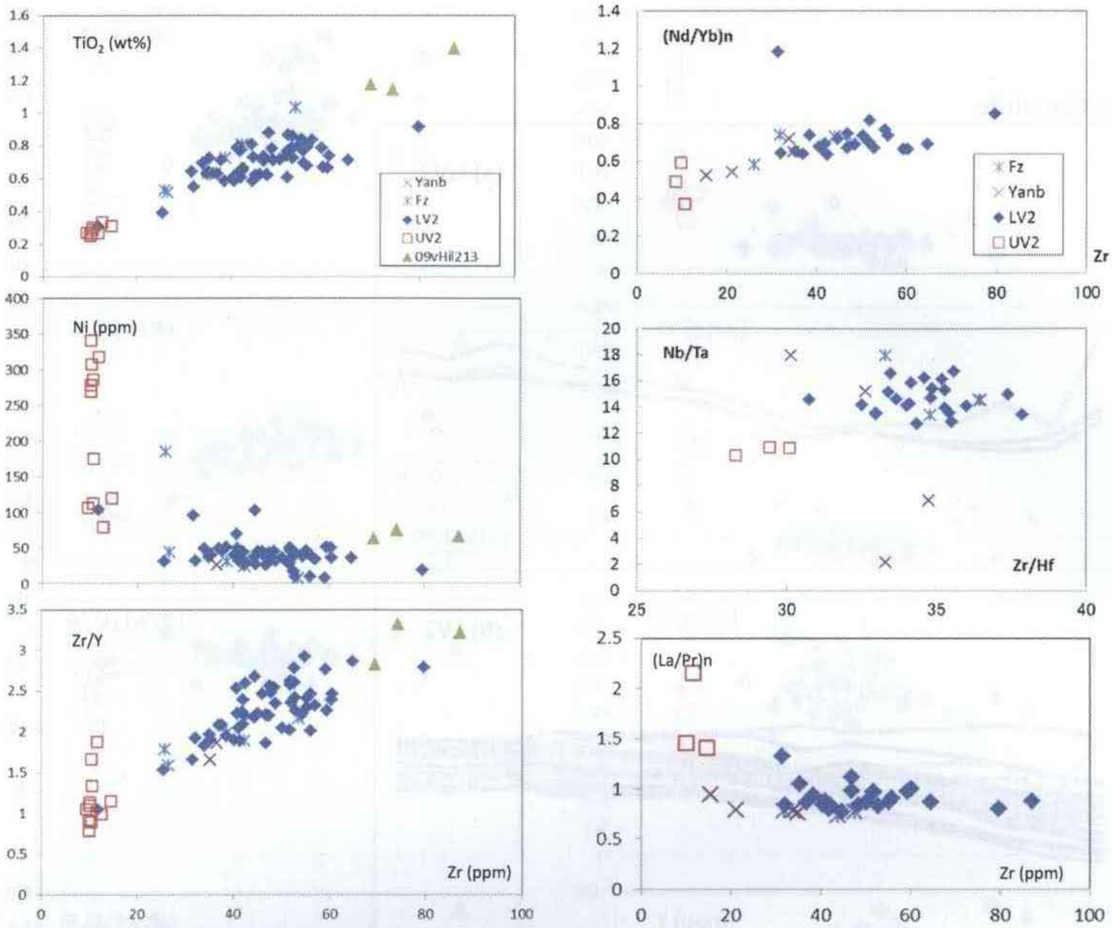

Figure 3.7 TiO$_2$, Ni, Zr/Y and chondrite normarized Nd/Yb ratios of V2 lava in the northern Oman ophiolite plotted against Zr. Nb/Ta versus Zr/Hf ratios are also shown. TiO$_2$ is based on an anhydrous basis.

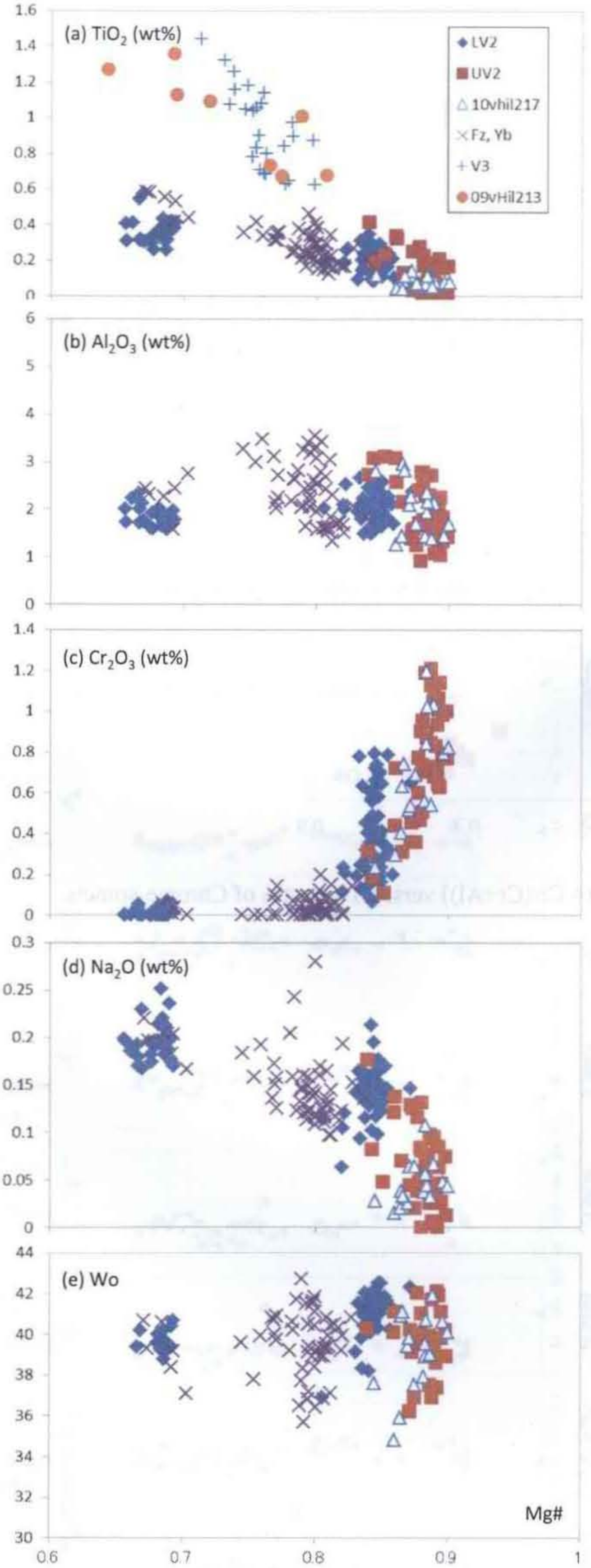

Figure 3.8 Clinopyroxexe Mg# versus (a) TiO_2, (b) Al_2O_3, (c) Cr_2O_3, (d) Na_2O and (e) Wo mol%.

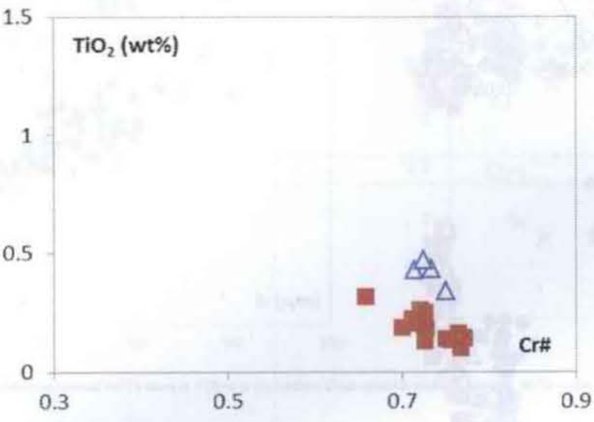

Figure 3.9 Plots of Cr# (= Cr/(Cr+Al)) versus TiO_2 wt% of Chrome-spinels.

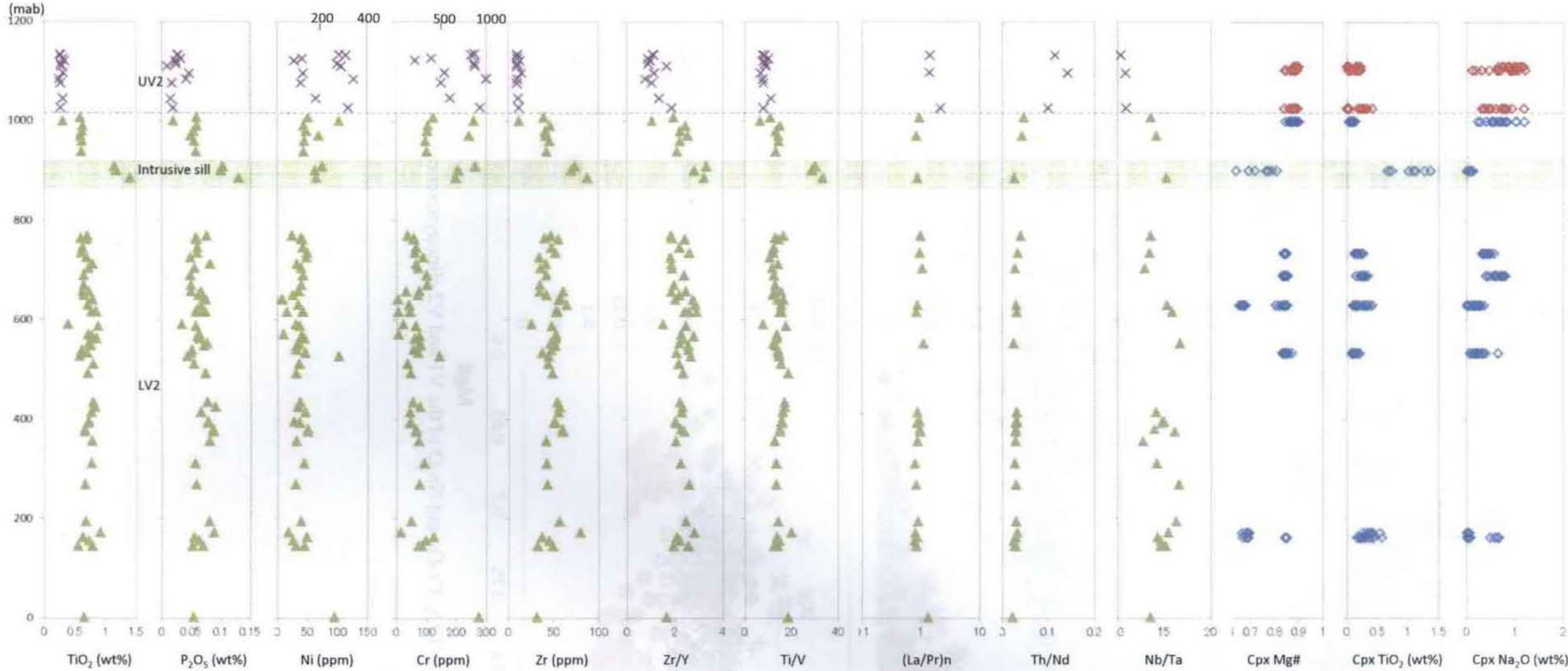

Figure 3.10 Stratigraphic variations of selected bulk-rock TiO_2, P_2O_5, Ni, Cr, Zr, Zr/Y, Ti/V, (La/Pr)n, Th/Nd, Nb/Ta and clinopyroxene Mg#, TiO_2 and Na_2O. Ni and Cr contents of UV2 samples shown in upper. See text for explanation.

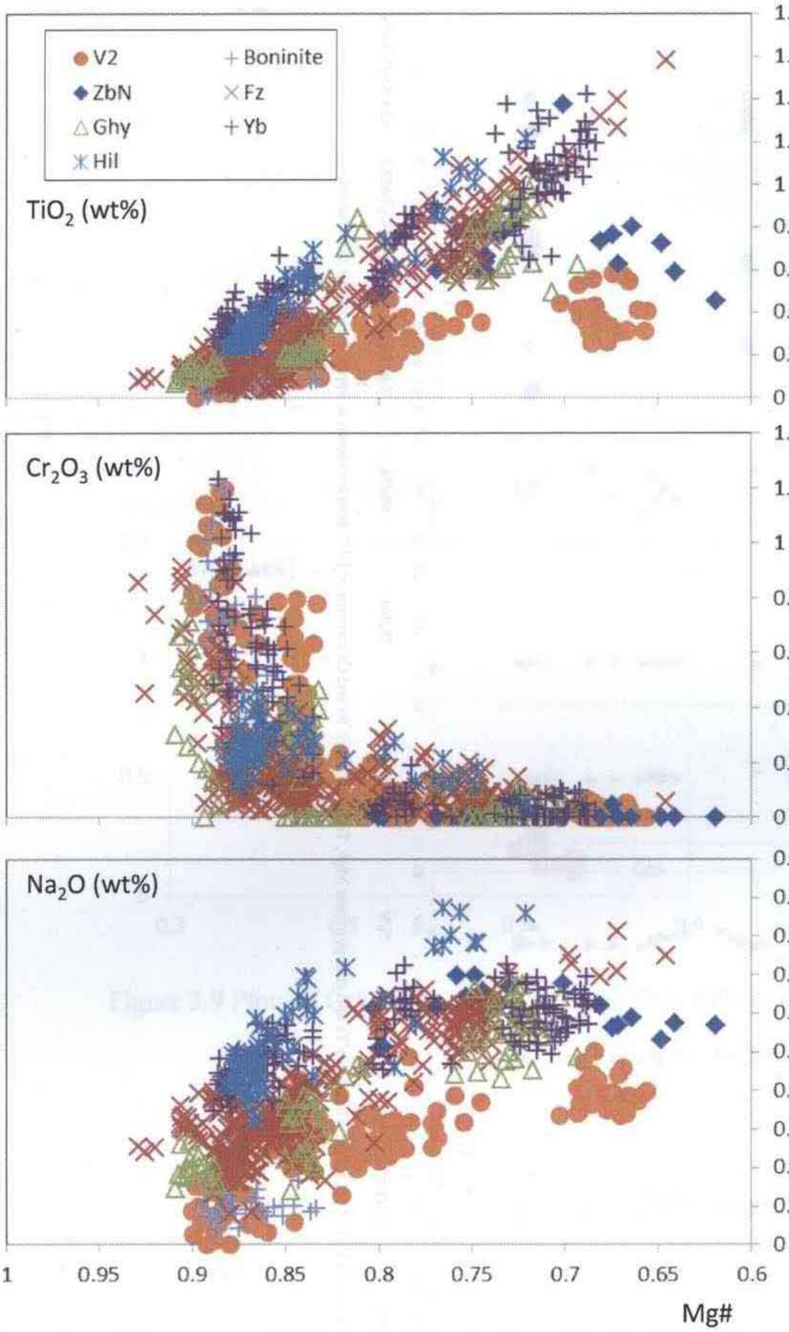

Figure 3.11 Clinopyroxexe Mg# versus TiO_2, Cr_2O_3 and Na_2O of the V1 and V2 clinopyroxenes.

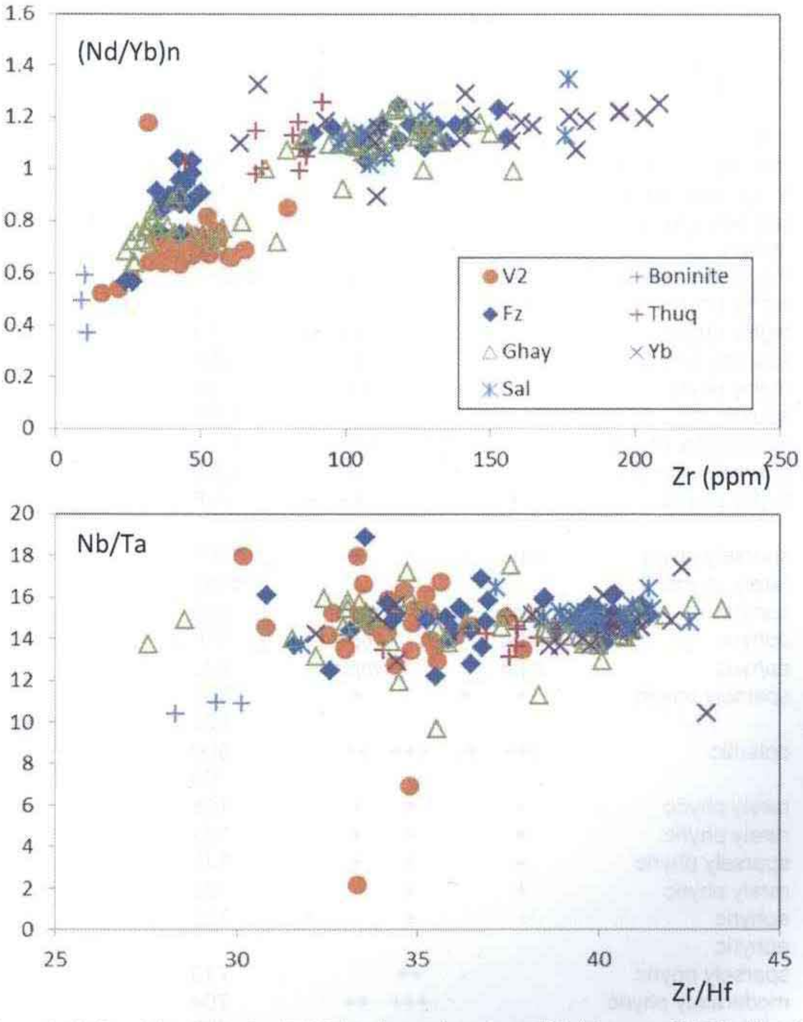

Figure 3.12 Chondrite normarized Nd/Yb ratios against Zr, and Nb/Ta versus Zr/Hf ratios of the V1 and V2 rocks.

Table 3.1 Locations, mode of occurrences and phenocryst assemblages of the Wadi Hilti V2 lava flows and dikes. Pl: plagioclase; Ol: olivine; Cpx: clinopyroxene; Opx: orthopyroxene; Sp: Chrome-spinel.

sample No.	Mode of occurrence	Mineral assemblages	Cpx	Opx	Pl	Ol	Sp	mab
UV2								
09vHil201	pillow lavas	highly phyric	++	+	++	+++		
09vHil202	pillow lavas	moderately phyric	+	+		+++		
10vHil201	pyroclastic rock							1149.5
10vHil203	pahoehoe flows	moderately phyric		+		++		1141
10vHil204	sheet flows	moderately phyric	+			++		1136
10vHil205	sheet flows	moderately phyric	++	++	+	++		1132
10vHil206	sheet flows	sparsely phyric				+		1125
10vHil207	pahoehoe flows	aphyric						1120
10vHil208	pahoehoe flows	moderately phyric				++		1115
10vHil209	pahoehoe flows	highly phyric	++			+++	+	1110
10vHil210	sheet flows	highly phyric	+++		++	+++	++	1103
10vHil211	sheet flows	sparsely phyric	+			+		1096
10vHil212	pahoehoe flows	highly phyric	+			++		1084
10vHil213	pahoehoe flows	aphyric						1075
10vHil214	sheet flows	moderately phyric				+++		1063
10vHil215	pahoehoe flows	sparsely phyric				+		1045
10vHil216	sheet flows	highly phyric	++			+++	++	1026
LV2								
09vHil206	sheet flows	sparsely phyric	mph	-	+	+		1007
09vHil207	sheet flows	rarely phyric				+		990
09vHil208	sheet flows	aphyric	mph			mph		980
09vHil209	sheet flows	aphyric	mph			mph		970
09vHil210	sheet flows	aphyric	mph			mph		960
09vHil211	sheet flows	sparsely phyric	+	+		+		938
09vHil212	pl-rich lava							926
09vHil213	sheet flows	doleritic	+++	++	+++	++		900
09vHil214	pahoehoe flows							769
09vHil215	massive	rarely phyric	+		+	+		765
09vHil216	massive	rarely phyric	+		+	+		762
09vHil217	pillow lavas	sparsely phyric	+		+	+		745
09vHil218	sheet flows	rarely phyric	+		+			735
09vHil219	pillow lavas	aphyric			+		+	725
09vHil220	pillow lavas	aphyric						
09vHil221	sheet flows	sparsely phyric		-	++			713
09vHil222	sheet flows	moderately phyric			+++	++		704
09vHil223	sheet flows	rarely phyric	+			+		690
09vHil224	sheet flows	sparsely phyric	+	-	++	+	+	670
09vHil225	pahoehoe flows	aphyric			mph	mph		657
09vHil226	pahoehoe flows	sparsely phyric	+		+++	++		650
09vHil227	sheet flows	sparsely phyric	+	+		+		640
09vHil228	pahoehoe flows	sparsely phyric	++	++	+	+		630
09vHil229	pahoehoe flows	aphyric	+			+		615
09vHil230		aphyric						591
09vHil231	sheet flows	rarely phyric	+			+	+	570
09vHil232	pillow lavas	rarely phyric	mph		+			657
09vHil233	sheet flows	sparsely phyric	+	+		+	+	640
09vHil234	sheet flows	sparsely phyric	+	+	+	+		630
09vHil236	sheet flows	rarely phyric		-		+		615
09vHil237	sheet flows	aphyric				mph		615
09vHil238	sheet flows	aphyric		-				587
09vHil239	sheet flows	sparsely phyric		-	++	++	+	567
09vHil240	pillow lavas	sparsely phyric	mph		+	+	+	562
09vHil241	sheet flows	sparsely phyric		-	++	+		553
09vHil242	pahoehoe flows	sparsely phyric		+	+++	++		548
09vHil243	sheet flows	sparsely phyric	+	+	++	+		540
09vHil244	sheet flows	sparsely phyric	+++		++	++		534
09vHil245	sheet flows	aphyric						435
09vHil246	sheet flows	aphyric						425
09vHil247	sheet flows	aphyric			mph			414
09vHil248	pahoehoe flows	aphyric			mph			396
09vHil249	pahoehoe flows	sparsely phyric	+			+		393
09vHil250	pahoehoe flows	aphyric						380

(continued)

sampleNo.	Mode of occurrence	Mineral assemblages	Cpx	Opx	Pl	Ol	Sp	mab
09vHil251	pahoehoe flows	moderately phyric			+++	++		375
09vHil252	pahoehoe flows	moderately phyric			+++	+		357
09vHil253	sheet flows	sparsely phyric		+	++	++		312
09vHil254	sheet flows	moderately phyric	mph		+++	+		269
09vHil255	pahoehoe flows	sparsely phyric	+	+	+	+		195
09vHil256	pahoehoe flows	sparsely phyric	+++		++	+		172
09vHil257	pahoehoe flows	sparsely phyric	mph	+	+	+		145
09vHil258	pahoehoe flows	sparsely phyric	+		++	++		155
09vHil259	pahoehoe flows	sparsely phyric	+		+++	++		163
09vHil260	pahoehoe flows	sparsely phyric	+		+	++		145
10vHil217	sheet flows	aphyric	mph			mph	+	1000
10vHil218	9-213 sheet flows	highly phyric	++		+++			909
10vHil219	9-213 sheet flows	doleritic	++		+++			885
10vHil220	sheet flows	rarely phyric	+					511
10vHil221	pahoehoe flows	aphyric						492
10vHil222	see pictures	moderately phyric	+		+	mph		527
10Sh 21	pahoehoe flows	sparsely phyric	++					2

Acknowledgments

I deeply appreciated to my supervisor Prof. S. Miyashita for giving me the great theme and dairy encouragement, and discussing everything. I appreciated to Prof. S. Umino (Kanazawa University) for giving a lot of advice about field survey and volcanology. I also deeply thank to Dr. Y. Adachi (Niigata University) for discussing my study and analyzing geochemical compositions.

I thank to Hilal Al Azri, Salim Hamaed Al-Busaidi, Durair A'shaikh, Mohamed Alaraimi (Ministry of Commerce and Industry of Oman), Y. Shibata (Mitsubishi Material Techno CO.), and Japanese Embassy in Oman for their kind supports during field survey.

I thank Dr. N. Tsuchiya (Iwate Univ.), Dr. T. Hiraga (Univ. of Tokyo), Ms. A. Akimoto (Asaka Riken Inc.), Mr. S. Tanaka, Mr. T. Hashimoto (Toshiba Home Tech. Co.), Mr. Y. Nogawa (Mitsubishi Material Techno Co.), Mr. R. Kaneko, Mr. K. Yoshida (Niigata University) and Ms. M. Hayashi (Foster Elec. Co., Ltd.) for helpful field working. I am also imbedded Drs. E. Takazawa, N. Fujibayashi, T. Kurihara and Mr. K. Hara (Niigata Univ.) for fruitful discussions. Thoughtful reviews by S.M. White and anonymous referee greatly improved this manuscript.

I would like to thank my parents and grandparents for all their help and encouragement during six years.

This study was supported by Sasagawa Scientific Research Grant from The Japan Science Society (21-711M) and Institute of Science and Technology Research Grant from the Niigata University (2010, 2011).

Reference list

Adachi, Y. and S. Miyashita (2003), Geology and petrology of the plutonic complexes in the Wadi Fizh area: Multiple magmatic events and segment structure in the northern Oman ophiolite., *Geochem. Geophys. Geosyst.*, 4, 8619, doi:10.1029/2001GC000272.

Alabaster, T., J.A. Pearce, and J. Malpas (1982), The volcanic stratigraphy and petrogenesis of the Oman ophiolite complex, *Contrib. Mineral. Petrol.*, 81, 168-183.

Alt, J.C. and J. Honnorez (1984), Alteration of the upper oceanic crust, DSDP site 417: Mineralogy and chemistry, *Contrib. Mineral. Petrol.*, 87, 149-169.

A'Shaikh, D., S. Miyashita, and H. Matsueda (2005), The petrological and geochemical characteristics of an ophiolite volcanic suite from the Ghayth area of Oman, *Jour. Mineral. Petrol. Sci.*, 100, 202-220.

Auzende, J.-M., V. Ballu, R. Batiza, D. Bideau, J.-L. Charlou, M.H. Cormier, Y. Fouquet, P. Geistdoerfer, Y. Lagabrielle, J. Sinton, and P. spadea (1996), Recent tectonic, magmatic, and hydrothermal activity on the East Pacific Rise between 17°S and 19°S: Submersible observations, *J. Geophys. Res.*, 101, 17995 – 18010.

Ballard, R.D., R.T. Holcomb, and T.H. van Andel (1979), The Galapagos Rift at 86°W: 3. Sheet flows, collapse pits, and lava lakes of the rift valley. *J. Geophys. Res.*, 84, 5407 - 5422.

Basaltic Volcanism Study Project (1981), *Basaltic Volcanism on the Terrestrial Planets.* Pergamon Press, Inc., New York. pp. 1286.

Batiza, R., Y. Niu, J.L. Karsten, W. Boger, E. Potts, L. Norby, and R. Butlar (1996), Steady and non-steady state magma chambers below the East Pacific Rise, *Geophys. Res. Lett.*, 23, 221-224.

Batiza, R., and J.D.L. White (2000), Submarine lavas and hyaloclastite, in *Encyclopedia of Volcanoes*. Academic Press, pp. 1000.

Blacic, T.M., G. Ito, J.P. Canales, R.S. Detrick, and J. Sinton (2004), Constructing the crust along the Galapagos Spreading Center 91.3°-95.5°W: Correlation of seismic layer 2A with axial magma lens and topographic characteristics, *J. Geophys. Res.*, 109, B10310, doi:10.1029/2004JB003066.

Boudier, F., G. Ceuleneer, and A. Nicolas (1988), Shear zones, thrusts and related magmatism in the Oman Ophiolite; initiation of thrusting on an oceanic ridge, *Tectonophysics*, 151, 275-296.

Canales, J.P., R.S. Detrick, D.R. Toomey, and W.S.D. Wilcock (2003), Segment-scale variations in the crustal structure of 150-300 kyr old fast spreading oceanic crust (East Pacific Rise, 8°15'N-10 (5'N) from wide-angle seismic refraction profiles, *Geophys. J. Int.*, 152, 794-799.

Coish, R.A. and L.A. Taylor (1979), The Effects of Cooling Rate on Texture and Pyroxene Chemistry in DSDP leg 34 Basalt: A Microprobe Study, *Earth Planet. Sci, Lett.*, 42, 389-398.

Cooper, L.B., T. Plank, R. J. Arculus, E.H. Hauri, P.S. Hall, and S.W. Parman (2010), High‐Ca boninites from the active Tonga Arc, *J. Geophys. Res.,*115, B10206, doi:10.1029/2009JB006367.

Crawford, A. J., T. J. Falloon, and D. H. Green (1989), Classification, petrogenesis and tectonic setting of boninites, in *Boninites and Related Rocks*, edited by A. J. Crawford, pp. 1–49, Unwin Hyman, London.

Crispini, L., P. Tartarotti, and S. Umino (2006), Microstructural features of a subaqueous lava from basaltic crust off the East Pacific Rise (ODP Site 1256, Cocos Plate), *Ofioliti*, 31, 117-127.

Dowry, E. (1976), Crystal structure and crystal growth: I I. sector zoning in minerals. *Am. Mineral.*, 61, 460-469.

Einaudi, F., M. Godard, P. Pezard, J.-J. Cocheme, T. Brewer, P. Hrvey, and C. Coulon (2003), Magmatic cycles and formation of the upper oceanic crust at spreading centers: geochemical study of a continuous extrusive section in the Oman ophiolite, *Geochem. Geophys. Geosyst.*, 4, 8608, doi:10.1029/2002GC000362.

Einaudi, F., P. Pezard, J.-J. Cocheme, T. Brewer, P. Hrvey, C. Coulon, C. Laverne, and M. Godard (2000), Petrography, geochemistry and physical properties of a continuous extrusive section from the Sarami massif, Semail ophiolite, *Mar. Geophys. Res.*, 21, 387-407.

Engels, J.L., M.H. Edwards, D.J. Fornari, M.R. Perfit, and J.R. Cann (2003), A new model for submarine volcanic collapse formation. *Geochem. Geophys. Geosyst.*, 4, 1077, doi:10.1029/2002GC000483.

Ernewin, M., C. Pflumio, and H. Whitechurch (1988), The death of an accretion zone as evidenced by the magmatic history of the Sumail ophiolite (Oman), *Tectonophysics*, 151, 247-274.

Falloon, T. J., D. H. Green, and M. T. McCulloch (1989), Petrogenesis of high‐Mg and associated lavas from the north Tonga Trench, in *Boninites and Related Rocks*, edited by A. J. Crawford, pp. 357–395, Unwin Hyman, London.

Fundis, A.T., S.A. Soule, D.J. Fornari, and M.R. Perfit (2010), Paving the seafloor: Volcanic emplacement processes during the 2005-2006 eruptions at the fast spreading East Pacific Rise, 9°50'N. *Geochem. Geophys. Geosyst.*, 11, Q08024, doi:10.1029/2010GC003058.

Fornari, D.J., R.M. Haymon, M.R. Perfit, T.K.P. Gregg, and M.H. Edwards (1998), Axial summit trough of the East Pacific Rise 9°-10°N: Geological characteristics and evolution of the axial zone on fast spreading mid-ocean ridges, *J. Geophys. Res.* 103, 9827-9855.

Fujimaki, H., M. Tatsumoto, and K. Aoki (1984), Partition coefficients of Hf, Zr and REE between phenocrysts and groundmasses, Proceedings of the fourteenth lunar and planetary science conference, Part 2, *J. Geophys. Res.* 89, Suppl. B662-B672.

Gamble, R.P., and L.A. Taylor (1980), Crystal/Liquid Partitioning in Augite: Effects of Cooling Rate, *Earth Planet. Sci, Lett.*, 47, 21-33.

Geshi, N., S. Umino, H. Kumagai, J.M. Sinton, S.M. White, K. Kishimoto, and T.W. Hilde (2007), Discrete plumbing systems and heterogeneous magma sources of a 24 km3 off-axis lava field on the western flank of East Pacific Rise, 14°S, *Earth Planet. Sci. Lett*, 258, 61-72.

Godard, M., J.-M. Dautria, and M. Perrin (2003), Geochemical variability of the Oman ophiolete lavas: Relationship with spatial distribution and paleomagnetic directions. *Geochem. Geophys. Geosys.*, 4, 8609 doi:10.1029/2002GC000452, 2003.

Gregg, T.K.P. and W.W. Jr. Chadwick (1996), Submarine lava-flow inflation: A model for the formation of lava pillars. *Geology*, 24, 981 - 984.

Gregg, T.K.P., and J.H. Fink (1995), Quantification of submarine lava-flow morphology through analog experiments, *Geology*, 23, 73-76.

Gregg, T.K.P., and J.H. Fink (2000), A laboratory investigation into the effects of slope on lava flow morphology, *J. Volcanol. Geotherm. Res.*, 96, 145-159.

Gregg, T.K.P. and D.K. Smith (2003), Volcanic investigations of the Puna Ridge, Hawai'i: relations of lava flow morphologies and underlying slopes. *J. Volcanol. Geotherm. Res.*, 126, 63 - 77.

Grenne, T., and J.F. Slack (2003), Paleozoic and Mesozoic silica-rich seawater: Evidence from hematitic chert (jasper) deposits. *Geology*, 31, 319-322.

Griffiths, R.W., and J.H. Fink (1992), Solidification and morphology of submarine lavas: a dependence on extrusion rate, *J. Geophys. Res.*, 97, 19729-19737.

Halbach, M., P. Halbacha, and V Lüders (2002), Sulfide-impregnated and pure silica precipitates of hydrothermal origin from the Central Indian Ocean. *Chem. Geol.* 182, 357-375

Hall, L.S., and J.M. Sinton (1996), Geochemical diversity of the large lava field on the flank of the East Pacific Rise at 8°17'S, *Earth Planet. Sci. Lett.*, 142, 241-251.

Hart, S.R., A.J. Erlank, and E.J.D. Kable (1974), Sea floor basalt alteration: Some chemical and Sr isotopic effects, *Contrib. Mineral. Petrol.*, 44, 219-230.

Hon, K., J. Kauahikaua, R. Denlinger, and K. Mackay (1994), Emplacement and inflation of pahoehoe sheet flows: Observations and measurements of active lava flows on Kilauea Volcano, Hawaii. *Geol.Soc.Amer.Bull.*,106, 351-370.

Honnorez, J. (1981), The aging of the oceanic crust at low temperature, in *The Sea,* edited by E. Emiliani, pp. 525-587, Wiley- Interscience, New York.

Hooft, E.E.E., R.S. Detrick, and G.M. Kent, (1997), Seismic structure and indicators of magma budget along the southern East Pacific Rise, *J. Geophys. Res.*, 102, 27319-27340.

Hooft. E.E.E., H. Schouten, and R.S. Detrick (1996), Constraining crustal emplacement processes from the variation in seismic layer 2A thickness at the East Pacific Rise, *Earth Planet. Sci. Lett.*, 142, 289-309.

Humphris, S.E., and G. Thompson (1978a), Hydrothermal alteration of oceanic basalts by seawater, *Geochim. Cosmochim. Acta*, 42, 107-125.

Humphris, S.E. and G. Thompson (1978b), Trace element mobility during hydrothermal alteration of oceanic basalts, *Geochim. Cosmochim. Acta*, 42, 127-136.

Ishikawa, T., K. Nagaishi, and S. Umino (2002), Boninitic volcanism in the Oman ophiolite: Implications for thermal condition during transition from spreading ridge to arc, *Geology*, 30, 899-902.

Ishikawa, T., S. Fujisawa, K. Nagaishi, and T. Masuda (2005), Trace element characteristics of the fluid liberated from amphibolite-facies slab: Inference from the metamorphic sole beneath the Oman ophiolite and implication for boninite genesis, *Earth Planet. Sci. Lett.*, 240, 355– 377.

Ishizuka, O., J. Kimura, Yi B. Li, R. J. Stern, M.K. Reagan, R.N. Taylor, Y. Ohara, S.H. Bloomer, T. Ishii, U.S. Hargrove III, and S. Haraguchi (2006), Early stages in the evolution of Izu–Bonin arc volcanism: New age, chemical, and isotopic constraints, *Earth Planet. Sci. Lett.*, 250, 385–401.

Karpoff, A.M., A.V. Walter, and C. Pflumio (1988), Metalliferous sediments within lava sequences of the Sumail ophiolite (Oman): Mineralogical and geochemical characterization, origin and evolution, *Tectonophysics*, 151, 223-245.

Langmuir, C.H., J.F. Bender, and R. Batiza (1986), Petrologic and tectonic segmentation of the East Pacific Rise, 5°30′-14°30′N, *Nature*, 322, 422-429.

Lippard, S.J., A.W. Shelton, and I.G. Gass (1986), *The Ophiolite of Northern Oman, Geol. Soc. Mem. Geol. Soc. London*, vol. 11, 178 pp., Vackwell Sci., Malden, Mass.

Lofgren, G.E., G.R. Huss, and G.J. Wasserburg (2006), An experimental study of trace-element partitioning between Ti-Al-clinopyroxene and melt: Equilibrium and kinetic effects including sector zoning. Am. Mineral., 91, 1596-1606.

Ministry of Petroleum and Minerals (1987), MAHAB-sheet NG40-14E-4, Geological map, 1:50,000, Muscat, Sultanate of Oman.

Miyashita, S., Y. Adachi, and S. Umino (2003), Along-axis magtmatic system in the northern

Oman ophiolite: Implications of compositional variation of the sheeted dike complex. *Geochem. Geophys. Geosys.*, 4, 8617, doi:10.1029/2001GC000235.

Morgan, J.P., and Y.J. Chen (1993) The genesis of oceanic crust: magma injection, hydrothermal circulation, and crustal flow, *J. Geophys. Res.*, 98, 6283-6297.

Mullen., E.D. (1983), $MnO/TiO_2/P_2O_5$: A minor element discriminant for basaltic rocks of oceanic environments and its implications for petrogenesis, *Earth Planet. Sci, Lett.*, 62, 53-62.

Nakamura, Y. (1973), Origin of Sector-Zoning of Igneous Clinopyroxenes. *Am. Mineral.*, 58, 986-990.

Nicolas, A. (1989), *Structures of Ophiolites and Dynamics of Oceanic Lithosphere*, 367 pp., Kluwer Acad., Norwell, Mass.

Niu, Y., and R. Batiza (1997), Trace element evidence from seamounts for recycled oceanic crust in the Eastern Pacific mantle, *Earth Planet. Sci. Lett.*, 148, 471-483.

Pearce, J.A. (1980), Geochemical evidence for the genesis and eruptive setting of lavas from Tethyan ophiolites, in *A Ophiolites*, edited by Panayiotou, A., Proceedings International Ophiolite symposium, Cyprus, 1979, Geol. Surv. of Cyprus, Nicosia

Pearce, J.A., M.J. Norry (1979), Petrogenetic implications of Ti, Zr, Y, and Nb variations in volcanic rocks, *Contrib. Mineral. Petrol.*, 69, 33-47.

Perfit, M.R., Fornari, D.J., Smith, M.C., Bender, J.F., Langmuir, C.H. and Haymon, R.M., 1994, Small scale spatial and temporal variations in mid-ocean ridge crest magmatic processes, *Geology*, 22, 375-379.

Perfit, M.R. and Jr.W.W. Chadwick (1998), Magmatism at mid-ocean ridges: Constraints from volcanological and geochemical investigations. in *Faulting and Magmatism at Mid-Ocean Ridges* edited by Vuck, W.R., Delaney, P.T., Karson, J.A. and Lagabrielle, Y., AGU Geophysical Monograph, 106, 59-116.

Reynolds, J.R., and C.H. Langmuir (2000), Identification and implications of off-axis lava flows around the East Pacific Rise, *Geochem. Geophys. Geosys.*, 1, doi:10.1029/1999GC000033

Roser, B., J. Kimura, and K. Hisatomi (2000), Whole-rock elemental abundances in sandstones and mudrocks from the Tanabe Group, Kii Peninsula, Japan, *Geosci. Rept. Shimane Univ.*, 19, 101-112.

Robertson, A.H.F., and A.J. Fleet (1986), Geochemistry and palaeo-oceanography of metalliferous and pelagic sediments from the Late Cretaceous Oman ophiolite, *Marine. Petrol. Geol.*, 3, 315-337.

Seyfried W.E.Jr., D.R. Janecky, and M.J. Mottle (1984), Alteration of the oceanic crust: Implications for geochemical cycles of lithium and boron, *Geochem. Cosmochim. Acta*, 48, 557-569.

Seyfried W.E.Jr., X. Chen, and L.-H. Chan (1998), Trace element mobility and lithium isotope exchange during hydrothermal alteration of seafloor weathered basalt: An experimental study at 350 ℃, 500 bars, *Geochim. Cosmochimi. Acta*, 62, 949-960.

Scheirer, D.S., and K.C. Macdonald (1993), Variation in cross-sectional area of the axial ridge along the East Pacific Rise: Evidence for the magmatic budged of a fast spreading center, *J. Geophys. Res.*, 98, 7841-7885.

Scheirer, D.S., and K.C. Macdonald (1995), Near-axis seamounts on the flanks of the East Pacific Rise, 8°N to 17°N, *Jour. Geophis. Res.*, 100, 2239-2259.

Shervais, J.W. (1982), Ti-V plots and the petrogenesis of modern and ophiolitic lavas, *Earth. Planet. Sci. Lett.*, 59, 101-118.

Sims, K.W.W., J. Blichert-Toft, D.J. Fornari, M.R. Perfit, S.J. Goldstein, P. Johnson, D.J. DePaolo, S.R. Hart, M.T. Murrell, P.J. Michael, G.D. Layne, and L.A. Ball (2003), Aberrant youth: Chemical and isotopic constraints on the origin of off-axis lavas from the East Pacific Rise, 9°-10°N, *Geochem, Geophys, Geosys.*, 4, 8621, doi:10.1029/2002GC000443.

Soule, S.A., D.J. Fornari, M.R. Perfit, M.A. Tivey, W.I. Ridley, and H. Schouten (2005), Channelized lava flows at the East Pacific Rise crest 9°-10°N: The importance of off-axis lava transport in developing the architecrure of young oceanic crust, *Geochem, Geophys, Geosys.*, 6, Q08005, doi:10.1029/2005GC000912.

Staudigel, H., and S. Hart (1983), Alteration of basaltic glass: Mechanisms and significance for the oceanic crust-seawater budget, *Geochim. Cosmochim. Acta*, 47, 337-350.

Sun, S.S., and W.F. McDonough (1989), Chemical and isotopic systematics of oceanic basalts: implications for mantle composition and processes. In Saunders, A. D. and Norry, M.J., eds., *Magmatism in the Ocean Basins. Geol. Soc. Special Pub.*, no.42, 313-345.

Taylor, R.N. (1990), Geochemical stratigraphy of the Troodos extrusive sequence: temporal developments of a spreading centre magma chamber, in Ophiolites: Oceanic Crustal Analogues, edited by J. Malpas et al., pp. 173-183, Geol. Surv. Dep., Minist. of Agric. and Nat. Resour., Nicosia, Cyprus.

Takahashi, T., and K. Shuto (1997), Major and trace element analyses of silicate rocks using X-ray fluorescence spectrometry RIX3000, *The Rigaku-Denki J.*, 28, 25-37.

Thompson, G. (1973), A geochemical study of the low temperature interaction of seawater and oceanic igneous rock, *EOS, Trans. Am. Geophys. Union*, 54, 1015-0-1019.

Tominaga, M., and S. Umino (2010), Lava deposition history in ODP Hole 1256D: Insights from log - based volcanostratigraphy, *Geochem. Geophys. Geosys.*, 11, Q05003, doi:10.1029/2009GC002933.

Umino, S., P.W. Lipman, and S. Obata, (2000), Subaqueous lava flow lobes, observed on ROV KAIKO dives off Hawaii, *Geology*, 28, 502-506.

Umino, S., S. Miyashita, F. Hotta, and Y. Adachi (2003), Along-strike variation of the sheeted dike complex in the Oman Ophiolite: Insights into subaxial ridge segment structures and the magma plumbing system, *Geochem. Geophys. Geosys.*, 4, 8618, doi:10 .1029/2001GC000233.

Umino, S., and S. Nakano (2007), *Geology of the Chichijima Retto District (in Japanese). Quadrangle Series, 1:50,000, Ogasawara Shoto (20)*, Geol Surv. Japan, 71pp, AIST.

Umino, S., S. Yanai, A.R. Jaman, U. Nakamura, and J.T. Iiyama (1990), The transition from spreading to subduction: Evidence from the Semail ophiolite, morthern Oman mountains. in *Ophiolites: Oceanic Crustal Analogues*, edited by J. Malpas et al., pp. 375-384, Geol. Surv. Dep., Minist. of Agric. and Nat. Resour., Nicosia, Cyprus.

Umino, S., S. Obata, P. Lipman, J.R. Smith, T. Shibata, J. Naka, and F. Trusdell (2002), Emplacement and inflation structure of submarine and subaerial pahoehoe lavas from Hawaii, in *Hawaiian Volcanoes: Deep Underwater Perspectives, Geophys. Monogr. Ser.*, vol. 128, edited by E. Takahashi et al., pp.85-101, AGU, Washington, D.C.

Walker, G.PL (1992), Morphometric study of pillow-size spectrum among pillow lavas, *Bull. Bolcanol.*, 54, 459-474.

White, S.M., K.C. Macdonald, and R.M. Haymon (2000), Basaltic lava domes, lava lakes, and volcanic segmentation of the southern East Pacific Rise, *J. Geophys. Res.*, 105, 23,519-23,536.

White, S.M., R.M. Haymon, D.J. Fornari, M.R. Perfit, and K.C. Macdonald (2002), Correlation between volcanic and tectonic segmentation of fast-spreading ridges: Evidence from volcanic structures and lava flow morphology on the East Pacific Rise at 9°-10°N, *J. Geophys. Res.*, 107(B8), 2173, doi:10.1029/201JB000571.

White, S.M., R.M. Haymon, S. Carbotte (2006), A new view of ridge segmentation and near-axis volcanism at the East Pacific Rise, 8°-12°N, from EM300 multibeam bathymetry, *Geochem. Geophys. Geosys.*, 7, Q12O05, doi:10.1029/2006GC001407.

White, S.M., S. Umino, and H. Kumagai (2006), Transition from seamount chain to intraplate volcanic ridge at the East Pacific Rise. *Geology*, 34, 293 - 296.

Appendix

Table 1 XRF analysis of this study
Table 2 ICP-MS analysis of this study
Table 3 Clinopyroxene composition
Table 4 Chrome-spinel composition

Appendix Table 1 Bulk-rock major and trace element compositions analyzed by XRF.

				(wt%)											(ppm)											
				SiO2	TiO2	Al2O3	FeO*	MnO	MgO	CaO	Na2O	K2O	P2O5	LOI	Nb	Ni	Pb	Rb	Sr	Th	Y	Zr	Ba	Cr	V
V1	Zabin		08zbN5	54.31	0.89	15.12	9.32	0.19	5.67	9.01	5.26	0.17	0.07	5.78	1.4	34.7	1.3	2.1	115.2	2.3	24.5	51.4	29	65	348
			08zbN10	62.42	1.82	13.86	8.79	0.15	3.56	3.38	5.70	0.05	0.27	3.01	4.8	-	1.2	1.6	74.5	6.2	57.3	174.5	-	5	140
			08zbN21	59.35	1.30	14.66	10.43	0.15	4.96	3.78	4.65	0.61	0.12	2.18	3.4	1.2	0.7	7.2	247.9	3.0	34.3	85.4	159	3	360
			08zbN32	44.79	1.39	19.95	9.81	0.16	0.95	22.54	0.07	0.08	0.26	4.96	5.6	-	1.9	0.8	48.2	5.7	55.6	166.2	-	4	130
			08zbN38	57.60	1.82	15.15	9.84	0.13	5.62	4.60	4.94	0.10	0.19	3.30	3.4	9.8	1.2	1.4	170.9	4.2	39.9	124.7	-	14	319
			08zbN45	68.16	1.21	14.03	5.49	0.09	1.18	2.56	6.91	0.06	0.30	0.99	5.6	-	2.1	1.5	84.4	8.6	64.1	203.1	-	3	50
			08zbN50	57.94	1.90	14.53	10.49	0.20	4.66	3.86	6.11	0.06	0.24	2.22	4.1	-	0.5	1.0	93.0	5.4	53.1	152.9	-	5	182
			08zbN54	63.92	1.60	14.07	7.30	0.15	2.89	3.15	6.58	0.06	0.28	1.63	6.1	-	2.3	0.6	78.5	6.3	56.5	173.7	1	3	110
			08zbN60	52.23	1.83	16.78	11.22	0.21	4.14	7.71	5.67	0.05	0.18	2.47	3.9	7.2	2.5	1.3	177.9	3.9	44.8	119.5	2	8	409
			08zbN64	61.11	1.40	14.46	8.42	0.15	3.79	4.25	6.17	0.04	0.20	2.21	3.4	7.5	1.1	0.7	68.8	4.7	45.8	129.5	0	8	143
			08zbN67	55.94	1.74	15.29	10.43	0.17	4.71	5.08	6.40	0.07	0.18	4.15	3.9	7.9	2.9	1.0	67.2	4.0	43.2	114.0	3	8	309
			08zbN71	52.46	1.78	16.01	11.00	0.20	5.14	7.97	5.23	0.06	0.16	1.99	3.1	14.4	1.5	1.6	188.5	3.0	37.9	103.6	-	11	487
	Fizh	LV1	07fizh5	51.31	1.89	15.39	10.04	0.32	6.34	8.96	4.95	0.66	0.13	4.40	3.1	32.3	3.8	8.7	192.2	-	41.2	110.8	89	51	324
			07fizh6	54.91	1.68	16.24	9.17	0.17	5.64	6.72	4.97	0.32	0.18	3.75	3.9	21.7	1.1	9.4	160.3	3.2	39.8	112.8	5	39	321
			07fizh7	52.27	1.47	14.96	9.22	0.20	6.45	9.31	5.75	0.23	0.13	5.02	3.8	32.2	1.4	3.2	163.3	-	31.6	87.3	30	41	308
			07fizh8	52.18	1.79	14.76	9.72	0.20	6.46	8.90	5.58	0.25	0.17	4.78	4.1	32.5	0.9	4.2	203.4	2.3	42.6	118.3	38	66	346
			07fizh9	52.83	1.53	14.49	9.24	0.16	5.93	9.54	5.27	0.85	0.15	4.41	3.5	31.3	2.5	13.4	147.1	0.8	32.5	93.2	210	38	296
			07fizh12	51.03	1.81	15.33	10.55	0.25	6.86	9.23	4.50	0.31	0.13	3.73	2.3	25.0	1.7	4.3	216.2	-	38.4	107.2	139	31	348
			07fizh13	51.98	2.07	14.37	11.27	0.23	7.24	7.06	5.30	0.29	0.20	4.38	4.9	24.2	0.8	4.3	172.6	1.7	49.1	141.2	35	17	379
			07fizh15	54.54	1.47	15.24	9.19	0.17	5.37	8.78	4.90	0.18	0.16	3.37	2.3	27.3	1.9	4.1	162.6	-	33.8	95.3	9	34	293
			07fizh17	53.42	1.51	14.90	9.03	0.26	6.05	8.20	5.65	0.86	0.13	4.62	3.6	22.0	2.8	8.3	213.9	-	32.1	86.3	116	17	342
			07fizh19	52.59	1.74	14.10	10.09	0.22	5.43	9.44	5.78	0.44	0.17	4.75	4.4	14.9	1.9	4.7	111.5	-	40.5	114.8	25	19	329
			07fizh20	53.27	1.90	15.38	8.88	0.27	4.89	9.04	6.09	0.14	0.14	4.97	2.1	38.9	2.0	3.9	136.2	0.5	38.5	106.7	9	30	350
			07fizh22	54.25	1.46	15.84	9.28	0.18	8.01	4.71	5.75	0.39	0.13	3.77	2.6	28.3	2.1	5.9	196.0	-	37.7	105.8	107	34	275
			07fizh23	61.57	1.47	13.38	8.58	0.18	7.53	1.90	5.15	0.08	0.16	3.63	4.4	12.8	0.9	2.9	76.6	3.2	39.1	118.3	-	11	227
			07fizh24	55.48	0.74	15.91	7.91	0.17	6.65	6.36	5.86	0.86	0.06	4.28	2.2	31.6	2.1	19.2	140.1	0.3	17.3	44.7	13	39	222
			07fizh26	55.06	2.09	14.54	11.10	0.25	6.12	4.33	6.15	0.18	0.19	3.32	5.1	22.9	2.0	4.6	90.4	3.2	44.4	127.1	-	13	331
			07fizh27	54.89	2.00	14.60	11.35	0.20	5.54	5.06	6.10	0.07	0.19	2.81	3.1	6.2	1.6	1.2	62.6	0.2	45.2	119.0	-	19	390
			07fizh28	55.74	1.91	14.87	10.28	0.15	5.65	4.33	6.80	0.08	0.19	2.90	4.9	11.6	0.9	2.6	109.5	3.1	45.4	127.5	-	15	370
			07fizh29	55.14	2.04	14.47	10.87	0.18	5.43	5.35	5.64	0.69	0.18	2.50	3.6	14.3	2.1	7.8	149.3	-	41.5	118.8	39	21	377
			07fizh31	53.28	2.01	14.29	12.24	0.25	7.07	4.94	5.40	0.35	0.19	2.88	4.7	14.3	1.7	7.3	123.8	-	45.1	122.1	20	18	401
			07fizh33	54.12	2.03	15.09	10.92	0.20	6.03	5.13	5.12	1.14	0.22	2.72	4.5	16.7	1.9	17.1	180.3	2.4	47.6	152.6	128	19	369
			07fizh34	52.97	2.25	15.55	11.09	0.63	6.94	4.53	5.49	0.30	0.25	3.59	5.3	11.3	2.7	3.3	113.6	0.1	51.8	155.4	107	18	374
			07fizh35	55.70	2.06	14.68	9.42	0.16	4.60	6.17	6.96	0.07	0.18	3.06	3.2	16.8	2.1	2.3	57.2	0.4	46.3	134.6	-	19	345
			07fizh36	55.27	1.88	15.47	9.79	0.16	4.43	7.92	4.81	0.10	0.19	4.84	4.2	14.2	1.0	3.7	108.0	2.6	46.2	137.7	4	17	402
			09vfz1	56.23	1.81	14.89	9.30	0.13	2.49	8.02	6.90	0.05	0.19	0.84	4.1	4.8	1.3	1.8	71.6	1.7	40.3	104.8	-	10	345
			09vfz2	54.72	0.79	16.50	8.21	0.17	6.31	6.72	5.84	0.67	0.06	4.79	1.3	41.4	1.8	11.5	196.2	0.9	18.6	47.0	-	44	214
			09vfz3	54.68	0.69	16.51	7.22	0.19	5.13	9.41	5.68	0.41	0.07	4.97	1.2	31.6	0.2	9.3	93.4	2.7	17.1	42.1	55	45	225
			09vfz4	55.24	0.77	16.86	7.90	0.17	5.16	7.93	5.47	0.44	0.06	4.37	2.2	25.3	0.9	9.1	206.2	1.1	19.0	46.9	60	36	250
			09vfz5	53.85	2.01	14.67	12.43	0.23	4.79	5.23	5.84	0.74	0.19	2.53	3.8	11.8	0.9	16.9	98.0	1.6	46.3	129.1	34	14	395
		MV1	07fizh37	54.40	0.64	14.34	7.48	0.41	7.68	8.77	5.86	0.36	0.06	6.52	0.9	48.6	9.5	8.4	132.5	0.4	16.5	36.2	26	63	257
			07fizh39	51.15	0.69	16.70	8.42	0.15	9.02	9.26	4.37	0.19	0.05	5.75	2.5	39.7	1.1	2.3	341.7	0.0	18.1	43.0	43	70	257
			07fizh40	54.26	0.63	15.38	8.45	0.18	7.74	7.97	4.83	0.52	0.05	3.61	1.7	34.4	2.2	7.6	218.3	-	16.6	35.3	41	48	245
			07fizh42	53.81	0.48	15.46	7.62	0.18	10.12	7.22	4.27	0.80	0.03	4.02	0.9	82.7	2.7	9.1	150.2	0.2	14.3	24.3	86	298	249
			07fizh43	56.24	1.64	14.82	9.27	0.17	5.16	5.39	6.49	0.67	0.16	3.00	3.5	16.1	2.0	16.0	82.1	3.0	37.1	112.2	15	17	321
			07fizh45	52.58	0.59	16.97	6.83	0.20	6.03	11.63	4.79	0.33	0.05	5.80	0.8	64.3	1.9	5.2	351.4	0.4	15.0	39.5	28	160	209
			07fizh46	52.76	0.68	16.64	7.92	0.18	7.11	9.28	4.84	0.52	0.06	6.23	1.8	67.2	1.7	10.1	284.6	1.4	17.5	42.1	13	136	226
			07fizh47	54.34	1.32	16.68	9.55	0.16	5.22	7.74	4.34	0.53	0.13	5.66	2.2	24.3	1.4	6.8	123.7	-	31.6	88.8	17	16	282
			07fizh48	50.70	0.70	17.08	8.40	0.20	9.03	9.23	4.38	0.22	0.05	6.25	1.7	57.7	0.5	4.5	378.2	1.3	17.4	44.5	29	146	235
			07fizh49	59.28	2.04	14.10	9.47	0.13	4.50	3.54	6.19	0.56	0.20	2.10	4.9	2.2	0.9	5.8	108.3	3.1	44.5	131.4	66	5	279
			07fizh50	53.96	2.12	14.54	10.50	0.21	7.09	5.13	5.40	0.87	0.17	3.04	2.9	29.0	1.6	18.4	189.2	-	44.8	126.1	90	18	342
			07fizh51	56.52	1.89	14.69	9.87	0.21	5.19	4.83	6.01	0.59	0.19	2.59	4.2	15.6	3.4	14.4	144.5	0.0	41.6	118.4	29	15	353

(Continued)

		(wt%)											(ppm)										
		SiO2	TiO2	Al2O3	FeO*	MnO	MgO	CaO	Na2O	K2O	P2O5	LOI	Nb	Ni	Pb	Rb	Sr	Th	Y	Zr	Ba	Cr	V
UV1	07fizh53	57.65	0.56	17.76	5.69	0.06	3.71	8.70	5.60	0.22	0.05	4.86	1.3	59.4	2.4	4.2	144.8	2.6	13.2	36.5	-	199	243
	07fizh55	51.72	0.62	17.58	8.26	0.16	7.13	9.71	4.62	0.14	0.05	5.49	0.8	32.1	2.3	1.9	209.0	0.5	19.2	34.9	3	70	296
	08fizh1	53.38	0.51	16.80	7.46	0.13	6.68	9.68	4.88	0.44	0.03	4.48	2.0	43.6	1.3	9.0	315.3	1.8	16.7	26.5	57	181	280
	08fizh3	55.23	0.71	15.53	8.48	0.16	7.44	7.21	4.90	0.28	0.06	4.63	1.2	46.9	1.0	6.5	134.7	1.7	18.2	42.0	22	34	257
	08fizh5	55.25	0.75	15.54	8.53	0.16	6.27	7.47	5.76	0.20	0.08	3.45	1.4	38.3	2.0	3.2	116.2	1.7	19.3	39.0	28	42	312
	08fizh6	55.30	0.62	14.80	7.16	1.47	4.39	10.41	5.52	0.24	0.09	3.59	2.2	47.8	1.3	5.7	693.0	2.2	20.5	46.3	203	28	241
	08fizh7	54.01	0.73	16.96	8.08	0.36	6.18	8.51	4.22	0.89	0.06	4.27	1.0	38.4		20.9	360.4	0.6	19.1	48.5	97	33	262
	08fizh8	57.15	0.65	15.03	7.18	0.14	4.85	8.84	5.21	0.84	0.10	5.92	1.7	32.1	1.1	19.9	360.1	2.6	18.0	42.9	271	32	261
	09vfz7	52.52	0.80	17.11	8.95	0.19	6.77	8.35	4.97	0.28	0.06	5.11	2.5	37.0	0.6	6.7	298.2	0.9	20.2	50.1	13	31	281
	09vfz9	54.70	0.76	16.48	7.51	0.16	5.87	8.31	5.46	0.68	0.06	5.62	2.1	71.3	0.3	7.4	104.3	1.0	19.4	42.7	83	73	231
Thuqbah	10vThu1	59.15	1.36	14.73	9.57	0.14	4.47	3.76	5.88	0.81	0.12	3.01	2.1	1.3	0.7	4.8	63.1	1.4	31.6	86.3	31	4	311
	10vThu2	63.29	1.27	14.56	8.18	0.11	2.49	2.78	6.39	0.81	0.11	1.95	3.3	1.1		6.1	106.3	2.8	31.2	81.6	33	5	372
	10vThu3	55.54	1.16	16.67	9.56	0.14	5.70	5.51	5.46	0.15	0.11	4.41	2.4	16.7	0.1	2.8	73.9	1.5	23.4	68.9	-	13	337
	10vThu6	56.87	1.47	15.29	10.89	0.14	5.61	3.13	4.64	1.84	0.12	4.24	3.0	5.7	0.7	13.7	114.6	1.7	34.2	84.3	146	5	370
	10vThu7	60.24	1.34	14.82	7.96	0.11	4.88	5.27	5.13	0.03	0.22	4.27	3.5	23.5	2.1	1.6	73.8	2.4	43.8	126.8	10	13	184
	10vThu8	58.39	1.22	16.04	7.05	0.14	3.60	8.26	4.89	0.29	0.13	6.88	2.8	17.7	2.3	3.6	337.2	2.1	30.1	83.7	11	8	278
	10vThu10	55.92	1.04	15.51	6.36	0.21	3.19	13.00	4.32	0.35	0.11	9.42	2.1	11.1	1.9	7.1	225.7	2.4	28.0	71.1	2	9	251
	10vThu11	53.60	1.27	16.29	7.84	0.12	4.02	13.56	2.59	0.58	0.14	7.95	2.9	39.0	1.7	9.5	949.3	1.6	26.5	84.1	97	113	283
	10vThu12	59.12	1.31	15.73	7.80	0.13	1.59	7.45	6.66	0.07	0.14	2.52	2.1	5.1	1.6	1.9	105.2	2.3	32.2	92.1	10	9	327
	10vThu13	56.04	0.72	17.05	6.39	0.08	2.84	9.72	7.09	0.00	0.07	3.64	2.4	30.5	1.0	0.3	66.9	1.0	18.5	44.5	12	65	239
	10vThu14	60.32	1.18	16.41	7.20	0.15	1.43	3.97	9.15	0.08	0.11	1.80	1.6	15.2	0.7	2.2	114.1	2.5	29.4	68.9	46	30	387
Ghayth	06ghay1	57.89	0.82	16.34	8.79	0.29	5.59	3.61	4.81	1.81	0.06	2.95	1.5	26.1	0.5	18.7	111.1	0.8	20.5	42.6	225	36	279
	06ghay2	56.78	0.73	14.94	7.97	0.65	7.49	4.16	6.24	0.99	0.06	3.45	1.4	49.3	2.3	10.1	112.9	0.3	23.7	50.7	144	61	261
	06ghay3	58.09	0.75	16.25	8.61	0.43	6.50	3.66	3.73	1.91	0.07	3.55	0.7	55.4	2.4	19.3	149.6	1.9	23.1	53.5	398	65	250
	06ghay4	61.01	1.71	14.85	9.31	0.16	3.11	3.94	5.46	0.30	0.16	2.20	3.0	7.2	2.6	4.3	62.1	2.1	36.0	104.3	13	9	328
	06ghay5	55.91	1.92	15.42	12.27	0.26	4.15	4.19	4.78	0.94	0.15	2.97	2.3	7.7	2.5	9.2	65.1	0.4	35.8	104.1	101	9	390
	06ghay6	57.17	1.91	14.95	11.52	0.23	4.22	4.43	5.06	0.35	0.16	1.53	1.3	10.1	1.9	4.3	52.8	0.6	37.5	103.4	18	8	404
	06ghay7	56.45	1.91	14.75	11.77	0.22	4.26	4.31	5.91	0.27	0.15	2.05	1.7	4.1	2.1	1.0	116.7	-	38.4	103.3	28	11	427
	06ghay14	54.85	2.07	14.60	11.60	0.24	3.87	6.15	5.73	0.66	0.22	4.00	3.9	7.3	1.3	5.2	110.2	-	48.8	141.9	103	12	349
	06ghay17	59.25	2.21	15.42	10.69	0.12	2.67	3.97	5.04	0.39	0.23	4.60	3.8	52.2	1.9	2.2	80.6	1.9	27.7	72.5	-	153	285
	06ghay19	52.91	1.20	15.25	8.32	0.13	5.81	11.12	5.05	0.11	0.10	4.80	5.7	10.4	2.5	3.3	129.5	3.2	50.2	157.9	-	9	420
	06ghay24	53.88	1.87	14.51	11.76	0.16	3.81	8.28	5.47	0.10	0.16	7.45	2.0	9.3	2.1	0.6	52.1	0.2	39.2	105.9	-	26	383
	06ghay27	67.69	1.35	14.44	6.47	0.09	1.50	2.71	5.43	0.16	0.15	2.96	2.0	6.2	1.5	4.9	60.7	3.5	32.6	96.2	3	1	206
	06ghay30	62.68	1.56	14.36	8.63	0.10	2.80	4.88	4.73	0.13	0.14	4.94	1.5	6.6	2.6	2.8	50.2	0.3	33.7	90.4	-	7	341
	06ghay34	60.91	1.40	14.33	7.74	0.13	2.73	6.37	6.18	0.10	0.12	5.63	2.1	8.9	2.4	0.0	41.9	0.8	29.8	79.8	-	11	328
	06ghay36	52.81	1.95	14.78	10.26	0.20	3.24	11.98	4.41	0.21	0.16	9.78	2.9	15.7	2.4	3.5	83.2	0.5	41.5	99.8	-	30	409
	06ghay40	62.56	1.41	14.67	8.17	0.15	2.21	5.02	5.11	0.57	0.12	4.29	1.7	6.8	2.3	5.8	106.6	0.8	27.2	79.7	35	11	340
	06ghay44	54.57	1.73	16.34	8.74	0.15	2.64	7.81	7.73	0.12	0.16	6.26	2.7	1.1	1.2	-	65.5	-	36.7	102.9	7	5	346
	06ghay47	62.64	1.45	15.34	7.61	0.15	2.39	2.98	7.15	0.08	0.20	3.14	4.0	4.3	1.6	0.6	34.4	4.8	47.7	146.3	-	15	142
	06ghay49	62.47	1.44	14.24	8.10	0.13	2.98	4.30	6.08	0.10	0.16	4.55	2.1	11.2	2.1	1.2	40.4		36.3	103.5	-	4	184
	06ghay54	61.52	1.49	14.93	8.94	0.22	3.64	2.44	6.57	0.12	0.13	3.21	1.0	5.8	4.4	1.1	55.9	0.8	31.2	85.2	2	8	333
	06ghay57	65.10	1.43	14.85	6.92	0.12	1.88	3.57	5.82	0.10	0.20	3.41	4.5	0.7	1.5	2.3	45.1	3.9	50.6	158.7	-	7	201
	06ghay61	65.12	1.40	15.65	7.03	0.12	2.26	2.13	6.01	0.10	0.17	2.48	2.9	4.6	2.6	3.0	45.1	3.6	38.2	116.5	-	4	141
	06ghay64	60.95	1.41	15.44	7.87	0.15	3.24	3.74	6.85	0.18	0.16	3.70	3.3	4.6	2.7	1.2	61.7	0.4	39.4	116.6	5	1	138
	06ghay69	56.78	1.65	16.05	9.75	0.21	4.27	4.26	6.70	0.20	0.14	4.19	1.6	7.9	0.8	1.0	80.0	0.6	34.0	100.0	11	16	348
	08ghay1	66.62	1.36	12.67	6.25	0.11	1.62	4.50	6.67	0.04	0.17	-	4.5		2.4	1.5	36.6	3.3	40.5	113.5	-	4	122
	08ghay2	66.89	1.06	14.36	6.30	0.10	2.22	1.61	7.17	0.13	0.16	-	3.4	2.7	1.8	3.0	88.9	3.5	36.5	120.7	-	17	99
	08ghay5	60.50	1.70	15.29	8.46	0.17	3.67	2.82	7.16	0.04	0.19	-	3.7	0.2	1.9	2.4	81.5	3.4	45.6	128.2	-	5	172
	08ghay11	67.25	1.43	13.39	7.39	0.08	1.28	1.90	7.08	0.04	0.16	-	3.6	1.9	1.2	1.8	74.2	3.4	34.6	108.2	-	6	218
	08ghay12	57.58	1.53	15.16	8.74	0.14	2.74	6.49	7.41	0.08	0.14	5.16	3.8	10.6	1.5	2.8	84.1	2.1	33.8	98.7	-	9	313
	10ghay1	58.90	1.65	14.08	9.93	0.32	3.67	4.96	6.28	0.04	0.16	5.01	3.3	12.0	2.9	2.2	38.6	2.7	40.9	108.5	-	10	331
	10ghay2	56.11	0.76	15.43	8.44	0.49	6.43	5.90	6.04	0.34	0.06	5.28	1.9	21.0	1.1	4.2	130.5	2.1	19.8	40.4	30	34	281
	10ghay3	60.71	0.90	15.14	9.45	0.20	3.41	2.64	6.30	1.18	0.07	2.94	1.6	3.3	0.2	9.6	85.5	1.7	27.0	56.6	173	8	342
	10ghay4	60.83	1.96	13.54	9.19	0.13	3.31	5.01	5.81	0.04	0.19	5.20	5.0	11.2	1.7	1.9	42.3	2.5	41.6	126.9	-	15	331

(Continued)

		(wt%)											(ppm)										
		SiO2	TiO2	Al2O3	FeO*	MnO	MgO	CaO	Na2O	K2O	P2O5	LOI	Nb	Ni	Pb	Rb	Sr	Th	Y	Zr	Ba	Cr	V
	10ghay5	60.82	1.72	14.66	9.63	0.21	3.02	2.82	6.77	0.09	0.26	3.25	4.8	2.4	1.2	3.1	55.3	3.9	52.5	150.0 -		5	125
	10ghay6	55.14	2.10	14.26	12.07	0.19	3.99	5.18	6.87	0.01	0.19	2.74	5.0	4.7	0.5	1.9	36.1	2.2	43.9	124.6 -		6	447
	10ghay7	61.76	1.66	13.72	7.91	0.23	2.86	5.20	6.46	0.03	0.16	4.85	2.6	18.9	1.6	2.0	61.0	3.1	36.3	99.7 -		8	336
	10ghay8	58.18	1.79	15.13	10.31	0.28	3.31	3.96	6.85	0.03	0.16	4.15	3.3	10.8	2.7	1.7	47.1	2.6	38.0	112.9 -		10	367
	10ghay9	59.87	1.67	15.09	8.64	0.19	3.15	3.93	7.18	0.08	0.21	3.58	4.0	5.0	1.2	2.5	47.8	3.6	46.5	133.2 -		7	163
	10ghay10	56.58	0.76	16.07	8.98	0.19	6.04	3.75	6.92	0.65	0.07	2.87	2.6	42.1	1.7	6.4	83.0	1.4	25.8	57.6	58	30	271
	10ghay11	56.41	1.72	15.85	10.07	0.13	4.83	3.34	7.06	0.44	0.15	3.73	3.3	11.8	2.3	4.7	110.5	2.1	33.5	99.4	49	12	415
	10ghay12	60.06	1.20	15.72	7.56	0.17	4.54	3.32	6.43	0.90	0.12	3.17	3.1	12.5	1.6	8.8	104.8	2.0	28.1	86.0	63	9	261
	10ghay14	56.71	0.79	15.64	8.86	0.15	5.75	5.28	5.92	0.85	0.06	4.78	2.2	36.4	0.6	9.4	137.8	1.4	25.2	53.6	77	30	285
	10ghay15	59.44	1.42	15.18	8.26	0.19	3.55	4.52	6.49	0.78	0.18	4.95	3.3	10.9	2.0	7.5	77.8	3.1	38.1	117.7	72	9	209
	10ghay16	58.12	1.41	15.98	9.18	0.14	4.08	3.35	7.30	0.28	0.17	2.68	3.5	11.9	0.7	3.5	117.9	2.7	36.6	116.1	33	7	212
	10ghay17	72.76	0.63	12.57	5.47	0.07	1.87	0.89	5.45	0.20	0.07	2.19	2.7	2.2	1.4	3.6	95.9	3.7	28.7	76.3	7	5	74
	10ghay18	53.34	1.97	14.35	11.66	0.19	4.35	7.07	6.57	0.34	0.17	2.95	4.3	19.8	0.2	3.0	88.9	1.4	43.6	117.5	50	25	400
	10ghay19	55.91	0.70	15.40	8.15	0.19	6.49	6.27	5.92	0.90	0.06	3.98	2.7	47.9	0.4	6.5	117.6	2.4	20.9	45.6	177	120	268
	10ghay20	54.42	2.12	14.80	11.42	0.17	4.10	5.83	6.85	0.10	0.19	2.49	4.0	14.2	0.2	2.4	60.1	1.7	43.2	128.6 -		14	393
	10ghay21	57.05	1.90	14.07	10.73	0.19	4.12	5.69	6.01	0.04	0.18	4.48	4.5	11.7	0.9	2.8	45.2	2.7	45.7	127.3 -		14	338
	10ghay22	58.83	1.76	14.62	10.40	0.18	4.48	3.23	6.29	0.05	0.16	4.50	3.2	10.3	1.4	2.8	44.0	2.7	39.2	112.6 -		11	350
	10ghay23	59.28	1.76	14.14	10.53	0.17	4.03	4.33	5.60	0.03	0.14	5.29	2.5	5.6	0.4	2.0	24.3	1.5	24.7	99.2 -		7	409
	10ghay24	56.22	1.86	15.59	10.95	0.16	4.35	3.53	7.11	0.04	0.19	4.00	4.1	12.6	1.4	2.3	64.8	2.6	44.4	125.0 -		11	363
	10ghay25	56.35	1.80	15.16	10.77	0.16	4.17	5.02	6.35	0.05	0.18	5.21	3.2	10.1	1.2	2.4	41.6	2.7	42.0	126.6 -		11	348
	10ghay26	61.22	1.64	13.37	9.30	0.13	3.44	4.68	6.03	0.05	0.13	4.50	3.8	5.2	0.8	2.3	28.9	2.3	31.7	94.3 -		9	390
	10ghay27	53.19	0.60	15.28	9.23	0.21	8.17	6.84	4.64	1.80	0.04	3.64	0.9	51.4	0.9	13.8	128.6	0.4	18.2	27.1	255	174	281
	10ghay28	56.23	1.62	14.66	10.45	0.16	4.52	4.59	7.44	0.18	0.15	2.73	3.0	13.9	0.8	2.9	66.2	1.9	35.6	100.4 -		26	361
	10ghay29	55.36	1.88	14.77	11.54	0.24	4.65	4.63	6.74	0.05	0.15	3.05	3.8	21.1	1.3	2.0	67.5	1.4	36.9	104.1 -		7	438
	10ghay30	58.30	1.68	14.73	10.48	0.39	4.82	3.19	6.19	0.06	0.16	3.73	3.5	12.8	1.5	1.7	55.2	2.0	38.2	109.0 -		10	343
	10ghay31	57.87	1.69	14.72	10.75	0.27	5.07	3.49	5.92	0.06	0.16	4.56	2.3	11.6	0.3	1.9	63.7	1.8	38.3	109.4 -		8	341
	10ghay32	56.12	0.60	15.82	7.89	1.07	6.79	5.32	4.86	1.48	0.04	7.17	1.5	33.7	0.7	14.2	110.5	1.9	17.3	33.7	115	41	262
	10ghay33	61.87	1.65	13.83	10.75	0.66	4.10	1.51	5.41	0.05	0.16	2.70	3.5	15.6	0.8	2.3	42.1	2.6	39.3	107.0	0	9	347
	10ghay34	57.98	0.57	15.46	8.54	1.02	6.98	3.61	5.63	0.17	0.04	4.57	0.3	27.7	1.5	2.8	63.6	1.9	14.1	31.1	4	34	284
	10ghay35	56.03	0.65	15.04	7.74	0.48	7.80	5.92	6.22	0.06	0.05	3.78	2.5	39.3	2.4	4.5	76.4	1.4	15.9	33.4 -		134	232
	10ghay36	55.60	1.96	15.09	11.48	0.26	4.80	4.13	6.01	0.49	0.18	4.75	4.0	5.0 -		4.4	70.6	3.3	44.0	130.1	42	10	382
	10ghay37	54.26	0.70	17.23	9.65	2.31	9.28	1.10	5.32	0.10	0.05	5.64	2.1	34.7	1.0	2.1	51.4	1.3	17.5	32.5	15	68	
	10ghay38	57.51	0.70	15.03	8.61	0.17	6.70	5.15	5.60	0.47	0.06	5.63	2.5	28.8	0.9	4.2	117.2	1.3	21.9	40.9	22	71	242
	10ghay39	57.39	0.47	15.73	7.53	1.27	9.14	3.35	4.92	0.16	0.03	6.81	2.7	33.0	0.7	4.6	62.1	1.9	11.8	24.1	12	40	227
	10ghay40	55.83	0.63	15.47	7.80	0.37	5.57	8.61	5.55	0.12	0.05	8.96	1.4	39.6	3.3	3.2	127.6	0.8	14.7	33.0 -		102	223
	10ghay41	56.51	0.58	15.76	7.98	2.38	8.23	2.82	5.43	0.27	0.04	5.71	1.8	32.2	1.8	3.8	106.2	1.4	15.8	27.1	51	27	338
	10ghay42	53.47	0.52	15.95	8.31	0.23	6.53	8.15	2.49	4.32	0.03	6.93	1.5	40.5	0.8	33.7	268.6 -		15.7	29.9	886	41	262
	10ghay43	52.98	0.48	16.26	8.02	0.15	7.45	9.55	5.00	0.09	0.03	3.69	1.6	44.1	0.7	2.1	66.7	1.2	12.7	26.2	1	42	234
	10ghay44	54.01	0.62	15.03	8.16	1.00	6.43	8.44	4.11	2.16	0.05	9.12	0.7	83.7	0.9	15.5	162.1	1.0	19.2	34.6	332	223	280
	10ghay45	56.36	0.61	14.55	7.53	0.35	6.87	5.78	5.02	2.89	0.05	2.32	1.6	41.3	0.9	19.9	93.9	1.3	15.1	31.7	425	108	236
	10ghay46	58.93	0.76	14.75	8.63	0.17	7.11	3.26	2.73	3.60	0.06	6.65	1.4	29.9	1.5	32.6	87.4	1.5	19.9	38.8	358	29	273
	10ghay47	53.03	1.06	16.93	10.78	0.38	7.35	1.93	3.03	5.42	0.08	6.11	2.4	17.6	2.6	49.4	107.5	0.5	29.8	64.2	362	17	331
	10ghay48	51.15	0.55	14.39	7.70	0.15	10.14	12.44	3.27	0.17	0.04	4.40	1.2	114.1	1.9	1.8	67.6	0.1	14.8	28.1	6	410	226
Yanbu	06sal6	50.07	0.98	17.71	8.30	0.33	6.63	13.49	1.78	0.64	0.08	3.74	1.1	120.7	1.7	8.4	184.9 -		23.9	63.2	109	357	206
	06sal8	57.41	2.16	14.92	10.58	0.20	4.72	3.95	3.56	2.31	0.19	3.35	4.2	18.3	0.3	21.9	118.6 -		44.1	129.9	182	13	371
	06sal9	58.35	2.26	14.88	10.42	0.24	3.95	3.89	5.49	0.28	0.25	3.19	3.5	2.1	1.8	1.3	195.2	0.3	53.7	164.4	19	1	215
	06sal10	54.40	2.49	15.93	13.06	0.18	4.42	3.00	3.56	2.77	0.19	4.24	3.5	17.0	1.4	27.4	128.4	0.3	44.4	133.7	115	11	382
	06sal11	58.10	2.05	15.50	9.84	0.19	3.78	5.21	4.67	0.37	0.29	5.13	5.0 -		0.8	4.8	160.8	2.2	60.0	184.6	31		154
	06sal12	59.93	2.20	14.67	8.69	0.16	3.48	5.23	4.85	0.53	0.26	4.54	4.0	5.3	1.3	5.3	78.9	0.9	58.5	163.1	29	1	191
	06vsal18	63.91	1.85	12.03	8.76	0.13	3.81	3.96	5.21	0.15	0.18	2.77	4.4 -		0.7	2.9	78.2	2.2	41.5	110.9 -		7	327
	06sal24	52.28	1.64	15.40	9.87	0.20	4.43	9.89	5.80	0.34	0.16	6.30	3.4	24.6	2.3	1.7	198.2		39.4	109.8	9	46	363
	06sal27	51.46	1.11	15.52	8.22	0.28	5.20	12.02	5.91	0.15	0.10	10.76	2.2	56.3	1.1	1.1	121.3	0.5	25.1	69.5	18	213	196
	10vsal2	65.62	1.11	15.06	6.92	0.12	2.35	1.23	7.26	0.07	0.28	2.53	5.6	0.0	2.5	2.9	82.5	5.0	56.4	179.9 -		5	52

(Continued)

		(wt%)											(ppm)										
		SiO2	TiO2	Al2O3	FeO*	MnO	MgO	CaO	Na2O	K2O	P2O5	LOI	Nb	Ni	Pb	Rb	Sr	Th	Y	Zr	Ba	Cr	V
	10vsal3	66.79	1.29	14.43	6.82	0.09	1.76	1.18	7.25	0.11	0.28	2.09	5.7	2.8	2.5	3.2	73.7	4.2	54.7	183.4		4	64
	10vsal4	56.03	1.79	16.30	10.91	0.18	3.52	3.19	7.74	0.05	0.29	3.75	6.1	3.2	0.7	3.0	63.4	3.9	67.6	203.0		4	188
	10vsal6	64.72	1.31	14.53	7.03	0.13	2.68	2.20	7.11	0.03	0.26	2.27	6.0	3.1	1.3	2.5	59.6	4.4	57.6	194.7		4	128
	10vsal8	66.65	1.33	13.74	6.73	0.11	2.07	2.20	6.86	0.06	0.26	1.38	6.2	7.0	0.9	2.9	71.8	4.0	60.3	208.5		4	125
	10vsal10	58.50	1.87	15.44	9.31	0.13	3.44	3.70	7.32	0.06	0.22	2.41	4.9		2.0	2.5	82.9	3.3	50.2	154.6		4	258
	10vsal12	60.40	1.54	15.10	8.49	0.20	3.33	7.09	3.21	0.49	0.15	8.17	2.3	22.2	1.7	4.8	468.5	1.9	35.0	110.8	251	20	276
	10vsal14	58.02	2.04	15.19	9.12	0.12	2.41	7.09	5.65	0.08	0.27	6.85	6.7		0.7	3.1	155.7	3.0	56.0	177.4		4	191
	10vsal15	61.57	1.89	14.21	8.19	0.16	2.03	6.42	5.16	0.12	0.24	6.90	5.6	5.2	2.6	2.7	174.3	3.2	51.1	160.3	26	4	196
	10vsal16	57.03	2.26	15.42	10.92	0.16	4.12	3.81	5.71	0.37	0.19	5.77	4.6	17.4	1.3	4.3	139.8	1.7	43.2	141.2	4	36	365
	10vsal19	58.80	1.85	15.30	9.22	0.15	3.99	3.48	6.95	0.05	0.22	4.14	5.7	11.3	1.6	2.1	56.5	3.8	49.4	139.9		18	227
	10vsal20	63.78	1.82	13.53	7.87	0.18	3.29	3.03	6.19	0.09	0.22	2.97	4.8	3.8	2.7	2.8	125.1	3.2	45.5	143.4		6	180
	06vsal13	58.47	1.81	13.54	11.22	0.18	4.91	3.94	5.50	0.27	0.17	5.15	4.3	6.7	1.2	2.9	149.1	1.2	38.0	108.1		8	341
	06vsal29	64.49	1.54	15.11	7.83	0.12	2.35	1.31	6.88	0.12	0.25	2.58	4.5	2.4	1.4	3.1	103.7	3.7	51.2	156.9		4	103
	06vsal30	56.71	1.38	15.75	10.53	0.20	2.65	5.44	6.77	0.26	0.30	5.57	6.0	2.8	2.4	4.6	127.6	2.9	62.9	194.5		6	83
	06vsal31	62.45	1.04	16.43	6.56	0.11	2.99	2.48	7.64	0.16	0.14	3.67	2.9	12.4	2.8	2.6	86.9	3.4	30.0	93.1		19	169
Salahi	07vsal29	56.10	1.75	13.67	8.03	0.23	4.42	8.39	5.27	1.97	0.16	3.47	3.4	14.9	4.0	11.6	73.8	0.3	40.1	105.0	354	27	332
	07vsal31	55.75	1.86	13.94	10.73	0.21	4.00	7.26	6.02	0.08	0.17	2.47	3.1	10.4	2.0	1.0	70.4		38.1	104.3	1	22	411
	07vsal32	55.76	1.75	13.39	10.49	0.25	6.18	6.18	5.68	0.16	0.15	2.27	3.0	17.8	2.1	1.9	63.2	1.0	37.0	98.6	20	32	363
	07vsal33	58.18	2.02	13.60	10.49	0.18	3.44	5.89	5.98	0.06	0.18	1.32	4.2	2.4	1.0	0.6	87.0	0.2	44.0	121.2		10	398
	07vsal34	66.71	1.50	14.04	6.81	0.13	2.22	2.05	6.23	0.11	0.20	1.95	3.5		3.4	1.3	46.3	2.3	45.0	126.9	1		130
	07vsal35	62.53	1.40	14.30	7.64	0.13	3.19	4.33	6.19	0.07	0.22	4.03	4.1	1.2	2.5	0.6	33.7	1.2	46.6	128.0		7	132
	07vsal37	55.56	1.60	15.14	9.85	0.30	5.46	6.04	5.82	0.06	0.17	6.22	4.3	7.9	3.2	0.8	39.1	1.0	38.7	113.3	11	12	278
	07vsal39	67.97	0.90	14.11	6.15	0.11	2.15	1.87	6.39	0.07	0.28	1.91	4.8	2.0	3.4	0.8	44.9	2.8	62.8	193.6	2		35
	07vsal41	56.06	1.69	15.22	9.36	0.16	5.42	5.68	6.19	0.06	0.16	5.35	3.0	31.0	3.4	0.8	34.0	1.0	40.4	105.5		24	346
	07vsal42	55.44	1.72	14.94	9.60	0.21	4.77	6.88	6.14	0.14	0.16	4.61	3.7	20.8	3.4	1.3	65.9	1.0	39.0	103.0	1	26	363
	07vsal45	58.15	1.57	14.55	9.88	0.13	4.03	5.48	6.01	0.04	0.15	5.29	2.8	7.6	2.6	0.7	42.2	0.4	35.8	97.9		21	332
	07vsal47	57.68	1.50	15.12	8.86	0.14	5.64	4.80	6.04	0.04	0.17	4.72	3.2	32.8	4.7	0.9	39.3	0.9	37.9	109.5		56	266
	07vsal48	61.67	1.60	14.07	8.79	0.12	3.89	3.84	5.83	0.05	0.16	3.68	3.8	4.5	3.1	0.7	35.9	0.5	37.7	108.4		8	276
	07vsal50	66.22	1.08	14.12	7.20	0.15	2.83	1.97	6.08	0.06	0.29	2.16	4.0		4.6	1.3	38.2	1.3	58.7	175.8			57
	07vsal51	63.83	1.18	14.89	7.72	0.10	2.53	3.88	5.55	0.04	0.28	2.05	4.1		4.6	0.8	181.2	1.4	55.3	163.4			71
	07vsal52	63.78	1.30	14.63	7.13	0.10	2.85	3.55	6.25	0.05	0.36	2.89	4.5		2.7	0.8	67.3	1.9	59.3	176.8			70
	07vsal54	65.04	1.23	13.63	7.52	0.13	2.31	4.36	5.40	0.05	0.34	2.66	5.6		4.1	1.4	87.1	1.6	54.6	171.2			55
Hilti	09vhil6	66.00	1.10	13.75	8.51	0.15	2.59	1.77	5.77	0.06	0.30	2.64	4.8	4.1	2.2	2.4	90.3	6.0	68.1	189.5		3	38
	09vhil10	54.75	2.29	14.14	12.68	0.26	4.05	5.81	5.59	0.21	0.22	2.58	5.9	1.0	1.3	1.7	78.8	2.5	51.1	140.9	21	8	288
	09vhil14	65.26	1.04	13.99	8.38	0.11	2.20	2.17	6.52	0.01	0.32	2.46	5.5	2.3	1.3	1.8	41.5	5.7	76.6	205.0		5	54
	09vhil20	53.08	0.91	15.60	8.55	0.23	7.64	8.94	4.87	0.12	0.07	3.08	2.4	77.7	0.6	2.1	95.9	0.9	23.3	46.7		221	236
	09vhil25	60.18	1.43	14.21	15.20	0.16	4.07	1.55	2.98	0.01	0.21	3.64	4.8	4.9	1.3	4.2	20.2	3.5	75.4	153.5		4	59
	09vhil37	62.24	1.32	14.50	9.44	0.21	3.37	2.35	6.28	0.01	0.27	2.19	4.7	0.7	2.4	1.2	40.7	3.7	67.1	179.3		4	57
	09vhil41	61.13	1.67	13.78	12.07	0.13	4.11	2.44	4.41	0.01	0.25	3.15	6.0	1.0	1.5	1.3	38.3	3.4	65.7	171.4		6	76
	09vhil45	58.94	1.67	14.50	10.90	0.15	4.93	3.59	5.03	0.02	0.27	3.34	4.3	9.5	1.5	1.6	72.4	3.6	67.2	187.0		13	195
	09vhil46	53.86	1.78	15.05	9.75	0.13	5.14	7.65	6.11	0.36	0.16	3.98	4.7	38.8	0.9	3.0	66.1	1.7	38.6	111.0	17	59	316
	09vhil48	50.22	1.67	15.01	11.01	0.23	6.78	10.23	4.37	0.34	0.15	4.25	4.3	30.7	0.9	4.5	319.7	1.3	36.9	105.0	39	50	325
	09vhil56	52.38	2.53	14.48	12.90	0.24	4.47	6.67	6.03	0.06	0.24	2.76	5.6	14.4	1.2	1.3	68.6	2.0	53.3	158.2		11	438
	09vhil58	53.59	2.07	15.66	9.95	0.15	2.38	9.45	5.98	0.53	0.22	2.11	4.4	8.9	1.0	2.8	48.1	2.9	50.3	147.4	9	12	382
	09vhil60	64.75	1.40	14.16	8.07	0.09	2.98	1.97	6.33	0.02	0.23	2.99	4.4	5.9	1.6	1.9	38.3	4.7	62.4	163.2		5	66
	09vhil63	53.41	1.96	14.92	9.22	0.13	3.67	10.62	5.86	0.04	0.17	3.21	4.9	44.0	1.4	1.5	62.4	1.9	42.2	104.8		42	358
Sheeted dikes, dikes																							
Fizh	07fizh1	53.76	1.65	14.20	11.00	0.24	7.47	5.91	5.55	0.10	0.12	2.21	2.6	24.0	3.4	1.8	66.9	0.1	33.3	86.8	18	20	356
	07fizh2	54.02	2.02	15.64	10.78	0.25	5.50	5.07	6.27	0.07	0.37	2.25	5.8	12.6	1.1	3.7	32.1	0.2	61.4	216.9		11	264
	07fizh3	52.35	2.20	14.35	12.30	0.29	6.24	6.63	5.39	0.05	0.20	2.01	4.7	21.1	1.3	2.6	60.9	1.9	48.7	131.6		21	398
	07fizh4	53.08	2.43	13.94	12.18	0.31	7.82	4.70	5.23	0.09	0.22	2.75	4.1	16.0	1.1	2.8	106.5		46.4	138.1		22	414
Ghayth	08ghay6												3.7	9.0	0.6	2.8	56.6	2.4	29.4	83.0		15	338
	08ghay8												3.6	18.0	2.0	2.0	52.5	3.2	33.5	108.7		87	100
	08ghay10												4.9	2.6	3.1	1.8	94.0	2.9	47.4	155.8		7	243

(Continued)

			(wt%) SiO2	TiO2	Al2O3	FeO*	MnO	MgO	CaO	Na2O	K2O	P2O5	LOI	(ppm) Nb	Ni	Pb	Rb	Sr	Th	Y	Zr	Ba	Cr	V
Salahi		07vsal43	56.87	0.73	14.71	8.95	0.18	6.84	5.69	5.20	0.77	0.05	2.26	2.1	40.6	3.2	5.2	121.6	1.2	18.5	36.3	137	84	
		07vsal55	63.12	1.41	14.27	8.57	0.15	3.82	2.69	5.60	0.06	0.30	2.89	4.3		3.1	1.0	32.4	1.0	53.1	165.9			329
Hilti		09vhil24	52.45	0.96	15.56	9.33	0.24	7.62	8.44	4.88	0.45	0.07	3.15	2.8	53.3	0.2	3.8	139.1	1.0	22.3	46.6	24	135	283
		09vhil36	51.59	1.02	14.99	9.63	0.21	8.14	9.95	4.25	0.17	0.07	2.93	2.0	65.3	0.3	2.3	61.3	0.5	26.4	47.1		107	285
		09vhil51	54.51	2.04	15.16	9.75	0.15	4.56	7.00	6.42	0.23	0.18	2.93	4.7	30.1	1.6	2.6	76.4	2.2	46.1	123.7		45	406
V2 lavas																								
Fizh		08fizh11	58.21	0.72	14.48	8.38	0.16	8.79	3.72	5.42	0.06	0.05	5.19	1.9	30.6	3.1	2.7	46.7	2.3	19.5	38.6		43	268
		08fizh13	59.83	0.81	14.48	8.28	0.13	8.52	2.55	5.29	0.05	0.06	5.29	1.6	24.0	0.9	2.8	55.5	2.5	22.4	42.3		36	301
		08fizh14	63.05	1.03	13.39	9.01	0.12	4.56	2.51	6.16	0.08	0.08	2.08	2.2	7.2	1.2	3.8	73.8	3.1	24.8	53.5		8	393
Yanbu		06sal3	60.72	0.63	14.82	8.10	0.14	3.40	8.90	2.94	0.30	0.06	6.27											
		06sal5	53.88	0.63	16.97	8.16	0.14	5.07	12.94	1.91	0.25	0.05	7.88											
boninite dike		08fizh4	56.18	0.24	12.15	8.46	0.15	12.85	9.18	0.54	0.24	0.01	2.65	1.7	270.3	2.2	4.0	43.3		7.8	9.0	30	972	231
V2 dike		08fizh17	51.02	0.53	14.04	7.45	0.46	7.19	13.62	5.54	0.12	0.04	8.89	1.8	184.1	0.7	2.7	112.7	0.2	14.5	25.8	37	628	242
Hilti	UV2	09vHil202	49.95	0.25	12.88	8.17	0.36	7.94	17.49	1.66	1.26	0.03	8.51	1.2	278.0	4.0	15.3	67.2	0.0	9.1	10.1	40	874	201
		10vHil205	55.16	0.27	13.39	7.55	0.11	9.46	10.42	3.22	0.38	0.03	3.77	2.0	307.8	1.1	6.2	78.9	0.5	9.0	10.2	8	838	186
		10vHil206	56.28	0.30	13.52	7.54	0.13	9.75	7.32	4.48	0.64	0.03	4.00	1.6	112.8	1.9	8.1	92.6	0.9	11.7	10.5	40	399	178
		10vHil207	57.23	0.34	14.74	7.46	0.10	8.12	5.38	6.57	0.04	0.02	2.63	1.9	78.9	1.0	0.7	76.6	1.8	12.7	12.6		220	253
		10vHil208	52.39	0.27	12.70	7.04	0.16	9.12	14.29	3.68	0.32	0.02	6.60	1.6	269.1	0.5	7.3	83.1	0.6	10.9	10.0	13	870	187
		10vHil209	54.24	0.29	14.29	7.56	0.12	9.77	9.33	4.03	0.36	0.01	2.91	1.1	286.9	2.1	6.6	99.3	0.4	6.3	10.5	7	877	192
		10vHil211	47.70	0.31	14.84	7.66	0.12	8.41	17.68	2.86	0.37	0.05	9.67	2.4	119.2		8.1	161.9	0.4	12.7	14.6	5	549	282
		10vHil212	48.48	0.25	11.24	7.47	0.19	12.03	17.78	1.67	0.85	0.04	9.74	1.2	341.2	1.4	9.2	108.7		12.8	10.1	6	999	196
		10vHil213	57.06	0.27	12.86	6.72	0.10	8.62	10.70	3.23	0.43	0.02	3.46	1.1	106.6	0.9	11.2	66.7	0.3	8.8	9.4	4	505	199
		10vHil215	63.83	0.31	9.92	7.10	0.07	7.34	6.44	4.89	0.07	0.02	2.33	1.5	174.8	1.8	3.0	53.1	1.9	7.9	10.6		605	163
		10vHil216	53.00	0.27	12.45	6.52	0.25	8.58	13.52	5.37	0.01	0.02	7.66	0.9	317.3	3.2	13.3	71.8	2.6	6.2	11.7		938	200
	LV2	09vHil206	56.26	0.59	15.49	7.54	0.15	5.94	8.35	5.58	0.05	0.06	5.07	1.3	51.4	2.5	1.2	78.5	1.7	19.8	38.6	1	123	325
		09vHil207	55.97	0.62	15.79	6.63	0.18	7.63	7.61	4.55	0.95	0.06	6.34	1.9	44.7	3.2	10.7	229.6	2.3	18.7	46.0	92	107	251
		09vHil208	55.88	0.62	15.59	8.26	0.16	6.05	9.24	3.34	0.81	0.05	4.45	2.2	48.6	1.9	25.2	133.6	1.5	18.4	40.8	44	103	280

	SiO2	TiO2	Al2O3	FeO*	MnO	MgO	CaO	Na2O	K2O	P2O5	LOI	Nb	Ni	Pb	Rb	Sr	Th	Y	Zr	Ba	Cr	V
09vHil209	55.55	0.59	15.27	8.14	0.12	10.04	6.81	3.16	0.28	0.05	4.70	0.8	68.9	1.3	2.5	178.0	1.4	16.0	40.7	65	240	248
09vHil210	57.02	0.62	15.89	7.72	0.14	6.73	7.69	3.54	0.59	0.06	4.27	2.3	44.8	2.3	4.4	184.3	2.0	20.3	45.2	59	98	259
09vHil211	56.36	0.61	15.58	7.56	0.35	4.08	10.21	5.09	0.10	0.06	5.04	1.1	43.8	6.6	2.0	99.5	2.2	20.1	42.0	12	101	273
09vHil213	49.70	1.18	16.85	8.20	0.18	6.43	13.90	3.23	0.23	0.10	4.83	3.5	62.9	1.2	0.9	230.3	1.1	24.6	69.5	19	206	248
09vHil214	64.74	0.71	13.63	6.81	0.12	3.92	4.26	5.63	0.11	0.08	3.06	2.9	25.2	2.6	2.3	142.6	2.9	25.2	46.9	6	38	256
09vHil215	53.46	0.60	16.55	8.46	0.06	2.80	13.35	4.62	0.03	0.06	3.65	2.1	40.0	2.4	0.5	46.3	1.1	21.2	40.2	5	57	277
09vHil216	57.89	0.70	15.68	8.26	0.11	5.98	6.47	4.24	0.61	0.06	5.61	2.5	42.6	2.4	14.0	412.4	2.1	22.9	55.3	49	60	290
09vHil217	52.50	0.63	17.56	7.83	0.08	2.85	13.82	4.57	0.10	0.06	4.89	1.6	43.0	1.4	1.6	226.6	0.9	21.6	47.4	16	65	303
09vHil218	59.79	0.61	14.94	7.17	0.14	2.99	9.87	4.17	0.26	0.06	5.15	2.5	50.1	0.5	7.0	656.0	1.0	19.7	51.8	37	62	298
09vHil219	54.35	0.70	16.45	9.14	0.16	5.72	8.49	4.85	0.09	0.05	4.91	2.0	49.1	0.8	3.8	210.9	1.0	18.5	33.9	24	90	397
09vHil221	59.36	0.80	15.60	7.91	0.14	3.71	8.27	3.82	0.31	0.08	6.88	1.4	33.5	1.9	7.9	317.4	1.0	22.0	41.5	75	66	335
09vHil222	57.79	0.73	15.18	8.27	0.13	3.50	9.81	4.47	0.06	0.06	3.57	2.2	39.9	1.1	2.1	162.6	2.4	18.5	35.3	17	73	377
09vHil223	54.47	0.65	16.07	8.73	0.13	4.54	13.53	1.57	0.27	0.05	8.86	2.4	43.7	1.0	5.5	692.6	1.1	17.6	42.0	41	99	311
09vHil224	55.84	0.64	16.03	8.84	0.11	5.18	9.73	3.25	0.34	0.05	7.31	1.1	40.2	1.8	8.5	333.7	0.6	17.8	35.1	31	102	298
09vHil225	54.96	0.63	15.91	8.95	0.09	4.71	10.31	4.28	0.12	0.05	4.69	1.8	36.4	0.7	5.6	311.3	3.0	18.6	34.8	5	77	297
09vHil226	59.81	0.65	15.28	7.34	0.12	3.26	8.54	4.76	0.18	0.06	4.89	1.8	25.9	1.6	4.5	661.1	1.9	19.3	42.3	26	70	325
09vHil227	64.63	0.79	13.32	9.03	0.11	2.81	3.38	5.47	0.37	0.07	2.75	2.2	9.2	0.9	8.3	65.3	2.9	27.8	56.0	0	5	342
09vHil229	65.24	0.78	12.91	7.85	0.21	2.83	4.70	5.40	0.01	0.07	2.74	2.6	16.1	1.4	1.8	34.7	1.7	20.2	52.6	0	5	311
09vHil230	52.15	0.39	17.44	7.29	0.09	3.21	14.42	4.96	0.01	0.04	4.66	0.9	31.2	1.0	1.8	54.6	1.2	16.6	25.4	0	21	307
09vHil231	64.46	0.73	13.40	8.26	0.15	1.49	5.74	5.64	0.08	0.06	2.28	1.6	9.9	1.9	1.9	75.1	2.6	23.4	52.9	0	6	316
09vHil232	59.39	0.74	15.44	7.95	0.13	3.62	7.94	3.84	0.88	0.07	6.56	1.7	35.4	0.0	18.3	755.1	2.7	24.6	60.5	133	32	285
09vHil233	67.19	0.79	12.44	8.71	0.14	3.10	2.79	4.22	0.55	0.07	3.93	1.8	7.6	1.6	13.3	233.6	1.2	21.4	59.1	23	5	284
09vHil234	57.78	0.71	15.74	8.36	0.14	4.82	9.66	2.00	0.71	0.07	7.75	2.3	35.7	1.1	14.7	1353.4	1.4	22.6	64.7	194	41	274
09vHil236	57.74	0.84	15.66	8.67	0.14	4.88	9.33	2.11	0.57	0.06	7.70	2.3	42.1	0.5	11.2	1285.6	1.9	18.7	54.8	522	43	337
09vHil237	58.12	0.86	14.78	8.86	0.19	3.69	11.15	1.70	0.58	0.07	7.92	2.9	43.3	0.8	13.6	710.8	2.1	21.8	52.9	49	46	324
09vHil238	56.24	0.88	15.42	10.02	0.14	5.87	7.86	3.07	0.44	0.06	5.74	2.0	37.1	1.4	8.8	535.6	0.9	19.3	48.0	28	65	298

(Continued)

		(wt%) SiO2	TiO2	Al2O3	FeO*	MnO	MgO	CaO	Na2O	K2O	P2O5	LOI	(ppm) Nb	Ni	Pb	Rb	Sr	Th	Y	Zr	Ba	Cr	V
	09vHil239	56.18	0.79	15.50	9.53	0.15	5.68	9.67	2.12	0.33	0.06	7.43	1.7	39.9	1.4	6.0	1224.4	0.8	18.9	52.7	112	77	346
	09vHil240	53.67	0.87	16.16	9.79	0.16	6.91	9.69	2.45	0.22	0.06	7.61	1.0	45.7	1.1	2.8	976.7	3.6	22.1	52.0	98	61	375
	09vHil241	55.71	0.74	16.49	8.04	0.14	4.32	10.73	3.53	0.25	0.08	6.50	2.1	36.1	0.9	4.6	983.6	1.8	21.3	46.9	313	77	360
	09vHil242	56.95	0.76	15.52	8.93	0.16	4.96	9.54	2.50	0.59	0.07	7.10	2.5	32.7	0.6	10.3	1154.9	2.3	20.1	51.8	59	78	349
	09vHil243	54.70	0.62	15.18	8.48	0.18	3.88	15.25	1.45	0.22	0.05	9.95	2.8	31.5	0.0	4.3	1280.2	0.9	18.6	47.6	221	56	259
	09vHil244	55.29	0.71	15.60	8.98	0.13	8.06	7.87	2.75	0.55	0.05	5.12	1.9	46.2	0.0	11.4	161.3	1.0	18.1	37.7	59	72	297
	09vHil245	55.71	0.81	15.29	8.27	0.19	4.49	12.30	1.79	1.07	0.08	9.42	2.9	37.6	0.0	26.1	198.0	2.3	24.6	54.4	26	54	283
	09vHil246	57.09	0.84	16.23	7.50	0.15	4.48	11.17	2.10	0.36	0.09	8.49	2.5	33.8	0.3	7.9	365.5	1.5	24.5	57.0	64	77	295
	09vHil247	58.24	0.77	15.82	8.32	0.12	4.16	8.01	3.05	1.43	0.07	6.39	2.1	45.8	0.9	30.6	263.5	2.5	24.1	55.2	25	44	282
	09vHil248	60.99	0.74	15.15	6.84	0.12	2.44	11.49	2.08	0.06	0.08	7.92	1.9	27.3	1.2	2.1	105.7	1.5	25.6	51.7	29	45	283
	09vHil249	63.59	0.72	13.92	7.33	0.15	3.44	8.23	1.91	0.66	0.08	6.41	2.4	36.2	0.7	17.3	133.0	0.8	24.6	50.3	37	44	264
	09vHil250	59.36	0.67	15.60	7.22	0.14	4.13	10.68	1.60	0.51	0.09	8.52	2.1	50.5	1.7	5.7	1318.0	2.7	26.3	59.4	99	64	265
	09vHil251	59.37	0.67	15.67	7.20	0.14	4.15	10.63	1.58	0.51	0.09	8.49	2.7	49.5	0.7	6.1	1316.2	2.6	25.3	60.3	95	63	265
	09vHil252	56.12	0.79	16.17	8.43	0.13	3.71	11.61	2.38	0.59	0.08	7.75	1.7	31.7	1.4	12.7	321.9	1.8	20.1	41.2	23	73	369
	09vHil253	59.40	0.77	15.17	8.13	0.14	4.16	10.24	1.57	0.37	0.06	8.43	3.0	44.7	1.3	4.8	499.3	0.6	18.7	41.9	28	92	341
	09vHil254	57.12	0.67	15.34	8.33	0.14	4.10	12.80	1.34	0.09	0.06	8.40	1.4	30.1	0.0	2.4	831.1	0.1	16.4	42.5	58	75	298
	09vHil255	56.18	0.68	16.54	7.96	0.16	4.43	11.66	1.99	0.32	0.08	8.83	1.9	39.6	1.7	4.3	869.7	2.6	22.8	56.0	127	50	282
	09vHil256	64.93	0.91	14.05	7.58	0.12	2.45	5.74	2.92	1.22	0.09	6.21	3.2	18.5	1.5	21.3	943.3	3.0	28.6	79.7	235	14	277
	09vHil257	57.57	0.79	14.88	9.44	0.13	4.89	10.02	1.78	0.42	0.07	7.69	1.4	45.0	1.5	6.6	797.9	1.0	19.1	48.5	51	74	334
	09vHil258	57.56	0.73	15.07	8.22	0.16	2.83	13.80	1.47	0.09	0.06	7.84	2.3	26.4	1.2	1.1	461.3	0.5	20.4	44.7	132	97	296
	09vHil259	57.25	0.63	15.75	7.89	0.17	5.81	10.32	1.85	0.28	0.05	7.90	2.1	49.0	0.9	4.5	492.2	1.2	17.8	37.0	74	123	274
	09vHil260	51.83	0.55	16.40	8.54	0.16	3.63	17.07	1.53	0.23	0.05	9.82	1.6	31.3	0.7	2.5	225.4	2.2	16.7	32.0	36	84	263
	10vHil217	53.59	0.31	15.12	8.22	0.09	6.12	11.89	4.64	0.01	0.02	3.55	2.6	103.5	1.4	0.9	61.4	0.5	11.3	11.8	5	258	288
	10vHil218	53.40	1.15	17.53	5.65	1.76	5.99	8.94	3.75	1.74	0.10	2.82	3.7	75.5	4.5	14.1	282.1	1.0	22.4	74.3	71	261	227
	10vHil219	51.13	1.40	16.24	8.73	0.17	7.07	11.69	3.21	0.23	0.13	3.64	4.0	65.7		1.6	204.0	1.4	27.1	87.1	11	198	251
	10vHil220	58.83	0.81	14.66	9.44	0.17	4.36	7.17	3.25	1.26	0.06	5.49	2.0	36.6	0.8	22.0	563.8	1.4	20.4	44.3	689	37	313
	10vHil221	60.20	0.71	15.86	6.43	0.13	4.60	7.04	4.61	0.35	0.07	5.70	1.4	31.7	0.8	3.0	835.7	2.0	20.8	48.9	24	47	231
	10vHil222	56.74	0.58	15.72	7.94	0.14	6.93	8.12	2.43	1.35	0.04	8.02	1.4	102.6	0.2	22.1	1130.5	1.5	16.6	44.5	1137	141	239
(Suhayli)	10SH21	54.78	0.64	13.34	7.10	0.22	5.35	13.81	4.22	0.49	0.05	5.70	2.2	95.5	3.4	4.4	65.2	0.2	19.0	31.5	52	274	210
V3 lavas																							
	07vsal V3	51.34	1.53	15.13	9.80	0.20	6.33	10.31	3.38	1.76	0.22	4.57	15.7	35.9	3.7	12.3	577.8	0.8	27.1	117.2	123	74	287
	09vHil203	53.83	1.89	14.96	10.78	0.49	6.77	5.15	5.77	0.08	0.28	5.62	19.9	20.0	2.4	1.5	78.9	3.7	27.9	124.8	23	41	333
	09vHil204	53.25	1.63	13.97	10.69	0.24	7.07	7.26	5.48	0.13	0.29	3.99	19.2	25.4	2.4	0.9	106.3	3.5	31.2	122.5	20	67	305
	09vHil205	53.06	1.73	14.55	10.89	0.19	6.67	6.69	4.67	1.28	0.28	3.21	20.8	18.5	1.7	11.6	163.4	3.7	30.6	135.2	251	55	316

Appendix Table 2 Bulk-rock major and trace element compositions analyzed by ICP-MS.

				(ppm) Li	Sc	V	Co	Zn	Ga	Rb	Sr	Y	Zr	Nb	Cs	Ba	La	Ce	Pr	Nd	Sm	Eu	Gd	Tb	Dy	Ho	Er	Tm	Yb	Lu	Hf	Ta	W	Pb	Th	U
V1	Fizh	LV1	07fizh5	11.53	34.21	372	39.86	141.13	18.08	7.93	196.6	43.6	121.1	2.99	0.12	96.0	5.15	14.63	2.30	12.71	4.26	1.54	5.82	1.02	6.64	1.52	4.34	0.68	3.99	0.61	3.12	0.21	2.36	0.30	0.10	0.10
			07fz6	10.41	30.54	339	33.57	94.32	16.52	7.40	159.7	41.4	120.7	2.79	0.14	26.4	4.95	14.25	2.38	12.51	4.14	1.42	5.53	1.00	6.45	1.42	4.24	0.63	3.89	0.58	3.01	0.20	10.63	0.97	0.29	0.12
			07fz8	14.99	37.69	376	40.09	102.24	16.59	2.85	198.3	44.3	127.0	3.00	0.09	45.9	4.97	14.49	2.45	12.56	4.26	1.53	5.64	1.05	6.76	1.55	4.47	0.67	4.10	0.61	3.21	0.21	2.96	1.03	0.27	0.15
			07fizh12	15.27	38.55	396	41.82	106.52	18.13	3.24	221.2	41.9	117.1	2.66	0.04	150.3	4.56	13.31	2.15	12.08	4.13	1.50	5.25	0.98	6.41	1.49	4.01	0.64	3.99	0.59	2.91	0.19	2.30	0.24	0.15	0.15
			07fizh13	15.42	36.23	393	35.87	106.85	20.36	2.93	175.2	51.6	147.2	4.16	0.03	53.3	6.49	17.83	2.98	15.31	5.06	1.77	6.85	1.22	7.81	1.76	4.90	0.77	4.77	0.72	3.68	0.27	2.35	0.51	0.39	0.14
			07fizh15	8.82	35.17	329	34.79	91.25	14.14	2.49	174.7	37.0	107.8	2.65	0.06	15.2	4.08	12.18	2.07	11.20	3.50	1.30	4.94	0.91	5.77	1.31	3.68	0.56	3.51	0.54	2.67	0.17	2.41	0.51	0.26	0.20
			07fizh17	12.53	34.31	393	39.56	95.80	14.13	10.16	222.7	35.7	93.3	2.12	0.29	125.6	3.83	11.36	1.91	10.45	3.33	1.22	4.69	0.84	5.43	1.23	3.43	0.56	3.51	0.52	2.42	0.13	1.22	0.24	0.07	0.06
			07fz20	10.51	31.52	406	52.65	110.31	21.15	1.42	136.8	40.8	119.9	2.64	0.11	13.8	4.39	13.06	2.22	11.37	3.89	1.43	5.30	0.99	6.34	1.43	4.24	0.63	4.02	0.60	3.00	0.18	2.64	0.72	0.28	0.12
			07fizh22	21.09	33.22	317	35.57	89.41	20.16	4.56	201.0	40.4	116.2	2.53	0.05	117.3	4.32	12.97	2.16	11.64	3.95	1.33	5.24	0.94	6.01	1.37	4.01	0.61	3.86	0.57	2.92	0.16	1.09	0.28	0.10	0.10
			07fizh23	13.17	23.22	205	27.45	65.83	17.65	0.62	74.7	40.6	124.0	2.70	0.01	11.1	4.87	14.61	2.31	12.11	4.01	1.41	5.42	0.96	6.36	1.40	4.14	0.64	3.99	0.60	3.13	0.18	3.28	0.79	0.32	0.09
			07fz24	7.46	32.09	247	33.41	65.21	14.61	21.33	139.2	18.9	46.9	0.64	0.16	14.3	1.77	4.97	0.89	4.71	1.75	0.68	2.41	0.45	2.93	0.66	1.91	0.30	1.80	0.27	1.31	0.05	1.83	0.53	0.21	0.10
			07fizh26	6.27	33.05	409	33.10	184.77	18.80	2.07	115.9	48.9	149.7	3.48	0.03	15.8	5.74	16.97	2.99	14.54	5.03	1.69	6.44	1.17	7.49	1.76	5.03	0.80	4.88	0.74	3.70	0.22	1.35	0.35	0.10	0.09
			07fz28	5.24	30.61	414	32.89	98.57	18.22	0.81	111.2	46.5	135.6	2.93	0.03	9.0	5.38	15.22	2.60	13.36	4.46	1.55	6.02	1.10	6.86	1.56	4.65	0.70	4.29	0.65	3.45	0.20	3.30	0.79	0.29	0.11
			07fz31	9.10	32.47	433	39.15	122.64	19.58	7.91	132.1	51.2	146.2	3.26	0.08	34.3	5.72	17.05	2.87	15.08	4.83	1.67	6.46	1.20	7.44	1.70	5.06	0.78	4.68	0.71	3.63	0.23	1.41	0.91	0.36	0.10
			07fizh33	10.20	34.35	336	35.48	102.19	20.86	17.52	184.3	51.7	156.5	3.60	0.04	122.1	5.98	18.90	3.17	17.04	5.49	1.83	7.21	1.29	8.47	1.78	5.40	0.80	5.04	0.75	4.07	0.23	0.85	0.40	0.12	0.11
			07fizh34	19.04	36.93	376	35.32	126.72	27.32	3.86	116.6	57.3	183.8	4.45	0.04	101.6	6.36	18.80	3.27	16.88	5.43	1.92	7.28	1.37	8.78	1.95	5.59	0.88	5.50	0.83	4.46	0.29	3.10	0.61	0.46	0.18
			07fizh35	7.07	35.55	347	34.52	94.21	18.02	0.75	55.8	47.7	147.1	3.55	0.03	9.4	5.44	16.29	2.75	14.13	4.70	1.65	6.30	1.15	7.37	1.66	4.78	0.73	4.66	0.70	3.58	0.23	4.29	0.66	0.35	0.28
			07fizh36	4.19	32.01	367	38.20	76.52	20.07	2.10	90.9	47.0	147.5	3.51	0.06	7.8	5.23	15.82	2.66	14.47	4.39	1.60	6.11	1.09	7.47	1.63	4.69	0.73	4.50	0.68	3.63	0.24	1.98	0.35	0.10	0.10
			09FZ1	1.05	28.39	321	16.75	73.75	15.24	0.78	65.5	39.8	107.7	2.27	0.05	6.1	4.27	12.44	2.20	11.12	3.55	1.36	5.06	0.94	6.02	1.33	3.94	0.61	3.59	0.54	2.71	0.15	19.09	0.78	0.23	0.14
			09FZ2	15.12	28.55	209	30.24	59.32	11.74	11.06	174.7	17.4	44.4	0.60	0.07	55.9	1.62	4.76	0.86	4.39	1.58	0.61	2.20	0.42	2.66	0.60	1.83	0.27	1.62	0.25	1.22	0.04	3.62	0.47	0.14	0.12
			09FZ3	7.42	25.86	196	25.24	53.56	11.78	7.51	79.4	15.5	39.5	0.53	0.06	6.0	1.56	4.03	0.75	4.12	1.42	0.58	1.91	0.37	2.38	0.54	1.58	0.22	1.45	0.23	1.07	0.04	2.68	0.75	0.14	0.08
			09FZ4	11.71	25.60	239	27.15	59.25	12.55	7.08	186.2	17.4	42.5	0.61	0.07	68.5	1.79	4.84	0.83	4.68	1.60	0.66	2.20	0.42	2.69	0.61	1.87	0.26	1.66	0.24	1.17	0.04	2.81	0.63	0.14	0.05
			09FZ5	8.92	28.30	360	33.09	113.11	17.29	15.69	89.3	45.4	129.9	2.95	0.12	41.2	5.16	15.11	2.58	13.37	4.24	1.51	5.92	1.07	6.83	1.56	4.91	0.72	4.23	0.66	3.22	0.20	2.55	0.68	0.31	0.08
		MV1	07fizh37	13.25	35.74	261	38.47	140.72	7.63	8.67	125.5	16.9	37.1	0.53	0.10	27.3	1.74	4.03	0.75	4.12	1.40	0.55	2.14	0.38	2.61	0.59	1.74	0.28	1.79	0.26	1.01	0.03	9.32	0.12	0.06	0.06
			07fizh39	12.48	45.08	266	41.61	81.69	17.27	1.56	350.8	19.3	38.0	0.61	0.04	42.8	1.38	4.07	0.72	3.94	1.49	0.59	2.20	0.44	2.97	0.67	1.87	0.31	1.91	0.30	1.08	0.04	1.58	0.79	0.13	0.09
			07fz40	9.43	38.41	281	35.98	71.50	12.49	6.99	214.1	16.4	31.2	0.47	0.15	38.4	1.24	3.55	0.60	3.52	1.33	0.52	2.00	0.38	2.46	0.59	1.71	0.26	1.68	0.25	0.94	0.03	2.01	0.34	0.13	0.13
			07fizh42	12.89	41.92	294	37.07	54.60	12.02	10.11	154.1	14.2	23.1	0.34	0.32	84.7	0.69	2.13	0.40	2.32	0.92	0.40	1.49	0.29	2.14	0.48	1.42	0.23	1.48	0.22	0.71	0.03	0.45	0.07	0.03	0.03
			07fz43	5.07	28.37	342	34.03	126.72	24.41	15.23	82.1	39.2	121.6	2.42	0.13	27.3	4.46	13.22	2.22	11.64	3.92	1.49	5.20	0.93	5.91	1.32	3.87	0.59	3.64	0.54	3.04	0.16	2.25	0.81	0.32	0.14
			07fizh45	8.00	36.34	230	34.70	53.05	15.47	5.27	353.4	15.7	33.3	0.49	0.19	37.1	1.45	3.95	0.60	3.66	1.33	0.62	2.02	0.39	2.51	0.56	1.52	0.25	1.52	0.22	0.99	0.03	0.83	0.14	0.05	0.05
			07fizh46	11.53	34.75	225	39.56	70.08	14.08	8.36	280.5	18.2	42.0	0.54	0.10	31.8	1.76	4.77	0.83	4.30	1.61	0.62	2.31	0.41	2.74	0.63	1.79	0.29	1.71	0.26	1.14	0.04	1.26	0.56	0.14	0.04
			07fz47	6.26	28.29	290	33.33	84.48	18.68	6.40	122.1	33.7	97.4	1.96	0.11	24.2	3.85	11.02	1.84	9.41	3.19	1.20	4.39	0.81	5.01	1.13	3.23	0.49	3.01	0.44	2.44	0.13	1.28	1.05	0.27	0.05
			07fizh48	13.60	36.74	237	39.36	61.91	15.88	3.25	374.5	16.5	39.2	0.58	0.10	31.6	1.53	4.67	0.77	4.29	1.63	0.63	2.18	0.40	2.76	0.60	1.68	0.26	1.66	0.24	1.14	0.04	1.42	0.15	0.00	0.00
			07fizh49	8.71	28.54	250	21.91	95.14	14.90	4.51	109.9	45.5	141.3	3.24	0.06	84.1	5.82	16.85	2.76	13.93	4.62	1.61	5.98	1.09	7.08	1.60	4.64	0.71	4.35	0.65	3.46	0.23	3.34	0.61	0.35	0.15
			07fizh50	17.02	35.96	357	46.84	117.85	20.50	20.18	192.3	49.0	141.7	3.48	0.32	94.8	5.43	16.16	2.73	14.15	4.77	1.59	6.23	1.15	7.31	1.64	4.77	0.72	4.48	0.66	3.53	0.24	1.96	0.69	0.33	0.18
			07fz51	8.12	31.13	370	29.90	102.80	14.62	14.96	145.9	46.0	134.7	3.35	0.20	36.3	6.52	17.30	2.85	14.13	4.63	1.60	6.19	1.09	6.93	1.53	4.48	0.66	4.13	0.61	3.26	0.22	1.69	4.03	0.32	0.16
		UV1	07fz53	2.80	32.36	250	17.00	29.93	15.05	2.32	140.4	12.4	33.9	0.52	0.05	14.1	1.43	3.63	0.61	3.27	1.09	0.47	1.55	0.29	1.90	0.43	1.30	0.21	1.35	0.21	0.95	0.04	4.89	0.83	0.12	0.12
			07fizh55	6.54	36.93	323	35.20	74.54	17.56	1.47	209.4	19.7	34.7	0.59	0.01	11.4	1.88	4.82	0.77	4.91	1.46	0.59	2.19	0.42	3.03	0.67	1.93	0.30	1.96	0.29	1.10	0.04	1.18	0.13	0.04	0.04
			08fizh1	6.24	43.78	301	32.35	73.01	16.18	7.39	320.3	15.6	21.8	0.39	0.06	60.9	1.09	2.61	0.47	2.61	1.05	0.45	1.69	0.34	2.37	0.55	1.65	0.26	1.68	0.26	0.71	0.02	2.00	0.45	0.06	0.08
			08fz3	4.54	23.84	166	23.48	44.52	10.08	2.66	89.2	12.8	29.6	0.43	0.05	21.2	1.13	3.35	0.54	3.06	1.09	0.42	1.59	0.28	1.88	0.44	1.29	0.19	1.24	0.19	0.81	0.03	6.10	0.46	0.10	0.06
			08fizh5	7.50	39.24	306	35.03	71.49	23.71	1.48	113.8	20.8	42.3	0.63	0.02	34.5	2.08	5.27	1.00	5.04	1.89	0.72	2.60	0.48	3.19	0.73	2.08	0.33	2.05	0.31	1.23	0.04	1.25	0.60	0.15	0.09
			08fz6	2.21	32.90	267	33.73	53.99	20.72	3.12	725.6	21.3	38.8	0.58	0.08	204.7	2.12	4.88	0.93	4.86	1.61	0.62	2.35	0.45	3.04	0.69	2.10	0.32	2.05	0.32	1.08	0.04	2.31	0.76	0.14	0.18
			08fizh7	9.47	37.74	255	32.99	68.09	15.41	22.04	363.9	19.8	44.5	0.66	0.54	94.8	1.87	5.24	0.89	4.84	1.71	0.63	2.36	0.46	2.97	0.67	2.08	0.31	1.98	0.31	1.20	0.04	1.63	0.50	0.16	0.10
			08fz8	3.86	33.30	276	24.29	63.82	12.26	20.28	356.9	17.9	39.3	0.61	0.17	275.1	1.76	5.10	0.88	4.06	1.57	0.57	2.20	0.41	2.74	0.61	1.76	0.28	1.71	0.27	1.09	0.04	1.46	0.48	0.14	0.15
			09FZ7	7.70	33.90	260	31.36	61.81	10.25	5.51	262.9	18.3	43.0	0.63	0.04	19.6	1.81	5.10	0.83	4.55	1.60	0.66	2.36	0.44	2.83	0.64	2.02	0.31	1.83	0.28	1.19	0.04	1.69	0.63	0.25	0.10
			09FZ9	6.42	28.52	210	25.43	78.18	12.07	6.02	91.0	16.9	38.7	0.54	0.13	77.9	1.59	4.41	0.73	4.19	1.41	0.61	2.08	0.40	2.54	0.62	1.77	0.28	1.59	0.25	1.13	0.03	1.69	0.46	0.13	0.08
	Thuqbah		10Thu1	4.66	27.67	302	27.10	86.84	15.48	4.04	62.0	33.3	93.5	1.39	0.04	40.7	3.37	10.40	1.75	9.08	3.31	1.12	4.40	0.80	5.04	1.14	3.40	0.50	3.16	0.49	2.49	0.11	4.48	0.58	0.29	0.13
			10Thu2	7.68	24.34	382	24.14	90.65	15.58	4.49	107.6	32.8	88.4	1.35	0.02	51.2	3.55	10.53	1.77	9.49	3.18	1.13	4.10	0.75	5.06	1.09	3.32	0.50	3.06	0.46	2.40	0.10	9.62	0.51	0.29	0.14
			10Thu3	10.86	33.21	338	33.23	88.11	18.91	1.40	72.6	24.4	70.9	1.21	0.02	15.4	2.68	7.77	1.32	7.09	2.39	0.89	3.14	0.59	3.77	0.85	2.50	0.42	2.25	0.33	1.89	0.08	1.78	0.62	0.26	0.11
			10Thu6	9.80	30.70	367	30.32	99.30	17.60	13.36	114.9	34.2	88.9	1.42	0.05	162.7	3.45	9.99	1.62	9.01	3.13	1.16	4.11	0.79	5.15	1.17	3.43	0.56	3.31	0.51	2.36	0.10	3.58	0.79	0.29	0.11
			10Thu7	27.52	24.09	177	20.85	81.66	16.30	0.60	70.5	44.1	134.4	2.28	0.02	21.2	4.72	14.10	2.33	13.01	4.36	1.36	5.64	1.05	6.63	1.51	4.44	0.67	4.16	0.63	3.51	0.15	6.87	0.85	0.46	0.23
			10Thu8	8.17	21.02	266	33.58	61.56	13.06	2.42	320.5	29.2	82.2	1.35	0.01	23.2	3.48	9.34	1.56	8.33	2.75	1.01	3.78	0.69	4.44	0.98	2.98	0.45	2.56	0.39	2.12	0.09	6.37	0.40	0.34	0.27
			10Thu10	5.99	29.37	259	22.86	76.78	9.07	3.67	209.6	27.3	70.9	1.38	0.09	23.9	3.05	8.11	1.39	7.30	2.62	0.97	3.59	0.64	4.11	0.95	2.85	0.47	2.65	0.40	1.88	0.10	4.59	0.78	0.34	0.25
			10Thu11	7.09	33.87	299	21.51	78.39	14.06	9.48	942.5	27.9	78.5	1.75	0.12	101.7	3.34	8.98	1.55	7.83	2.89	1.03	3.82	0.66	4.24	0.95	2.95	0.42	2.64	0.40	2.02	0.12	3.90	1.05	0.28	0.12
			10Thu12	3.99	27.56	329	17.18	81.64	23.80	1.79	105.7	32.1	96.2	2.14	0.08	26.3	4.02	10.73	1.90	9.74	3.27	1.21	4.33	0.75	4.88	1.08	3.19	0.52	2.82	0.43	2.51	0.15	6.09	1.05	0.36	0.27
			10Thu13	3.73	33.25	263	19.32	45.22	17.02	0.92	67.7	18.5	46.8	0.94	0.07	20.0	1.97	5.16	0.94	5.12	1.86	0.69	2.36	0.43	2.80	0.65	1.90	0.30	1.82	0.27	1.37	0.07	3.73	0.97	0.19	0.27
			10Thu14	4.72	29.04	412	16.41	74.19	15.29	1.97	117.1	30.3	76.7	1.35	0.11	62.2	2.84	8.38	1.40	7.73	2.88	1.07	3.94	0.71	4.50	1.03	3.07	0.47	2.87	0.44	2.03	0.09	6.36	0.87	0.26	0.21
	Ghayth		06ghay1	-	45.04	-	40.35	68.39	15.10	23.40	116.7	22.2	46.8	0.70	0.05	227.4	1.75	5.18	0.90	5.19	1.87	0.70	2.64	0.51	3.31	0.75	2.18	0.33	2.10	0.32	1.32	0.07	-	1.29	0.15	0.51
			06ghay2	-	37.52	-	43.51	74.37	12.94	10.42	112.5	25.1	56.6	1.09	0.05	128.0	1.92	5.61	0.97	5.23	1.92	0.68	2.92	0.55	3.69	0.86	2.52	0.40	2.54	0.40	1.51	0.06	-	1.46	0.17	0.13
			06ghay7	-	36.26	-	41.84	118.52	19.23	2.52	124.7	42.3	120.3	2.44	0.02	34.0	4.41	13.41	2.33	12.11	3.94	1.50	5.35	0.99	6.54	1.45	4.33	0.66	4.04	0.62	3.02	0.16	-	1.38	0.29	0.12
			06ghay14	-	35.74	-	42.55	112.09	19.85	6.33	116.9	56.0	166.6	3.99	0.02	110.8	6.44	19.52	3.19	16.54	5.46	1.84	7.06	1.27	8.45	1.84	5.50	0.82	5.14	0.78	4.06	0.26	-	0.71	0.39	0.20
			06ghay17	-	33.30	-	29.67	108.20	19.63	3.38	126.3	51.9	166.6	3.95	0.04	14.6	5.43	16.40	2.84	14.54	4.84	1.70	6.57	1.21	7.91	1.80	5.38	0.84	5.30	0.80	4.09	0.28	-	3.37	0.41	0.16
			06ghay19	-	40.26	-	41.59	61.68	14.24	0.69	78.7	29.2	75.3	1.91	0.00	6.1	2.94	8.95	1.51	7.61	2.79	1.09	3.81	0.71	4.61	1.05	2.92	0.47	2.79	0.42	1.95	0.13	-	1.38	0.18	0.12
			06ghay24	-	36.26	-	41.12	377.96	18.76	0.25	53.5	42.5	116.6	2.62	0.01	5.4	4.67	13.45	2.25	11.48	3.95	1.53	5.41	1.02	6.46	1.44	4.23	0.66	3.92	0.60	2.87	0.18	-	2.08	0.26	0.10
			06ghay34	-	27.85	-	32.81	70.35	15.05	0.41	40.6	30.1	83.5	1.65	0.00	5.1	3.45	9.53	1.65	8.24	2.73	1.04	3.75	0.68	4.55	0.99	2.96	0.46	2.79	0.43	2.08	0.13	-	0.82	0.25	0.13
			06ghay44	-	28.21	-	34.48	85.38	18.57	0.66	63.7	37.4	109.5	2.38	0.07	9.7	4.78	13.16	2.30	11.06	3.79	1.41	5.00	0.96	5.92	1.30	3.70	0.64	3.67	0.59	2.86	0.21	-	1.70	0.38	1.04
			06ghay47	-	21.53	-	24.24	51.63	18.11	0.20	32.2	49.0	157.9	3.10	0.00	14.4	6.52	18.06	2.97	14.93	4.79	1.61	6.38	1.18	7.57	1.64	4.82	0.78	4.60	0.71	3.86	0.21	-	0.69	0.42	0.29
			06ghay49	-	24.83	-	22.15	121.01	16.75	0.63	40.6	37.2	114.4	2.31	0.01	7.4	4.07	11.94	2.01	10.50	3.51	1.20	4.58	0.85	5.41	1.22	3.63	0.55	3.42	0.52	2.79	0.16	-	0.99	0.31	0.22

(Continued)

		(ppm) Li	Sc	V	Co	Zn	Ga	Rb	Sr	Y	Zr	Nb	Cs	Ba	La	Ce	Pr	Nd	Sm	Eu	Gd	Tb	Dy	Ho	Er	Tm	Yb	Lu	Hf	Ta	W	Pb	Th	U
	06ghay54	-	26.94	-	30.49	186.11	16.58	0.80	53.5	30.5	92.4	1.81	0.01	11.1	3.73	10.08	1.66	8.89	2.85	1.04	3.91	0.75	4.55	1.01	3.05	0.47	2.90	0.45	2.30	0.12	-	2.13	0.28	0.29
	06ghay64	-	23.50	-	23.10	90.52	17.59	1.36	60.6	40.2	127.6	2.47	0.02	13.2	4.66	13.86	2.33	11.64	3.94	1.28	5.29	0.98	6.14	1.34	4.01	0.64	3.80	0.57	3.20	0.18	-	1.81	0.39	0.21
	06ghay69	-	26.25	-	32.52	108.06	18.94	1.45	79.2	35.0	110.6	2.14	0.02	16.2	3.89	11.28	1.97	10.38	3.38	1.22	4.57	0.86	5.40	1.20	3.49	0.55	3.29	0.50	2.72	0.14	-	1.81	0.33	0.23
	08ghay1	6.47	18.82	93	12.66	67.35	14.71	0.42	34.3	42.6	126.7	2.53	0.01	5.8	4.86	14.06	2.31	12.00	4.02	1.40	5.51	0.98	6.40	1.39	4.21	0.65	4.11	0.62	3.11	0.17	6.72	0.88	0.33	0.26
	08ghay2	4.98	16.78	69	10.73	78.84	14.72	1.48	83.8	38.3	131.6	2.33	0.03	11.0	5.39	14.37	2.28	11.94	3.84	1.27	5.04	0.91	5.80	1.25	3.80	0.60	3.53	0.53	3.28	0.16	5.62	1.26	0.48	0.29
	08ghay5	6.37	22.52	144	16.84	98.04	19.08	0.71	78.4	46.3	142.1	2.89	0.01	11.4	5.49	15.88	2.60	13.43	4.51	1.53	6.14	1.10	7.10	1.57	4.74	0.72	4.42	0.69	3.56	0.20	3.98	0.98	0.37	0.46
	08ghay11	5.30	21.44	190	16.35	74.89	12.50	0.49	68.8	36.7	116.9	2.37	0.00	8.4	4.62	13.09	2.22	10.90	3.62	1.24	4.82	0.87	5.77	1.22	3.84	0.59	3.56	0.54	2.97	0.16	6.65	0.87	0.34	0.20
	10ghay1	6.88	22.44	272	20.35	63.59	14.16	0.36	29.5	34.1	96.7	1.83	0.00	4.7	3.22	10.21	1.75	9.06	3.09	1.13	4.30	0.80	5.09	1.15	3.27	0.49	3.13	0.47	2.35	0.12	3.63	2.26	0.22	0.13
	10ghay2	5.51	33.78	259	31.91	91.05	12.56	2.98	117.2	18.5	39.7	0.59	0.03	40.5	1.48	4.36	0.79	4.46	1.59	0.56	2.25	0.42	2.82	0.64	1.89	0.32	1.85	0.29	1.11	0.04	4.67	1.29	0.12	0.12
	10ghay3	4.49	28.04	312	25.66	86.06	14.74	6.75	78.6	26.5	57.9	0.87	0.02	169.6	1.78	5.51	1.00	5.43	2.04	0.71	3.03	0.60	4.13	0.94	2.74	0.45	2.77	0.43	1.73	0.06	6.61	0.56	0.17	0.13
	10ghay4	9.59	28.94	307	26.97	92.35	15.16	0.33	36.8	39.6	131.8	2.98	0.00	6.0	3.19	11.18	2.00	10.72	3.83	1.32	5.08	0.92	6.08	1.34	4.03	0.58	3.91	0.60	3.04	0.19	4.51	1.00	0.30	0.31
	10ghay5	6.34	22.58	100	16.78	124.96	18.11	0.66	48.0	49.2	150.9	3.23	0.01	10.8	5.50	16.28	2.76	14.28	4.77	1.61	6.14	1.13	7.12	1.62	4.69	0.68	4.57	0.69	3.61	0.21	6.11	1.16	0.36	0.24
	10ghay6	3.76	33.67	432	32.39	115.10	17.56	0.24	34.2	44.5	135.2	2.98	0.00	5.9	4.87	14.43	2.43	12.81	4.32	1.43	5.77	1.07	6.77	1.49	4.37	0.64	4.08	0.61	3.18	0.19	4.35	0.41	0.29	0.17
	10ghay7	7.57	26.97	321	32.99	69.60	13.93	0.37	54.7	35.2	102.6	2.04	0.01	6.9	3.64	10.93	1.87	9.74	3.30	1.13	4.39	0.82	5.20	1.17	3.46	0.55	3.24	0.49	2.58	0.15	5.83	1.39	0.26	0.59
	10ghay8	3.64	26.77	325	25.41	84.89	18.78	0.11	42.2	36.1	113.5	2.24	0.01	4.1	4.11	12.51	2.14	11.11	3.61	1.30	4.77	0.91	5.75	1.27	3.61	0.50	3.39	0.51	2.90	0.16	4.21	1.59	0.27	0.13
	10ghay9	3.63	21.53	144	15.69	78.03	17.15	0.81	44.1	46.0	135.9	2.78	0.01	7.7	5.02	14.92	2.54	13.04	4.27	1.46	5.72	1.04	6.69	1.49	4.49	0.68	4.31	0.65	3.35	0.19	6.16	0.82	0.36	0.18
	10ghay10	3.07	32.75	254	30.10	92.02	15.31	4.90	77.4	24.9	46.4	1.17	0.08	69.8	1.86	5.55	0.96	5.31	1.98	0.61	2.99	0.57	3.81	0.87	2.47	0.39	2.52	0.39	1.40	0.07	3.66	0.71	0.15	0.09
	10ghay11	4.19	27.60	409	27.83	78.56	18.50	2.68	107.1	34.4	105.4	2.05	0.02	69.6	3.84	11.57	1.86	10.05	3.39	1.21	4.47	0.85	5.39	1.20	3.48	0.55	3.31	0.51	2.68	0.14	6.37	0.73	0.30	0.28
	10ghay12	3.80	21.70	241	22.34	68.20	15.70	6.46	95.1	26.8	86.3	1.66	0.07	78.7	3.49	9.80	1.57	8.00	2.77	0.93	3.30	0.67	4.15	0.95	2.65	0.41	2.61	0.40	2.14	0.11	5.89	0.63	0.30	0.15
	10ghay14	4.33	33.16	276	30.55	59.18	15.47	7.68	131.1	24.2	54.4	1.05	0.11	84.3	1.78	5.16	0.88	4.92	1.85	0.66	2.69	0.53	3.52	0.82	2.43	0.37	2.50	0.39	1.52	0.08	3.97	0.45	0.16	0.11
	10ghay15	8.26	22.82	200	22.77	74.48	16.46	6.40	74.8	38.2	126.3	2.30	0.02	78.2	4.70	13.59	2.27	11.95	3.91	1.38	5.20	0.95	5.98	1.32	3.78	0.57	3.51	0.52	3.16	0.17	5.02	1.11	0.32	0.53
	10ghay16	4.82	22.75	193	23.33	76.97	17.52	2.17	108.1	36.1	123.6	2.24	0.01	39.6	4.14	12.61	2.11	11.26	3.74	1.28	4.85	0.86	5.59	1.25	3.51	0.54	3.34	0.50	3.01	0.15	4.23	0.45	0.31	0.13
	10ghay17	14.37	16.99	62	9.10	70.62	12.64	1.91	86.9	25.0	54.8	1.13	0.02	17.0	1.96	5.88	1.05	5.60	2.09	0.37	2.96	0.56	3.87	0.92	2.85	0.47	2.83	0.44	1.74	0.08	14.57	0.65	0.19	0.36
	10ghay18	2.24	32.64	371	35.92	85.36	15.90	1.50	81.2	42.9	122.8	2.77	0.02	65.1	4.70	14.35	2.31	12.65	4.29	1.42	5.44	1.06	6.68	1.48	4.36	0.70	4.06	0.61	3.11	0.20	4.70	0.25	0.29	0.15
	10ghay19	4.02	32.97	256	28.59	96.87	13.84	4.59	105.5	20.2	44.2	0.95	0.01	168.7	1.58	4.67	0.78	4.18	1.56	0.56	2.24	0.45	2.95	0.69	2.01	0.29	2.01	0.31	1.22	0.06	4.58	0.44	0.13	0.11
	10ghay20	3.22	30.53	368	31.14	90.05	19.43	0.53	55.2	42.7	133.3	3.17	0.01	11.9	4.88	15.10	2.48	13.00	4.35	1.52	5.68	1.08	6.77	1.49	4.23	0.68	4.00	0.59	3.32	0.21	3.97	0.55	0.32	0.16
	10ghay21	4.67	26.59	318	28.60	104.67	18.41	0.45	42.4	44.4	128.0	3.07	0.01	7.2	4.99	15.11	2.52	13.07	4.43	1.51	5.68	1.05	6.65	1.51	4.38	0.64	4.17	0.64	3.19	0.20	4.55	0.57	0.32	0.16
	10ghay22	9.53	28.28	335	28.47	98.52	18.96	0.42	41.6	39.6	117.7	2.31	0.01	5.7	3.95	12.40	2.11	11.30	3.90	1.40	5.11	0.96	6.21	1.37	4.04	0.64	3.81	0.58	3.06	0.16	5.50	1.49	0.28	0.20
	10ghay23	15.89	28.10	368	34.74	93.39	19.23	0.31	22.7	23.7	101.1	1.97	0.01	7.1	2.67	7.91	1.37	7.36	2.46	0.73	3.11	0.58	3.80	0.89	2.72	0.46	2.91	0.48	2.53	0.13	5.48	1.37	0.23	0.20
	10ghay24	4.43	27.21	333	26.62	102.00	18.32	0.36	61.4	43.3	127.4	2.43	0.02	9.6	4.60	13.87	2.28	12.56	4.29	1.45	5.36	1.05	6.74	1.51	4.29	0.65	4.06	0.61	3.22	0.18	6.32	0.66	0.32	0.60
	10ghay25	4.38	28.01	331	28.12	87.31	18.62	0.52	39.3	40.3	129.3	2.53	0.01	7.7	4.55	13.61	2.29	12.53	4.19	1.44	5.46	0.98	6.43	1.40	4.03	0.66	3.85	0.59	3.26	0.17	6.34	0.50	0.32	0.20
	10ghay26	7.58	28.21	388	20.50	85.35	15.04	0.53	28.4	28.8	47.7	1.94	0.01	3.2	3.21	9.33	1.61	8.73	3.18	1.04	3.94	0.76	4.95	1.08	3.07	0.49	2.90	0.46	1.67	0.13	6.25	0.44	0.21	0.16
	10ghay27	7.69	39.86	284	37.46	59.89	11.73	12.70	119.7	15.9	16.7	0.38	0.97	224.5	0.91	2.80	0.49	2.87	1.09	0.47	1.70	0.35	2.45	0.56	1.60	0.27	1.63	0.24	0.61	0.03	5.71	0.29	0.07	0.04
	10ghay28	2.48	26.78	345	25.24	48.25	16.19	1.13	63.6	34.1	68.8	2.05	0.01	13.8	3.57	10.96	1.91	9.90	3.48	1.19	4.51	0.83	5.31	1.16	3.43	0.57	3.11	0.47	2.06	0.14	4.28	0.26	0.23	0.19
	10ghay29	3.78	30.62	411	39.45	117.23	17.79	0.44	64.5	37.7	106.6	2.22	0.01	8.0	3.42	11.24	1.94	10.95	3.71	1.30	4.99	0.92	5.97	1.30	3.85	0.63	3.67	0.56	2.86	0.15	4.01	0.88	0.26	0.26
	10ghay30	4.68	28.44	337	29.10	120.53	18.84	0.47	54.8	40.5	118.2	2.33	0.01	8.8	3.95	12.47	2.17	11.48	3.87	1.37	5.21	0.95	6.27	1.36	4.01	0.64	3.83	0.59	3.01	0.16	9.73	1.12	0.29	0.25
	10ghay31	6.00	28.33	330	32.62	95.42	19.39	0.61	62.2	38.9	114.8	2.27	0.01	8.4	4.37	12.70	2.15	11.41	3.80	1.31	4.97	0.91	6.15	1.34	3.95	0.61	3.67	0.55	3.02	0.15	5.60	0.75	0.30	0.33
	10ghay33	5.77	25.29	314	26.63	75.34	15.72	0.76	39.6	37.8	107.6	2.15	0.01	5.4	3.35	12.00	2.08	11.16	3.68	1.34	5.06	0.91	5.89	1.30	3.76	0.61	3.63	0.55	2.80	0.14	5.74	0.95	0.27	0.19
	10ghay32	8.63	37.33	258	37.62	187.82	14.16	12.56	103.2	16.8	33.1	0.41	0.08	104.6	1.31	3.82	0.64	3.83	1.39	0.47	1.97	0.37	2.48	0.59	1.67	0.25	1.66	0.25	0.98	0.03	4.76	0.82	0.15	0.26
	10ghay34	6.39	34.13	262	31.89	216.94	12.91	0.96	60.5	13.2	29.5	0.36	0.01	12.2	0.80	2.65	0.49	2.79	1.16	0.35	1.51	0.31	2.15	0.47	1.34	0.23	1.30	0.19	0.86	0.03	4.18	0.68	0.13	0.13
	10ghay35	3.54	34.07	216	33.24	109.24	9.38	0.26	70.4	15.4	30.6	0.54	0.01	8.5	1.03	3.22	0.59	3.32	1.24	0.43	1.81	0.36	2.41	0.54	1.60	0.27	1.50	0.22	0.91	0.04	2.96	1.43	0.11	0.15
	10ghay36	6.32	26.67	346	26.26	99.58	16.94	2.68	65.2	43.1	128.9	2.61	0.01	47.0	4.72	14.59	2.41	12.80	4.29	1.45	5.63	1.06	6.78	1.48	4.26	0.71	4.09	0.61	3.23	0.18	2.50	0.60	0.33	0.29
	10ghay37	7.90	35.34	783	32.33	177.88	15.04	0.53	46.4	16.0	31.6	0.48	0.01	5.7	1.13	3.32	0.63	3.21	1.23	0.45	1.80	0.37	2.40	0.55	1.63	0.26	1.63	0.25	0.91	0.03	2.07	0.42	0.11	0.17
	10ghay38	5.76	33.09	236	29.14	82.24	12.80	2.53	111.3	20.3	39.7	0.68	0.08	35.7	1.46	4.07	0.72	4.28	1.59	0.53	2.33	0.46	3.15	0.70	2.07	0.36	2.07	0.32	1.22	0.04	2.14	0.73	0.15	0.16
	10ghay39	9.26	34.74	206	31.01	184.68	11.82	0.89	54.9	11.1	22.0	0.28	0.02	14.8	0.80	2.19	0.38	2.19	0.84	0.31	1.26	0.25	1.66	0.38	1.11	0.20	1.16	0.18	0.67	0.02	2.55	0.83	0.10	0.16
	10ghay40	9.75	34.33	220	31.99	123.72	12.70	0.95	117.9	14.8	33.2	0.51	0.03	13.1	1.26	3.34	0.61	3.22	1.30	0.48	1.69	0.33	2.20	0.50	1.50	0.26	1.47	0.23	0.89	0.03	2.70	1.39	0.11	0.23
	10ghay41	7.75	38.07	328	35.57	361.11	14.97	1.82	97.7	15.4	27.2	0.39	0.03	38.2	0.83	2.74	0.48	2.80	1.15	0.43	1.73	0.34	2.27	0.54	1.60	0.25	1.60	0.24	0.82	0.03	1.65	1.93	0.10	0.14
	10ghay42	10.56	36.19	248	34.47	52.29	11.82	32.16	249.4	12.9	21.8	0.30	0.10	802.7	1.02	2.76	0.45	2.66	0.98	0.39	1.55	0.29	1.97	0.46	1.33	0.20	1.34	0.21	0.68	0.02	2.47	0.40	0.10	0.09
	10ghay43	7.25	37.40	226	34.75	59.26	12.98	0.53	60.6	12.4	24.8	0.30	0.00	11.7	0.96	2.68	0.45	2.61	1.01	0.39	1.45	0.28	1.93	0.45	1.31	0.20	1.31	0.21	0.72	0.02	2.35	0.62	0.10	0.12
	10ghay44	9.67	34.95	261	34.21	142.17	11.35	13.09	144.8	16.5	28.6	0.48	0.06	289.8	1.15	3.30	0.59	3.28	1.25	0.47	1.93	0.36	2.43	0.56	1.62	0.22	1.56	0.24	0.85	0.03	2.65	1.93	0.10	0.17
	10ghay45	4.86	33.95	228	30.37	73.45	9.59	19.38	88.1	15.3	31.6	0.52	0.01	386.0	0.93	3.10	0.61	3.24	1.24	0.46	1.80	0.36	2.35	0.53	1.57	0.25	1.52	0.23	0.89	0.04	3.87	1.29	0.11	0.11
	10ghay46	16.50	31.87	266	29.10	64.04	13.37	29.87	79.2	18.3	37.4	0.49	0.04	312.9	1.28	3.69	0.65	3.86	1.44	0.51	2.19	0.42	2.80	0.63	1.89	0.26	1.81	0.27	1.11	0.03	2.99	0.75	0.11	0.13
	10ghay47	15.91	34.36	327	35.55	91.78	17.75	48.52	101.0	30.2	65.7	1.20	0.04	319.6	2.36	6.94	1.20	6.66	2.44	0.77	3.47	0.68	4.54	1.03	3.17	0.47	3.05	0.48	1.89	0.08	20.06	4.49	0.20	0.18
	10ghay48	7.78	39.05	235	38.45	56.78	14.40	0.88	63.1	14.2	27.6	0.44	0.02	22.3	1.12	3.13	0.54	2.89	1.12	0.43	1.66	0.31	2.14	0.49	1.46	0.20	1.39	0.22	0.80	0.04	1.62	1.06	0.10	0.07
Yanbu	06vsal13	6.22	24.95	276	22.48	183.44	14.55	1.47	128.9	34.4	102.7	2.24	0.03	15.0	4.31	12.54	2.05	10.68	3.54	1.29	4.83	0.86	5.43	1.22	3.58	0.53	3.45	0.52	2.66	0.16	5.12	0.95	0.24	0.17
	06vsal29	3.15	16.46	77	10.64	214.82	15.64	1.09	91.5	49.0	157.9	3.27	0.01	13.3	6.26	17.67	2.92	15.05	4.79	1.21	6.32	1.17	7.47	1.67	5.02	0.79	4.95	0.75	3.97	0.24	14.60	1.19	0.38	0.21
	06vsal30	3.85	16.00	56	11.81	248.40	17.88	2.35	114.2	60.6	194.7	3.97	0.02	17.3	8.58	23.70	3.86	19.66	6.12	1.97	8.35	1.49	9.26	2.08	6.10	0.96	5.85	0.89	4.86	0.27	3.66	1.38	0.50	0.23
	06vsal31	4.58	18.67	135	15.66	172.88	13.98	0.98	73.2	27.8	90.3	1.71	0.02	8.6	3.34	10.14	1.70	8.63	2.95	0.94	3.79	0.71	4.42	0.97	2.86	0.43	2.65	0.39	2.28	0.12	4.87	0.66	0.30	0.14
	06sal6	-	43.65	-	45.66	65.96	14.50	10.21	180.8	23.2	65.2	0.75	0.22	110.5	2.33	7.17	1.25	6.50	2.16	0.86	3.05	0.55	3.49	0.78	2.24	0.35	2.15	0.33	1.52	0.07	-	0.72	0.07	0.03
	06sal9	-	3.38	-	12.97	54.98	8.25	1.03	91.3	26.8	85.8	2.12	0.01	10.2	3.37	9.74	1.61	8.11	2.68	0.92	3.50	0.65	4.14	0.93	2.67	0.41	2.53	0.37	2.10	0.05	-	0.39	0.21	0.09
	06sal18	7.15	28.39	332	26.23	90.58	13.46	0.86	78.2	43.6	122.9	2.80	0.03	9.9	5.07	14.49	2.46	12.79	4.14	1.47	5.79	1.02	6.81	1.42	4.29	0.70	4.02	0.59	3.06	0.17	0.46	0.31	0.49	0.48
	06sal24	-	35.09	-	39.83	88.64	16.79	2.46	169.8	37.4	104.0	2.49	0.01	21.1	4.62	12.95	2.16	10.86	3.59	1.30	4.90	0.89	5.68	1.28	3.82	0.58	3.60	0.54	2.58	0.07	-	1.03	0.25	0.56
	06sal27	-	42.62	-	39.89	113.86	20.55	2.58	127.2	27.6	80.1	1.87	0.02	11.8	4.55	11.96	1.91	9.39	2.99	1.07	3.89	0.69	4.37	0.93	2.65	0.42	2.58	0.40	1.89	0.11	-	1.26	0.19	0.08

(Continued)

		Li (ppm)	Sc	V	Co	Zn	Ga	Rb	Sr	Y	Zr	Nb	Cs	Ba	La	Ce	Pr	Nd	Sm	Eu	Gd	Tb	Dy	Ho	Er	Tm	Yb	Lu	Hf	Ta	W	Pb	Th	U
	10vsal2	5.19	13.66	35	10.35	139.55	16.97	0.43	73.4	54.9	185.5	3.67	0.00	8.9	6.18	18.44	3.12	15.81	5.28	1.41	6.84	1.28	8.54	1.90	5.62	0.84	5.37	0.80	4.56	0.25	5.70	0.88	0.47	0.26
	10vsal3	3.81	12.88	43	9.15	128.28	15.21	0.84	50.4	44.6	190.0	3.89	0.01	9.5	5.91	15.79	2.87	14.92	4.72	1.18	6.00	1.12	7.18	1.58	4.79	0.71	4.58	0.70	4.72	0.26	6.83	0.91	0.38	0.16
	10vsal4	5.88	19.93	150	20.02	102.41	19.08	0.35	51.6	64.2	209.0	4.54	0.00	12.3	7.55	22.33	3.78	19.53	6.30	2.01	8.21	1.51	9.76	2.14	6.32	0.91	5.93	0.90	5.09	0.30	4.29	1.09	0.49	0.16
	10vsal6	4.57	16.92	103	11.51	67.17	15.95	0.44	54.0	56.3	197.6	4.08	0.00	7.5	7.62	22.21	3.59	18.18	5.71	1.71	7.45	1.34	8.69	1.96	5.72	0.90	5.43	0.84	4.88	0.28	6.29	0.55	0.50	0.28
	10vsal8	2.93	16.70	105	12.17	55.69	14.70	0.66	64.5	59.0	213.2	4.38	0.00	11.3	8.11	23.59	3.86	18.81	5.96	1.70	7.69	1.41	9.03	1.99	5.87	0.87	5.47	0.81	5.08	0.29	9.23	0.43	0.53	0.28
	10vsal10	2.35	23.90	217	24.28	47.65	16.98	0.49	72.1	47.9	152.8	3.34	0.00	12.5	5.82	16.99	2.83	14.89	4.95	1.48	6.45	1.16	7.56	1.69	4.94	0.67	4.44	0.67	3.81	0.22	5.43	0.48	0.39	1.08
	10vsal12	6.41	16.50	188	24.03	0.00	11.74	1.84	342.0	29.2	76.9	0.00	0.02	203.7	2.27	6.82	1.32	7.01	2.48	0.90	3.56	0.65	4.41	1.00	2.98	0.47	2.86	0.43	2.02	0.00	1.76	0.92	0.10	0.09
	10vsal14	4.97	23.38	175	21.48	89.78	17.03	1.37	165.8	55.2	173.5	4.32	0.06	27.4	7.45	20.57	3.39	17.08	5.66	1.76	7.27	1.28	8.33	1.85	5.34	0.84	5.18	0.78	4.24	0.30	1.07	1.22	0.47	0.22
	10vsal15	4.95	21.34	169	15.53	71.74	15.02	1.64	174.7	48.7	156.0	3.83	0.05	45.5	6.76	18.65	3.03	15.26	4.96	1.53	6.38	1.13	7.51	1.67	4.87	0.79	4.70	0.69	3.89	0.27	1.70	0.89	0.42	0.36
	10vsal16	4.96	31.60	323	27.02	103.59	17.18	3.45	161.7	40.5	138.4	3.42	0.07	31.7	5.74	16.34	2.59	13.39	4.29	1.43	5.49	0.97	6.38	1.40	4.12	0.63	3.78	0.59	3.43	0.24	1.04	1.72	0.37	0.19
	10vsal19	6.63	25.65	203	20.63	102.97	19.27	1.60	90.1	48.4	140.7	3.25	0.06	15.9	5.44	16.42	2.84	14.07	4.93	1.55	6.26	1.12	7.37	1.64	4.88	0.80	4.58	0.69	3.59	0.22	1.27	1.10	0.38	0.20
	10vsal20	5.81	24.08	167	17.10	109.91	15.60	1.66	150.9	44.1	143.2	3.25	0.07	13.1	5.63	16.56	2.73	14.05	4.64	1.50	5.98	1.06	7.10	1.54	4.47	0.71	4.24	0.63	3.68	0.24	2.47	1.24	0.38	0.19
	07vsal108	10.35	31.11	338	16.26	77.82	9.98	19.98	445.7	25.9	51.9	0.81	0.20	44.4	1.96	5.28	0.97	5.20	1.95	0.74	2.91	0.55	3.90	0.87	2.62	0.42	2.64	0.41	1.51	0.06	4.04	0.74	0.16	0.20
	07vsal110	4.86	28.77	330	28.45	54.07	18.70	0.81	36.4	48.9	159.3	4.03	0.02	3.3	6.25	18.23	3.00	15.30	4.98	1.74	6.61	1.20	7.68	1.64	4.89	0.76	4.64	0.70	3.91	0.27	3.07	0.36	0.42	0.20
	07vsal113	7.80	40.84	314	38.75	85.73	14.64	20.22	145.1	18.2	34.4	0.62	0.05	160.9	1.23	3.37	0.57	3.16	1.32	0.50	1.97	0.40	2.67	0.62	1.86	0.30	1.86	0.29	1.00	0.04	1.55	0.59	0.10	0.07
	07vsal116	8.09	39.91	290	39.56	82.14	13.62	10.90	221.2	14.6	26.2	0.48	0.12	137.1	0.95	2.63	0.45	2.57	1.03	0.43	1.63	0.33	2.19	0.49	1.50	0.24	1.53	0.24	0.77	0.03	1.80	1.16	0.08	0.05
	07vsal117	12.74	38.81	274	37.07	48.63	13.63	6.59	137.6	16.7	31.2	0.55	0.04	262.4	0.97	2.98	0.51	2.98	1.19	0.46	1.78	0.37	2.52	0.57	1.80	0.27	1.81	0.28	0.97	0.04	0.98	0.42	0.09	0.07
	07vsal118	4.66	39.34	239	39.85	59.00	14.98	15.41	271.1	26.2	76.1	2.00	0.09	107.0	3.00	8.91	1.49	7.58	2.58	0.95	3.52	0.65	4.22	0.92	2.67	0.41	2.49	0.38	1.90	0.13	1.37	0.79	0.18	0.07
	07vsal119	5.72	36.99	238	35.80	69.54	14.14	0.42	136.7	22.1	60.2	1.29	0.01	8.1	2.62	7.20	1.17	6.23	2.09	0.77	3.01	0.52	3.40	0.71	2.13	0.34	2.06	0.30	1.58	0.09	1.67	1.19	0.21	0.09
	07vsal120	4.08	24.52	205	19.84	37.98	19.29	0.44	65.3	36.7	123.4	2.42	0.01	6.3	4.84	13.48	2.23	10.99	3.68	1.20	4.75	0.88	5.61	1.21	3.85	0.60	3.62	0.55	3.08	0.16	1.53	0.71	0.36	0.24
	07vsal122	3.92	17.74	58	12.81	117.63	21.14	0.42	66.9	48.6	195.2	3.89	0.00	7.3	3.25	9.72	1.63	8.78	3.15	0.90	4.64	0.91	6.48	1.61	5.47	0.89	5.74	0.92	4.91	0.27	1.50	0.93	0.53	0.28
	07vsal123	6.77	33.10	340	36.19	95.36	19.75	2.60	64.8	45.6	161.6	4.04	0.01	29.9	6.62	19.12	3.18	16.21	5.25	1.99	6.68	1.18	7.70	1.64	4.95	0.80	4.95	0.78	3.93	0.28	1.38	1.97	0.42	0.29
Salahi	07vsal4	8.77	27.28	200	27.80	158.09	10.46	19.93	85.1	15.0	24.9	0.47	0.02	374.0	0.96	2.89	0.50	2.83	1.11	0.41	1.69	0.34	2.32	0.51	1.60	0.26	1.54	0.24	0.78	0.03	1.82	1.43	0.07	0.16
	07vsal6	3.97	29.57	382	35.81	231.05	16.34	0.38	61.2	39.1	115.7	2.60	0.00	4.1	4.38	13.18	2.19	11.69	3.95	1.41	5.10	0.98	6.30	1.33	4.12	0.62	3.82	0.56	2.89	0.18	1.75	1.14	0.27	0.25
	07vsal8	4.27	26.72	358	22.37	225.41	12.09	0.16	44.5	44.1	114.7	2.58	0.00	8.5	3.84	12.31	2.31	12.43	4.17	1.44	5.74	1.03	6.54	1.47	4.28	0.64	4.04	0.59	2.88	0.17	2.84	1.94	0.27	0.10
	07vsal10	4.41	29.92	267	30.88	246.13	13.94	2.42	50.2	21.9	49.8	1.00	0.02	31.6	1.82	5.03	0.81	4.39	1.65	0.58	2.49	0.48	3.27	0.76	2.32	0.31	2.31	0.36	1.41	0.07	3.52	1.92	0.15	0.09
	07vsal11	4.65	19.61	196	19.58	241.38	15.73	0.88	51.3	35.5	109.6	2.18	0.01	19.3	3.31	10.35	1.89	10.00	3.45	1.17	4.48	0.84	5.49	1.22	3.64	0.52	3.39	0.51	2.85	0.15	2.41	1.80	0.33	0.15
	07vsal12	3.46	21.35	285	17.73	81.93	13.93	0.37	58.5	33.4	95.5	1.96	0.01	14.4	4.51	11.55	1.88	9.87	3.20	1.08	4.09	0.76	4.95	1.11	3.36	0.52	3.23	0.49	2.42	0.13	7.19	1.27	0.27	0.23
	07vsal15	3.14	25.74	328	26.10	168.64	16.50	0.86	67.2	33.2	96.1	1.97	0.01	26.4	3.67	10.57	1.75	9.27	3.13	1.13	4.30	0.79	4.94	1.11	3.31	0.48	3.13	0.47	2.44	0.13	3.18	1.12	0.27	0.22
	07vsal20	3.55	19.07	185	16.11	108.08	15.29	0.75	60.1	36.9	116.6	2.33	0.01	11.7	4.72	13.13	2.17	11.10	3.71	1.23	4.66	0.89	5.64	1.22	3.79	0.53	3.55	0.54	2.87	0.15	8.36	1.55	0.31	0.18
	07vsal26	2.03	23.75	290	26.73	78.02	13.89	0.36	60.1	36.4	107.6	2.28	0.00	8.7	4.17	12.21	2.06	10.97	3.58	1.28	4.54	0.88	5.61	1.23	3.70	0.52	3.45	0.54	2.69	0.15	6.15	0.90	0.28	0.14
	07vsal56	1.30	23.71	299	24.17	112.17	17.13	1.42	90.7	36.7	106.3	2.26	0.01	27.5	4.39	12.64	2.08	10.55	3.55	1.34	4.67	0.86	5.57	1.23	3.75	0.52	3.47	0.53	2.73	0.15	7.82	3.41	0.28	0.18
	07vsal57	1.40	23.46	244	25.86	116.28	17.06	0.45	53.7	40.9	127.4	2.68	0.00	6.4	4.96	14.81	2.39	12.48	4.14	1.35	5.21	0.99	6.43	1.40	4.18	0.59	3.95	0.62	3.23	0.18	6.22	2.41	0.35	0.17
	07vsal58	1.63	25.76	275	23.94	103.74	12.68	0.50	74.0	37.0	107.3	2.35	0.01	13.6	4.09	12.47	2.07	10.59	3.58	1.19	4.52	0.87	5.53	1.23	3.77	0.53	3.53	0.55	2.63	0.16	7.13	0.63	0.28	0.39
	07vsal60	1.99	26.64	306	31.99	117.51	17.96	0.51	62.4	31.9	99.3	2.01	0.01	11.2	3.84	10.75	1.86	9.34	3.24	1.11	4.03	0.79	4.97	1.09	3.34	0.44	3.10	0.48	2.50	0.14	5.65	0.86	0.25	0.10
	07sal29	3.48	34.38	356	29.06	65.36	16.02	8.95	74.8	42.1	120.7	2.87	0.00	360.7	4.69	14.04	2.35	11.95	3.93	1.54	5.53	1.00	6.40	1.49	4.14	0.66	3.91	0.60	2.96	0.20	2.13	0.26	0.41	0.41
	07sal32	2.19	34.24	357	37.81	379.54	16.65	1.00	60.0	39.8	112.3	2.57	0.00	26.7	4.27	13.28	2.14	11.24	3.91	1.37	5.13	0.99	6.37	1.39	3.96	0.65	3.66	0.55	2.74	0.16	0.79	0.23	0.11	0.11
	07sal34	4.80	17.73	117	11.11	59.36	14.72	0.73	46.4	47.4	150.4	3.04	0.01	13.4	5.00	16.29	2.95	14.78	4.80	1.67	6.50	1.21	7.61	1.63	4.90	0.79	4.40	0.65	3.63	0.20	0.98	0.37	0.30	0.29
	07sal37	4.52	28.00	279	30.24	154.69	19.13	0.25	39.2	41.3	128.2	2.61	0.00	7.9	3.93	12.63	2.09	11.61	4.10	1.27	5.56	1.02	6.41	1.43	4.20	0.66	4.05	0.60	3.02	0.18	1.10	0.35	0.37	0.36
	07sal41	3.96	32.13	348	42.45	77.74	19.73	0.41	36.4	43.3	125.1	2.58	0.00	5.5	4.62	13.75	2.29	12.62	4.07	1.47	5.82	1.04	6.77	1.43	4.38	0.71	4.04	0.61	3.21	0.17	0.71	0.30	0.36	0.36
	07sal45	4.17	29.79	330	27.90	76.75	18.49	0.19	41.5	38.7	112.7	2.43	0.00	5.5	4.50	13.49	2.22	11.37	3.90	1.31	5.09	0.94	6.03	1.34	3.96	0.63	3.77	0.57	3.03	0.15	0.93	0.27	0.43	0.43
	07sal48	4.40	22.57	271	23.54	76.17	17.29	0.27	34.6	40.8	125.1	2.51	0.00	6.5	4.13	12.94	2.23	11.14	3.85	1.26	5.03	1.00	6.32	1.43	3.94	0.61	3.99	0.58	3.17	0.17	0.54	0.32	0.22	0.21
	07sal50	4.27	14.91	47	10.80	75.80	18.29	0.37	39.5	63.4	207.1	3.85	0.01	8.5	7.14	22.16	3.66	19.17	6.21	1.87	8.45	1.52	9.85	2.17	6.29	0.98	6.19	0.92	5.22	0.26	0.68	0.56	0.41	0.40
	07sal52	3.85	17.76	53	13.44	89.18	19.13	0.11	65.7	63.6	211.9	4.37	0.00	6.2	8.53	24.46	4.23	20.82	6.84	2.32	9.19	1.61	10.35	2.14	5.96	0.89	5.63	0.82	5.12	0.27	0.59	0.57	0.45	0.44
Sheeted dikes																																		
Fizh	07fizh1	3.91	35.43	401	28.54	136.42	17.54	1.21	68.1	36.0	98.6	2.16	0.00	17.8	3.79	11.61	1.86	10.62	3.56	1.20	4.43	0.86	5.68	1.29	3.51	0.57	3.35	0.51	2.63	0.17	0.58	0.26	0.05	0.05
Ghayth	08ghay6	6.42	26.88	319	24.94	77.31	16.88	0.85	55.3	31.7	90.9	1.80	0.01	7.9	3.68	9.96	1.68	8.97	3.02	1.09	4.11	0.74	4.90	1.10	3.31	0.48	3.00	0.46	2.38	0.12	3.26	0.75	0.27	0.28
	08ghay8	4.52	18.31	83	13.33	63.52	16.51	0.46	49.4	34.9	120.2	2.10	0.01	6.0	4.41	12.56	2.06	10.35	3.56	1.16	4.67	0.81	5.32	1.16	3.47	0.53	3.30	0.50	3.05	0.14	4.01	0.96	0.43	0.29
	08ghay10	3.45	25.97	222	20.39	68.85	15.87	0.60	89.9	50.4	170.5	3.52	0.01	12.2	6.18	18.55	3.07	15.03	5.05	1.43	6.75	1.21	7.71	1.65	5.17	0.78	4.67	0.72	4.18	0.23	2.35	0.54	0.46	0.49
Salahi	07sal55	3.26	17.85	50	11.89	121.46	20.82	0.33	31.0	56.9	195.8	4.17	0.00	6.7	7.75	21.22	3.82	18.24	6.16	2.06	8.01	1.46	9.08	1.99	5.65	0.86	5.39	0.80	4.78	0.28	0.70	0.52	0.20	0.20
V2 lavas																																		
Fizh	08fizh11	5.54	33.93	271	33.85	37.12	14.89	0.52	45.1	21.5	44.0	0.69	0.01	3.8	1.43	4.52	0.78	4.28	1.67	0.62	2.47	0.48	3.22	0.75	2.15	0.35	2.14	0.33	1.26	0.05	1.54	0.36	0.19	0.11
	08fizh13	6.26	34.01	268	31.99	52.89	14.37	0.48	52.2	23.6	47.6	0.79	0.01	4.6	1.61	4.70	0.84	4.65	1.86	0.68	2.61	0.53	3.55	0.81	2.50	0.37	2.45	0.38	1.30	0.05	1.12	0.43	0.13	0.10
	08fizh14	2.50	16.30	173	14.74	29.32	7.83	0.54	40.0	14.5	32.0	0.51	0.02	4.2	1.11	3.22	0.57	3.03	1.14	0.42	1.59	0.32	2.17	0.51	1.52	0.24	1.50	0.23	0.88	0.04	1.59	0.06	0.09	0.07
	07vsal1	10.88	35.23	204	27.86	243.96	11.08	76.87	47.7	10.9	15.5	0.24	0.04	353.5	0.79	1.54	0.34	1.78	0.72	0.31	1.26	0.25	1.70	0.39	1.17	0.20	1.24	0.19	0.51	0.01	1.29	2.81	0.05	0.05
	06sal3 V2	-	34.38	-	30.19	69.18	12.35	6.76	178.4	19.5	34.9	0.45	0.09	295.3	1.20	3.68	0.63	3.55	1.44	0.54	2.08	0.44	2.86	0.64	2.00	0.31	1.99	0.31	1.05	0.21	-	0.73	0.10	0.11
	06sal5 V2	-	36.33	-	29.44	59.28	22.13	5.53	160.5	20.6	33.9	0.40	0.13	132.1	1.22	3.54	0.62	3.61	1.42	0.57	2.07	0.43	2.82	0.65	1.97	0.29	1.83	0.27	0.97	0.06	-	0.50	0.10	0.10
	07vsal107	8.98	45.06	272	39.34	62.85	14.60	2.31	118.5	14.0	21.2	0.29	0.15	28.2	0.75	1.96	0.38	2.08	0.94	0.39	1.44	0.30	2.04	0.48	1.43	0.22	1.40	0.22	0.65	0.02	1.19	0.44	0.07	0.07
V2 dike	08fizh17	10.98	41.28	254	39.48	67.19	16.24	0.94	113.2	15.2	26.2	0.43	0.02	39.1	0.80	2.44	0.45	2.51	0.99	0.38	1.63	0.33	2.29	0.53	1.63	0.25	1.58	0.25	0.79	0.02	1.23	0.33	0.08	0.28
Boninite dike	08fizh4	12.86	50.91	254	51.71	74.09	10.39	5.23	43.9	7.4	9.2	0.61	0.08	31.4	0.69	1.55	0.22	1.05	0.41	0.16	0.68	0.16	1.07	0.25	0.84	0.14	0.99	0.16	0.30	0.05	2.08	0.76	0.20	0.12
Hilti LV2	09vHil209	37.85	33.46	215	28.98	56.22	11.24	2.59	141.0	13.4	33.6	0.72	0.03	45.4	1.01	2.88	0.49	2.72	0.97	0.41	1.61	0.32	2.06	0.48	1.36	0.27	1.46	0.23	0.99	0.05	4.25	0.83	0.12	0.10
	10vHil219	11.11	34.59	226	33.89	67.72	14.58	1.41	170.9	23.8	81.5	2.92	0.02	25.0	3.67	10.33	1.68	7.94	2.53	1.03	3.41	0.61	3.82	0.87	2.43	0.38	2.24	0.33	1.92	0.19	2.77	0.42	0.21	0.09
	09Hil218	14.32	29.40	283	27.81	60.78	18.04	4.84	586.5	17.5	42.8	0.78	0.03	34.7	1.69	4.03	0.70	3.93	1.37	0.54	2.14	0.39	2.69	0.62	1.82	0.25	1.76	0.28	1.13	0.06	18.96	1.07	0.13	0.30
	09Hil222	14.32	34.07	386	26.68	63.08	20.48	1.01	149.1	17.8	34.2	0.61	0.01	21.4	1.54	3.37	0.59	3.28	1.24	0.51	1.93	0.37	2.53	0.61	1.82	0.30	1.83	0.29	0.96	0.05	12.80	0.99	0.09	0.21
	09Hil234	10.02	29.93	250	25.97	61.76	12.57	13.83	1246.4	20.1	42.6	0.79	0.17	163.7	1.52	4.33	0.70	3.91	1.45	0.57	2.36	0.44	3.09	0.70	2.10	0.35	2.07	0.33	1.21	0.05	9.18	0.66	0.12	0.10
	09Hil237	7.49	31.38	319	27.98	74.99	13.69	12.55	652.9	20.7	40.8	0.79	0.18	47.4	1.41	3.94	0.68	3.85	1.47	0.59	2.35	0.47	3.04	0.73	2.20	0.36	2.09	0.34	1.19	0.05	4.48	0.60	0.12	0.29

(Continued)

			Li (ppm)	Sc	V	Co	Zn	Ga	Rb	Sr	Y	Zr	Nb	Cs	Ba	La	Ce	Pr	Nd	Sm	Eu	Gd	Tb	Dy	Ho	Er	Tm	Yb	Lu	Hf	Ta	W	Pb	Th	U
		09Hil241	4.86	29.86	328	21.45	60.47	13.96	3.21	852.1	18.4	32.3	0.58	0.03	256.0	1.67	3.72	0.60	3.69	1.23	0.53	2.03	0.36	2.55	0.60	1.84	0.30	1.81	0.29	0.91	0.03	7.53	0.81	0.09	0.08
		09Hil247	8.15	31.21	276	27.11	67.94	12.41	28.33	235.3	22.3	51.0	0.98	0.26	43.9	1.76	4.86	0.81	4.54	1.80	0.62	2.57	0.49	3.34	0.76	2.21	0.33	2.17	0.33	1.42	0.07	4.72	0.57	0.15	0.11
		09Hil248	5.64	25.67	254	17.35	54.26	16.37	1.06	90.7	22.4	48.1	0.93	0.03	38.0	1.97	5.00	0.81	4.40	1.64	0.58	2.45	0.47	3.24	0.75	2.23	0.34	2.29	0.37	1.29	0.06	10.37	0.92	0.15	0.14
		09Hil249	9.40	26.78	245	24.21	60.03	9.82	15.10	113.8	22.3	47.6	0.96	0.14	38.2	1.80	4.64	0.84	4.56	1.66	0.57	2.54	0.46	3.25	0.75	2.25	0.37	2.26	0.35	1.37	0.07	11.22	0.60	0.13	0.11
		09Hil250	9.17	30.52	261	24.37	165.75	13.55	5.48	1215.5	24.1	42.5	0.82	0.07	97.5	1.91	4.68	0.79	4.29	1.62	0.56	2.45	0.48	3.24	0.75	2.36	0.36	2.36	0.37	1.20	0.06	4.06	0.88	0.13	0.12
		09Hil251	5.07	34.59	360	21.55	88.25	14.34	11.11	287.0	19.3	35.4	0.68	0.14	29.8	1.55	3.85	0.62	3.44	1.39	0.55	2.08	0.41	2.70	0.61	1.92	0.30	1.90	0.30	1.01	0.04	6.64	1.44	0.10	0.11
		09Hil252	12.69	36.30	335	25.55	250.96	22.94	0.79	792.9	17.7	33.2	0.66	0.02	29.1	1.29	3.48	0.59	3.33	1.29	0.50	2.00	0.39	2.61	0.60	1.81	0.28	1.81	0.28	0.97	0.05	7.32	1.10	0.10	0.49
		09Hil253	10.19	34.25	319	27.92	66.17	11.68	4.33	446.9	17.4	33.4	0.65	0.07	34.9	1.17	3.33	0.59	3.33	1.27	0.51	2.01	0.39	2.63	0.59	1.78	0.27	1.75	0.27	1.03	0.05	7.06	0.65	0.09	0.14
		09Hil254	8.73	31.47	265	27.72	90.90	16.54	0.91	735.0	15.1	28.6	0.55	0.02	49.5	1.00	2.80	0.48	2.68	1.16	0.43	1.72	0.33	2.28	0.52	1.59	0.22	1.54	0.24	0.86	0.03	10.83	0.72	0.08	0.16
		09Hil255	7.68	31.42	274	24.50	92.54	15.71	4.38	799.5	20.7	42.8	0.83	0.07	123.1	1.67	4.46	0.74	4.19	1.57	0.53	2.25	0.44	2.99	0.70	2.07	0.32	2.08	0.33	1.24	0.05	4.15	0.99	0.13	0.14
		09Hil256	7.48	25.53	264	20.36	81.81	10.22	21.05	907.3	26.8	65.7	1.30	0.19	221.2	2.18	6.25	1.09	5.96	2.19	0.79	3.25	0.60	4.06	0.90	2.71	0.37	2.55	0.39	1.88	0.08	12.41	0.69	0.20	0.13
		09Hil257	8.37	31.76	297	29.34	129.54	13.93	5.62	717.8	17.0	32.7	0.61	0.08	51.8	1.15	3.29	0.55	3.37	1.32	0.51	1.91	0.38	2.61	0.59	1.77	0.26	1.78	0.28	0.97	0.04	6.73	0.78	0.09	0.08
		09Hil258	7.42	29.66	265	26.08	79.89	16.09	0.47	405.7	18.7	31.4	0.60	0.02	122.9	1.20	3.58	0.62	3.61	1.37	0.51	2.06	0.41	2.76	0.63	1.79	0.27	1.83	0.28	1.02	0.04	9.24	0.83	0.09	0.15
		09Hil259	8.71	33.92	251	27.53	141.89	10.71	3.61	430.8	15.4	28.4	0.52	0.04	71.0	1.04	2.86	0.48	2.73	1.10	0.42	1.64	0.34	2.25	0.50	1.54	0.23	1.56	0.24	0.83	0.04	5.38	0.63	0.08	0.06
		09Hil260	3.35	30.59	237	24.62	234.37	23.32	1.22	196.4	14.7	25.4	0.48	0.04	44.8	0.94	2.52	0.45	2.55	0.98	0.40	1.53	0.31	2.15	0.47	1.45	0.22	1.45	0.22	0.76	0.03	4.81	0.65	0.08	0.07
		10sh21	6.01	40.96	214	33.57	85.11	14.36	3.77	96.9	17.6	30.5	0.58	0.06	54.7	3.64	4.72	1.10	5.43	1.64	0.59	2.30	0.42	2.65	0.62	1.75	0.29	1.68	0.26	0.93	0.04	0.83	2.57	0.12	0.34
	UV2	09vhil206	9.68	36.14	334	30.00	92.66	14.59	1.62	112.0	17.6	37.4	0.89	0.06	11.8	1.66	4.01	0.71	3.62	1.39	0.48	1.93	0.38	2.54	0.61	1.82	0.30	1.79	0.29	1.13	0.07	4.76	1.48	0.17	0.16
		09vhil214	20.25	31.86	259	22.26	102.46	10.26	2.58	170.6	24.2	45.7	0.97	0.07	17.0	2.29	5.29	0.94	4.55	1.78	0.59	2.56	0.48	3.32	0.81	2.38	0.40	2.48	0.39	1.29	0.07	10.71	1.19	0.18	0.19
		10vhil205	20.49	41.20	204	46.82	93.16	8.41	5.08	115.3	8.9	8.8	0.52	0.08	22.3	1.00	1.91	0.28	1.36	0.50	0.18	0.78	0.17	1.21	0.31	0.95	0.16	1.00	0.16	0.31	0.05	5.60	2.66	0.16	0.09
		10vhil211	13.50	44.37	299	36.27	105.67	14.46	8.04	188.4	11.4	10.8	0.60	0.13	10.4	0.89	1.68	0.25	1.28	0.51	0.21	0.88	0.19	1.45	0.37	1.18	0.23	1.26	0.21	0.36	0.05	2.09	1.41	0.18	0.18
		10vhil216	10.77	44.10	220	43.63	110.18	7.56	1.72	117.1	8.1	10.0	0.56	0.07	12.0	2.30	2.17	0.43	1.65	0.56	0.17	0.79	0.17	1.20	0.30	0.91	0.17	1.02	0.17	0.34	0.05	2.80	4.48	0.16	0.22
V3 lavas																																			
Hilti		07salV3	5.14	39.42	319	36.67	42.07	16.39	10.59	582.6	28.6	122.1	18.52	0.02	140.2	14.97	30.45	4.09	16.16	4.15	1.50	4.71	0.79	4.74	1.00	2.85	0.42	2.54	0.38	2.68	0.86	0.49	2.40	0.50	0.49

Appendix Table 3 Representative clinopyroxene analyses.

			Name	(wt%) SiO2	TiO2	Al2O3	Cr2O3	FeO	MnO	MgO	CaO	Na2O	Total	Ca	Mg	Fe	Mg#
V1	Zabin		08ZbN50	51.04	0.45	1.14	0.00	14.97	0.51	13.65	17.82	0.28	99.88	36.80	39.10	24.10	0.62
			08ZBN71	50.89	0.49	1.84	0.00	7.68	0.16	16.87	19.80	0.26	97.97	40.20	47.60	12.10	0.80
	Fizh	LV1	07fizh5	49.71	1.10	3.13	0.05	11.10	0.25	14.24	19.76	0.37	99.71	41.00	41.10	17.90	0.70
			07fizh17	51.57	0.39	2.04	0.00	6.58	0.17	17.35	20.73	0.22	99.05	41.40	48.30	10.30	0.82
			07fizh22	52.09	0.18	2.19	0.13	4.53	0.19	18.39	22.07	0.18	99.95	43.10	50.00	6.90	0.88
			07fizh24	52.11	0.15	2.15	0.03	5.14	0.17	18.32	21.54	0.18	99.79	42.20	49.90	7.90	0.86
			07fizh26	51.49	0.62	2.16	0.16	9.26	0.20	15.82	19.85	0.29	99.85	40.40	44.80	14.70	0.75
			07fizh33	50.46	0.91	2.90	0.08	9.25	0.31	15.26	20.53	0.32	100.02	41.90	43.30	14.70	0.75
		MV1	07fizh40	53.07	0.09	2.76	0.74	2.80	0.06	17.94	21.68	0.13	99.27	44.40	51.10	4.50	0.92
			07fizh42	51.78	0.17	2.14	0.26	6.08	0.21	18.15	20.68	0.12	99.59	40.80	49.80	9.40	0.84
			07fizh43	50.68	0.68	2.59	0.00	9.04	0.23	16.07	19.88	0.28	99.45	40.30	45.40	14.30	0.76
			07fizh45	52.90	0.15	1.95	0.11	4.84	0.12	18.69	21.02	0.11	99.89	41.40	51.20	7.40	0.87
			07fizh47	51.53	0.51	2.84	0.10	6.53	0.16	17.19	20.59	0.21	99.66	41.50	48.20	10.30	0.82
			07fizh48	52.86	0.15	2.17	0.43	3.63	0.08	17.98	22.37	0.15	99.82	44.60	49.80	5.70	0.90
		UV1	07fizh52	54.68	0.14	1.90	0.25	4.43	0.06	18.22	20.17	0.11	99.96	41.20	51.70	7.10	0.88
			07fizh55	53.90	0.17	2.03	0.14	4.77	0.15	18.18	19.79	0.14	99.27	40.50	51.80	7.60	0.87
			08fizh2	52.84	0.25	2.24	0.05	6.10	0.25	18.50	19.04	0.17	99.44	38.40	52.00	9.60	0.84
			08fizh3	53.06	0.37	2.25	0.00	5.82	0.14	17.89	19.22	0.20	98.95	39.50	51.10	9.30	0.85
			08fizh6	52.87	0.20	2.40	0.16	5.51	0.18	17.86	20.61	0.16	99.95	41.40	49.90	8.60	0.85
			08fizh7	53.03	0.15	2.64	0.21	5.56	0.16	17.89	20.01	0.16	99.81	40.60	50.50	8.80	0.85
			08fizh8	53.47	0.23	1.57	0.06	5.87	0.09	18.52	20.00	0.17	99.98	39.70	51.20	9.10	0.85
	Ghayth		06Ghay1	52.01	0.25	1.78	0.00	6.17	0.05	17.66	21.04	0.13	99.08	41.70	48.80	9.50	0.84
			06Ghay2	52.79	0.21	1.93	0.34	5.86	0.14	17.76	20.69	0.17	99.89	41.40	49.40	9.20	0.84
			06Ghay7	51.62	0.63	1.53	0.06	11.18	0.31	15.93	17.69	0.23	99.17	36.40	45.60	18.00	0.72
			06Ghay14	50.58	0.94	2.83	0.10	10.27	0.22	15.30	19.06	0.34	99.65	39.40	44.00	16.60	0.73
			06Ghay69	51.60	0.58	1.72	0.00	9.14	0.11	16.15	18.92	0.22	98.44	39.00	46.30	14.70	0.76
	Yanbu		06vsal8	50.39	1.07	2.70	0.00	10.28	0.30	14.57	20.04	0.31	99.66	41.50	41.90	16.60	0.72
			06vsal9	49.91	1.29	3.17	0.00	11.32	0.26	14.02	20.06	0.32	100.36	41.40	40.30	18.20	0.69
			06vsal11	51.92	0.64	1.72	0.03	10.87	0.33	15.58	19.43	0.26	100.78	39.20	43.70	17.10	0.72
			06vsal12	50.57	1.23	3.62	0.01	9.66	0.15	15.20	19.42	0.35	100.21	40.40	44.00	15.70	0.74
			06vsal24	51.75	0.68	1.88	0.00	9.11	0.10	16.25	19.09	0.23	99.10	39.10	46.30	14.60	0.76
			07sal118	51.30	0.43	2.96	0.74	4.58	0.07	17.01	21.67	0.24	99.00	44.30	48.40	7.30	0.87
			07sal119	50.77	0.53	3.79	0.12	5.15	0.16	17.38	21.41	0.19	99.48	43.20	48.70	8.10	0.86
			07sal120	51.97	0.25	1.97	0.54	4.36	0.13	18.82	20.22	0.24	98.51	40.60	52.60	6.80	0.89
			07sal111	49.91	1.17	3.72	0.00	10.87	0.32	15.73	18.57	0.34	100.63	37.90	44.70	17.30	0.72
	Hilti		09vHil24	51.31	0.30	2.24	0.24	4.36	0.10	17.39	21.99	0.21	98.16	44.30	48.80	6.90	0.88
			09vHil36	52.01	0.36	2.58	0.23	4.66	0.18	18.08	21.11	0.24	99.44	42.30	50.40	7.30	0.87
			09vHil51	50.79	0.73	2.51	0.24	7.55	0.08	16.58	20.38	0.32	99.17	41.30	46.80	12.00	0.80
			09vHil57	50.26	0.54	2.93	0.27	5.91	0.13	16.71	21.16	0.30	98.19	43.20	47.40	9.40	0.83

				(wt%)													
			Name	SiO2	TiO2	Al2O3	Cr2O3	FeO	MnO	MgO	CaO	Na2O	Total	Ca	Mg	Fe	Mg#
V2	Fizh		08fizh11	50.22	0.31	2.02	0.07	8.74	0.18	16.43	19.80	0.15	97.92	40.00	46.20	13.80	0.77
		Boninite dike	08fizh4	52.56	0.08	1.94	0.21	6.21	0.25	17.86	20.22	0.04	99.37	40.50	49.80	9.70	0.84
	Yanbu		06vsal3	51.61	0.34	3.04	0.09	7.30	0.14	17.45	19.92	0.13	100.03	39.90	48.60	11.40	0.81
			07vsal103	51.72	0.16	1.55	0.01	7.26	0.15	17.19	20.36	0.14	98.54	40.80	47.90	11.30	0.81
			07vsal104	51.79	0.20	2.42	0.09	7.73	0.17	18.13	18.20	0.11	98.83	36.80	51.00	12.20	0.81
	Hilti	LV2	09vHil213	49.97	1.13	2.86	0.04	10.71	0.32	13.62	20.90	0.35	99.91	43.40	39.30	17.30	0.69
			09vHil218	52.12	0.16	1.75	0.36	5.58	0.14	17.76	20.85	0.12	98.84	41.80	49.50	8.70	0.85
			09vHil223	52.00	0.16	2.10	0.69	5.72	0.22	17.93	19.86	0.15	98.83	40.30	50.60	9.10	0.85
			09vHil228	50.61	0.31	1.73	0.00	13.07	0.36	14.03	19.43	0.20	99.72	39.60	39.70	20.80	0.66
			09vHil234	52.37	0.15	1.71	0.19	5.66	0.14	17.79	20.41	0.16	98.58	41.20	49.90	8.90	0.85
			09vHil244	52.52	0.10	1.70	0.20	5.29	0.17	17.93	20.49	0.12	98.52	41.30	50.30	8.30	0.86
			09vHil256	50.32	0.39	1.98	0.06	11.40	0.38	14.37	18.78	0.20	97.87	39.40	41.90	18.70	0.69
			09vHil259	50.56	0.43	1.65	0.00	11.90	0.30	14.45	19.01	0.25	98.56	39.30	41.50	19.20	0.68
			10vHil217	52.56	0.12	2.80	0.23	6.23	0.19	19.11	18.95	0.03	100.21	37.60	52.80	9.70	0.85
		UV2	10vHil210	53.13	0.07	1.07	0.68	4.56	0.12	20.43	19.12	0.09	99.27	37.40	55.60	6.90	0.89
			10vHil216	53.05	0.28	1.71	0.60	4.57	0.10	18.25	20.96	0.12	99.64	42.00	50.80	7.20	0.88
V3	Hilti		09vHil203	49.27	0.97	3.95	0.06	7.43	0.16	14.85	21.14	0.35	98.19	44.40	43.40	12.20	0.78

Appendix Table 4 Chrome-spinel compositions of V2 lavas.

		SiO2	TiO2	Al2O3	Cr2O3	FeO	MnO	MgO	CaO	Total	Mg#	Cr#
UV2	10vHil209SP3	0.04	0.18	13.43	53.48	19.95	0.21	12.49	0.06	99.85	0.597	0.728
		0.07	0.25	13.03	51.75	22.43	0.31	10.63	0.10	98.57	0.522	0.727
	10vHil209SP1	0.06	0.32	17.00	49.07	19.58	0.31	13.08	0.01	99.43	0.615	0.659
		0.10	0.25	12.89	50.91	22.46	0.34	10.84	0.08	97.87	0.536	0.726
		0.08	0.13	13.38	52.71	20.50	0.35	11.84	0.02	99.00	0.575	0.726
		0.12	0.20	12.97	50.97	25.54	0.37	8.71	0.05	98.93	0.433	0.725
	10vHil209SP2	0.08	0.38	13.02	50.09	23.05	0.35	8.70	0.26	95.92	0.446	0.721
		0.02	0.26	13.35	51.45	18.62	0.19	12.43	0.21	96.53	0.614	0.721
		0.21	0.18	14.98	52.25	18.91	0.25	14.79	0.10	101.67	0.682	0.701
	10vHil216SP1	0.07	0.22	14.33	52.81	20.53	0.19	10.66	0.05	98.86	0.518	0.712
		0.10	0.14	11.34	57.36	19.09	0.24	10.81	0.01	99.10	0.532	0.772
		0.05	0.22	13.90	52.07	21.24	0.23	11.41	0.12	99.22	0.552	0.715
		0.09	0.24	13.12	51.86	22.42	0.31	10.57	0.38	98.99	0.523	0.726
		0.09	0.20	14.09	52.49	19.92	0.25	10.67	0.44	98.16	0.53	0.714
		0.08	0.22	13.98	53.13	20.21	0.14	10.81	0.56	99.13	0.533	0.718
	10vHil216SP2	0.07	0.16	11.70	57.04	20.64	0.30	10.83	0.04	100.77	0.525	0.766
		0.06	0.15	11.27	56.59	20.99	0.26	10.32	0.10	99.73	0.508	0.771
		0.08	0.10	11.68	57.98	19.47	0.28	10.77	0.17	100.54	0.526	0.769
		0.05	0.24	13.69	53.87	20.83	0.29	9.30	0.81	99.07	0.47	0.725
		0.07	0.14	12.60	56.80	18.27	0.23	10.13	0.93	99.17	0.514	0.751
		0.09	0.13	12.19	56.18	18.94	0.23	10.04	0.78	98.58	0.51	0.756
LV2	10vHil217	0.06	0.43	13.94	52.03	20.24	0.35	8.94	0.39	96.36	0.456	0.715
		0.05	0.44	12.64	52.16	21.83	0.37	9.96	0.28	97.72	0.499	0.735
		0.04	0.47	13.20	51.88	22.09	0.34	9.59	0.20	97.82	0.477	0.725
		0.09	0.34	12.10	54.45	20.14	0.32	9.31	0.31	97.05	0.473	0.751